

**Development of Condition Monitoring System for Railway Crossings  
Condition Assessment and Degradation Detection for Guided Maintenance**

Liu, X.

**DOI**

[10.4233/uuid:aadbb312-4596-4072-86f3-b43b3532ab40](https://doi.org/10.4233/uuid:aadbb312-4596-4072-86f3-b43b3532ab40)

**Publication date**

2020

**Document Version**

Final published version

**Citation (APA)**

Liu, X. (2020). *Development of Condition Monitoring System for Railway Crossings: Condition Assessment and Degradation Detection for Guided Maintenance*. [Dissertation (TU Delft), Delft University of Technology]. <https://doi.org/10.4233/uuid:aadbb312-4596-4072-86f3-b43b3532ab40>

**Important note**

To cite this publication, please use the final published version (if applicable).  
Please check the document version above.

**Copyright**

Other than for strictly personal use, it is not permitted to download, forward or distribute the text or part of it, without the consent of the author(s) and/or copyright holder(s), unless the work is under an open content license such as Creative Commons.

**Takedown policy**

Please contact us and provide details if you believe this document breaches copyrights.  
We will remove access to the work immediately and investigate your claim.

# DEVELOPMENT OF CONDITION MONITORING SYSTEM FOR RAILWAY CROSSINGS

Condition Assessment & Degradation Detection  
for Guided Maintenance

*Xiangming Liu 刘向明*

# **Development of Condition Monitoring System for Railway Crossings**

Condition Assessment and Degradation Detection for  
Guided Maintenance

**XIANGMING LIU**

# **Development of Condition Monitoring System for Railway Crossings**

Condition Assessment and Degradation Detection for  
Guided Maintenance

Proefschrift

ter verkrijging van de graad van doctor  
aan de Technische Universiteit Delft,  
op gezag van de Rector Magnificus, prof.dr.ir. T.H.J.J. van der Hagen  
voorzitter van het College voor Promoties,  
in het openbaar te verdedigen op  
woensdag, 2 december, 2020 om 12.30 uur

door

**Xiangming LIU**

Spoorweg ingenieur, Universiteit Centraal Zuid, China  
geboren te Qinhuangdao, China

Dit proefschrift is goedgekeurd door de

promotor: Prof.dr.ir. R.P.B.J. Dollevoet

copromotor: Dr. V.L. Markine.

Samenstelling promotiecommissie bestaat uit:

Rector Magnificus,	voorzitter
Prof. dr.ir. R.P.B.J. Dollevoet	Technische Universiteit Delft, promotor
Dr. V.L. Markine	Technische Universiteit Delft, copromotor

Onafhankelijke leden:

Prof. dr. R.M.P. Goverde	Technische Universiteit Delft
Prof. J.C.O. Nielsen	Technische Universiteit Chalmers, Zweden
Prof. E. Kassa G	Wetenschap en Technische Universiteit Noors, Noorwegen
Prof. R. Chen	Jiaotong Universiteit Zuidwesten, China
Prof. dr.ir. S.M.J.G. Erkens	Technische Universiteit Delft, reservelid

Overig lid:

Dr. I.Y. Shevtsov                      ProRail

This dissertation is funded by China Scholarship Council and Delft University of Technology, and partly supported by ProRail.



**TU Delft ProRail**

Keywords: railway crossing, condition monitoring, degradation detection, maintenance guidance

Cover Design: Xiangming Liu

Printed by: GILDEPRINT

Copyright © 2020 by Xiangming Liu (X.Liu0805@gmail.com)

ISBN: 9789464190786

All rights reserved. No part of the material by this copyright notice may be reproduced or utilized in any form or by any means, electronic or mechanical, including photocopying, recording or by any information storage and retrieval system, without written permission of the author.

谨以此书献给我的家人

# **Propositions**

pertain to the dissertation

## **Development of Condition Monitoring System for Railway Crossings**

by

**Xiangming Liu**

1. Structural Health Monitoring system is the only way to keep railway crossings sustainable.
2. In railway track maintenance, a crossing must be treated as a part of the railway track system rather than an independent element.
3. All the physical measures aiming to sustainable railway crossings end up to target on reducing the wheel impact forces.
4. Maintenance is a beneficial way to reduce investment for contractors, but not for the infrastructure manager.
5. Voluntary-based peer review of journal articles ends up with low quality reviews.
6. Writing a paper is like making a movie, the writing style of the final version must be exciting.
7. Experience is a plus for an engineer only when it is combined with an open mind to others.
8. Obsessive-compulsive disorder is the best character for researchers.
9. Researchers need to stay in the happy mood to overcome difficulties in doing research.
10. Make a feasible plan and stick with it is the only way keep research on track.

These propositions are regarded as opposable and defensible, and have been approved as such by the (co)promoters Prof.dr.ir. R.P.B.J. Dollevoet and Dr. V.L. Markine.

### Summary

Railway crossings are essential components of the railway track system that allow trains to switch from one track to another. Due to the complex wheel-rail interaction in the crossing panel, crossings are vulnerable elements of railway infrastructure and usually have short service lives. The crossing damage not only results in substantial maintenance efforts but also leads to traffic disruptions and can even affect traffic safety. In the Netherlands, the annual maintenance cost on railway crossings is more than 50 million euros.

Due to the lack of monitoring systems, the real-time information on crossing condition is limited. As a result, the present maintenance actions on railway crossings are mainly reactive that take place only after the occurrence of visible damage. Usually, such actions (repairs) are carried out too late and result in unplanned disruptions that negatively affect track availability. In the Netherlands, around 100 crossings are urgently replaced every year, accompanied by traffic interruptions.

Also, there is a considerable number of crossings with the service life of only 2-3 years. The maintenance methods used by the contractors on such crossings are somewhat limited and usually ended up with ballast tamping. In this case, the root causes of the fast crossing degradation are usually not resolved, and the crossings are still operated in degraded conditions after the maintenance.

In order to improve the efficiency of the current maintenance of railway crossings aiming for better crossing performance, the goal of this study is to develop a **monitoring system** for railway crossings using which the crossing **condition** can be assessed, and the **sources** of the degradation can be detected. Using such a system timely and proper **maintenance** on railway crossings can be provided.

The main steps in achieving this goal were as follows:

- Based on the measured dynamic responses of railway crossings due to passing trains, several **condition indicators** were proposed;
- To provide the fundamental basis for the proposed indicators a **numerical model** for the analysis of vehicle-crossing interaction was developed;
- The effectiveness of the proposed indicators was demonstrated using the data from long-term monitoring of 1:9 and 1:15 crossings.

The railway crossing conditions can be reflected in the changes in the **dynamic responses** due to passing trains. In this study, the responses were obtained from the crossing instrumentation and wayside monitoring system. The responses reflect the **wheel-rail interaction**, which consists of the wheel impact accelerations, impact locations and the rail displacements due to the impacts, etc. Based on the correlation analysis of the responses, the **indicators** related to the **wheel impact**, **fatigue area** and **ballast support** were proposed. The indicators form a basis for the structural health monitoring (SHM) system for the railway crossings.

To verify the effectiveness of the proposed indicators, and to explain the experimental

findings, a numerical vehicle-crossing model is developed using the **multi-body** system (MBS) method. The model is validated using the measurement results and further verified using the finite element (FE) model.

The proposed indicators and the MBS model were applied to the condition stage identification and damage source detection of the crossings. The main outcomes are presented below.

In the condition monitoring of normally degraded crossings, the proposed indicators were capable to catch the **main degradation stages** of the railway crossing ranging from newly installed to damaged and repaired ones. With the assistance of these indicators, the maintenance actions can be **timely** applied before the occurrence of severe damage. The proposed indicators can also be used for **assessing** the effectiveness of the performed maintenance (repair welding and grinding, ballast tamping, etc.). It was demonstrated that ballast tamping has no positive effect on the performance of the monitored 1:9 crossing.

The proposed indicators can also help to detect the **root** causes of the crossing damage. In some cases, the degradation is caused by adjacent structures, and therefore the maintenance should be performed not on the crossing itself but of the track nearby. In this study, the fast degradation of the monitored 1:9 crossing was found to be caused by the lateral track deformation in front of the crossing. The numerical results confirmed the phenomenon that the train **hunting** motion activated by the track deviation. It was the source of the extremely high impacts recorded by the monitoring system that ultimately resulted in the fast crossing degradation. By knowing the damage sources, **proper** maintenance can be performed rather than the currently used ineffective ballast tamping.

Additionally, it was found that crossing degradation can also result from external disturbances. It was proven that highly increased rail **temperature** due to the long duration of sunshine would amplify the existed geometry deviation in turnout. Considering the high sensitivity of wheel-rail interaction in the crossing, higher standards for crossing maintenance and construction are required for better crossing performance.

This study contributes to the development of the condition monitoring system for railway crossings. The application of the condition indicators is a big step forward for the current maintenance philosophies from damage repair to **predictive** maintenance, and from “failure reactive” to “failure proactive”. The outcomes in this study will contribute to the better performance of railway crossings.

### Samenvatting

Puntstukken zijn essentiële onderdelen in het spoorwegsysteem waarmee treinen van het ene spoor naar het andere kunnen rijden. Vanwege de complexe wiel-rail interactie ter hoogte van het puntstuk, zijn puntstukken kwetsbare onderdelen van spoorweginfrastructuur en hebben meestal een korte levensduur. De puntstukschades leiden niet alleen tot aanzienlijke onderhoudsinspanningen, maar ook tot verkeersverstoringen en de schades kunnen zelfs de verkeersveiligheid beïnvloeden. In Nederland bedragen de jaarlijkse onderhoudskosten aan puntstukken meer dan 50 miljoen euro.

Vanwege het ontbreken van een monitoringssysteem is de real-time-informatie over de puntstukconditie beperkt. Als gevolg hiervan zijn de huidige onderhoudsacties op puntstukken hoofdzakelijk reactief die alleen plaatsvinden na het optreden van zichtbare schade. Gewoonlijk worden dergelijke acties (reparaties) te laat uitgevoerd en resulteren in ongeplande verstoringen die de beschikbaarheid van het spoor negatief beïnvloeden. In Nederland worden jaarlijks ongeveer 100 puntstukken met spoed vervangen, gepaard met verkeersonderbrekingen.

Er is ook een aanzienlijk aantal puntstukken met een levensduur van slechts 2-3 jaar. De onderhoudsmethoden die door de aannemers op dergelijke puntstukken worden gebruikt zijn zeer beperkt en komen meestal neer op ballast stoppen. In dit geval worden de oorzaken voor de snelle puntstukdegradatie meestal niet opgelost en worden de puntstukken na onderhoud nog steeds in aangetaste toestand bereden.

Om de efficiëntie van het huidige onderhoud van puntstukken te verbeteren met het oog op betere puntstukprestaties, is het doel van deze studie het ontwikkelen van een **monitoringssysteem** voor spoorwegkruisingen waarmee de **puntstukconditie** kan worden beoordeeld en de bronnen van de degradatie kunnen worden gedetecteerd. Met behulp van een dergelijk systeem kan tijdig en correct onderhoud aan spoorwegkruisingen worden gepleegd.

De belangrijkste stappen om dit doel te bereiken waren als volgt:

- Gebaseerd op de gemeten dynamische reacties van puntstukken als gevolg van passerende treinen, werd een aantal **conditie-indicatoren** voorgesteld;
- Om de fundamentele basis voor de voorgestelde indicatoren te bieden, werd een **numeriek model** voor analyse van voertuig-puntstuk interactie ontwikkeld;
- De effectiviteit van de voorgestelde indicatoren werd aangetoond met behulp van de gegevens van lange termijn monitoring van 1:9 en 1:15 puntstukken.

De ontwikkeling van puntstuk conditie wordt weerspiegeld in de veranderingen van de **dynamische reacties** als gevolg van passerende treinen. In deze studie werden de antwoorden verkregen vanuit metingen aan puntstukken en via een monitoringssysteem langs de baan. De responsies laten de **wiel-rail interactie** zien, die bestaat uit de wielimpact versnellingen, impactlocaties en de railverplaatsingen als gevolg van de slagwerking, enz., Op basis van de correlatieanalyse van de responsies werden de **indicatoren** met betrekking tot de **slagwerking**, het **vermoeidheidsgebied** en de **ballastondersteuning** voorgesteld. De

indicatoren vormen een basis voor de structurele gezondheidsmonitoring (SGM) systeem voor de spoorwegkruisingen.

Om de effectiviteit van de voorgestelde indicatoren te verifiëren en de experimentele bevindingen te verklaren, is een numeriek voertuig-kruisend model ontwikkeld met behulp van de **Multi-body** system (MBS) methode. Het model is gevalideerd met behulp van de meetresultaten en verder geverifieerd met behulp van het eerder ontwikkelde eindige elementen (EE) model.

De voorgestelde indicatoren en het MBS-model worden toegepast bij de identificatie van de puntstuk conditie stadium en de detectie van de schadebronnen. De hoofdresultaten worden hieronder gepresenteerd.

Bij de conditiebewaking van normaal gedegradeerde puntstukken, waren de voorgestelde indicatoren in staat om de belangrijkste afbraakfasen van de puntstukken te bepalen, variërend van nieuw geïnstalleerde tot beschadigde en gerepareerde. Met behulp van deze indicatoren kunnen de onderhoudsacties tijdig worden uitgevoerd voordat ernstige schade optreedt. De voorgestelde indicatoren kunnen ook worden gebruikt voor het beoordelen van de effectiviteit van het uitgevoerde onderhoud (reparatie lassen en slijpen, ballast aanstampen, enz.). Er werd aangetoond dat ballast stoppen geen positief effect heeft op de prestaties van de bewaakte 1:9 kruising.

De voorgestelde indicatoren kunnen ook helpen om de **grondoorzaken** van de kruisingsschade op te sporen. In sommige gevallen wordt de degradatie veroorzaakt door nabije constructies, en daarom moet het onderhoud niet op het puntstuk zelf worden uitgevoerd, maar op het omliggende spoor. In deze studie werd aangetoond dat de snelle degradatie van de bewaakte 1:9 kruising werd veroorzaakt door de laterale vervorming van het aangrenzende spoor vóór het puntstuk. De numerieke resultaten bevestigden het fenomeen dat zelfsturende effect van de trein werd geactiveerd door de spoorafwijking, die de oorzaak was van de extreem hoge impacts die werden geregistreerd door het bewakingssysteem, uiteindelijk resulteerde in de snelle degradatie. Door de oorzaken van schade te kennen, kan **passend** onderhoud worden uitgevoerd in plaats van het momenteel ineffectieve ballast stoppen.

Aanvullend, bleek dat de puntstukdegradatie ook kan worden veroorzaakt door de externe verstoringen. Het is bewezen dat een sterk verhoogde railtemperatuur vanwege de lange zonneshijn bestaande geometrieafwijkingen kunnen vergroten. Gezien de hoge gevoeligheid van wiel-rail interactie bij het puntstuk, zijn hogere normen voor puntstukonderhoud en puntstukconstructie vereist voor betere puntstukprestaties.

Deze studie draagt bij aan de ontwikkeling van het conditiebewakingssysteem voor spoorwegkruisingen. De toepassing van de conditie-indicatoren is een grote stap voorwaarts voor de huidige onderhoudsfilosofieën, van schadeherstel naar **voorspellend** onderhoud, en van "faal reactief" naar "falen proactief". De resultaten in deze studie zullen bijdragen aan de betere prestaties van puntstukken.

## 综述

道岔作为辅助火车变道的结构，是铁路轨道系统中不可或缺的组成部分。由于在车轮过岔时复杂的轮轨相互作用，道岔也是铁路轨道中的薄弱环节，使用寿命也相对较短。道岔的伤损不仅会导致高昂的养护维修成本，同时也会造成交通中断，严重时甚至会影响通行安全。在荷兰，每年花费在道岔上的维护费用高达五千万欧元。

由于缺乏有效的监测系统，实时的道岔工况信息非常有限。因此，现阶段的道岔维护主要还是在可见伤损出现以后再采取措施。通常情况下，采取这些维护措施的时候已经为时已晚，这就导致了计划外的线路中断，严重影响铁路的可用性。在荷兰，每年约有一百个道岔被紧急更换，伴随而来的就是交通中断。

此外，有一些道岔的使用寿命非常短，甚至只有两到三年。对于这些问题道岔，承包商们除了进行道砟捣固以外并没有太多的养护维修措施。在这种情况下，导致道岔快速劣化的根本原因并没有得到解决，而道岔在养护维修之后依然在存在伤损的工况下运行。

为了提高现有的道岔区养护维修的有效性，改善道岔动力表现，本研究旨在开发一个道岔监测系统来实时的获取道岔的工况，并准确地检测道岔伤损的根本来源。利用这个系统，可以对道岔区的病害及时地进行有针对性的养护维修。

实现上述目的的主要步骤如下：

- 基于列车过岔时道岔的动力响应，提出几个主要的道岔状态指标；
- 建立一个分析车辆-道岔相互作用的数值模型，为上述状态指标提供基本依据；
- 在对 1: 9 和 1: 15 等多个道岔的长期监测中验证道岔状态指标的有效性。

铁路道岔的工况可以反映在列车过岔时道岔的动力响应上。在本研究中，道岔的动力响应主要通过仪器化道岔以及路旁监测来获得。这些动力响应反映了轮轨的相互作用，包括了车轮冲击产生的加速度，冲击位置以及冲击引起的钢轨的位移等。基于对这些响应的相关性分析，提出了与车轮冲击，疲劳区间和道砟支撑度等相关的状态指标。这些指标构成了铁路道岔健康监测系统的一个基础。

为了验证这些状态指标的有效性以及为了解释实验中的一些发现，在本研究中基于多体动力学分析软件建立了一个车辆-道岔模型。这个模型用实验结果进行了验证，并用有限元模型进行了进一步的查证。

上述状态指标和多体模型被应用到了道岔的工况识别和伤损源检测中。主要发现如下。

在监测正常劣化的道岔的过程中，这些状态指标可以识别道岔从新到损坏，再到修缮的主要工况。在这些指标的帮助下，养护维修工作可以在出现严重伤损之前及时地开展。这些指标也可以帮助评估养护维修作业（焊接打磨，道砟捣固等）的有效性。结果显示，道砟捣固对一个 1: 9 道岔的动力响应表现没有提升。

这些状态指标还可以帮助检测造成道岔伤损的根本原因。在一些情况下，道岔劣化是由相邻的轨道结构导致的，因此养护维修也应该在这些轨道区间进行，而不是在道岔区间。在本研究中，我们监测的一个 1: 9 的道岔的快速劣化是由道岔前段轨道的横向不平顺所导致的。数值分析结果确认了这种现象，即轨道的横向不平顺激发了列车的晃动。车辆的晃动是造成监测系统所记录的非常高的轮轨冲击的主要

因素，最终也导致了道岔的迅速劣化。通过掌握这些伤损源，养护维修作业可以更加合理地实施，以替代现在通常采用的无效的道砟捣固。

另外，外界环境的因素也会造成道岔的劣化。经证实，长时间日照引起的过高轨温会加剧轨道中现有的不平顺。考虑到道岔区轮轨相互作用的高敏感度，为了提高道岔的表现，道岔区轨道的铺设和维护需要采用更高的标准。

本研究对于铁路道岔监测系统的开发具有重要的指导意义。本文提出的道岔状态监测指标将促使道岔养护维修策略从普通的伤损维修升级转变为预防性维护，从“故障响应模式”升级为“故障预响应模式”。这将是道岔养护维修策略的一大进步。最终，本文的研究成果将推动道岔结构的进一步优化设计，为提高车辆一道岔动力学性能做出贡献。

# Thesis Contents

This thesis consists of two main parts. Part I is an extended summary, and Part II is papers appended to support Part I. The appended papers are listed below.

## Paper A

X. Liu, V.L. Markine, H. Wang, I.Y. Shevtsov, Experimental tools for railway crossing condition monitoring, *Measurement*, vol. 129, 2018, p. 424-435.

## Paper B

X. Liu, V.L. Markine, MBS Vehicle-Crossing Model for Crossing Structural Health Monitoring, *Sensors*, 20 (10), 2020, 2880.

## Paper C

X. Liu, V.L. Markine, Correlation Analysis and Application in the Railway Crossing Condition Monitoring, *Sensors*, vol. 19 (19), 2019, 4175.

## Paper D

X. Liu, V.L. Markine, Train Hunting Related Fast Degradation of a Railway Crossing – Condition Monitoring and Numerical Verification, *Sensors*, 20 (8), 2020, 2278.

# CONTENTS

Summary .....	I
Samenvatting .....	III
综述 .....	V
Thesis Contents .....	VII
Part I: Extended Summary	
Chapter 1 Introduction .....	1
1.1 Railway turnout crossings .....	1
1.2 Research motivation .....	2
1.2.1 Problems in railway crossings.....	2
1.2.2 SHM system in railway engineering .....	3
1.2.3 Numerical models for crossing behaviour .....	4
1.3 Research goal and approach .....	5
1.4 Thesis structure .....	5
Chapter 2 Condition monitoring – tools and indicators .....	7
2.1 Crossing instrumentation .....	7
2.1.1 Wheel impacts .....	8
2.1.2 Fatigue area .....	8
2.1.3 Impact angle .....	9
2.2 Wayside monitoring system .....	10
2.2.1 Rail Vertical displacement.....	10
2.3 Geometry measurement device .....	11
Chapter 3 MBS vehicle-crossing model .....	13
3.1 Model development .....	13
3.1.1 Geometrical parameters .....	13
3.1.2 Vehicle-crossing model.....	14
3.1.3 Model parameters.....	14
3.2 Model validation and verification .....	15

3.2.1	Transition region.....	16
3.2.2	Impact acceleration.....	17
3.2.3	Fatigue area analysis.....	18
3.2.4	Vertical contact forces.....	19
Chapter 4	Assessment of crossing conditions.....	21
4.1	Assisting in crossing condition monitoring.....	21
4.1.1	Condition stage identification.....	21
4.1.2	Damage source detection and verification.....	24
4.2	Maintenance and condition development.....	26
4.2.1	Effect of repair welding and grinding.....	26
4.2.2	Effect of local ballast tamping.....	28
4.2.3	Effect of fastening system renovation.....	29
4.3	Summary.....	31
Chapter 5	Detection of root damage causes.....	32
5.1	Track misalignment and fast degradation.....	32
5.1.1	Measured abnormal performance and analysis.....	32
5.1.2	Inspected track misalignment.....	34
5.1.3	Numerical verification of the damage sources.....	34
5.1.4	Effects of track curve and gauge deviation.....	37
5.2	Weather-related performance variation.....	38
5.2.1	Weather variation and crossing responses.....	38
5.2.2	Correlation analysis.....	39
5.2.3	Sunshine caused track deviations.....	42
5.3	Summary.....	44
Chapter 6	Conclusions and future work.....	45
6.1	Main conclusions.....	45
6.1.1	Condition stage identification.....	45
6.1.2	Maintenance effectiveness assessment.....	45

6.1.3	Damage source investigation.....	46
6.2	Recommendations for future work .....	46
6.2.1	Remote monitoring and data reading .....	46
6.2.2	Simplified failure alarm.....	47
6.2.3	Coupled numerical tools for design optimization .....	47
	References .....	48
Part II: Appended papers		
	Paper A.....	55
	Paper B.....	77
	Paper C .....	103
	Paper D .....	129
	Publications .....	151
	Acknowledgements.....	153



## **Part I: Extended Summary**



## Chapter 1 Introduction

In this chapter, an introduction of railway turnout and the wheel-rail interaction in the turnout crossing are firstly presented. Followed with these, the requirement for improving the current crossing maintenance, as well as the lack of particular research, are briefly discussed. Regarding the current status and the requirement for improvement, the research goal is brought forward. At the end of this chapter, the approach is described, and the thesis outline is provided.

### 1.1 Railway turnout crossings

Railway turnouts (switches and crossings) are essential components in the railway track system to the trains to transfer from one track to the other. A standard railway turnout contains three main parts:

- The switch panel that controls train travelling directions;
- The crossing panel that provides the intersection of two tracks;
- The closure panel that connects the other two panels.

A sketch view of a standard left-hand turnout is shown in Figure 1.1.

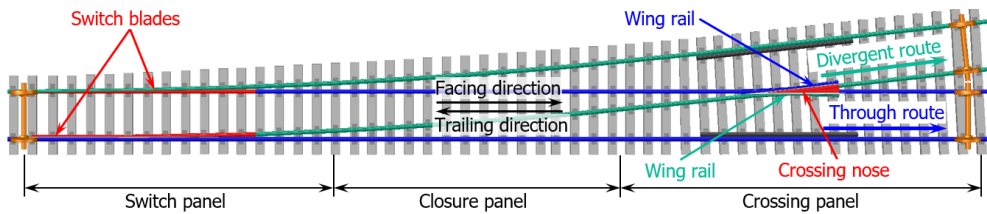


Figure 1.1. Standard left-hand railway turnout with a 1:9 crossing.

It can be seen from Figure 1.1 that the crossing panel is featured to provide the flexibility for trains to pass on different routes. An example of the wheel-rail interaction for the trains passing in the facing through route is given in Figure 1.2. The wheel-rail contact points along the track are shown as the yellow strips.

The wheel firstly approaches the crossing from the wing rail (Figure 1.2 (a)-(b), looking from the right side, the same below), and then follows with the transition of the wheel from the wing rail to the nose rail (c), after which the wheel continues running over the crossing nose (d) and the through rail. In section (c), the wheel load is transferred from the wing rail to the crossing nose, where the impact occurs on the nose rail. This section is then referred to as the transition region. Apparently, the smoother the wheel load transition is, the smaller the amplification of the wheel-rail impact forces due to the rail gap.

The high wheel-rail impact forces resulted from the presence of the gap between wing rail and nose rail are the leading causes of the degradation and failure of the railway crossings. In the Dutch railway, unlike the divergent route traffic, the train velocity in the through route

is not restricted and can be up to 140 km/h as same as in the normal track [1]. Such high train velocity may amplify the wheel-rail impacts and further shorten the service life of the crossing. Guarantee the good performance of railway crossings is a challenging task for railway infrastructure managers.

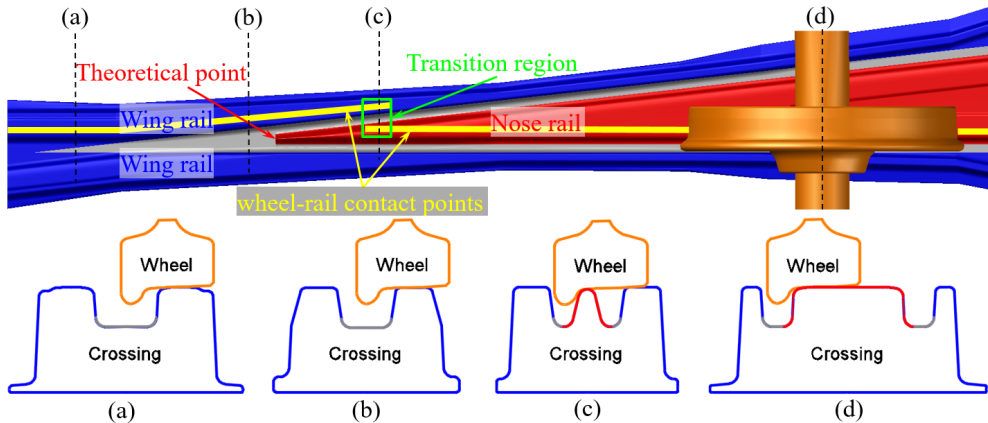


Figure 1.2. Main stages of wheel passing through a turnout crossing: approaching crossing (a)-(b), the transition from wing rail to crossing nose (c), continue moving on the crossing and through rail (d).

## 1.2 Research motivation

### 1.2.1 Problems in railway crossings

The high wheel-rail impacts in the railway crossings make them vulnerable elements in the railway infrastructure. Such high impacts result in not only substantial damages on the crossing rail (e.g., cracks and spalling on the railhead (Figure 1.3 (a)), broken rail foot (Figure 1.3 (b)), etc.), but also failures in the related track components (e.g., broken clips (Figure 1.3 (c)) and uneven ballast settlement (Figure 1.3 (d)), etc.).

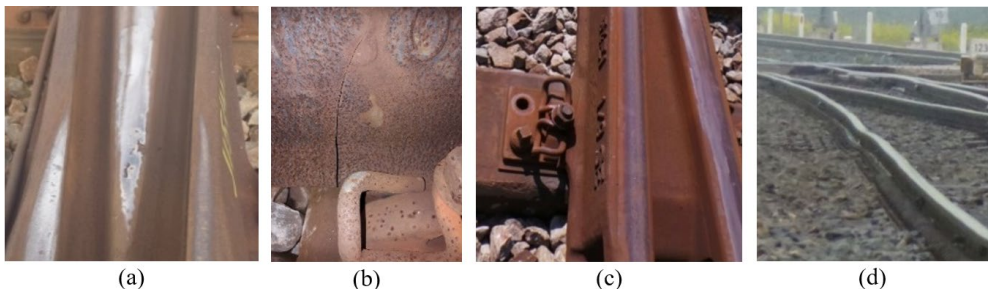


Figure 1.3. Crossing damages in the Dutch railway. (a): spalling on the railhead; (b): broken rail foot (photo from I.Y. Shevtsov); (c): Broken clips; (d): Uneven ballast settlement.

The crossing damage not only cost substantial maintenance efforts but also lead to traffic disruptions and can even affect traffic safety. In the Netherlands, the annual maintenance cost on railway crossings is more than 50 million euros. Among the 7000 crossings, around 100

of them are urgently replaced every year [2] accompanied by traffic interruptions. It was also mentioned in [2] that compared with the average crossing usage of around 18 years, there is a considerable amount of crossings that suffer from the extremely short service life of only 2-3 years.

Correspondingly, the current crossing maintenance actions are mainly reactive damage repair and routine preventive check. The former only takes place after the occurrence of visible damage. Such actions are usually carried out too late and result in unplanned disruptions that negatively affect track availability. While for the latter ones, the maintenance methods used by the contractors are limited. Even for the problematic crossings with short lives, they are usually ended up with ballast tamping. In this case, the root causes of the fast crossing degradation are usually not resolved, and the crossings are still operated in degraded conditions after the maintenance. It can be seen that the current maintenance philosophies are unable to meet the requirement for sustainable railway crossings. Necessary guidance for the maintenance actions in railway crossings is highly required to improve the current situation.

### 1.2.2 SHM system in railway engineering

The ineffective maintenance actions are mainly due to the limit of real-time information on crossing conditions. Such situations are resulted by the lack of monitoring systems. Therefore, one practical solution to improve maintenance is based on the principles of Structural Health Monitoring (SHM). Typically, SHM consists of five levels of activities [3], namely

- **Determine** the presence of structural damage;
- **Localize** the existed damage in the structure;
- **Assess** the structural condition;
- **Predict** the structural degradation and the remaining life;
- Seek for effective **remediation**.

To obtain sufficient information for the structural damage detection, localization and condition assessment, it is essential to get insight into the structural performance based on the monitoring data from the site. Nowadays, SHM systems are already well developed and applied to various civil engineering structures, such as large bridges and buildings with sensors and other monitoring devices installed during construction [4]-[7]. In railways, the use of SHM systems is still in the initial stages of local defects detection and localization. The main methods based on the inspection train consist of ultrasonic testing [8], image recognition [9]-[10], acoustic detection [11] and guided wave inspection [12], etc. Besides, the vehicle-based monitoring systems have been applied in the track stiffness measurement [13] and estimation [14], track alignment estimation [15], hanging sleepers detection [16] and track fault detection [17], etc.

Regarding railway turnouts, unlike in the switch panel where sensors are instrumented for condition monitoring [18]-[19] and remaining useful life prediction [20], The development of the crossing condition monitoring is still in the primary exploration stage [21]. Due to the increasingly restricted track access as well as the high cost for field measurements,

experimental methods such as instrumented wheel [22]-[22] and rail [24]-[25] are mainly used for numerical model validation. Therefore, it is quite necessary to develop a monitoring system for railway crossings. Such a system should be able to provide sufficient information for the assessment of the crossing condition and the detection of the degradation sources.

### 1.2.3 Numerical models for crossing behaviour

For the crossing condition assessment and damage detection, only on-site monitoring is not enough. A reliable numerical model that can be applied to verify the experimental findings is also necessary. In recent years, the numerical approaches are widely applied as practical alternatives to condition monitoring for crossing performance analysis. These numerical methods mainly consist of the multi-body system (MBS) methods [22], [25]-[35] and the finite element (FE) methods [23]-[24], [36]-[39].

The MBS methods can take into account the dynamic behaviour of both vehicle and track and featured with fast simulation. Using the MBS software, E. Kassa et al. [26]-[28] studied the dynamic interaction between train and railway turnout. The work of B. Pålsson et al. [29]-[30] contributed to the crossing damage analysis and crossing profile optimization. C. Wan et al. [31]-[33] used the MBS vehicle-crossing models optimized the railway crossing from rail geometry to the elastic track properties based on the wheel-rail interaction. Based on an MBS program, X. Shu et al. [34] developed a tool for advanced crossing performance analysis. J. Wegdam [35] developed an expert tool for the crossing geometry assessment.

Compared with the MBS methods, the FE methods are mainly used for detailed wheel-rail contact analysis. With the assistant of the FE models, M. Wiest et al. [36] studied the crossing nose damage due to the passing wheels. Z. Ren et al. [37] proposed a method to determine the transition region of the wheel load in a turnout. To combat rolling contact fatigue, V.L. Markine et al. [38] investigated the influence of track elastic properties on the wheel-rail contact. T. Arts [39] developed a full FE turnout model and studied the geometrical changes due to the variation of temperatures. Using the explicit FE approach, M. Pletz et al. [40]-[41] developed a wheelset-crossing model for the dynamic analysis of railway crossing. Based on the validated FE model [24], A.A. Mashal [42] analysed the dynamic performance of railway crossing and proposed ways for improvement. L. Xin et al. [43]-[45] developed a long-term behaviour model to analyse the dynamic interaction between wheelset and crossing, assess the effectiveness of repair welding and grinding and predict the crossing fatigue life. J.C.O. Nielsen and R. Skrypnik et al. [46]-[48] developed an iterative procedure to analyse wheel-crossing interaction and to predict the crossing geometry degradation. P.T. Torstensson et al. [49] investigated the influence of vehicle speed and crossing dip angle on the wheel-crossing interaction generated noises. Also, the MBS simulation results can be used as input data in the FE model to calculate the degradation of rail profiles [50].

Also, some other numerical models are developed and applied to analyse the performance of railway crossings. S. Alfi et al. [51] developed a mathematical model for train-turnout interaction. M. Wiest et al. [52] compared four different methods. They pointed out that the wheel-rail contact pressure calculated using Hertz and non-Hertzian methods correlate well with the FE method in case of no material plasticization. S. Chiou et al. [53] developed three functions to model the crossing geometry and compared the simulation results with the

measured vehicle vibration. X. Ma et al. [54] compared the efficiency and accuracy of three engineering approaches (Kik-Piotrowski, Ayasse-Chollet and Sichani) with Kalker's 3-D theory and FE model in terms of rail damage assessment.

It can be seen that the current numerical studies are usually focusing on specific problems and lack of connection with the crossing conditions. Real-life situations are usually much more complex, and the dynamic performance of a crossing can be affected by many internal and external factors. To assess the crossing condition and detect damage, especially in the fast degraded crossings, a numerical model that can provide a fundamental basis for the experimental findings is still needed.

### 1.3 Research goal and approach

Based on the above discussion, it is clear that to improve the performance of railway crossings, current maintenance actions need to be guided appropriately based on sufficient condition information. Therefore, the goal of this study is to develop a **monitoring system** for railway crossings, using which the crossing **condition** can be adequately assessed, and the **sources** of the crossing degradation can be accurately detected. The outcomes of this study will then be applied to guide **maintenance** actions on railway crossings. To achieve this goal, this study was initiated with the following main steps:

The first step was to select experimental tools to measure the dynamic responses of railway crossings. The experimental tools require limited track occupation and can catch the main dynamic features of railway crossings. Based on the responses, the indicators for the crossing condition assessment were proposed.

To provide a fundamental basis for the proposed crossing condition indicators, in the second step, an MBS vehicle-crossing model for the analysis of crossing performance was developed. Such a model was validated and verified using both the measurement results and the simulation results from an FE model. The developed MBS model is featured with fast simulation and sufficient options to verify the experimental findings.

In the third step, the effectiveness of the proposed indicators was demonstrated with the assistance of the MBS model. The demonstrations were based on the measurement data from long-term monitoring of 1:9 and 1:15 crossings and consist of the following parts:

- Identification of the crossing condition stages;
- Detection of the root causes for the fast degradation of a crossing;
- Investigation of the weather effects on the crossing performance.

All the steps are presented in this dissertation.

### 1.4 Thesis structure

This thesis is organized in the following chapters.

- Chapter 1: A brief introduction including research motivation, goal and approach;
- Chapter 2: Tools and indicators for crossing condition monitoring
- Chapter 3: Development of MBS vehicle-crossing model.
- Chapters 4-5 demonstrate the effectiveness of the developed monitoring system:
  - Chapter 4: Crossing condition stage identification and maintenance effectiveness analysis;
  - Chapter 5: Root causes investigation of the fast degraded crossing.
- Chapter 6 concludes this research and prospects the future work.

The thesis outline is presented in the flow chart below.

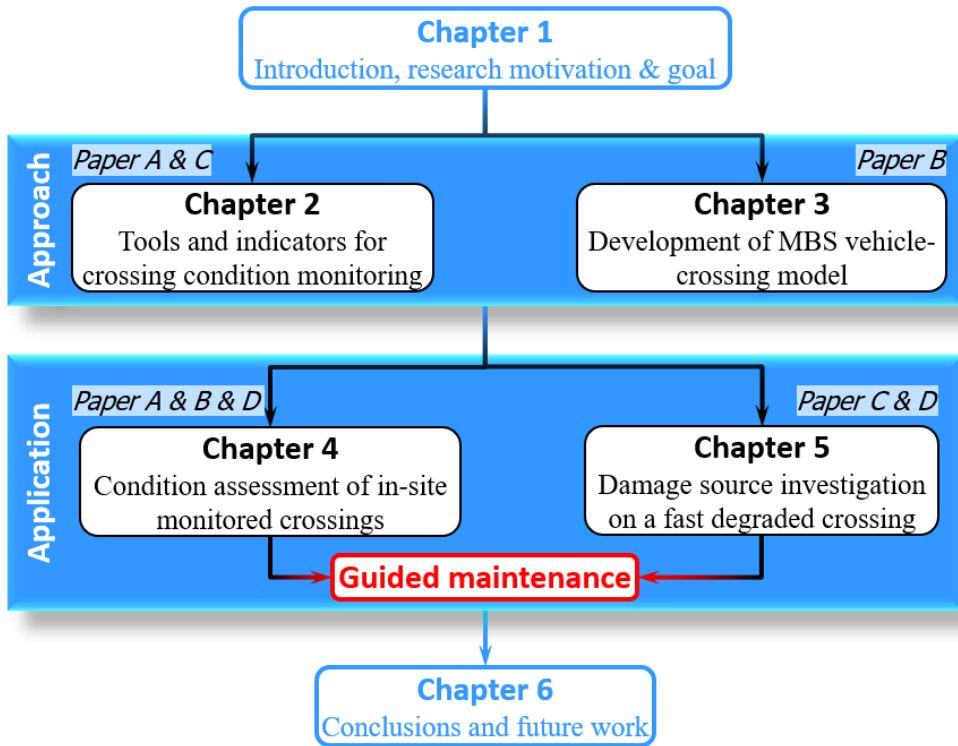


Figure 1.4. Thesis outline.

## Chapter 2 Condition monitoring – tools and indicators

The development of railway crossing conditions is reflected in the changes in the dynamic responses due to the passing trains. The responses that reflect the wheel-rail interaction, including the wheel impact accelerations, impact locations and the rail displacements due to the impacts, etc., are the bases of the proposed methodology. Therefore, the selected experimental tools should be able to measure the above mentioned dynamic responses for the crossing condition assessment. Also, the increasingly strict railway safety rules in the Netherlands demand the measurements be performed without track possession.

Based on the requirements mentioned above, two devices have been selected for crossing response measurements. The one is an accelerometer-based ESAH-M (Elektronische System Analyse Herzstückbereich-Mobil) for crossing instrumentation. The other is the digital image correlation (DIC)-based displacement measurement device called Video Gauge System (VGS) for wayside monitoring. Based on the measured dynamic responses, the indicators related to the wheel impact, fatigue area and ballast support were proposed.

### 2.1 Crossing instrumentation

The main components of the crossing instrumentation are an accelerometer attached to the crossing nose rail for 3-D acceleration measurement, a pair of inductive sensors attached in the closure panel for train detection and velocity calculation. All the data will be collected in the Main Unit located out of the track, which allows the measurements to be performed continuously without track access. An overview of the instrumented crossing is shown in Figure 2.1.

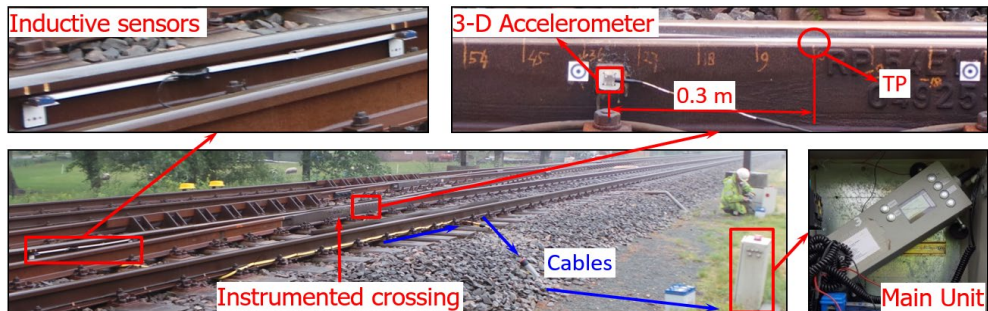


Figure 2.1. Crossing instrumentation based on ESAH-M.

The main outputs of the crossing instrumentation are the dynamic responses of the crossing nose, including the wheel-rail impact accelerations and locations, etc. All these responses are calculated within the transition region (Figure 1.2). In practice, the transition region of a crossing is where the shining bands on both the wing rail and the nose rail are overlapped, which can be obtained through field inspection. For crossings with different angles, the transition regions are usually quite different. Figure 2.2 shows two examples of the inspected crossing transition regions. For the 1:9 crossing (Figure 2.2 (a)), the estimated transition region is 0.15-0.40 m measured from the theoretical point (TP) of the crossing, while for the 1:15 crossing (Figure 2.2 (b)), such region is around 0.30-0.60 m from the TP.

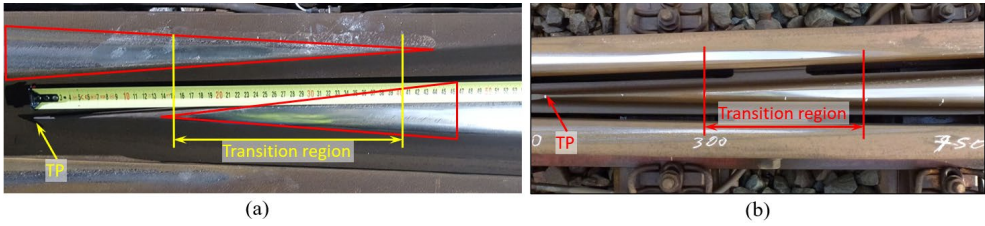


Figure 2.2. Inspected transition regions of crossings with different angles. (a): 0.15-0.40 m in a 1:9 crossing; (b): 0.30-0.60 m in a 1:15 crossing.

Based on these measured responses and the correlation analysis between the responses, two indicators respectively related to the **wheel impact** and **fatigue area** were proposed. Detailed information regarding the correlation analysis is presented in Paper C.

### 2.1.1 Wheel impacts

The wheel impact is reflected by the vertical accelerations, which are obtained on the crossing and processed through statistical analysis. This indicator is mainly based on the magnitude of the impacts due to each passing wheel (Figure 2.3 (a)). The distribution of the impacts due to multiple wheel passages can then be used to estimate the condition of the monitored crossing. Figure 2.3 (b) shows an example of the measured impacts in a 1:15 crossing (Figure 2.2 (b)) in different condition stages. It can be seen that with the crossing condition was degraded from the “Worn” stage to the “Damaged” stage, the wheel impacts overall shifted to a higher level.

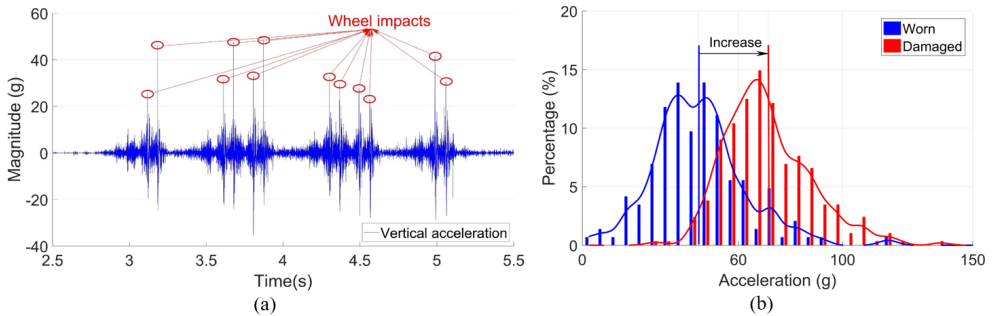


Figure 2.3. Indicator for the wheel impact. (a): Procedure for the obtainment of wheel impacts; (b): variation of the wheel impacts in different condition stages.

### 2.1.2 Fatigue area

On the railway crossing, the fatigue area is defined as the region where the majority of the wheel impacts located, and ultimately the cracks initiate, as demonstrated in Figure 2.4 (a). In practice, the fatigue area can be simplified as the confidence interval of  $[a-\sigma, a+\sigma]$ , where  $a$  is the mean value of the wheel-rail impact locations, and  $\sigma$  is the standard deviation. The location and size of the fatigue area are critical indicators for the assessment of crossing wear and plastic deformation. It is demonstrated in Figure 2.4 (b) that for the 1:15 crossing (Figure 2.2 (b)), when the crossing condition was degraded from the “Worn” stage to the “Damaged”

stage, the fatigue area became much narrower and shifted further from the TP.

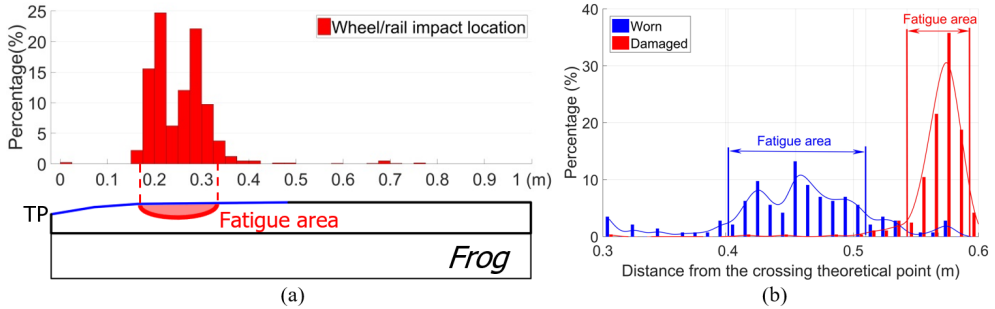


Figure 2.4. Fatigue area. (a): Definition; (b): Development in different crossing condition stages.

It can also be seen from Figure 2.3 and Figure 2.4 that the wheel impact and impact location are quite unstable and vary from one passing wheel to another. The statistical results of the wheel impacts and fatigue area based on a large amount of the measurement data can dramatically reduce the measurement error and better estimate the crossing condition.

### 2.1.3 Impact angle

Additionally, it was found that the crossing performance is, to a large extent, determined by the wheel-rail interaction in the transition region. Normally during the wheel transition, contact occurs on the wheel gauge corner (Figure 2.5 (a)), and the dominant impact acceleration is in the vertical direction. However, in some cases, when the wheel enters the crossing with a certain angle, the impact can occur on the wheel flange (Figure 2.5 (b)-(c)). In these situations, the magnitude of the accelerations is much higher than that in the normal situation with largely increased lateral impact accelerations. Obviously, impacts on the wheel flange are more damaging for a crossing than the impact on the wheel gauge corner.

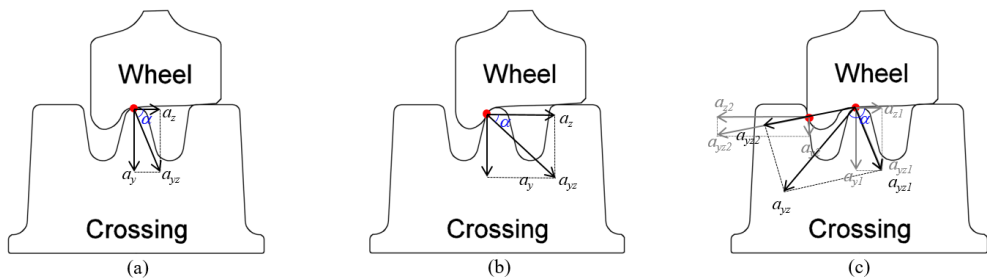


Figure 2.5. Wheel/rail contact situations. (a): Regular contact; (b): Irregular (positive) flange-nose rail contact; (c): Irregular (negative) flange-wing rail contact.

The wheel transition can be assessed by analysing the angle of the impact accelerations. To distinguish these contact situations, a simplified method to identify irregular contact is introduced in this measurement system based on the impact angle. Define the wheel impact angle  $\tan \alpha = |a_z / a_y|$ , when  $\tan \alpha \geq 1$ , the impact acceleration in the lateral direction is higher than that in the vertical direction, and the wheel-rail contact situation is considered as

irregular contact. Otherwise, the contact situation is regular. The irregular contact can be further divided into two categories: positive and negative. The positive contact is when the wheel flange has an impact on the crossing rail (Figure 2.5 (b)), and the negative contact when the flange impact is accompanied by the contact between the inner wheel and the wing rail (Figure 2.5 (c)).

Irregular contact might occur incidentally due to the bad wheel or wrong geometry of the crossing rail. However, if the proportion of irregular contact wheels in the overall passing wheels increases, it can indicate some changes in the crossing geometry. Therefore, this proportion can also be used as an indicator for the assessment of the crossing condition.

## 2.2 Wayside monitoring system

The VGS for wayside monitoring is a DIC-based remote measurement device. It uses high-speed digital cameras to measure the dynamic movements of the selected targets in the track. The system setup and the installed targets on the crossing rail are shown in Figure 2.6 (a), and the demo of displacement measurement is shown in Figure 2.6 (b). The main output is the vertical displacements of the tracked targets and the sampling frequency is up to 200 Hz.



Figure 2.6. Wayside monitoring. (a): system setup; (b) Screen of displacements measurement.

### 2.2.1 Rail Vertical displacement

Due to the limitation of the experimental conditions, the wayside monitoring system is usually set up close by the side of the track. Due to the ground vibration activated by the passing trains, there will be extra noise in the measured displacement results. In order to improve the accuracy of the measurement, the noise part needs to be eliminated.

The noise is mainly coming from the ground-activated camera vibration, by hammering the ground near the camera, such vibration can be manually activated. The manually activated camera vibration responses in both the time domain and frequency domain are shown in Figure 2.7. It can be seen from Figure 2.7 (b) that the main resonance of the camera vibration is around 15-45 Hz. According to the elaboration results shown in the previous study [55], The train-track components related to displacement responses are mainly distributed below 10 Hz, which means that they are not overlapped with the camera vibration in the frequency domain. The noise part due to camera vibration can then be reduced through 15 Hz low-pass filtering. An example of the measured rail displacements before and after filtering is shown

in Figure 2.8.

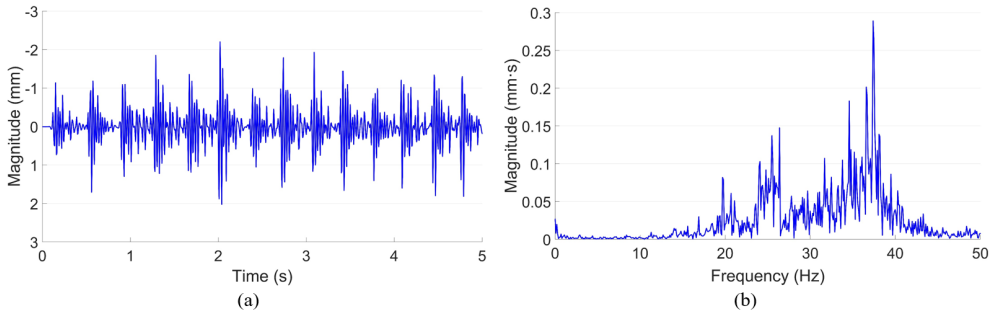


Figure 2.7. Ground activated camera vibration. (a): Time-domain signal; (b): Frequency domain responses.

The magnitude of the vertical rail displacement directly reflects the intensity of the track movement due to the passing trains. By comparing the measured rail displacement with the reference level, the ballast settlement level of the monitored location can be estimated. The reference level of the rail displacement can be obtained from the numerical simulation with the validated MBS model using the parameters in the designed condition, which will be discussed in the next chapter.

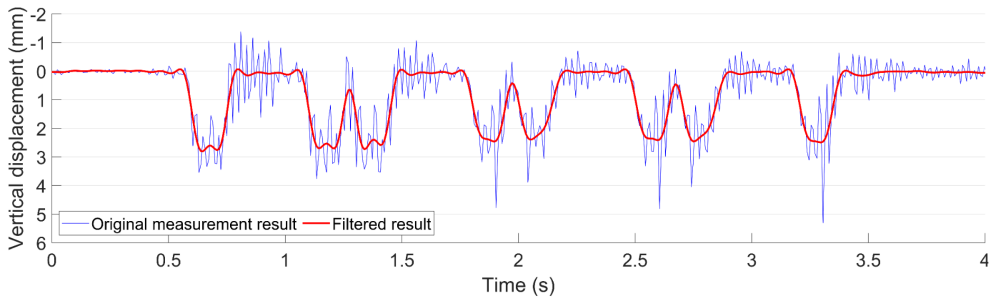


Figure 2.8. Examples of the measured rail vertical displacement.

### 2.3 Geometry measurement device

The device for the measurement of the crossing geometry is the laser rangefinder-based Calipri system. This device consists of a laser emitter sensor, a linear guide to control the positioning of the sensor, and a tablet to operate measurement and display the result (Figure 2.9 (a)).

By using this system, the critical sections of a crossing can be measured one after another. Together with all the measured cross-sections, the crossing geometry can be described (Figure 2.9 (b)). The direct application of the measured crossing geometry is to estimate rail wear and plastic deformation quantitatively. Examples of the measured crossing geometries in different states are shown in Figure 2.10. It can be seen that in the “Damaged” state, both wing rail and nose rail were worn and deformed. Such plastic deformations may lead to the change of the wheel-rail interaction and further cause the increase of the impact acceleration responses. After repair, the measured rail profiles along this crossing have clearly shown that



## Chapter 3 MBS vehicle-crossing model

To verify the effectiveness of the proposed indicators, as well as to explain the experimental findings, a numerical vehicle-crossing model is developed using the MBS method. The MBS model is validated and verified using both the field measurement results and the simulation results from the previously developed FE model. In this chapter, the model development, validation and verification are presented.

### 3.1 Model development

#### 3.1.1 Geometrical parameters

To ensure the MBS vehicle-crossing model simulates the same real-life situation as the previously developed FE model [24], the main parameters in the MBS model are set to be consistent with the monitored 1:9 cast manganese crossing in the Dutch railway. The vehicle model is developed based on the double-deck train VIRM [54], which is the most commonly used train type in the monitored track section. The wheel type used in the VIRM train is S1002, and the rail type used in the track is UIC54 E1. The main parameters of the S1002 wheel profile and UIC54 E1 rail profile are shown in Figure 3.1.

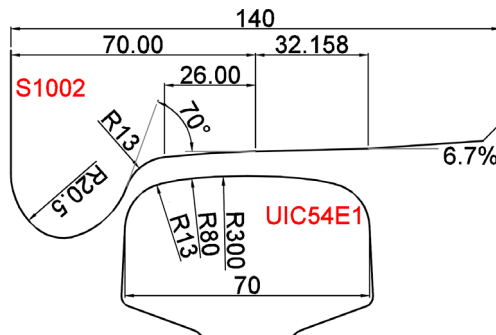


Figure 3.1. UIC54 E1 rail profile and S1002 wheel profile applied in the MBS model. Unit: mm.

The crossing geometry is one of the critical components in the development of the MBS vehicle-crossing model. The design drawing of the modelled 1:9 cast crossing is shown in Figure 3.2. The total length of the crossing is approximately 3.7 m.

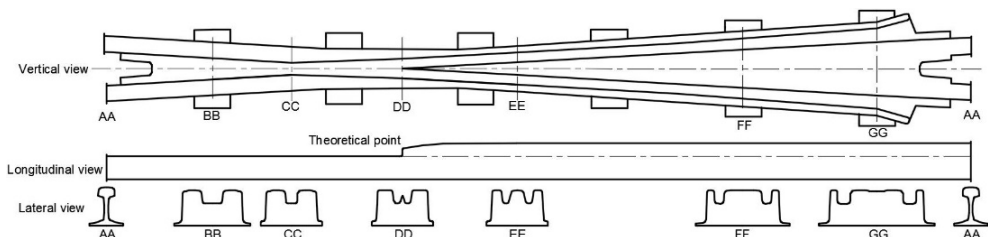


Figure 3.2. Geometry of the 1:9 cast crossing with defined major critical cross-sections. (Photo from Y. Ma)

In this drawing, a group of critical cross-sections from AA to GG are defined to describe the crossing rail geometry. The TP is located in section DD, the change of the rail geometry is mainly from section CC (-0.50 m from the TP) to section FF (1.51 m from the TP). In order to precisely define the crossing geometry, additional critical sections are added to control the curvature of the arcs in the rail profiles and the height of the nose rail. In this crossing model, the crossing geometry is defined by the overall 23 control sections.

### 3.1.2 Vehicle-crossing model

The model for the analysis of the vehicle – track interaction developed using the MBS method (implemented in VI-Rail software) is shown in Figure 3.3 (a). The track model is a straight line with the crossing panel (Figure 3.3 (b), critical sections are marked as red) situated in the middle of the track. This study is concentrated on the wheel-rail interaction in the crossing panel. Therefore, the switch panel (Figure 1.1) is simplified to a normal track. The profiles between two adjacent sections are automatically interpolated using the third-order spline curve. The total length of the track model is 100 m, which allows enough preloading space (around 1 m) before the vehicle entered into the crossing panel as well as enough space after the vehicle passed through the crossing.

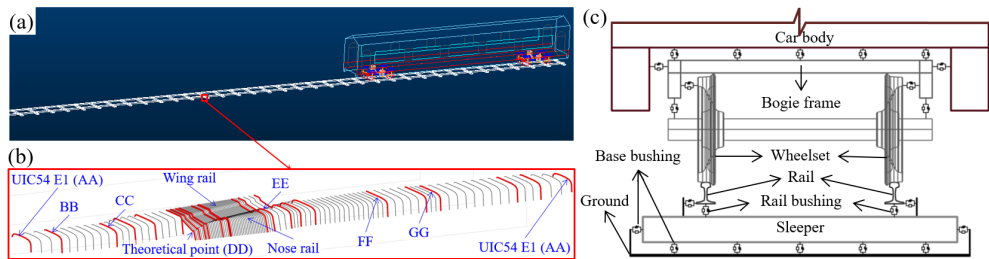


Figure 3.3. MBS model: (a) Vehicle-track model; (b) Flexible connections in the model; (c): Input crossing profiles, the control sections are marked in red colour.

The vehicle model is developed based on the VIRM train with a total length of 27.5 m. The car body, the bogie frames and the wheelsets are modelled as rigid bodies with both primary suspension and secondary suspension taken into account [56] (Figure 3.3 (c)). The wheel-rail contact model is defined as the general contact element that uses the actual wheel and rail profiles as input, which allows variable wheel and rail profiles and the visualized contact graphic.

The main outputs of the MBS model include the wheel displacements, rail accelerations (optional), wheel-rail contact forces and contact area, etc. The computation of the wheel-rail contact force is based on the Hertz contact theory. The elastic deformation is estimated through undeformed penetration, which will be used for the contact area calculation. More information about the methodologies can be found in [56].

### 3.1.3 Model parameters

Before the simulations, the properties of the track and the corresponding elements in the MBS models were thoroughly checked and adjusted to ensure that the MBS model and the FE

model (used for the model verification) describe the same real-life railway system (the monitored crossing). The vehicle/wheelset properties used in the MBS model are given in Table 3.1. The total axle load results from the wheelset, bogie and car body masses, which is 10 t in this model. In the FE model [24], the axle load is also 10 t, while the weights of the bogies and the car body are all integrated into the simplified half moving wheelset.

Table 3.1. Vehicle configuration of the MBS model

Items		Value
Wheel	Profile	S1002
	Radius, m	0.46
Wheelset	Mass, kg	1100
Bogie	Mass, kg	3800
Car body	Mass, kg	68000

The main properties of the rail model are Young's modulus and density. For the rail pad and ballast, the stiffness and damping in both vertical and lateral directions are taken into account. The main track properties are given in Table 3.2, referring to [57].

Table 3.2. Track properties of the MBS model

Track components		Values
Rail	Young's modulus, GPa	210
	Mass density, kg/m <sup>3</sup>	7900
Rail pad	Vertical stiffness, MN/m	1300
	Vertical Damping, kN·s/m	45
	Lateral stiffness, MN/m	280
	Lateral Damping, kN·s/m	58
Ballast	Vertical stiffness, MN/m	45
	Vertical Damping, kN·s/m	32
	Lateral stiffness, MN/m	45
	Lateral Damping, kN·s/m	32

### 3.2 Model validation and verification

In the previous study [24], the FE wheel-crossing model for the crossing performance analysis was already developed and validated. The explicit FE model can take the plastic deformation and hardening of the material on a local scale into account, which will be quite helpful for a better understanding of wheel-rail interaction. To allow the combination of the MBS model with the FE model for thoroughly study the dynamic performance of railway crossings, it is of great importance that the MBS model is not only comparable with the measurement results but also to close to the output of the FE model. Therefore, the developed vehicle-crossing MBS model is validated using the measurement results from the crossing instrumentation and verified using the simulation results from the FE model.

To better compare with the measurement and FE simulation results, the train running direction is set to the facing through route and the time step is adjusted to 0.0001 s, which is

consistent with that in the FE simulation and the sampling frequency of the measurement data. The following response quantities that reflect the performance of the crossing are used to validate and verify the MBS model:

- The transition region where the wheel load transit from the wing rail to the nose rail, which is considered as the most vulnerable region in the crossing;
- The vertical impact acceleration within the transition region.

Besides, some other output data from both the MBS and the FE simulations, including the vertical wheel trajectory and contact forces are compared further to prove the compatibility of the two numerical models. All these results are presented and analysed in the following sections.

### 3.2.1 Transition region

In the MBS simulation, the transition region is where the wheel and crossing rail has two-points contact and recognized as the interval between the start of wheel-nose rail contact and the end of wheel-wing rail contact. The size and location of the transition region reflect the smoothness of the wheel-rail contact transition from the wing rail to the nose rail. The transition region calculated using the MBS model is 0.196-0.227 m, as shown in Figure 3.4.

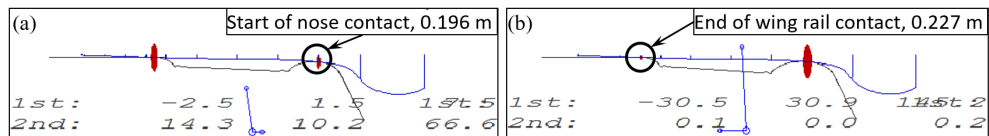


Figure 3.4. Transition region calculation in the MBS model. (a): Start contact with the nose rail; (b): End contact with the wing rail.

In the real-life situation, the transition region is obtained through field inspection and recognized as the overlapped shining bands on both the wing rail and the crossing nose. For the monitored crossing, the observed transition region is around 0.16-0.35 m with a size of 0.19 m, as shown in Figure 3.5. It can be seen that the transition region in the MBS simulation is within the observed one, but much smaller with the size of only 0.031 m. Such a phenomenon can be explained by the ideal initial conditions (no lateral angle or displacement) of the wheels used in the simulations and absence of the wheel or rail irregularities. Moreover, the crossing in situ was not new and had a certain level of plastic deformations and wear. In reality, every wheel passes the crossing with a certain angle and lateral shift that results in earlier/later contact in the transition region. The fact that the simulated transition region is included in the transition region of the real crossing proves the correctness of the MBS simulation results.

The transition region in the FE model simulation is 0.180-0.223 m, with a size of 0.043 m, which is 30% larger than that obtained from MBS simulation. Considering that in the MBS model, the wheels and rails are simulated as rigid bodies without taking the material deformation into account, the transition regions in both methods are close to each other, which proved the compatibility of the MBS models with the FE model.

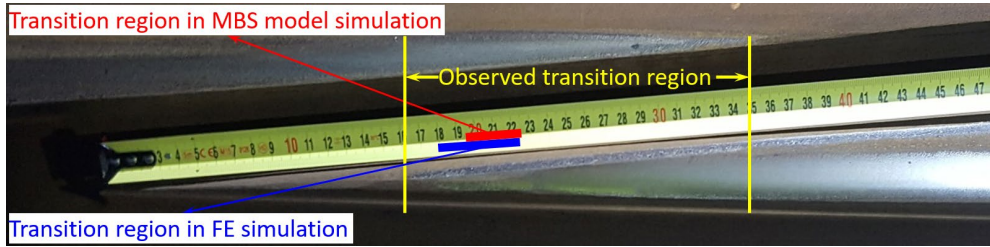


Figure 3.5. Transition regions obtained from the field observation and the numerical simulations.

### 3.2.2 Impact acceleration

The measured acceleration signals for the model validation contain more than 1000 wheels from 90 trains. In both numerical models, no track or rail irregularities were considered, which means that in the numerical simulations, the wheel (wheel-set) does not experience any additional disturbance when passing the crossing. As a result, the contact situation in these simulations is always regular (Figure 2.5 (a)). Therefore, only the regular contact wheels from the measurement are taken into account, which resulted in 500 selected passing wheels. The distribution of the impact accelerations due to these passing wheels is shown in Figure 3.6. The resulted histogram can be considered as a normal distribution, the mean value  $\mu = 47.15 \text{ g}$ , and the standard deviation  $\sigma = 17.65 \text{ g}$ .

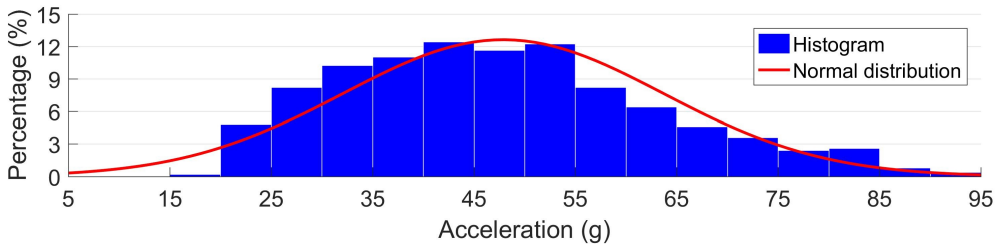


Figure 3.6. Histogram of the measured vertical accelerations.

The time domain representation of the selected measured acceleration responses used in Figure 3.6 is given in Figure 3.7 (a). For a better interpretation, the time histories were aligned horizontally to the wheel-rail impact point (Figure 3.7 (b)), which were used for validation of the numerical model.

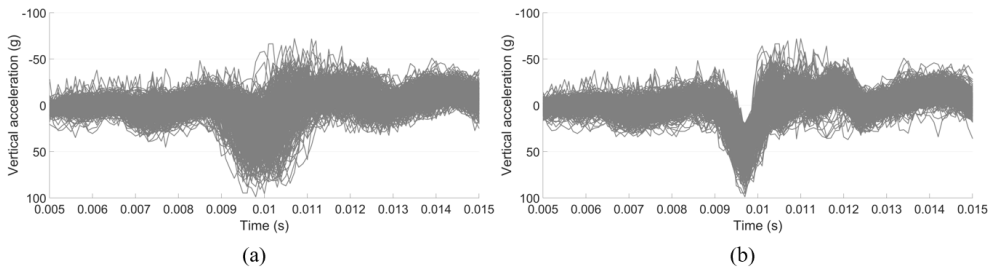


Figure 3.7. Measured acceleration responses: (a): Original time domain results; (b): Modified results: time histories aligned horizontally to the impact point.

In the MBS model, the selected element for acceleration extraction is the rail with lumped mass (Figure 3.8 (a)) located 0.3 m from the TP, which is the same as the location of the accelerometer in the crossing instrumentation (Figure 2.1). The comparison of the MBS simulation results with the measured responses and the FE simulation results is shown in Figure 3.8 (b). In general, the MBS simulation results have acceptable correlations with the measured accelerations. The amplitude of the simulated vertical acceleration is 61.8 g, which is 21 % higher than the mean value of the measured acceleration, and 62 % higher than the FE simulation results (38.1g). The big difference between MBS simulation and FE simulation results can be explained by different assumptions in these models. It can also be noted that some of the measured accelerations have rebounded after the impact (0.01-0.011 s), and the shape of the MBS simulation correlated well with these accelerations. While in the FE model, the impact acceleration is much smoother.

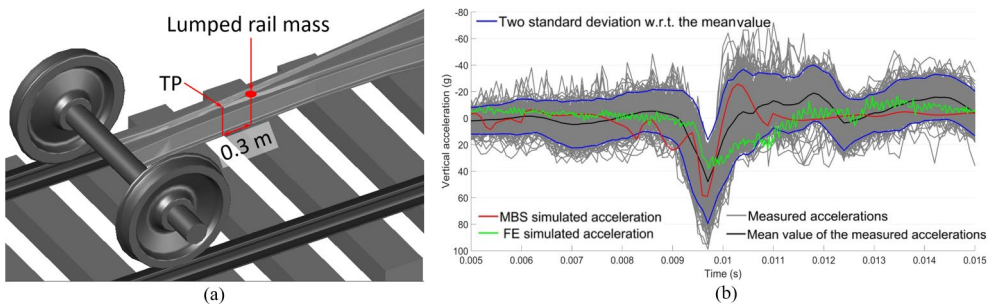


Figure 3.8. (a): Rail element for acceleration extraction in the MBS model; (b): Comparison of simulated accelerations with measured ones in the time domain.

The discrepancy between the MBS and the FE simulations are mainly due to the different assumptions in these models. In the MBS model, the wheelsets, rails and sleepers are all modelled as rigid bodies. In this case, the elasticity and damping of the vehicle-track system are underestimated, which leads to the relatively higher amplitude of rail acceleration. While in the FE model, the crossing rail is modelled as a solid element without hollow inside. It means that the rail mass and stiffness are overestimated and resulting in relatively small accelerations. Nevertheless, both simulation results are located within the interval  $[\mu-\sigma, \mu+\sigma]$  of the measured accelerations, meaning that although tolerable discrepancies exist, the MBS model is reasonably compatible with field measurement as well as the FE model.

### 3.2.3 Fatigue area analysis

For the selected measurement data, the distribution of wheel impact location is shown in Figure 3.9. Based on these results, the fatigue area of the crossing is calculated, which is 0.221-0.249 m from the TP.

In the MBS simulation, the wheel impact is located at 0.231 m from the TP, which is very close to the centre of the fatigue area, as marked in Figure 3.9. The fatigue area obtained from field measurement represents the degree of concentration of the wheel impacts, while the impact location in the MBS simulation is only from one wheel passage. Still, the close results proved the correctness of the MBS model.

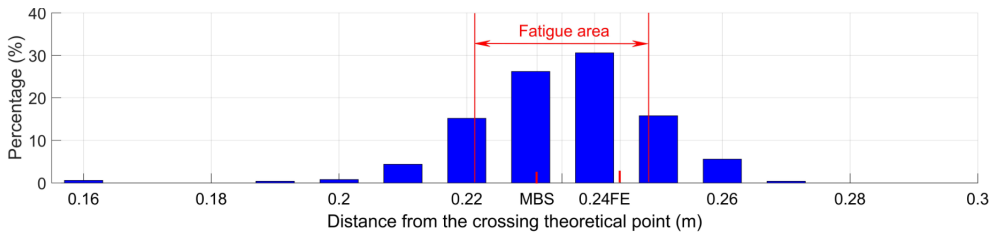


Figure 3.9. Distribution of wheel impact locations.

Comparatively, the impact location in the FE simulation is 0.244 m, which is within the fatigue area as well. The close impact locations obtained from the MBS and the FE simulations further proved the compatibility of these two models. It has to be noted that the wheel impacts and the fatigue area are calculated based on the selected wheels, which all have regular wheel-rail contact and the deviation is quite limited. Therefore, the resulted wheel impacts and fatigue area cannot fully represent the real-life situation, which should not be used to assess the crossing condition.

### 3.2.4 Vertical contact forces

The wheel-rail contact forces are related to the local properties and reflect the accuracy of the modelling of the wheel-rail contact. To further verify the compatibility of the MBS model with the FE model, the wheel-rail contact forces of these two models are compared. The results are presented in Figure 3.10. For the MBS simulation, the results from the first wheelset of the vehicle are applied.

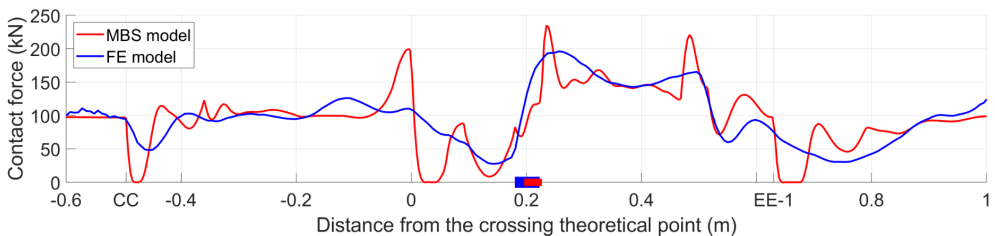


Figure 3.10. Comparison of vertical wheel-rail contact forces.

It can be seen from Figure 3.10 that the contact forces of both models are close to each other. In the MBS simulation, there are circumstances of the loss of wheel-rail contact near the sections of CC, DD and EE-1, which are consistent with the locations where the rail geometries are variated (Figure 3.3 (b)). Comparatively, the wheel-rail contact forces in the FE model developed smoother than those in the MBS models with less fluctuation.

The decrease in the contact forces of both models near section CC (Figure 3.10) indicates the beginning of the wing rail. At this point, the wheel-rail contact point on the wheel shifts farther from the wheel flange. In the MBS model, the sudden increase of the contact force near the TP reflects the effect of geometry change of the wing rail. It has to be noted that the first peak values (after passing through the TP) of both models occur after the respective transition regions. In the MBS simulation, the pick value is 235 kN that located in 0.235 m

from the TP. While in the FE model, it is 196 kN in 0.256 m. The second peak values are respectively 221 kN in 0.484 m in the MBS model and 165 kN in 0.496 m in the FE model.

It can be concluded that the contact forces obtained from the MBS model are comparable to those from the FE model. Some saltation in the MBS simulation is caused by modelling the wheel and rail elements as rigid bodies without considering the flexibilities of them. The slight hysteresis of the contact force calculation in the FE model is due to the effect of material deformation. From this point of view, the FE simulation is closer to the real situation. Still, as a much more efficient alternative, the MBS model can also provide acceptable results.

The comparable results of the MBS model simulation with the FE model simulation further confirmed that both models describe the same real-life system. For the same simulation presented in this section, the calculation time in the FE model is a couple of days while that in the MBS model is only a few minutes. Therefore, the MBS model can be better applied in repetitive simulations such as rail geometry optimization and track irregularity analysis. For the dynamic performance analysis of railway crossings, this MBS model can be applied for the preliminary simulations to find out the critical situations. The obtained critical situations can be then used as input in the FE model for detailed wheel-rail contact analysis. The combined MBS-FE methods form an integrated tool that can be applied to study the dynamic performance of railway crossings thoroughly.

In this chapter, the MBS model for the dynamic vehicle-crossing interaction analysis has been described. The model has been validated and verified using the measurement results and the FE simulation results. Although tolerable discrepancies exist, the MBS model is reasonably compatible with field measurement as well as the FE model. It can be concluded that the MBS model can catch the main features of the wheel-rail impact in crossing. In the condition monitoring of railway crossings, the MBS model will be applied to verify the effectiveness of the proposed indicators as well as explain the experimental findings.

## Chapter 4 Assessment of crossing conditions

The proposed indicators based on the crossing condition monitoring and the developed MBS model for vehicle-crossing interaction analysis are applied in the crossing condition stage identification. Also, by comparing the crossing performance before and after some maintenance actions, the effect of maintenance on the crossing condition development can be assessed as well. The main outcomes are presented in this chapter.

### 4.1 Assisting in crossing condition monitoring

Using the crossing condition monitoring tool, the condition assessment is made based on the changes in the dynamic performance indicators during the monitored period. In some cases, when the monitoring has to be performed on already operated (not newly installed) crossing, its condition stage at that moment is difficult to determine, especially for a new type of crossing for which no monitored history is available. With the help of the MBS model developed in this study, the condition stage can be determined by comparing the measurement results with the simulation results based on the new (designed) crossing condition.

In case that the monitored crossing was identified to be in a degraded condition, the damage sources will need to be inspected. The inspected crossing damage can be then used as input in the MBS model to simulate the crossing performance in the degraded condition. By comparing the simulation results with the measured ones, the damage sources of the crossing degradation can be verified. By knowing the crossing damage sources, proper maintenance actions can be timely implemented to avoid fatal defects and unexpected track disruptions.

In this section, the above-mentioned applications (identify condition stages and verify damage sources) are demonstrated in a monitored 1:9 trailing crossing, as presented below.

#### 4.1.1 Condition stage identification

The studied 1:9 trailing crossing is located in the same double crossover as the facing crossing used for model validation in Section 3. Similarly, the trains were passing the crossing mainly in the through route with the velocities up to 140 km/h. In contrast to the crossing analysed in Section 3, this crossing was passed in the trailing direction. Nevertheless, the same MBS model presented in Section 3 is used here to assess the crossing performance. The in-situ performance of the crossing was obtained using the instrumentation (Figure 2.1). By comparing the measurement results with the simulation results of the crossing in the designed condition, the actual condition stage of the crossing is identified.

##### 4.1.1.1 Measurement results and analysis

To process the measured data, the transition region in the crossing was inspected, as shown in Figure 4.1. The transition region is recognized as the region with overlapped shining bands. Using the track dimensions (the sleeper width is 0.20 m, and the clip is located in 0.30 m from the TP), the transition region of this crossing was located between 0.15-0.40 m from the TP.

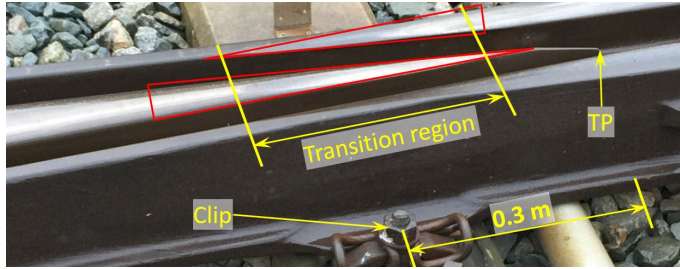


Figure 4.1. Transition region inspection of the monitored 1:9 trailing crossing.

The measurement data used for the crossing performance analysis consisted of the multiple wheel passages from one monitoring day. To be consistent with the numerical simulation, only the results from the VIRM trains with velocities of around 140 km/h, as it was used in the model, were selected, which resulted in the sample size of 78 passing wheels. The magnitude and location of the impacts due to these wheels are analysed in Figure 4.2.

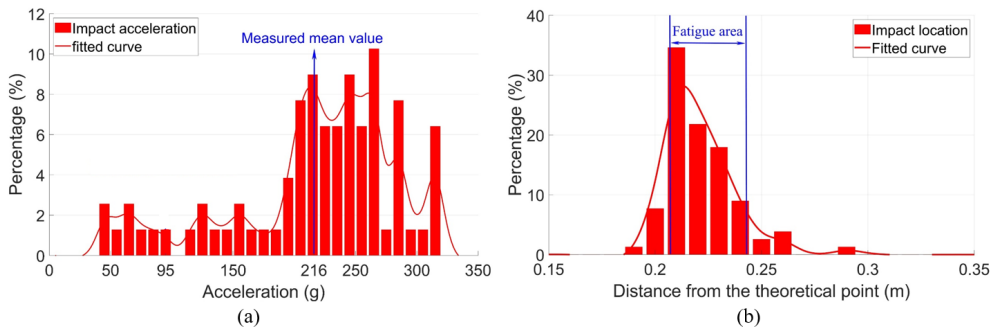


Figure 4.2. Measured dynamic responses. (a): Wheel impact distribution; (b): Impact location distribution.

Figure 4.2 (a) shows the magnitude distribution of the measured impact acceleration responses. The mean value is 216 g and the standard deviation is 68 g. The impact location distribution is shown in Figure 4.2 (b), from which it can be seen that the majority of the wheel impacts (the fatigue area) is located on the distance 0.207-0.243 m from the TP resulting in the size of the fatigue area of 0.036 m.

The wheel impact based results are the most representative ones that reflect the condition of the crossing. In the next section, these results will be compared with the simulation results of the crossing in the designed condition to identify the actual condition stage of the monitored crossing.

#### 4.1.1.2 Numerical simulation and condition stage identification

The MBS vehicle-crossing model used here to analyse the crossing performance in the designed condition is the same as the one presented in Section 3. The only difference is that the vehicle is now moving in the trailing direction, meaning that the wheel load in the crossing panel is transferred from the crossing nose to the wing rail. Using the designed (not worn)

crossing shape and the other model parameters given in Section 3, the dynamic performance of the 1:9 trailing crossing is analysed.

Determination of the transition region using the simulation results is demonstrated in Figure 4.3. On contrast to the facing crossing, the wheel load in the trailing crossing is transit from crossing nose to the wing rail. Therefore, the transition region starts from the wheel-wing rail contact (Figure 4.3 (a)) and end up with the loss of wheel-crossing nose contact (Figure 4.3 (b)). The determined transition region is then 0.182-0.225 m from the TP. This region is located within the one obtained during field inspection (0.15-0.40 m) shown in Figure 4.1. Thus, this confirms that the MBS model developed for the trains passing in the facing direction is also valid for the trailing crossing analysis.

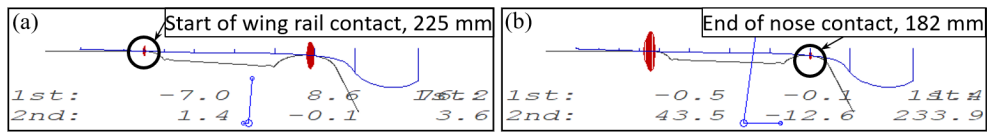


Figure 4.3. Transition region calculation of 1:9 trailing crossing in designed condition. (a): Start contact with the wing rail; (b): End contact with the nose rail.

Figure 4.4 shows the vertical acceleration responses of the crossing rail due to the first passing wheel. It can be seen that the maximum acceleration (due to the wheel impact) is 95 g. This value is much lower than the mean value of the measured impact acceleration (216 g) shown in Figure 4.2 (a). Based on the significant difference (increase) between the measured and the simulated crossing accelerations (in the designed condition), it can be concluded that the monitored crossing was in a highly degraded condition. This conclusion is in agreement with the experimental results of the 1:15 crossing (Figure 2.3 (b)), wherein the significant increase (68%) in the observed measured acceleration was correlated with the visible damage of the crossing rail.

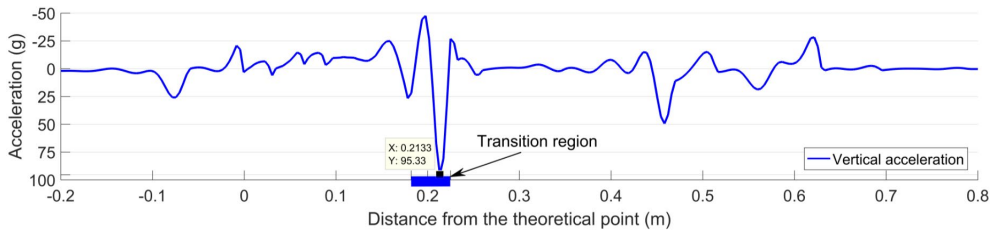


Figure 4.4. Rail vertical acceleration responses of 1:9 trailing crossing in designed condition.

The fatigue area in the designed condition cannot be determined from the numerical simulation. Yet, the wheel impact location can be obtained, which is 0.213 m from the TP (Figure 4.4). Similar to the transition region, the impact location is within the measured fatigue area (0.207-0.243 m, Figure 4.2 (b)).

It can be seen that in the degraded condition, the main change is the increased wheel impact acceleration, while the change in the impact location is rather limited. In the next step, the damage sources of this crossing are detected and verified, as presented in the next section below.

## 4.1.2 Damage source detection and verification

In the previous section, the highly degraded condition of the monitored crossing was identified, which is corresponding to the first step of SHM activities. The next step is then to localize the damage to provide guidance for crossing maintenance.

### 4.1.2.1 Degraded crossing geometry

For regularly degraded railway crossing, one of the typical damage sources is rail wear and deformation. In the monitored crossing, the rail profiles in the critical sections are measured, and compared with the designed profiles, as shown in Figure 4.5.

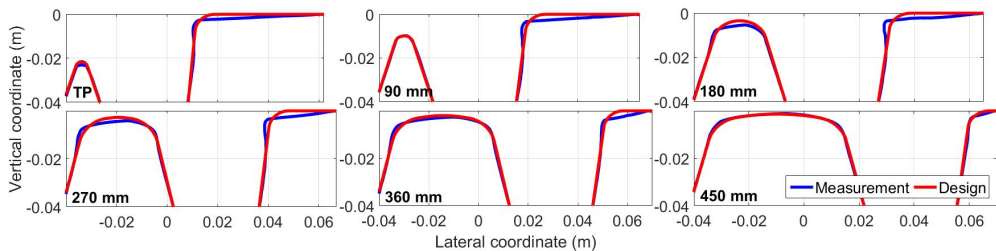


Figure 4.5. Measured crossing profiles in critical sections compared with the designed profiles.

It can be clearly seen from Figure 4.5 that the crossing rail is worn and deformed. The most severe material damage on both the wing rail and the nose rail occurs in the section of 0.18-0.27 m, which is consistent with the distribution of the wheel impact locations (0.207-0.243 m, Figure 4.2 (b)). It can also be seen that wear and deformation of the wing rail are continued to the section of 0.00-0.18 m, meaning that the rail degradation is extended out of the transition region. From this point of view, the crossing had been operated under the degraded condition for a specified period.

### 4.1.2.2 Numerical verification

The geometry measurement results presented in the previous section indicate the worn and deformed condition of the crossing and wing rails. In order to verify the effect of this damage on the crossing performance, the measured rail profiles were implemented in the MBS model and the numerical simulations were performed again.

The calculated transition region was 0.244-0.264 m, as shown in Figure 4.6. It can be seen that due to the severe wear and deformation of the wing rail, the initial wheel-wing rail contact (Figure 4.6 (a)) occurs earlier than that in the designed condition (0.225 m, Figure 4.3 (a)). Also, the size of the transition region is reduced to only 0.020 m (compared with 0.043 m in the designed condition). The damaged rail geometry resulted in that the transition region was shifted further away from the TP and sharper transit of the wheel load from the crossing nose to the wing rail. The narrowed transition region with a shift farther from the TP can indicate degraded crossing rail geometry. Such a changing pattern is in agreement with the development of the fatigue area that was observed in the previous study of a 1:15

facing crossing (Figure 2.4 (b)).

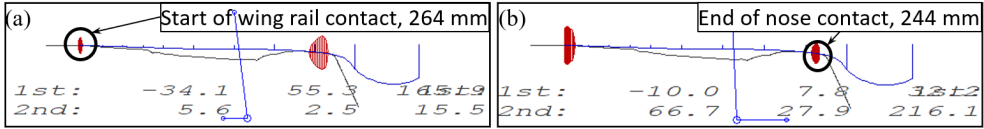


Figure 4.6. Transition region calculation of 1:9 trailing crossing using measured rail geometry. (a): Start contact with the wing rail; (b): End contact with the nose rail.

The simulation time history of the crossing acceleration due to the first passing wheel is shown in Figure 4.6. Compared with the designed condition (Figure 4.4), the crossing acceleration in the degraded condition is increased from 95 g to 214 g, and such a result is quite close to the mean value of the measured results (216 g, Figure 4.2 (a)). These results indicate that the degraded rail geometry is the main cause of the increased accelerations.

It should be noted that the simulated wheel impact is located in 0.256 m from the TP, which is not consistent with the measured fatigue area (0.207-0.243 m, Figure 4.2 (b)). Also, this location is 0.043 m farther than the wheel impact in the designed condition (0.213 m, Figure 4.4). Such a result indicates that besides the degraded crossing rail geometry, there might also be some other degraded elements in the monitored crossing (e.g. uneven ballast settlement), which need to be further investigated in combination with displacement measurement results.

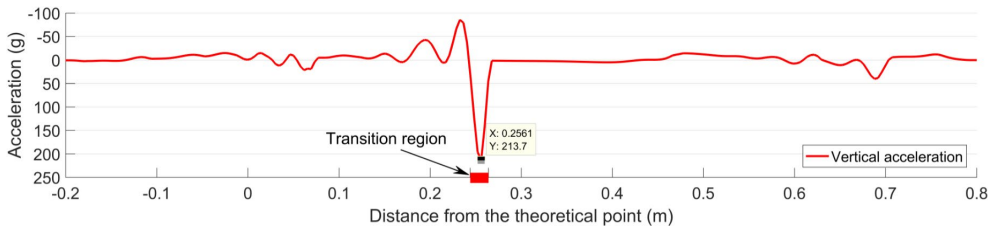


Figure 4.7. Simulation results of 1:9 trailing crossing with rail wear and deformation are taken into account.

In order to analyse the developments in the wheel-rail interaction, the contact forces in both the designed and degraded conditions are compared as well. The results are presented in Figure 4.8.

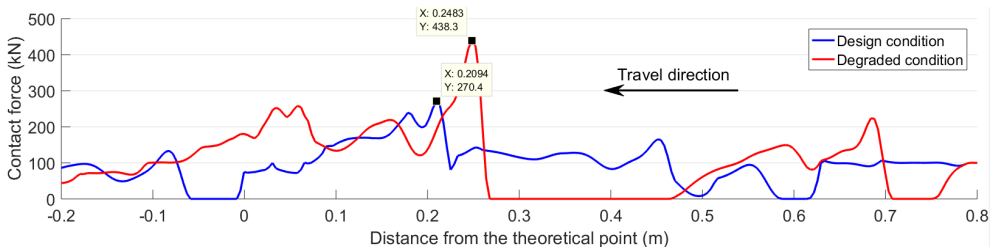


Figure 4.8. Wheel-rail contact forces in different rail conditions.

Beside the dramatically increased impact force (438 kN in the degraded condition vs 270 kN

in the designed condition), the rail damage resulted in the loss of wheel-rail contact in 0.27-0.46 m. Such results clearly show the influence of rail wear and deformation on wheel behaviour. Due to the interaction with the other wheel from the same wheelset as well as the influence of the other wheelset within the same bogie, the wheel that running through the crossing cannot fully follow the damaged rail profile. Consequently, when the wheel resumed contact with the rail, the contact force is dramatically increased and the wheel load is sharply transit from the crossing nose to the wing rail. Such a sharp transition of the wheel load will in return lead to higher impact on the crossing.

In this section, the developed MBS model is successfully applied to help to identify the condition stage of a crossing and to verify the damage sources in the combination of field inspection. Based on the results and analysis, it can be concluded that the monitored 1:9 trailing crossing was in a highly degraded condition. The high wheel-rail impacts are mainly correlated with the worn and deformed rail geometry. Repair welding and grinding in this crossing are urgently required to avoid further damage (e.g. cracks, spalling, etc.).

The application of the MBS model in the condition monitoring of the 1:9 trailing crossing further confirmed that the condition indicators proposed based on the 1:15 facing crossing are applicable for different types of crossings (e.g. angle, traffic direction, etc.), which provides a better opportunity for the promotion of the condition monitoring system.

The deformed crossing geometry in the studied crossing is the dominated factor of the degradation, there is still likely to be some other damage that is not detected, e.g. ballast settlement, track misalignment, etc. The developed MBS model is proved to be sufficient in the crossing condition stage identification and damage source verification, yet necessary track inspection is still required. The better way to master the crossing condition is to combine the MBS model with condition monitoring. With sufficiently detected damage sources, proper maintenance actions can be planned timely, which will help improve the crossing performance and ultimately lead to sustainable railway crossings.

## 4.2 Maintenance and condition development

In the railway track operation, maintenance activities are necessary to keep the crossings in good condition. Therefore, it is of great importance to make sure that the implemented maintenance actions are useful. Due to the limited information on the crossing condition, the current crossing maintenance actions are mainly damage repair and preventive check. Typical damage repair activities include repair grinding and welding of the crossing rail, renovation of the fastening clip, etc. For the preventive check, there are usually limited methods for the contractors and usually ended up with ballast tamping.

In this section, the effectiveness of the maintenance actions in several monitored crossings is assessed using the condition indicators. The assessment results will then be used to guide the arrangement of the maintenance actions.

### 4.2.1 Effect of repair welding and grinding

For damages on the crossing nose rail (Figure 1.3 (a)), the standard treatment is to grind out

the damaged material, weld it, and then grind again to reshape it. In this procedure, the quality of the repair work highly depends on the grinder & welder. With the assistance of the condition indicators, the effect of the repair grinding and welding in a 1:15 crossing is assessed.

The crossing was measured continuously three times. Based on the maintenance record and the track inspections, the crossing condition stages can be respectively considered as “Worn”, “Damaged” and “Repaired”. In the “Worn” and “Damaged” stages, the wheel impacts and fatigue area of this crossing have already been demonstrated in Section 2.1 (Figure 2.3 (b) and Figure 2.4 (b)). The inspected transition regions in different condition stages are shown in Figure 4.9. It can be seen that from the “Worn” stage to the “Damaged” stage, the transition region was stable in 0.30-0.60 m (from the TP), while in the “repaired” stage, the transition region was enlarged to 0.30-0.70 m. Such results indicate that after the repair, the crossing geometry was reshaped and different from the previous one.

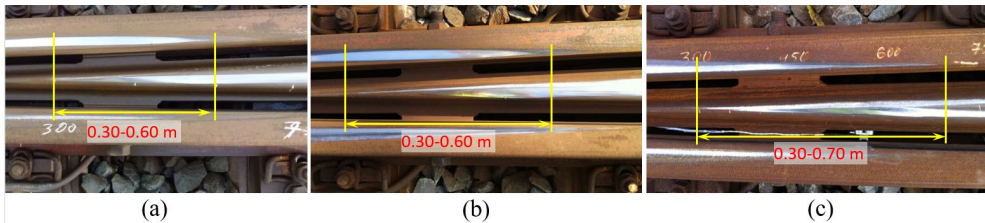


Figure 4.9. Inspected transition regions of the monitored 1:15 crossing in different condition stages. (a): “Worn” stage; (b): “Damaged” stage; (c): “Repaired” stage.

Based on the observed transition regions, the wheel impact accelerations and the fatigue area were calculated, as presented in Figure 4.10. Apparent changes can be seen from Figure 4.10 (a) that after the repair, the acceleration responses reduced to the level even below that of the “Worn” stage. These results indicate that the repair work had a positive effect, and the condition of the crossing was improved as compared to the condition in the “Worn” stage.

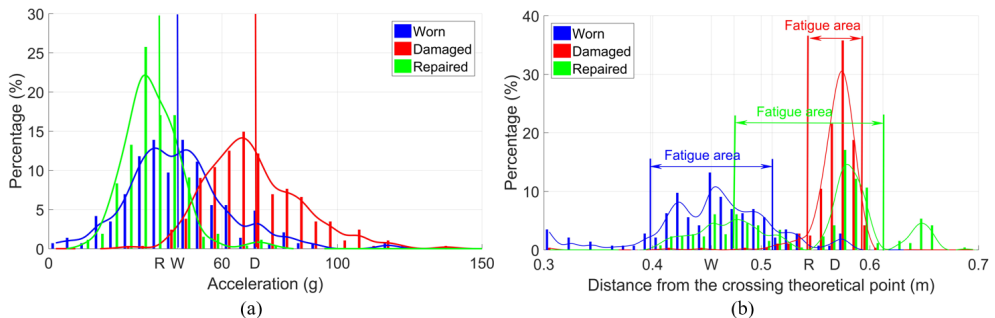


Figure 4.10: Dynamic responses of the monitored crossing. (a): Distribution of the impact acceleration; (b): Distribution of the impact location.

\*Marks in x axes represent the mean values in different conditions: W-“Worn”; D-“Damaged”; R-“Repaired”.

In the “Worn” stage, the fatigue area was around 0.398-0.510 m (size=0.112 m). While in the “Damaged” stage, the fatigue area dramatically reduced to 0.543-0.593 m with a size of

only 0.050 m, and this was also the region where visible cracks are initiated. After the repair of the crossing nose, the wheel impact locations were widely distributed in three different regions with an estimated fatigue area of 0.475-0.612 m (size=0.137 m), which is even wider than that in the “Worn” stage. Moreover, the wheel impact locations were shifted further away from the TP where the crossing rail is much thicker. Such a change is also helpful for the performance of the crossing.

Based on the above analysis, it can be concluded that the repair welding and grinding of the crossing nose were successful. Afterwards, the wheel impacts were dramatically reduced and the fatigue area was widened and shifted further away from the TP. The condition of the crossing was improved after the repair work.

### 4.2.2 Effect of local ballast tamping

As mentioned in Chapter 1 that in the Dutch railway network, some problematic crossings are suffering from adequately short service lives. In a monitored 1:9 facing crossing, the service life was only around three years. In the face of such a situation, the local contractor frequently performed ballast tamping in this track section. To assess the ballast condition, and the effectiveness of the tamping operation, the vertical displacement of the crossing rail was monitored using the wayside monitoring system. The measured vertical displacements of the crossing rail are presented in Figure 4.11. The calculated displacement results using the MBS model are presented as well.

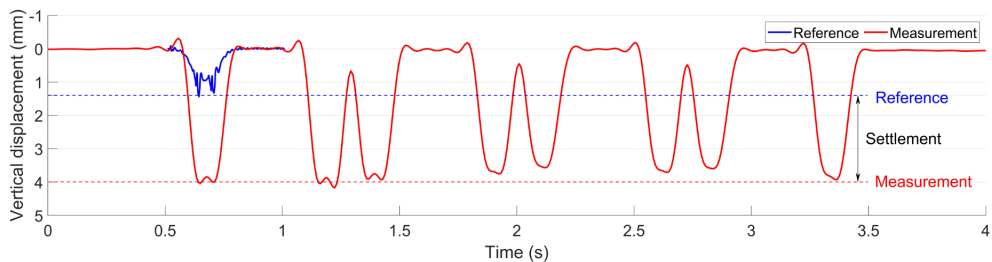


Figure 4.11. Ballast settlement in the monitored crossing.

It can be seen from Figure 4.11 that the measured vertical rail displacement was around 4 mm. The measured displacement result can be considered to have two main parts: the elastic deformation and the gap between the sleeper and ballast. Considering that the ballast settlement is the accumulated effect due to multiple wheel passages, the plastic deformation caused by each passing train can be neglected. Due to the high impacts in the crossing panel, the ballast is usually settled unevenly, which results in hanging sleepers. Using the validated MBS model, it was calculated that the rail displacement in the reference condition is 1.4 mm (Figure 4.11), which only consisted of the elastic deformation part. By comparing these two results, it could be calculated that the gap between the sleeper and ballast was 2.6 mm, which can be estimated as the settlement of ballast.

In Paper A, it has been shown that track irregularities such as rail joints and crossings can lead to the fast deterioration of the ballast, and the ballast settlement will in turn accelerate the degradation procedure of other related track components. Comparatively, the 2.6 mm

ballast settlement in this crossing is already higher than those in the previously monitored welded joints ( $\approx 1.5$  mm) and movable crossings ( $\approx 2$  mm), which indicate the severely deteriorated ballast condition.

Due to the lack of maintenance facilities, the ballast tamping was mainly performed using the squeezing machine (Figure 4.12 (a)). In this case, the track geometry was not corrected. The comparison of the rail displacement results before and after tamping is presented in Figure 4.12 (b).

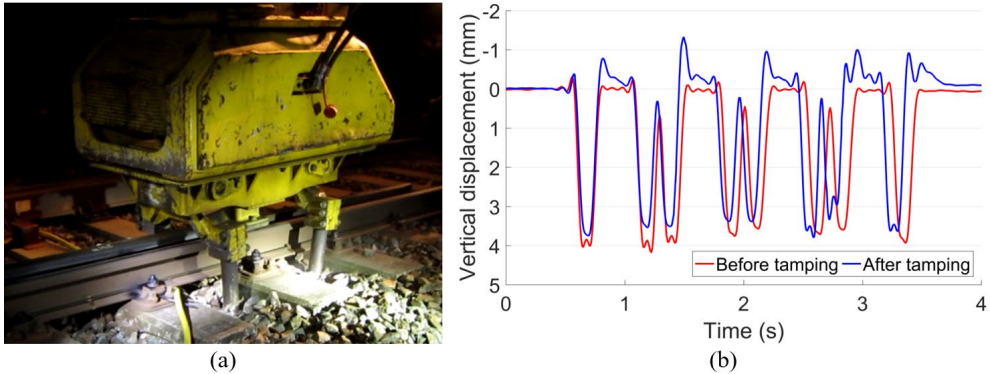


Figure 4.12. (a): Squeezing machine used for ballast tamping in the monitored crossing; (b): Measured rail displacement before and after ballast tamping.

It can be seen from Figure 4.12 (b) that after tamping, the reduction of the rail displacement was quite limited. Moreover, the rebound of the rail became much higher after tamping, which might be caused by the intensified ballast with less elasticity. It can be concluded that such frequently implemented ballast tamping was ineffective, and either the ballast condition or the dynamic performance of the monitored crossing was improved. Before figuring out the root causes of the fast crossing degradation, such ballast tamping should be suspended.

### 4.2.3 Effect of fastening system renovation

For the same crossing mentioned in Section 4.2.2, the fastening system was found to be degraded with some broken bolts during the monitoring period. Such degradation can affect the lateral stability of the track. Therefore, the fastening system, mainly the bolts in the guard rails and the clips, was renovated, as shown in Figure 4.13.

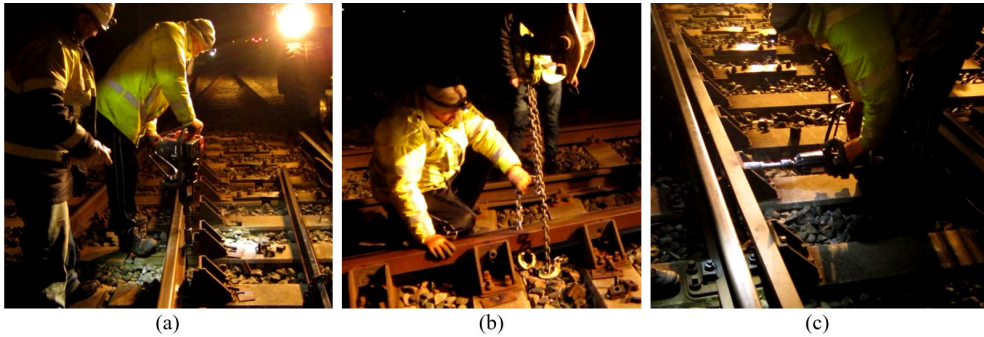


Figure 4.13. Fastening system renovation. (a): Remove the broken bolts; (b): Reposition the guard rail; (c): Install new bolts.

Besides wayside monitoring, the crossing was also monitored using the instrumentation. The development of the wheel-rail impacts before and after renovation is shown in Figure 4.14. In the upper figure, each point represents the mean value of the wheel impacts due to multiple wheel passages in one monitoring day, and the lower figure gives the ratio of different impact levels in each monitoring day corresponding to the value in the upper figure.

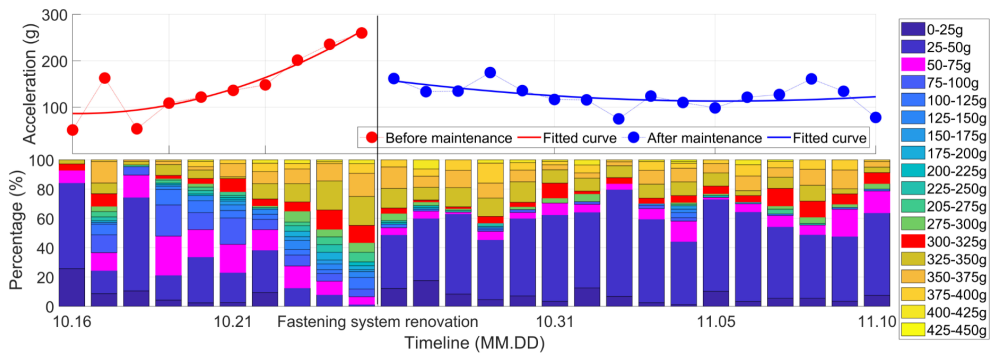


Figure 4.14. Effect of fastening system renovation on the dynamic performance of the crossing.

It can be seen from Figure 4.14 that before the renovation, the wheel-rail impact shows a clear increasing trend with the impact values widely distributed from 0 to 450 g. Such a trend clearly indicates that maintenance was urgently required due to the defects of the fastening system. After the renovation, the wheel-rail impacts were dramatically reduced in terms of the mean value. The impacts of the majority of the passing wheels are reduced to the level of 0-50 g. It can be concluded that the fastening system renovation was effective and the crossing performance was improved afterwards.

It has to be noted that after renovation, the impact accelerations indicate precisely polarized distribution with a large proportion of impacts above 300 g. For a crossing in a relatively new condition, such performance is quite abnormal and might be the reason for the fast crossing degradation. From this point of view, the fastening system renovation was forced maintenance action due to the appearance of damaged components, and the root causes were remain unsolved after maintenance. In the next chapter, the damage sources for this crossing

will be investigated.

### 4.3 Summary

This chapter has presented some applications of the monitoring tools and indicators as well as the MBS model in the condition monitoring of railway crossings. The application in a monitored 1:9 trailing crossing has proved that the MBS model can help identify the condition stage and verify the damage source. It has also been proved that the condition indicators can be applied in different types of railway crossings. The MBS model and the indicators formed a sound basis of the condition monitoring system for railway crossings. The promotion of such a system will help discover the crossing defects in the early stage and allow necessary maintenance actions to be timely applied.

For the other applications in the crossing condition assessment, the maintenance effects were taken into account. Among the studied cases, the repair welding and grinding of the 1:15 crossing were necessary and sufficient and the crossing performance was highly improved. The fastening system renovation in the monitored 1:9 crossing was helpful but incomplete with partly improved crossing performance. For the same 1:9 crossing, the frequently performed local ballast tamping turned out to be ineffective with no help to the crossing performance improvement. Such applications have provided references for the contactors to arrange maintenance activities.

It can be concluded that with the assistance of the crossing condition monitoring, the crossing maintenance can be better planned. The necessary maintenance actions can be timely implemented to reduce unexpected track disruptions, and those ineffective ones should be rather suspended before pointing out the sources of the crossing damage.

## Chapter 5 Detection of root damage causes

In the previous chapter, it is presented that the monitored 1:9 facing crossing was suffering from fast degradation with a considerable amount of extremely high wheel impacts. In this chapter, the abnormal crossing performance is further analysed in detail to investigate the root causes of the damage. With the assistance of field inspection and the MBS model, the actual sources for the crossing damage are further verified.

### 5.1 Track misalignment and fast degradation

The monitored 1:9 crossing is part of a facing crossover, meaning that the trains mainly pass in the facing through route with the maximum velocity of around 140 km/h. The on-site view of the crossing is shown in Figure 5.1 (a).

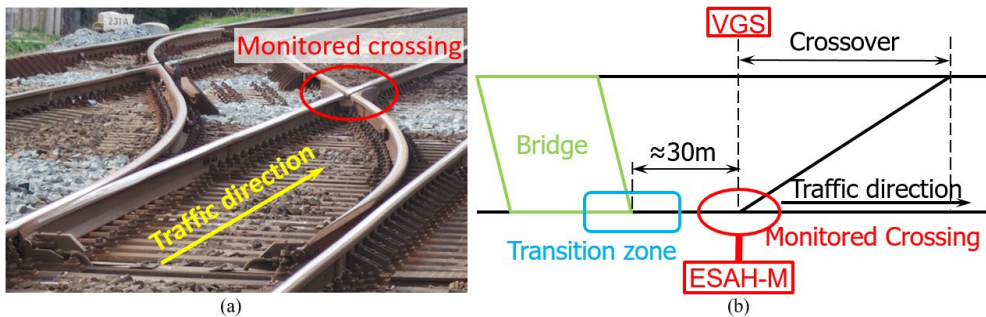


Figure 5.1. Overview of the monitored crossing. (a): Sketch view; (b): On-site view.

Figure 5.1 (b) gives a sketch view of the crossing, including the setup of the monitoring devices and the layout of the adjacent structures, especially the small bridge in front of the crossing. Considering that the bridge is located quite close to the monitored crossing, the performance of the crossing might be affected by the bridge, which will be discussed later.

#### 5.1.1 Measured abnormal performance and analysis

In this section, the measurement results based on the crossing instrumentation are presented and analysed. The instrumentation results were obtained from one monitoring day with multiple train passages. Similar to the trailing crossing presented in 4.1, the selected results are restricted to the VIRM trains with a velocity of around 140 km/h. The estimated transition region is 0.15-0.40 m, which has already been demonstrated in Figure 2.2 (a).

Based on the estimated transition region, the wheel impact accelerations are calculated. The distribution of the wheel impacts due to multiple wheel passages is shown in Figure 5.2 (a). The sample size, in this case, is 78 passing wheels. It can be seen that the wheel impacts presented a bimodal distribution. Around 80 % of the wheel impacts are below 50 g. In the meantime, the rest of 20 % of the wheel impacts are incredibly high with a mean value of around 350 g. Such polarized distribution of impacts indicates the highly unstable wheel-rail interaction in this crossing. In the MBS model validation, it has already been demonstrated

that for this type of railway crossing, the average level of the wheel impacts is around 50 g, meaning that the 20 % high impacts of the monitored crossing are already more than seven times higher than the average impact level. It can be imagined that such high impacts will dramatically accelerate the degradation procedure of the crossing.

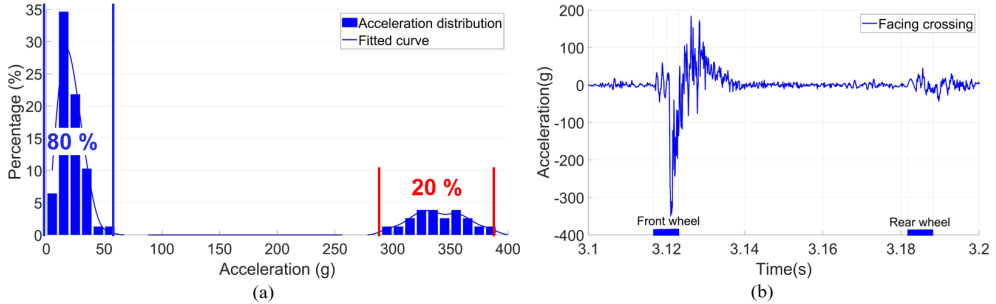


Figure 5.2. Vertical acceleration responses of the monitored crossings. (a): Distribution based on multiple train passages in one day; (b): Example of impacts due to one bogie.

An example of the impact acceleration response in time-domain due to the first bogie of a VIRM train is shown in Figure 5.2 (b). It can be seen that for the two passing wheels from the same bogie, the impacts can be quite different. The impact due to the front wheel was up to 350 g, while the rear wheel activated vertical acceleration is only 20 g. It has to be noted that the high impacts were not always introduced by the front wheel but appeared to have random occurrences. Such results further confirmed the instability of wheel-rail interaction in this crossing.

The measured fatigue area of the monitored crossing is presented in Figure 5.3. It can be seen that the wheel impacts are widely distributed in 0.22-0.38 m from the TP with the fatigue area size of 0.16 m. Considering that the transition region is around 0.15-0.40 m, the fatigue area widely covered 64 % of the transition region, which can be considered to be in line with the expectation of a new crossing profile. Such results further confirmed that the crossing rail was not worn or deformed.

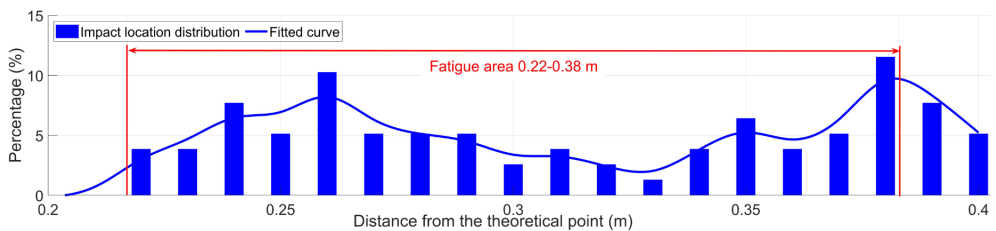


Figure 5.3. Measured fatigue area of the monitored crossing.

It has to be noted that the fatigue area does not conform to a normal distribution (referring to the mid-term stage demonstrated in Figure 2.4 (b)). Combined with the results of the wheel impacts, such fatigue area further confirmed the instability of the wheel-rail contact in the monitored crossing.

### 5.1.2 Inspected track misalignment

Generally, the crossing degradation is accompanied by the increase of wheel-rail impacts and the reduction of the fatigue area. The large amount of extremely high wheel-rail impacts and the relatively wide fatigue area indicate the abnormal performance of the monitored crossing. Find out the root causes of such abnormality is the key to improve the dynamic performance of the crossing.

In the field inspection, it was found that the bridge was not well aligned in the track but deviated around 15 cm, as shown in Figure 5.4 (a). Such deviation resulted in a curve that was likely to be out of design since no elevation was set up in the outer rail. It can be imagined that the trajectory of the passing trains will not be along the central line of the track but tend to have flange contact with the outer rail, which eventually leads to the severe wear in the switchblade (Figure 5.4 (b)).

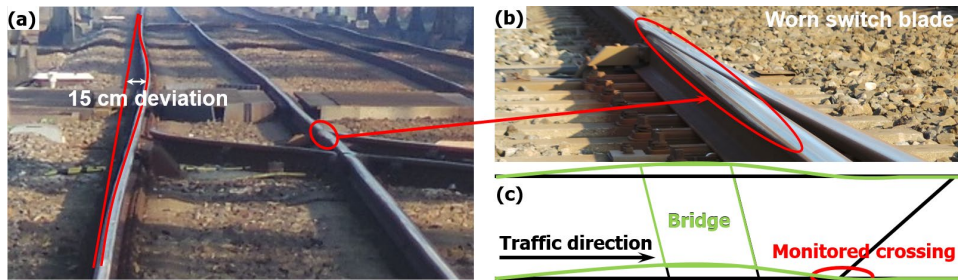


Figure 5.4. Track deviation in front of the crossing. (a): Inspected curve introduced by the bridge; (b): Worn switch rail; (c): Demonstration of the bridge deviation.

The accumulated effect of the track deviation was also reflected in the varied track gauge. It was shown in the track gauge measurement results that the gauge variations along the whole turnout were up to 3 mm, as presented in Table 5.1. Considering that the monitored crossing is located quite close to the bridge (Figure 5.4 (c)), such track misalignment, including the track deviation in the bridge and track gauge variation along the turnout, may affect the wheel-rail interaction in the crossing.

Table 5.1. Track gauge measurement results in critical sections along the turnout

Location	A	B	C	D	E	F	G
Deviation (mm)	+2	+3	-2	-2	+2	+3	0

### 5.1.3 Numerical verification of the damage sources

To verify the effect of the track lateral misalignment on the performance of the crossing, both

the bridge-introduced curve and the track gauge variation are input into the MBS vehicle-crossing model. The equivalent lateral track irregularities as model input are shown in Figure 5.5.

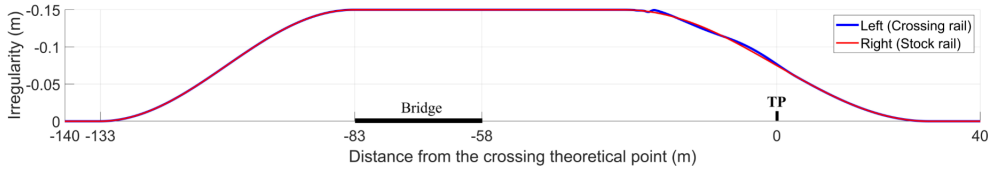


Figure 5.5. Equivalent lateral irregularities in the track.

With the track misalignment taken into account, the crossing condition is considered as degraded. The simulation results of both wheels in the bogie, including the wheel impact accelerations and transition regions, are compared with the results in the designed condition (Figure 3.8 (b)), as shown in Figure 5.6.

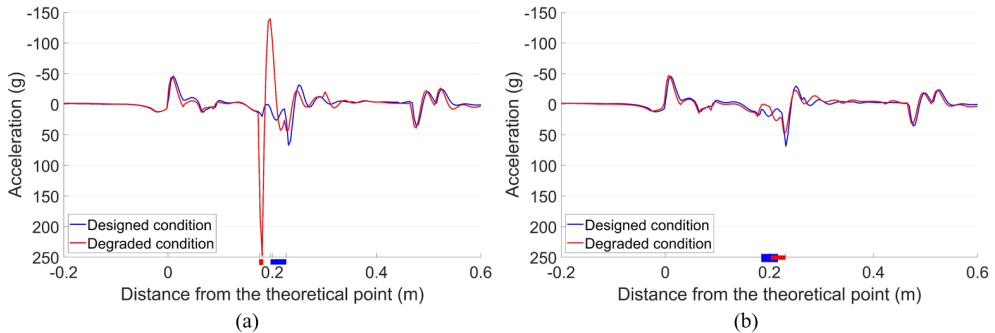


Figure 5.6. Impact acceleration responses and transition regions. (a): Front wheel; (b): Rear wheel.

It is shown in Figure 5.6 (a) that due to the influence of the lateral irregularity, the impact of the front wheel is dramatically increased to 247 g, which is four times higher than the reference value (around 60 g) in the designed condition. While for the rear wheel from the same bogie, the impact is 48 g, which is even lower than the reference value. Despite the slight difference in the absolute values, the simulation results are consistent with the measurement results (Figure 5.2). Meanwhile, the transition region of the front wheel is 0.176-0.182 m from the TP with a size of only 0.006 m. Compared with the reference value (0.196-0.217 m with a size of 0.031 m), it is much narrower and closer to the TP, indicating earlier wheel impact and much sharper wheel load transition in the crossing. For the rear wheel, although the transition region is located farther from the TP, the size is almost the same as the reference value.

Such results clearly show that the curve and lateral track misalignment in front of the crossing can lead to the unstable wheel-rail contact in the crossing and sometimes result in extremely high impacts. Also, the different dynamic responses between the front wheel and the rear wheel indicate that the performance of the rear wheel is not independent but can be affected by the front wheel.

For the wheel-rail contact forces, the tendency is similar to the acceleration responses, as shown in Figure 5.7. With the degraded track condition, the maximum contact force of the front wheel in the degraded condition is 468 kN, which is twice higher than that in the designed condition (235 kN). While for the rear wheel, the difference between the degraded condition and the designed condition is limited.

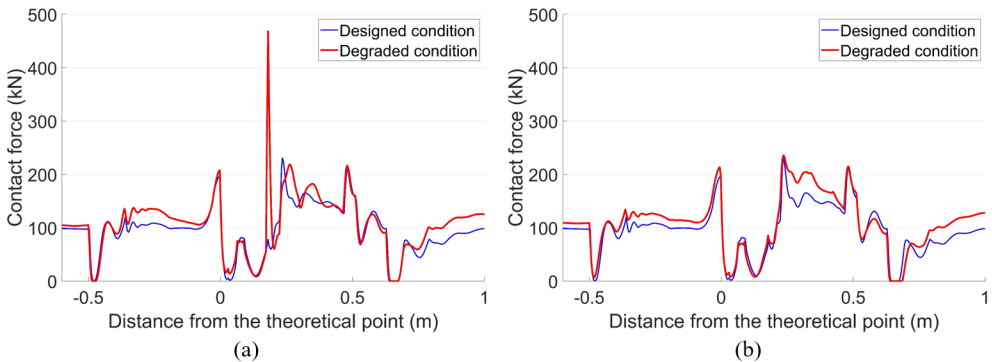


Figure 5.7. Vertical wheel-rail contact responses of the facing crossing. (a): Front wheel; (b): Rear wheel.

To figure out how is the track misalignment affects the wheel-rail interaction in the crossing, the relationship between the wheel lateral displacements and wheel-rail contact forces are analysed. Before that, the wheel lateral displacement in the designed condition is presented in Figure 5.8. It can be seen that when the train enters the crossing panel, the varied rail geometry will lead to the lateral movement of the wheel. The maximum lateral displacement is around 0.7 mm.

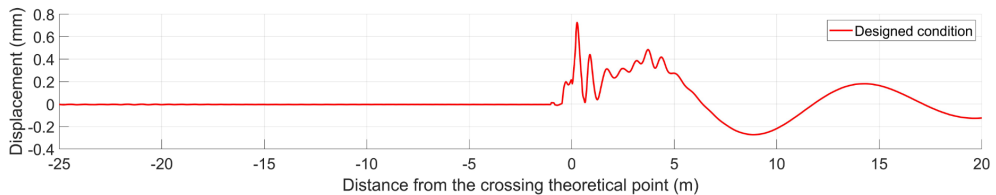


Figure 5.8. Wheel lateral displacement in the designed condition.

In the degraded condition with track lateral irregularities, the lateral displacements of the wheels are dramatically changed, as shown in Figure 5.9. It can be seen that both the front wheel and the rear wheel have shown activated hunting oscillation before and after passing through the crossing, but the trajectories are quite different. For the front wheel, the lateral movement is more intense, and it is running towards the crossing nose rail. The maximum lateral displacement corresponding to the position with the highest contact force is 2.3 mm (Figure 5.9 (a)), which means that compared with that in the designed condition, the wheel flange is around 1.6 mm closer to the nose rail.

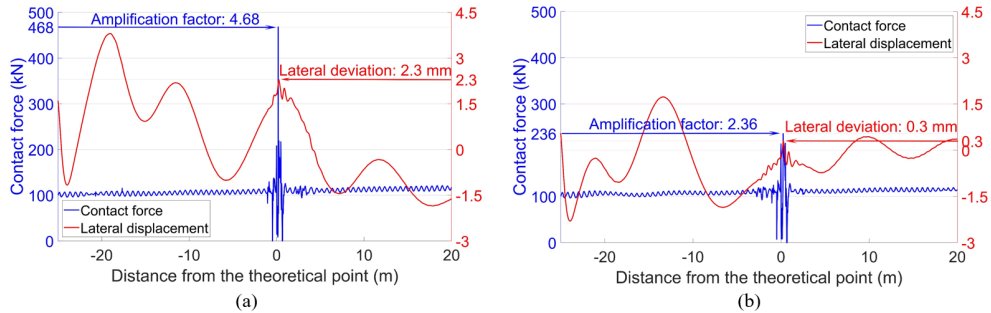


Figure 5.9. Wheel-rail contact forces and lateral wheel displacements. (a): Front wheel; (b): Rear wheel.

Comparatively speaking, the maximum lateral displacement of the rear wheel is only 0.3 mm (Figure 5.9 (b)). Such results indicate that the wheel-rail impact is profoundly affected by the movement of the wheel. When the wheel is approached closer to the crossing nose, the wheel-rail impact is likely to be increased. It can be concluded that the train hunting activated by the lateral track misalignment in front of the crossing is the main cause of the extremely high wheel-rail impacts.

The train hunting effect also explains the unstable wheel-rail impacts. For the rear wheel, the lateral movement is affected not only by the track misalignment but also by the front wheel from the same bogie. As a result, these two wheels lead to quite different wheel trajectories. It can be imagined that in the real-life situation, there are many more factors that may affect the hunting motion of each passing wheelset. These factors include the initial position of the wheel when entering the misaligned track section, the mutual interaction between the adjacent wheelsets, the lateral resistance of the track, and even the weather condition, etc. The combined effect of all these factors eventually resulted in the polarized distribution of the impact acceleration responses (Figure 5.2 (a)).

### 5.1.4 Effects of track curve and gauge deviation

It can be noticed that in the previous analysis, the input track misalignment consists of two parts: the lateral curve introduced by the bridge and the track gauge deviation. In this section, the effects of these two parts are further analysed respectively, and the results are presented below.

The wheel-rail contact forces and the wheel the lateral displacements with the bridge-introduced lateral curve taken into account are presented in Figure 5.10. It can be seen that for the front wheel, the lateral curve mainly resulted in the lateral shift of the wheel trajectory due to the centripetal force. Such a shift is only 0.5 mm near the crossing nose compared with the designed condition, and the effect on the wheel impact is limited. For the rear wheel, the combined effect of the curve and the motion of the front wheel resulted in the lateral deviation of 0.9 mm, which is quite close to that in the designed condition and has no significant influence on the wheel-rail impact.

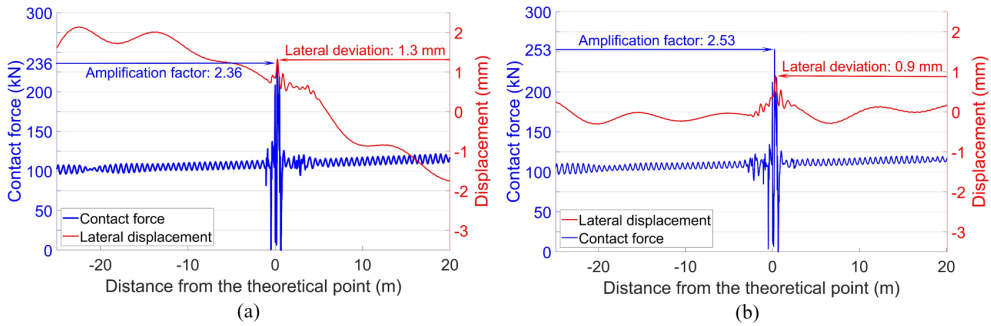


Figure 5.10. Wheel-rail contact forces and lateral wheel displacements. (a): Front wheel; (b): Rear wheel.

The effect of the track gauge deviation on the wheel-rail interaction is demonstrated in Figure 5.11. Different from the effect of the bridge-introduced curve, the deviated track gauge activated the hunting motion of the passing wheels. Yet, the resulted lateral wheel displacements are not large enough to amplify the wheel-rail impact. The maximum displacements corresponding to the wheel impacts are respectively 1 mm due to the front wheel and 0.4 mm due to the rear wheel.

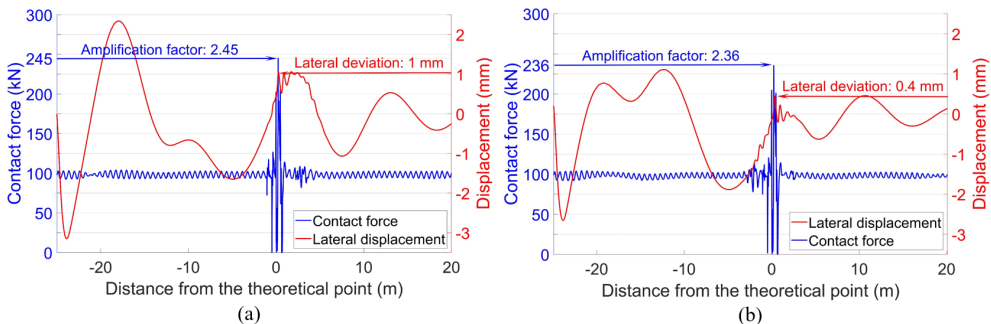


Figure 5.11. Wheel-rail contact forces and lateral wheel displacements. (a): Front wheel; (b): Rear wheel.

## 5.2 Weather-related performance variation

In the real-life situation, the wheel-crossing interaction can be affected by a lot of factors, not only those related to the train-track system but also some factors that related to the environment, e.g., the contaminants on the rail [58]-[59] and rail temperature variation [39]. For the monitored crossing with track misalignment, the varied weather condition may also have an impact on the crossing performance. To have a better understanding of the crossing performance, the influence of the weather has to be analysed as well.

### 5.2.1 Weather variation and crossing responses

It can be seen from the upper figure in Figure 4.14 that even after the renovation of the fasting system, the vertical acceleration responses of the monitored crossing fluctuated from 80 g to 180 g during a short period. Considering that such fluctuation is unlikely to be related to structural degradation, one possible cause might be the continuously changed weather

conditions.

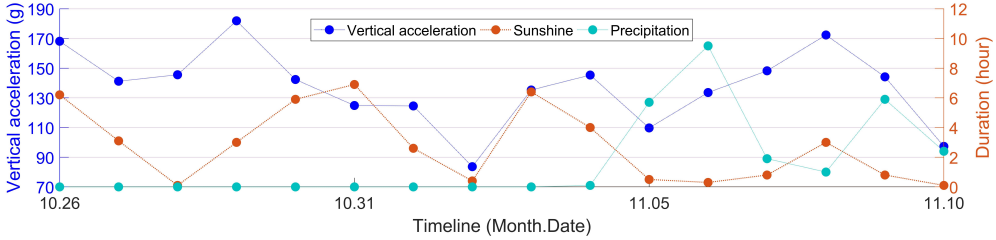


Figure 5.12. Development of vertical acceleration together with the sunshine and precipitation durations

By comparing the weather conditions with the dynamic crossing responses, it has been discovered that the daily sunshine duration shows a similar pattern with the crossing vertical acceleration responses, as shown in Figure 5.12 (the weather information is obtained from the KNMI [61]). There seems to be a connection between these two variables. For the precipitation duration, the connection with the acceleration responses is lower.

To quantitatively assess the weather impact, the correlations between the weather variables and the condition indicators are analysed. The representative weather variables consist of the following items:

- Sunshine duration per day ( $D_s$ );
- Precipitation per day ( $D_p$ ).

The analysed indicators consist of the following parts:

- Vertical acceleration responses ( $a_y$ );
- Wheel impact location ( $L_o$ );
- The size of the fatigue area ( $F_a$ ).

### 5.2.2 Correlation analysis

In statistics, the linear correlation between two variables is usually measured using Pearson's correlation coefficient  $r$ . For two variables  $X$  and  $Y$  with the same sample size of  $n$ ,  $r$  can be obtained using the following formula:

$$r_{X,Y} = \frac{\text{cov}(X,Y)}{\sigma_X \sigma_Y} = \frac{E[(X - \mu_X)(Y - \mu_Y)]}{\sigma_X \sigma_Y} = \frac{1}{\sigma_X \sigma_Y} \cdot \frac{1}{n} \sum_{i=1}^n [(x_i - \mu_X)(y_i - \mu_Y)] \quad (5-1)$$

$$X = X(x_1, x_2, \dots, x_n), \quad Y = Y(y_1, y_2, \dots, y_n) \quad (5-2)$$

where

- $\text{cov}(X, Y)$  is the covariance of  $X$  &  $Y$
- $\sigma_X$  &  $\sigma_Y$  are respectively the standard deviations of  $X$  &  $Y$
- $\mu_X$  &  $\mu_Y$  are respectively the mean values of  $X$  &  $Y$
- $E[\dots]$  is the expectation of the given variables

When  $X$  is in direct/inverse proportion to  $Y$ , then the correlation coefficient is

$$r_{X,Y} = \frac{E[(X - \mu_X)(Y - \mu_Y)]}{\sigma_X \sigma_Y} = \pm \frac{\sigma_X \sigma_Y}{\sigma_X \sigma_Y} = \pm 1 \quad (5-3)$$

If  $X$  and  $Y$  are independent, then the variable of  $(x_i - \mu_X)(y_i - \mu_Y)$  (5-1) could be a random positive or negative value. In the case of a large amount of data ( $n \rightarrow \infty$ ),

$$\lim_{n \rightarrow \infty} \frac{1}{n} \sum_{i=1}^n [(x_i - \mu_X)(y_i - \mu_Y)] = 0 \quad (5-4)$$

Therefore, the value range of the correlation coefficient is  $r_{X,Y} = [-1, 1]$ .  $r_{X,Y} = \pm 1$  means that the two variables  $X$  and  $Y$  are perfectly correlated, and  $r_{X,Y} = 0$  means that  $X$  and  $Y$  do not correlate with each other. Otherwise,  $X$  and  $Y$  are considered partly correlated.

In different research fields, the gradation of the correlation index may have notable distinctions [62]. In this study, the structural responses and the weather are indirectly associated. The three-level guideline modified from [63] is applied for the correlation strength analysis, as shown in Table 5.2.

Table 5.2. The three-level correlation strength guideline

r	Correlation Strength
$ r  < 0.3$	Weak
$0.3 \leq  r  < 0.5$	Moderate
$0.5 \leq  r  < 1$	Strong

In the analysis presented here, the correlations between the dynamic crossing responses ( $a_y$ ,  $L_o$  and  $F_a$ ) and the weather-related variables ( $D_s$  and  $D_p$ ) are studied. The data used for the correlation analysis are from 16 monitoring days (same as in Figure 4.13 after fastening system renovation,  $n=16$  in (5-2)). The correlation within each group of the parameters as well as the cross-correlation between these two groups of the parameters will be analysed.

Table 5.3. Correlation coefficients for dynamic responses and weather variables

$r$	$a_y$	$L_o$	$F_a$	$D_s$	$D_p$
$a_y$	1	-0.37	-0.51	0.36	-0.17
$L_o$		1	0.36	-0.39	0.14
$F_a$			1	-0.63	0.38
$D_s$				1	-0.54
$D_p$					1

The results are presented in Table 5.3. Nomenclature in the table is presented earlier in section. The strong, moderate and weak correlation coefficients are marked with red, blue and black colour respectively. The correlation results are to be analysed and presented below.

It can be seen from Table 5.3 that the size of the fatigue area ( $F_a$ ) is strongly correlated with ( $a_y$ ) with a negative value, which means that the increase of  $a_y$  is usually accompanied by the reduction of  $F_a$ . The correlations of the impact location ( $L_o$ ) with  $a_y$  and  $F_a$  are not strong, meaning that it is relatively independent from the other dynamic responses. The detailed correlation results  $F_a - a_y$  and  $a_y - L_o$  are shown in Figure 5.13.

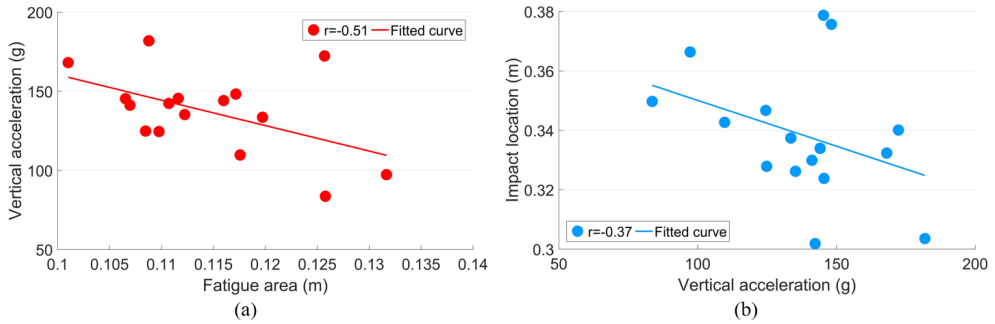


Figure 5.13. Correlation results between the dynamic crossing responses. (a):  $F_a - a_y$ ; (b):  $a_y - L_o$ .

The precipitation duration ( $D_p$ ) is strongly correlated with the sunshine duration ( $D_s$ ) with a negative value (Figure 5.14 (a)). For the weather variables,  $D_s$  and  $D_p$  can be considered as two opposite weather conditions. From this point of view, the correlation coefficient  $r = -0.54$  is not very strong. Such results can be explained by the existence of the cloudy/overcast conditions, and the weather in a day can switch among sunny, rain and cloudy/overcast. It can be noticed that in the monitored period, precipitation only occurred in 6 over 16 days, which to some extent, shows the complicity of the weather condition.

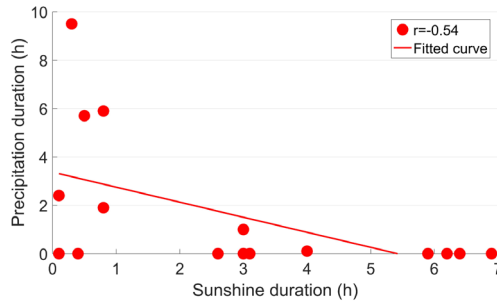


Figure 5.14. Correlation results between the sunshine duration  $D_s$  and the precipitation duration  $D_p$ .

Among the cross-correlation results between the dynamic crossing responses and the weather variables, the correlation  $D_s - F_a$  is stronger than the others ( $r = -0.63$ ), meaning that the sunshine initiated rail displacements is likely to result in centralized impact locations first and further increase the chance of higher wheel impacts. From this point of view, the connection between  $D_s$  and  $a_y$  is likely to be indirect. Therefore, the resulted correlation strength is moderate ( $r = 0.36$ ). Comparatively, the impact from  $D_p$  on the dynamic responses is less than that from  $D_s$ .

### 5.2.3 Sunshine caused track deviations

In general, the solar radiation is one of the major sources of thermal rail forces. Depending on the sunshine duration, the associated rail temperature can be up to  $40^\circ\text{C}$  higher than the ambient air temperature [64]. The change in rail temperature will increase rail stress and amplify the lateral rail displacements. The lateral rail displacements will then increase the uncertainty of the wheel impact angle in the crossing, eventually leading to an increase of the acceleration responses of the passing wheels.

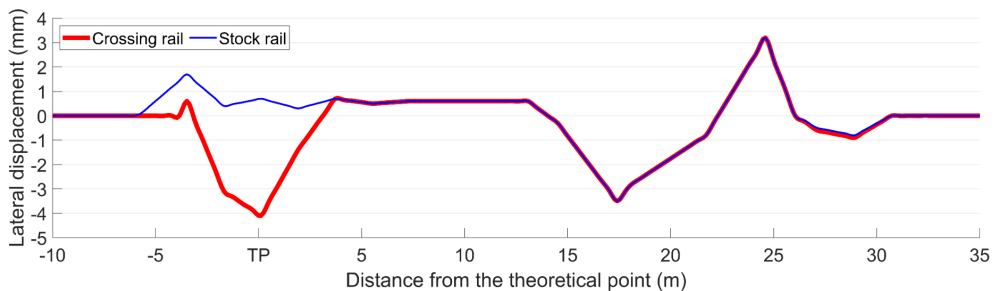


Figure 5.15. Temperature initiated lateral rail displacement in FE simulation (Figure 11.15 in [39]).

In [39], the displacements of a turnout due to the change of the rail temperature were analysed using a FE model. The simulation results indicated that when the rail temperature was increased (from stress-free temperature) by  $40^\circ\text{C}$ , the lateral displacements of the turnout rails were up to 4 mm, as shown in Figure 5.15.

It has already been found that the monitored crossing is suffering from severe track misalignment, so the lateral rail displacement resulted from the increased temperature is acted on the degraded track. In this case, the lateral rail displacement due to the effect of the temperature is superposed to the existing track misalignment (Figure 5.5) and input in the MBS model. To simplify the situation, the ballast settlement and broken clips are not taken into account.

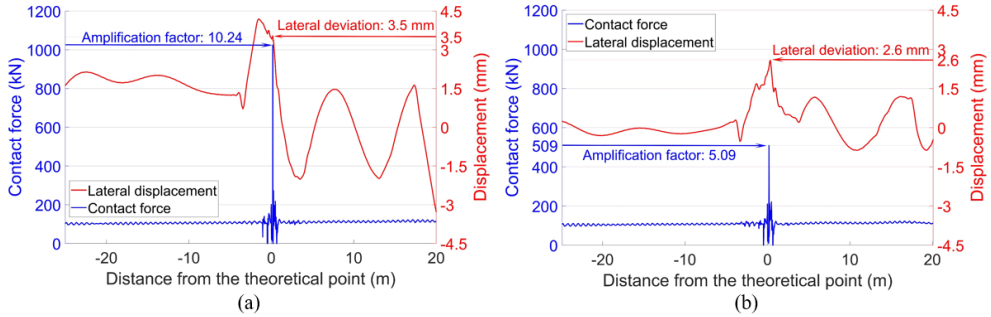


Figure 5.16. Wheel-rail contact forces and lateral wheel displacements. (a): Front wheel; (b): Rear wheel.

The simulated wheel-rail contact forces, together with the lateral wheel displacements due to the superposed track irregularities, are presented in Figure 5.16. It can be seen that with the additional lateral rail displacements, the hunting oscillation of the wheels is more violent (compared with the results in Figure 5.9). For the front wheel, the lateral deviation during the wheel impact is up to 3.5 mm, and the resulted impact force is 1024 kN, which is over four times higher than that in the designed condition (235 kN, Figure 3.10). Even for the rear wheel with less hunting oscillation, the lateral deviation is 2.6 mm, and the resulted impact force is 509 kN.

The vertical acceleration responses and the corresponded transition regions are shown in Figure 5.17. It can be seen that for the front wheel, the impact acceleration is 638 g, which is even higher than the measurement range of the instrumented accelerometer (500 g). Also, the resulted transition region is only 0.012 m, which is much narrower than that in the designed condition Figure 3.4.

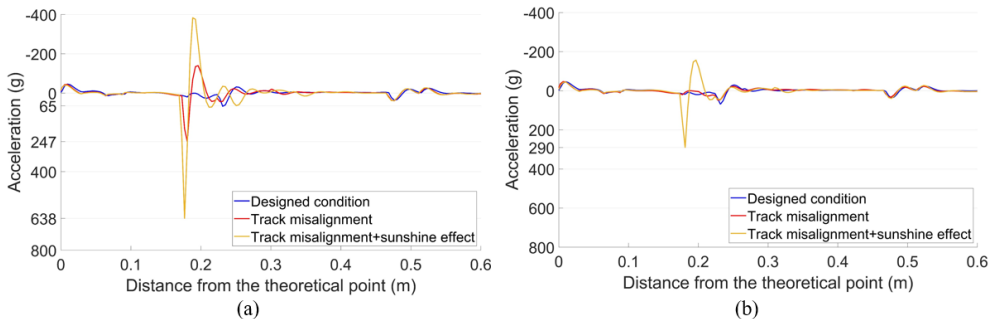


Figure 5.17. Vertical rail accelerations due to the passing wheels. (a): Front wheel; (b): Rear wheel.

Despite that the lateral input irregularity in the MBS model is an extreme situation, the simulation results confirmed the correlation results (Figure 5.14 (a)-(b)) that the long sunshine duration, which will result in higher temperature in the rail, can lead to the centralized impact locations and higher impact accelerations in the crossing. Such an effect can be amplified by the existed degradations. Moreover, the precipitation can also affect the performance of the crossing by reducing the friction coefficient in the wheel-rail interface. More information regarding the weather effects can be found in Paper C.

### 5.3 Summary

In this chapter, the root causes of the fast degradation of a 1:9 crossing in the Dutch railway have been investigated. The effect of the varied weather conditions on the performance of the crossing has been analyzed as well.

The fast crossing degradation was directly caused by the extremely high wheel-rail impacts, and the root cause for such high impacts was the hunting of the passing trains that activated by the track lateral misalignment in front of the crossing. When the maximum wheel lateral displacement reached to a certain level (e.g., 2.3 mm), the wheel-rail impact was dramatically amplified. To improve the current situation, such track misalignment needs to be eliminated.

The simulation results further confirmed the effectiveness of the previously proposed condition indicators in the damage sources investigation of the crossing. Since the root causes for the fast degradation was the deviated track in front of the crossing, it means that the degradation detection is not only restricted to the crossing itself but can also take the adjacent structures into account.

The correlation analysis and the numerical verification results proved that the varied weather conditions, especially the long-duration of sunshine, can also affect the crossing performance. Such an effect can be amplified by the existed track degradations.

Considering that railway crossings are very sensitive to the wheel-rail interactions, higher standards for the track installation (e.g., stress-free temperature control) and maintenance (e.g., tolerable track gauge variations) in railway crossings are required.

## Chapter 6 Conclusions and future work

This study contributes to the development of the condition monitoring system for railway crossings. The purpose of this study is to obtain the condition information of the in-service railway crossings, which will help to provide necessary guidance for the current crossing maintenance actions. Ultimately the optimized maintenance philosophy will lead to better performance and longer service life of the railway crossings. The main conclusions of this study, as well as some recommendations for future work, are given below.

### 6.1 Main conclusions

Concerning the increasingly restricted track access, several experimental tools that can catch the dynamic features of railway crossings are selected and tested. Based on the measured crossing dynamic responses and correlation analysis, several critical **indicators** that are respectively representing **wheel impact**, **fatigue area** and **ballast settlement** for the crossing condition assessment were proposed. To better understand the dynamic performance of railway crossings as well as to provide explanations for the experimental findings, and MBS model for the vehicle-crossing interaction analysis is developed, validated and verified. The proposed condition indicators and the MBS model are further applied in the crossing condition stage identification, effectiveness analysis of typical maintenance actions and the root causes investigation of the fast degradation of a railway crossing. Based on the applications, the following conclusions can be drawn.

#### 6.1.1 Condition stage identification

In the condition monitoring of normally degraded crossings, the proposed indicators were capable to catch the **main degradation stages** of the railway crossings. In a monitored 1:15 crossing, three critical condition stages ranging from “Worn”, “Damaged” to “repaired” were identified. For the monitored 1:9 trailing crossing, the degraded condition with rail wear and deformation was identified and further verified using the MBS model. With the identified crossing condition, the maintenance actions can be **timely** applied before the occurrence of severe damage, which will effectively avoid unplanned disruptions.

Moreover, the successful applications on two different types of crossings proved the broad applicability of the proposed condition indicators. Such a feature makes it possible to promote the monitoring system in the Dutch railway network without much additional adjustment.

#### 6.1.2 Maintenance effectiveness assessment

With the assistance of the proposed indicators, the effectiveness of the typical crossing maintenance actions can be **assessed**. The repair welding and grinding in the monitored 1:15 crossing was proved to be effective with dramatically improved performance.

For the monitored 1:9 facing crossing that suffered from fast crossing degradation, the frequently performed local ballast tamping was proved to no positive effect on the crossing performance. The renovation of the fastening system was helpful to a certain extent, but could not improve the crossing performance to the level of the designed condition. Such results

proved that either the ballast settlement or the broken clips were the root cause of the fast crossing degradation. In this case, ballast tamping should be suspended, and the root damage sources should be investigated.

### 6.1.3 Damage source investigation

Based on the proposed indicators and the assistance of the MBS model, the root causes for the fast degradation of the monitored 1:9 crossing were successfully detected and verified. It was shown that the fast crossing degradation was mainly caused by the lateral deformation of the adjacent track introduced by the bridge in front of the crossing. The numerical results in the MBS model confirmed the phenomenon that the train **hunting** motion activated by the track deviation, which was the source of the extremely high impacts recorded by the monitoring system, ultimately resulted in the fast crossing degradation.

By knowing the damage sources, **proper** maintenance can be performed rather than the currently used ineffective ballast tamping. In the studied case, the degradation is caused by adjacent structures, and therefore the maintenance should be performed not on the crossing itself but of the track nearby.

Additionally, it has been found that crossing degradation can also be affected by varied weather conditions. It was proved that high rail **temperature** due to the long duration of sunshine could amplify the existed geometry deviation in turnout, which may lead to more violent train hunting and result in higher dynamic responses. Considering the high sensitivity of wheel-rail interaction in the crossing, higher standards for crossing maintenance and construction are required for better crossing performance.

The development of the monitoring system and the application of the condition indicators is a big step forward for the current maintenance philosophies **from damage repair to predictive maintenance**, and **from “failure reactive” to “failure proactive”**. The outcomes in this study will contribute to the better performance of railway crossings.

## 6.2 Recommendations for future work

This research is the start of the SHM system for railway turnout crossings developed by TU Delft. For future research, it can be extended in the following aspects: Remote monitoring and data reading, simplified failure alarms as well as coupled numerical tools for design optimization.

### 6.2.1 Remote monitoring and data reading

The current monitoring system still requires manual operation by the track. It not only costs a lot of fieldwork to read data, change the battery and install/uninstall measurement devices, but also the measurement data are poor in timeliness. In case of unexpected defects, e.g., broken accelerometer and bad contact cables, they cannot be found out in time, and the measurement data in a certain period will be missing. Improve the monitoring system with permanent installation and remote control (e.g., data reading, start/stop trigger, etc.) can be the solution to reduce the existed drawbacks.

### **6.2.2 Simplified failure alarm**

The current procedure for data processing has already been simplified through correlation study, still analysing the data requires knowledge of computational methods, structural dynamics, etc. Further, simplify the procedure for data processing and analysis and set up simple failure alarms (e.g., critical values of the wheel impacts, fatigue area and the rail displacement, etc.) will improve the practicability of the monitoring system. To set up these alarms, more information on the target crossing in the whole degradation procedure will be required.

### **6.2.3 Coupled numerical tools for design optimization**

The developed MBS model was proved to be able to provide comparable results with the previously developed FE model. The MBS model is featured with fast simulation, and the FE model can provide more detailed information (e.g., stress distribution). By coupling these two models, the strength of each model can be drawn. The MBS model can be applied in the repetitive simulations such as the rail geometry optimization and track irregularity analysis, and the preliminary determined critical conditions can be used as input in the FE model for detailed analysis. The combination of using these two models can dramatically improve the efficiency of wheel-crossing interaction analysis.

## References

- [1] ProRail, Ontwerpvoorschrift (Baan en Bovenbouw) Deel 6.1: Wissels en kruisingen Alignment, tussenafstanden, overgangsvrije zones en bedieningsapparatuur, V006, The Netherlands, 2015, p. 12.
- [2] I.V. Shevtsov, Rolling Contact Fatigue problems at railway turnouts - experience of ProRail, [https://www.sim-flanders.be/sites/default/files/events/Meeting\\_Materials\\_Nov2013/mm\\_13112013\\_ivan\\_shevtsov\\_prorail.pdf](https://www.sim-flanders.be/sites/default/files/events/Meeting_Materials_Nov2013/mm_13112013_ivan_shevtsov_prorail.pdf), 13 November 2013.
- [3] D. Huston, Structural Sensing, Health Monitoring, and Performance Evaluation, University of Vermont, Burlington, USA, 2011.
- [4] D. Pines, A. E. Aktan, Status of structural health monitoring of long-span bridges in the United States, *Progress in Structural Engineering and Materials*, vol. 4, 2002, p. 372-380.
- [5] I.N. Robertson, Prediction of vertical deflections for a long-span prestressed concrete bridge structure, *Engineering Structures*, vol. 27, 2005, p. 1820-1827.
- [6] J.M. Ko, Y.Q. Ni, Technology developments in structural health monitoring of large-scale bridges, *Engineering Structures*, vol. 27, 2005, p. 1715-1725.
- [7] J.M.W. Brownjohn, Lateral loading and response for a tall building in the non-seismic doldrums, *Engineering Structures*, vol. 27, 2005, p. 1801-1812.
- [8] H.A. Toliyat, K. Abbaszadeh, M.M. Rahimian, L.E. Olson, Rail defect diagnosis using wavelet packet decomposition, *IEEE Transactions on Intelligent Transportation Systems*, vol. 39 (5), 2003, p. 1454-1461.
- [9] L.F. Molina, E. Resendiz, J.R. Edwards, J.M. Hart, C.P.L. Barkan, N. Ahuja, Condition Monitoring of Railway Turnouts and Other Track Components Using Machine Vision, *Proceedings of the Transportation Research Board 90th Annual Meeting*, January 2011.
- [10] Y. Li, H. Trinh, N. Haas, C. Otto, S. Pankanti, Rail component detection, optimization, assessment for automatic rail track inspection, *IEEE Transactions on Intelligent Transportation Systems*, vol. 15 (2), 2014, p. 760-770.
- [11] N.A. Thakkar, J.A. Steel, R.L. Reuben, Rail-wheel contact stress assessment using acoustic emission: A laboratory study of the effects of wheel flats, *Proceedings of the Institution of Mechanical Engineers, Part F: Journal of Rail and Rapid Transit*, vol. 226, 2012, p. 3-13.
- [12] D. Cantero, B. Basu, Railway infrastructure damage detection using wavelet transformed acceleration response of traversing vehicle, *Structural Control and Health Monitoring*, vol. 22, 2015, p. 62-70.
- [13] P. Wang, Li. Wang, R. Chen, J. Xu, J. Xu, M. Gao, Overview and outlook on railway track stiffness measurement, *Journal of Modern Transportation*, Vol. 24 (2), 2016, p. 89-102.
- [14] G.J. Yeo, Monitoring Railway Track Condition Using Inertial Sensors on an in-Service Vehicle, PhD thesis, University of Birmingham, Birmingham, United Kingdom, June 2017.

- [15] A. De Rosa, S. Alfi, S. Bruni, Estimation of lateral and cross alignment in a railway track based on vehicle dynamics measurements, *Mechanical Systems and Signal Processing*, vol. 116, 2019, p. 606-623.
- [16] F. Balouchi, A. Bevan, R. Formston, Detecting Railway Under-Track Voids Using Multi-Train in-Service Vehicle Accelerometer, 7th IET Conference on Railway Condition Monitoring, Birmingham, United Kingdom, 27-28 September 2016.
- [17] H. Tsunashima, Condition Monitoring of Railway Tracks from Car-Body Vibration Using a Machine Learning Technique, *Applied Sciences*, vol. 9, 2019, No. 2734.
- [18] A.T. Cornish, Life-time monitoring of in service switches and crossings through field experimentation, PhD thesis, Imperial College London, London, UK, May 2014.
- [19] L.F. Molina, E. Resendiz, J.R. Edwards, J.M. Hart, C.P.L. Barkan, N. Ahuja, Condition Monitoring of Railway Turnouts and Other Track Components Using Machine Vision, *Proceedings of the Transportation Research Board 90th Annual Meeting*, November 2010.
- [20] C. Chen, T. Xu, G. Wang, B. Li, Railway turnout system RUL prediction based on feature fusion and genetic programming, *Measurement*, vol. 151, 2020, No. 107162.
- [21] S. Kaewunruen, Monitoring structural deterioration of railway turnout systems via dynamic wheel/rail interaction, *Case Studies in Nondestructive Testing and Evaluation*, vol. 1, 2014, p. 19-24.
- [22] E. Kassa, J.C.O. Nielsen, Dynamic interaction between train and railway turnout: full-scale field test and validation of simulation models, *Vehicle System Dynamics*. Vol. 46, 2008, 521-534.
- [23] Z. Wei, C. Shen, Z. Li and R. Dollevoet, Wheel–Rail Impact at Crossings-Relating Dynamic Frictional Contact to Degradation, *Journal of Computational and Nonlinear Dynamics*, vol. 12 (4), 2017, p. 041016 1-11.
- [24] Y. Ma, A.A. Mashal, V.L. Markine, Modelling and experimental validation of dynamic impact in 1:9 railway crossing panel, *Tribology International*, vol. 118, 2018, p. 208-226.
- [25] C. Wan, V.L. Markine, I.Y. Shevtsov, Analysis of train/turnout vertical interaction using a fast numerical model and validation of that model. *Proceedings of the Institution of Mechanical Engineers Part F: Journal of Rail and Rapid Transit*, vol. 228, 2014, p. 730-743.
- [26] E. Kassa, C. Andersson, J.C.O. Nielsen, Simulation of dynamic interaction between train and railway turnout, *Vehicle System Dynamics*. Vol. 44, No. 3, 2006, 247-258.
- [27] E. Kassa, J.C.O. Nielsen, Stochastic analysis of dynamic interaction between train and railway turnout, *Vehicle System Dynamics*. Vol. 46, No. 5, 2008, p. 429-449.
- [28] E. Kassa, J.C.O. Nielsen, Dynamic train-turnout interaction in an extended frequency range using a detailed model of track dynamics, *Journal of sound and vibration*, vol. 320, 2009, p. 893-914.

- [29] B. Pålsson, J. Nielsen, Wheel-rail interaction and damage in switches and crossings, *Vehicle System Dynamics*, Vol. 50, 2012, p. 43-58.
- [30] B. Pålsson, Optimisation of railway crossing geometry considering a representative set of wheel profiles, *Vehicle System Dynamics*, vol. 53, 2015, p. 274-301.
- [31] C. Wan, V.L. Markine, I.Y. Shevtsov, Improvement of vehicle–turnout interaction by optimizing the shape of crossing nose, *Vehicle System Dynamics*, vol. 52, 2014, p. 1517-1540.
- [32] C. Wan, V.L. Markine, I.Y. Shevtsov, Optimisation of the elastic track properties of turnout crossings. *Proceedings of the Institution of Mechanical Engineers Part F: Journal of Rail and Rapid Transit*, vol. 230, 2016, p. 360-373.
- [33] C. Wan, V.L. Markine, R.P.B.J. Dollevoet, Robust optimisation of railway crossing geometry. *Vehicle System Dynamics*, vol. 54, 2016, p. 617-637.
- [34] X. Shu, N. Wilson, C. Sasaoka, J. Elkins, Development of a real-time wheel/rail contact model in NUCARS and application to diamond crossing and turnout design simulations, *Vehicle System Dynamics*, vol. 44, 2006, p. 251-260.
- [35] J. Wegdam, Expert tool for numerical & experimental assessment of turnout crossing geometry, MSc thesis, Delft University of Technology, Delft, the Netherlands, December 2018.
- [36] M. Wiest, W. Daves, F.D. Fischer, H. Ossberger, Deformation and damage of a crossing nose due to wheel passages, *Wear*, vol. 265, 2008, p. 1431-1438.
- [37] Z. Ren, S. Sun, G. Xie, A method to determine the two point contact zone and transfer of wheel rail forces in a turnout, *Vehicle System Dynamics*. Vol. 48, No. 10, 2010, p. 1115-1133.
- [38] V.L. Markine, M.J.M.M. Steenbergen, I.Y. Shevtsov, Combatting RCF on switch points by tuning elastic track properties. *Wear*, vol. 271, 2011, p. 158-167.
- [39] T.M.H. Arts, Measuring the neutral temperature in railway track during installation and use, MSc thesis, Delft University of Technology, Delft, the Netherlands, 2011.
- [40] M. Pletz, W. Daves, H. Ossberger, A wheel set/crossing model regarding impact, sliding and deformation - explicit finite element approach, *Wear*, vol. 294, 2012, p. 446-456.
- [41] M. Pletz, W. Daves, H. Ossberger, A wheel passing a crossing nose: dynamic analysis under high axle loads using finite element modelling, *Proceedings of the Institution of Mechanical Engineers Part F: Journal of Rail and Rapid Transit*, vol. 226, 2012, p. 603-611.
- [42] A.A. Mashal, Analysis & Improvement of railway crossing using explicit finite element method, MSc thesis, Delft University of Technology, Delft, the Netherlands, 2016.
- [43] L. Xin, V.L. Markine, I.Y. Shevtsov, Numerical analysis of the dynamic interaction between wheelset and turnout crossing using explicit finite element method, *Vehicle System Dynamics*, vol. 54, 2016, p. 301-327.
- [44] L. Xin, V.L. Markine, I.Y. Shevtsov, Analysis of the effect of repair welding / grinding on performance of railway crossings using field measurements and finite element

- modelling, *Proceedings of the Institution of Mechanical Engineers Part F: Journal of Rail and Rapid Transit*, vol. 232, 2018, p. 645-662.
- [45] L. Xin, V.L. Markine, I.Y. Shevtsov, Numerical procedure for fatigue life prediction for railway turnout crossings using explicit finite element approach, *Wear*, vol. 366-367, 2016, p. 167-179.
- [46] J.C.O. Nielsen, X. Li, Railway track geometry degradation due to differential settlement of ballast/subgrade – Numerical prediction by an iterative procedure, *Journal of Sound and Vibration*, vol. 412, 2018, p. 441-456.
- [47] R. Skrypnik, J.C.O. Nielsen, M. Ekh, B.A. Pålsson, Metamodeling of wheel-rail normal contact in railway crossings with elasto-plastic material behaviour, *Engineering with Computers*, Vol. 35, 2019, p. 139-155.
- [48] R. Skrypnik, M. Ekh, J.C.O. Nielsen, B.A. Pålsson, Prediction of plastic deformation and wear in railway crossings – Comparing the performance of two rail steel grades, *Wear*, Vol. 428-429, 2019, p. 302-314.
- [49] P.T. Torstensson, G. Squicciarini, M. Krüger, B.A. Pålsson, J.C.O. Nielsen, D.J. Thompson, Wheel-rail impact loads and noise generated at railway crossings – influence of vehicle speed and crossing dip angle, *Journal of Sound and Vibration*, vol. 456, 2019, p. 119-136.
- [50] A. Johansson, B. Pålsson, M. Ekh, J.C.O. Nielsen, M.K.A. Ander, J. Brouzoulis, E. Kassa, Simulation of wheel-rail contact and damage in switches & crossings, *Wear*, vol. 271, 2010, p. 472-481.
- [51] S. Alfi, S. Bruni, Mathematical modelling of train-turnout interaction, *Vehicle System Dynamics*. Vol. 47, No. 5, 2009, p. 551-574.
- [52] M. Wiest, E. Kassa, W. Daves, J.C.O. Nielsen, H. Ossberger, Assessment of methods for calculating contact pressure in wheel-rail/switch contact, *Wear*, vol. 265, 2008, p. 1439-1445.
- [53] S. Chiou, J. Yen, Modeling of railway turnout geometry in the frog area with the vehicle wheel trajectory, *Proceedings of the Institution of Mechanical Engineers Part F: Journal of Rail and Rapid Transit*, vol. 232(6), 2018, p. 1598-1614.
- [54] X. Ma, P. Wang, J. Xu, R. Chen, J. Wang, Assessment of Non-Hertzian Wheel-rail Contact Models for Numerical Simulation of Rail Damages in Switch Panel of Railway Turnout, *Wear*, vol. 432-433, 2019, 120912.
- [55] H. Wang, V.L. Markine, X. Liu, Experimental analysis of railway track settlement in transition zones, *Proceedings of the Institution of Mechanical Engineers Part F: Journal of Rail and Rapid Transit*, vol. 232 (6), 2018, p. 1774-1789.
- [56] VI-grade GmbH, VI-Rail 16.0 Documentation, © 2014 VI-grade engineering software & services, Marburg, Germany, 2014.
- [57] M. Hiensch, J.C.O. Nielsen, E. Verheijen, Rail corrugation in The Netherlands—measurements and simulations, *Wear*, vol. 253, 2002, p. 140-149.

- 
- [58] O. Arias-Cuevas, Low Adhesion in the Wheel-Rail Contact, PhD thesis, Delft University of Technology, Delft, the Netherlands, 2010.
- [59] H. Chen, T. Ban, M. Ishida and T. Nakahara, Effect of water temperature on the adhesion between rail and wheel, Proceedings of the Institution of Mechanical Engineers, Part J: Journal of Engineering Tribology vol. 220, 2006, p. 571-579.
- [60] M. Ertz, F. Bucher, Improved creep force model for wheel/rail contact considering roughness and temperature, Vehicle System Dynamics, vol. 37, 2002, p. 314-325.
- [61] Koninklijk Nederlands Meteorologisch Instituut, <https://www.knmi.nl/nederland-nu/klimatologie/daggegevens>, 2015.
- [62] H. Akoglu, User's guide to correlation coefficients, Turkish Journal of Emergency Medicine, vol. 18, 2018, p. 91-93.
- [63] J. Cohen, Statistical Power Analysis for the Behavioral Sciences 2<sup>nd</sup> Edition, New York University, New York, USA, 1988.
- [64] ProRail, Instruction of Procedures at Extreme Weather Conditions RLN00165, Version 002, Utrecht, the Netherlands, 10 December 2003.
- [65] T. Ohyama, Tribological studies on adhesion phenomena between wheel and rail at high speeds. Wear, vol. 144, 1991, p. 263-275.

## **Part II: Appended papers**



# Paper A

## Experimental Tools for Railway Crossing Condition Monitoring

X. Liu, V.L. Markine, H. Wang, I.Y. Shevtsov

*Measurement*, vol. 129, 2018, p. 424-435.

<https://doi.org/10.1016/j.measurement.2018.07.062>

A

### Abstract

Two experimental tools to measure the railway crossing dynamic responses are presented. One system is ESAH-M equipped with a 3-D accelerometer and a speed detection sensor that featured for crossing instrumentation and characterised by fast installation/ uninstallation, automatic data recording and processing. The other system is a Digital Image Correlation (DIC) based Video Gauge System (VGS) that record the dynamic displacements of the rail/sleepers. A number of measurements have been performed aiming to explore the feasibility of these experimental tools, establish the relation between the measured dynamic responses and condition of the monitored crossings and estimate the effectiveness of crossing maintenances. The measurements based on crossing instrumentation show that the crossing degradation process can be described using the dynamic responses. The wayside monitoring in different problematic track sections have shown the capability of detecting and quantifying ballast conditions. Both systems will be further applied in long-term monitoring of railway crossings.

**Keywords:** Railway Crossing, Condition Monitoring, Crossing Instrumentation, Wayside Monitoring, Structural Health Monitoring System.

## 1 Introduction

In railway track system, a turnout is an essential component that is needed to guide a train when it is passing from one track to the other. However, rail discontinuity in the turnout crossing makes it a vulnerable part in the railway track system. The high wheel/rail impact forces due to this discontinuity accelerate the crossing degradation and lead to high costs of turnout maintenance. In the Dutch railway network, there are more than 7000 crossings, and about 100 crossings among them are urgently replaced every year. The service life of some crossings is only 2-3 years [1]. Moreover, the high impact forces can lead to other types of crossing damage, such as broken clips, geometry deterioration and ballast settlement, etc. (Figure 1.1). Damage in the crossing may in turn result in further amplification of the wheel impact forces and accelerate the degradation of the track structure. Improving the performance of turnout crossing is very important in extending the crossing service life, reducing the maintenance cost, enhancing the track stability and guaranteeing the track safety.

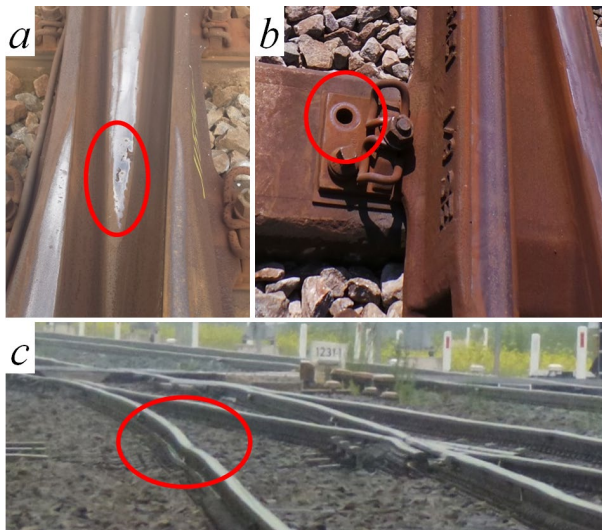


Figure 1.1. Typical problems in railway crossings.

(a): Cracks in crossing nose; (b): broken clips; (c): ballast settlement.

Currently, turnout crossing maintenance in the Netherlands consists of two main activities: preventive check and damage repair. The former are periodic inspections, while latter is only performed when visible damage has occurred. The inspection trains are widely applied to collect railway track information, but with the constrained possession time and limited amount of the inspection trains, it is very difficult to get the real-time information on the condition of railway crossings. In this case, the inspection (preventive check) cannot fully eliminate potential damage risk with limited information and when it comes to damage repair, it often resulted in complete replacement of the crossing.

One solution for maintenance improvement is timely performing it in the predictive way based on the principles of Structural Health Monitoring (SHM). Typically, SHM consists of five levels of activities, namely detection, localization, assessment, prognosis and

remediation [2]. Predictive maintenance requires the SHM developed to the level of assessment and prognosis. Nowadays, SHM systems are well developed and applied to various civil engineering structures, such as large bridges and buildings with sensors and other monitoring devices installed during construction [3]-[6]. In railways, the use of SHM systems is mainly in the stages of defects detection and localization. The main methods of detection/localisation are ultrasonic testing [7], image recognition [8]-[9], acoustic detection [10], guided wave inspection [11], manual inspections, etc. Regarding to railway crossings, most of the studies are numerical concerning crossing performance analysis and design optimization [12]-[13]. Experimental methods such as instrumented wheel [14]-[17] and rail [18] are mainly used for numerical model validation. Therefore, development of SHM Systems for railway crossings that include damage detection, localization and condition assessment, as well as damage prognosis and remediation is highly requested.

This paper presents two experimental tools for crossing condition monitoring and shows how the crossing structural behaviour and wheel-crossing interaction can be characterised based on the measured responses (Detection and Localization stages of SHM). In Section 2, a brief introduction of the wheel-rail interaction in the railway crossing is given. The experimental tools, accelerometer-based crossing instrumentation and Digital Image Correlation (DIC)-based wayside monitoring tool are described in Section 3. In Section 4, the performance of a crossing in various condition stages is analysed and relations between the dynamic responses and the crossing condition are determined. In addition, the effect of maintenance on the crossing nose is briefly discussed. Measurements and analysis of the performances of ballast in various conditions using wayside monitoring tool is presented in Section 5, followed by conclusions given in Section 6. The presented condition monitoring tools will be used as the basis of SHM system for railway turnout crossings.

## 2 Wheel-rail interaction in railway crossings

A standard right-hand turnout (Figure 2.1) has four passing directions: the facing (from switch panel to crossing panel) and trailing (the opposite facing) directions in the through and divergent routes. In order to allow trains to intersect two tracks on the same level, there is a gap between the wing rail and the nose rail (Figure 2.1). When passing the crossing nose, a significant amplification of the wheel force can occur due to the presence of this gap.

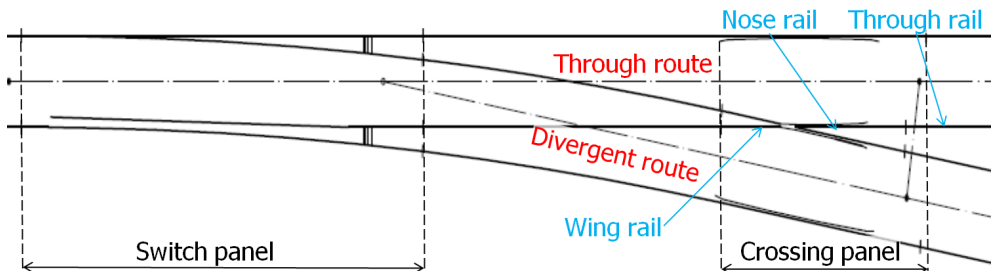


Figure 2.1. Demonstration of a standard right-hand turnout.

An example of wheel-rail interaction when the train runs in the through facing direction is given in Figure 2.2, and the wheel-rail contact points along the track are shown as the yellow

strips. The wheel firstly approaches the crossing from the wing rail ((a)-(b), looking from the right side, the same below), and then follows with the transition of the wheel from the wing rail to the nose rail (c), after which the wheel continues running over the crossing nose (d) and the through rail.

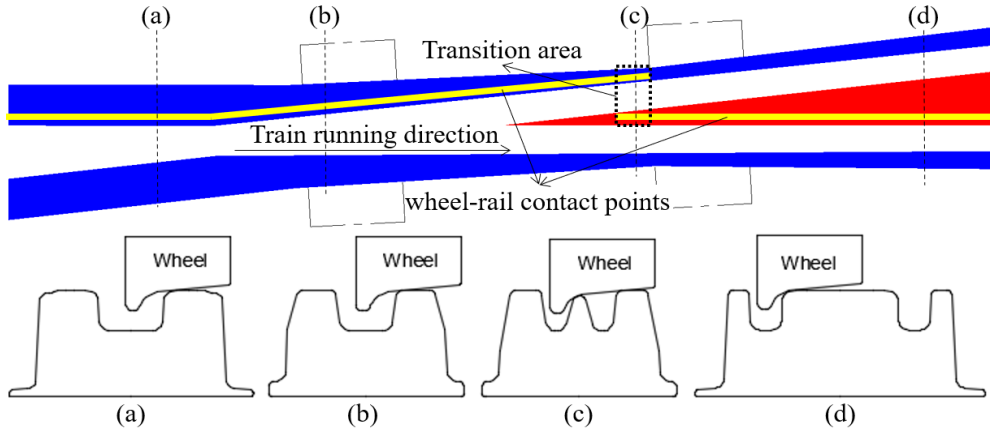


Figure 2.2. Main stages of wheel passing through a turnout crossing: approaching crossing (a)-(b), transition from wing rail to crossing nose (c), continue moving on crossing and through rail (d).

In section (c) (Figure 2.2), the wheel load is transferred from the wing rail to the crossing nose, where impact occurs on the nose rail. This section is then referred to as the transition area. Apparently, the smoother the transition of the wheel from the wing rail to the crossing nose, the smaller the amplification of the wheel forces (impact forces) due to the rail gap.

The presence of the gap (and the resulting impact force) is the main cause of the fast degradation and failure of the railway crossing. The forces can be extremely high because of high train velocity (140 km/h as same as in normal track) when passing the crossings in the through direction. The high wheel (impact) forces ultimately lead to the crossing rail failure (cracks). As it was shown in the previous experimental studies [19]-[22] the geometry of the crossing deteriorates not only locally due to rail plastic deformations, but also overall due to the settlement of ballast that in turn results in further increase of the wheel forces. In the forthcoming sections, the link between the crossing condition/degradation and the measured responses will be established.

### 3 Experimental tools for condition monitoring

In order to timely detect and localise the possible crossing defects, proper experimental tools are highly required. To be suitable for crossing condition monitoring, these tools should satisfy the following requirements:

- Easy to install in and uninstall from the crossing;
- Able to measure the crossing condition related responses;
- Capable to perform the measurement continuously.

The increasingly strict railway safety rules in the Netherlands demand the measurements to be performed without track possession. Among the dynamic responses, accelerations and displacements are the major indexes for assessment of structural performance. The rail accelerations due to passing trains provide information on the track vibrations that can reflect the condition of the crossing; the rail/sleeper displacements on the other hand, mainly reflect the condition of the supporting structure of the track (mainly the ballast). Therefore, rail accelerations together with the rail and sleeper displacements can be used for crossing condition assessment.

Based on the above-mentioned requirements, two devices have been selected for crossing responses measurements. The one is an accelerometer-based ESAH-M (Elektronische System Analyse Herzstückbereich-Mobil) for crossing instrumentation. The other is the DIC-based displacement measurement device called Video Gauge System (VGS) for wayside monitoring. Both devices are described below.

### 3.1 Instrumentation of crossings

The acceleration measurement device presented here has already been introduced and actively used in the previous studies [19]-[22]. The device and the measured responses for the assessment of the crossing condition are described below.

#### Crossing instrumentation

The main components of the crossing instrumentation are a 3-D accelerometer, a pair of inductive sensors, an optional sleeper sensor and the Main Unit. The 3-D accelerometer is mounted on the crossing rail to measure the accelerations of the crossing nose rail due to the passing wheels. The pair of the IS is attached to the rails (under the railhead) near the crossing to detect the passing train and to measure the velocity of each passing wheel. This system continuously measures the responses of the crossing and automatically saves the data when a passing train is detected. Figure 3.1 shows the instrumentation of a railway crossing. All the data is processed and saved in the Main Unit. No track access is required for data collection and battery replacement. It should be noted that in order to satisfy the above-mentioned requirements for SHM system, the original ESAH-M system has been modified. The main unit has been put outside of the track (Figure 3.1) so that the measurements can be performed continuously.

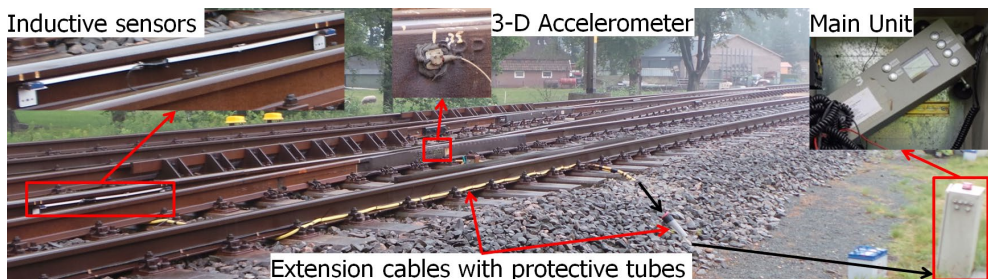


Figure 3.1. Overview of crossing instrumentation.

### Responses based on one passing train

An example of the measured vertical acceleration response in the time domain due to the passage of one train is shown in Figure 3.2 (similar responses in longitudinal and lateral directions are obtained as well). The measurement range of the acceleration sensor is 500 g (5000 m/s<sup>2</sup>) and the sampling frequency is 10 kHz. The high peaks in the acceleration response shown in Figure 3.2 correspond to the wheel impacts on the crossing nose.

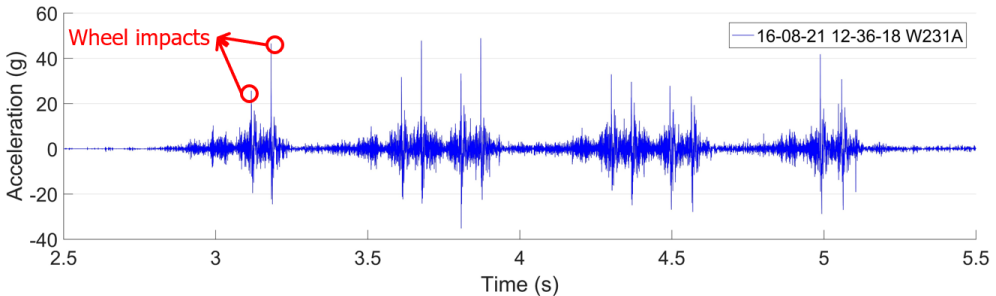


Figure 3.2. Vertical acceleration response of one train (12 wheelsets).

In the previous study [20], it has already been shown that the magnitude and location of the impact can reflect the performance/condition of the crossing. In this instrumentation, the velocities of the passing wheels are calculated from the inductive sensors. Together with the distance between the inductive sensor and the crossing nose point, the location of the impact of each passing wheel on the crossing nose can be detected. The impact itself is defined by the maximum acceleration within the monitored area on the crossing nose (Figure 3.3).

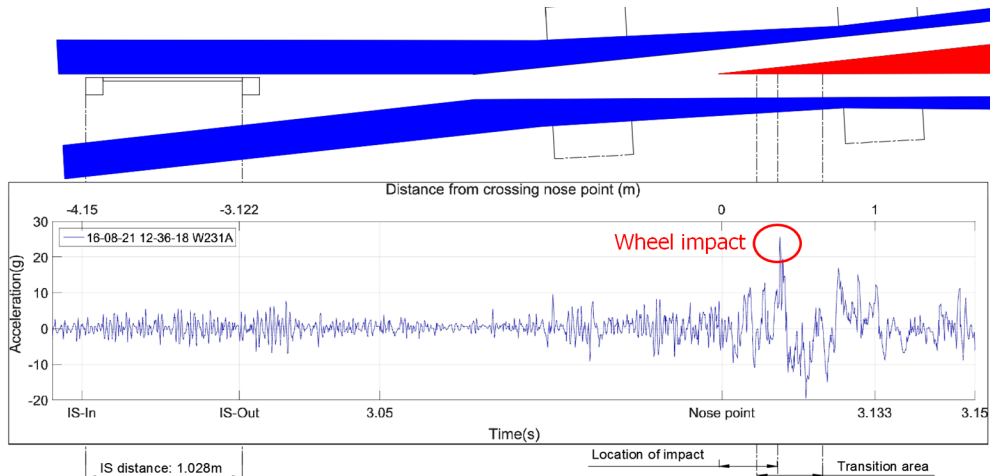


Figure 3.3. Detection of wheel impact and its location.

It should be noted that only the maximum acceleration in the transition area (Figure 2.2) is recognized as impact. The transition area can vary considerably for crossings of different angles and usages, but normally can be covered by the 1 m monitored area (Figure 3.3).

Sometimes, high acceleration responses beyond the transition area might be misidentified as impact due to the defects of wheel or rail. The proportion of these responses is normally quite small and their influence on the crossing performance assessment can be neglected.

The vertical acceleration response due to the first bogie of a passing train is shown in Figure 3.4 (zoomed in from Figure 3.2). It can be seen that the sphere of influence of single passing wheel is mainly within the 1 m monitored area. Considering that the wheelbase of a train bogie is normally around 2.5 m, which is much longer than the 1 m monitored area, the influence of one passing wheel on the neighbour wheels is negligible. In this case, each passing wheel can be regarded as an independent excitation on the crossing.

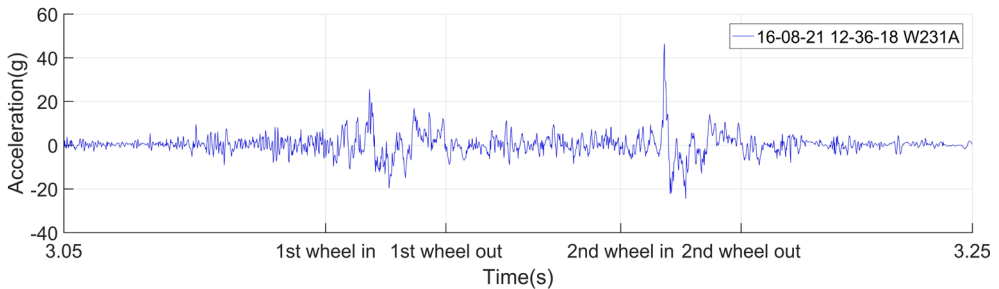


Figure 3.4. Vertical acceleration response due to the first bogie of a train.

Performance of a crossing is to a large extent determined by the way of the wheel and rail interaction in the transition area (Figure 2.2). This interaction is influenced by various factors ranging from the crossing design, condition and maintenance to the vehicle properties. Normally during the wheel transition, contact occurs on the wheel gauge corner (Figure 3.5 (a)) and the dominant impact acceleration is in the vertical direction. However, in some cases when the wheel enters the crossing with a certain angle, the impact can occur on the wheel flange (Figure 3.5 (b)-(c)). In these situations, the magnitude of the accelerations is much higher than that in the normal situation, and the dominant impact acceleration in this case is in the lateral direction. Obviously, impacts on the wheel flange are more damaging for a crossing than the impact on the wheel gauge corner.

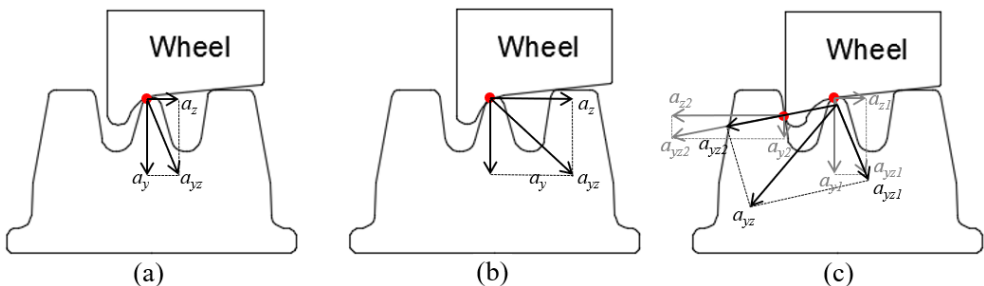


Figure 3.5. Wheel/rail contact situations: (a) Regular contact; (b) Irregular positive contact with wheel flange hit on the crossing nose; (c) Irregular negative contact with wheel flange impact on the outside wing rail.

Using the presented crossing instrumentation, the wheel transition can be assessed by analysing the angle of the impact accelerations. To distinguish these contact situations, the

regular and irregular contact defined based on the angle are introduced in this measurement system. Define the wheel impact angle  $\tan \alpha = |a_z / a_y|$ . When  $\tan \alpha < 1$ , the acceleration response of the crossing in the vertical direction is higher than that in the lateral direction. In this case, the wheel-rail contact is considered as regular. Otherwise, the contact is considered as irregular. The irregular contact can be further divided into two categories: positive contact when the wheel flange has impact on the crossing rail (Figure 3.5 (b)) and negative contact when the flange impact is accompanied by the contact between the inner wheel and the wing rail (Figure 3.5 (c)).

A

Irregular contact might occur incidentally due to the bad wheel or wrong geometry of the crossing rail. However as it will be shown later in this paper, if the proportion of irregular contact wheels in the overall passing wheels increases, it can indicate some changes in the crossing geometry. Therefore, this proportion (number of irregular contact wheels/number of overall passing wheels) will be used as an indicator for the assessment of crossing condition.

### Responses based on multiple train passages

As discussed previously, wheel-rail interaction in crossing is affected by many factors. As it can be seen from the example of vertical acceleration distribution given in Figure 3.6, the magnitude of wheel impact can vary considerably from one passing wheel to another. In this case, the impact acceleration due to a single passing wheel is not representative. In order to analyse these data, the distribution of the accelerations due to multiple wheel passages is used to characterize the performance of the crossing for condition assessment.

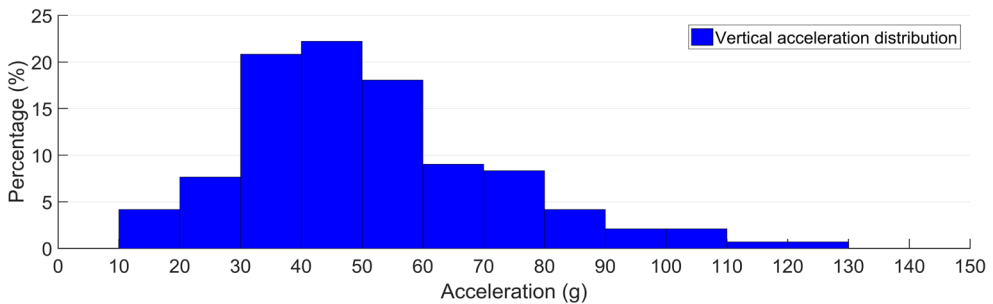


Figure 3.6. An example of vertical acceleration distribution of trains in one measurement day.

Beside the impact accelerations, the impact locations on the crossing nose also vary from one passing wheel to another [20]. The region where most of the wheel impacts are located is defined as the **fatigue area** (Figure 3.7). The size and location of the fatigue area can be used for the assessment of the crossing performance/condition. It was found in the previous study [21] that the crossing with highly worn nose rail has a relatively narrow fatigue area (100 mm), which resulted in the rolling contact fatigue defects in the crossing. During the service life of a crossing, the location and size of the fatigue area can change, especially when the welding or grinding maintenance is performed. It should be noted that the vehicle properties (the primary suspension system of the passing vehicles, wheel profile, etc.) also have an effect on the size of the fatigue area. The fatigue area and the distribution of impact accelerations can help to analyse the big amount of the collected data and estimate the

crossing condition, as it will be demonstrated later in this paper.

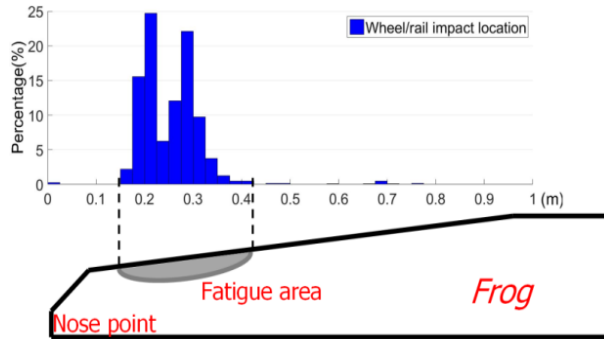


Figure 3.7. Fatigue area detection by the crossing instrumentation.

### 3.2 Wayside monitoring system

The second experimental tool is a wayside monitoring system called VGS. It has already been introduced in the previous studies [23]-[24]. It is a DIC-based remote measurement system that uses high speed digital cameras to measure the dynamic movements of the selected targets in the track. The major advantage of this system is that the whole measurement process can be performed without track possession. In the crossing section, it is used to measure the displacements rail and multiple sleepers to assess ballast condition and detect hanging sleepers. The field installation and device capabilities of this system are presented below.

#### Components and field installation

The main components of this wayside monitoring system are the high speed video cameras with suitable lenses connected to an operation computer with DIC software. In principle, any target can be recognized as long as the grey value of this target is different from the surrounded points. However, a more recognizable target can improve the tracking stability and provide more accurate measurement results. Therefore, if condition permits, it is better to install special targets on the monitored objects. The recommended target type for this monitoring system is rotationally symmetric circles with blurry edges as shown in Figure 3.8. This figure shows a setup of this system for crossing monitoring with the targets installed on the crossing rail and sleepers.

#### Features for track condition assessment

In the field measurement, the cameras make videos of the real-time movements of multiple targets within the monitored region. The accuracy of this system can be up to 0.01 mm, and the maximum sampling frequency with full screen (1024×768 pixels) is 117 Hz, which can be increased up to 400 Hz when using cropped screen.

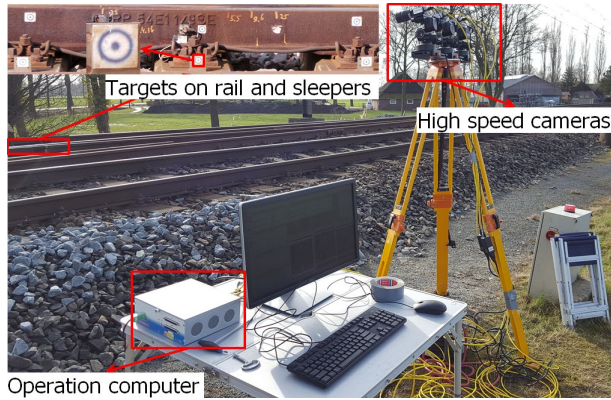


Figure 3.8. Wayside monitoring system setup.

Figure 3.9 shows an example of displacement measurement using cropped screens (300×400 pixels). The displacements of the selected targets (three targets on the rail in Figure 3.9) can be obtained and displayed on the screen online as the train is passing by. It is also possible to use this system to make only videos in the field without targets setup, and to post-process the videos afterwards (offline), which can help to save time during the field measurements.

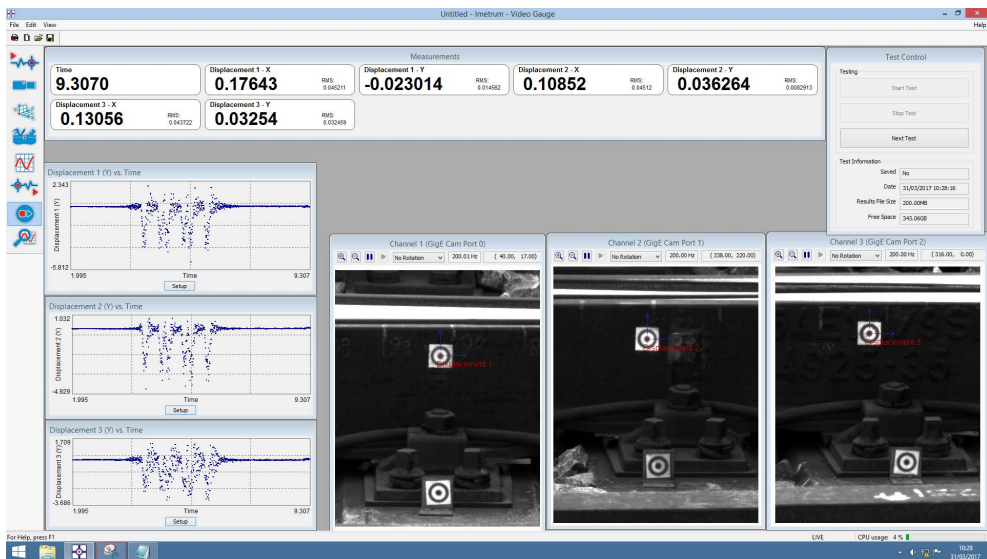


Figure 3.9. Screen of displacements measurement.

In [22] it was shown that the measured rail and sleeper displacements are realistic (in the order of several millimetres), and the main responses are in the frequency range of 0-10 Hz that corresponds to vehicle configuration and train velocity. Therefore, this system is sufficient to perform dynamic displacements measurement of the railway crossing. Moreover, this measurement system is capable to track up to 100 targets simultaneously using multiple cameras, which can be used to measure the displacements of several sleepers and assess the

ballast condition in a critical section [24].

## 4 Condition monitoring analysis using instrumentation

In this section, the results of monitoring a 1:15 railway crossing using the instrumentation that described in Section 3.1 are presented. This study aims to determine the relation between the measured dynamic responses and the crossing conditions and to evaluate the effectiveness of crossing maintenance (repair grinding and welding).

### 4.1 Measurement and maintenance activities in the monitored crossing

The monitored crossing was subsequently measured in different condition stages according to the visual inspection and maintenance. The first measurements were performed when the crossing was after some time of operation and the crossing nose was worn but no visible damage was observed. The crossing state at that time was referred to as “**Worn**” (Figure 4.1 (a)). The second measurements took place seven months later when there were already visible cracks on the rail. In this stage, the crossing condition was referred to as “**Damaged**” (Figure 4.1 (b)). About one month after the second measurement, this crossing was manually repaired. During the repair, firstly the damaged material on the crossing nose was cut off, then new material was added using electrode welding, and finally the crossing was grinded to restore the rail profile. It should be noted that the quality of the crossing geometry after repair highly depends on the skills and experience of the welder, which means that the repaired crossing profile could be different from the original design. The third measurements were performed one month after repair, and the condition of the crossing in this stage was referred to as “**Repaired**” (Figure 4.1 (c)).

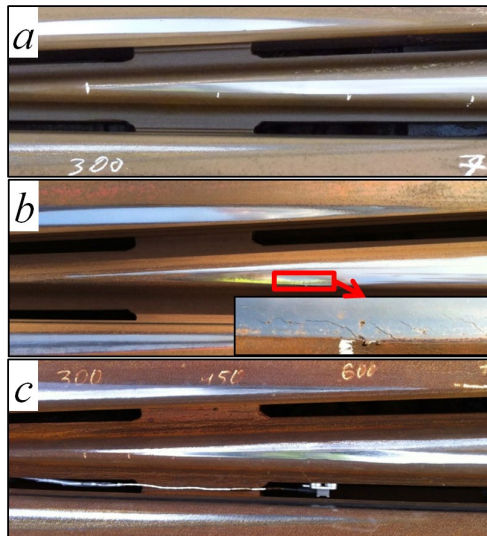


Figure 4.1. Different condition stages of the monitored crossing. (a): Worn; (b): Damaged; (c): Repaired.

## 4.2 Analysis of impact accelerations

On the monitored crossing, the trains were running in the through facing direction with the velocity around 130 km/h. As mentioned previously, the train configuration has an influence on the track responses. In order to eliminate the influence of the train, only the trains of one type (double floor VIRM train with six wagons) were taken into account in the analysis. The amount of the measured trains (wheelsets) in each measurement series that fit the above filter conditions is given in Table 4.1.

A

Based on the selected trains, the mean values of the 3-D impact accelerations were calculated (Table 4.1). The percentages of the wheels with irregular positive and negative contacts (Figure 3.4) are given as well.

Condition	Total wheelsets	Mean values of accelerations, g			Positive Contact, %	Negative Contact, %
		Longitudinal	Vertical	Lateral		
Worn	144	23.4	52.0	34.0	2.1	0.7
Damaged	288	48.9	73.4	51.9	0	20.1
Repaired	264	20.3	43.6	22.6	0.4	3.0

Table 4.1. Measured acceleration results in the monitored crossing.

From this table it can be seen that from “Worn” to “Damaged” state, the impact accelerations were dramatically increased (around 40 % in the vertical and lateral directions, and more than 100 % in the longitudinal directions). At the same time, the percentage of the wheels with irregular negative contact was tremendously increased from 0.7 % to 20.1 %. The increase of the magnitude of the accelerations and increase of irregular (negative) contact were clearly related to deterioration of the crossing condition. The measured rail profiles of the monitored crossing in the critical sections indicate that in the “Damaged” state, both wing rail and nose rail were worn/deformed (Figure 4.2). These plastic deformations lead to the change of the wheel-rail interaction and further caused the increase of lateral acceleration.

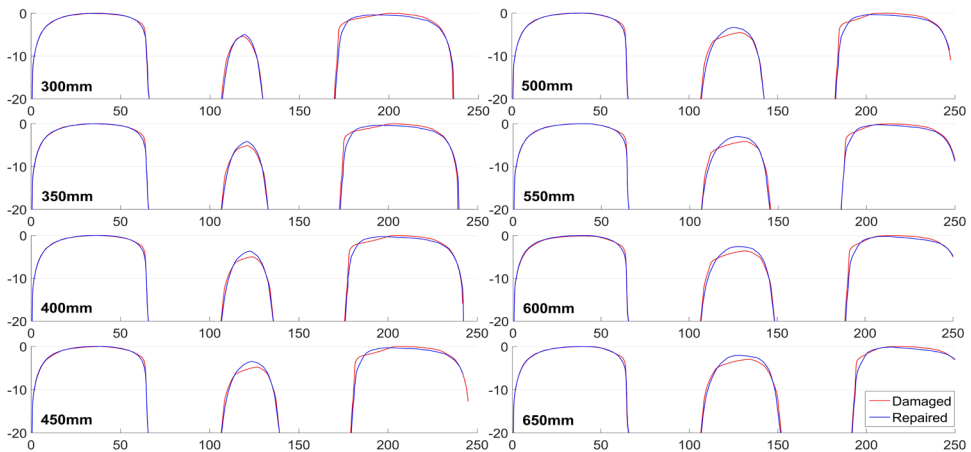


Figure 4.2. Measured rail profiles along instrumented crossing – examples for profiles at 300 mm to 650 mm from nose point.

After repair, the percentage of the wheels with irregular contact was reduced from 20.1 % to 3.3 %, which was already of the same level as in the “Worn” state (2.8 %). It can also be seen that the accelerations in the “Repaired” state were reduced even below the level of the “Worn” state, especially in the lateral direction was significantly reduced. The measured rail profiles along this crossing have clearly shown that the rail shape was restored. These results indicate that the repair work had a positive effect and the condition of the crossing was improved as compared to the condition in the “Worn” state.

As mentioned earlier, the crossing accelerations vary per passing wheelset. Therefore, the distributions of acceleration responses (in vertical and lateral directions) that can better reflect the performance of the crossing were obtained and given in Figure 4.3.

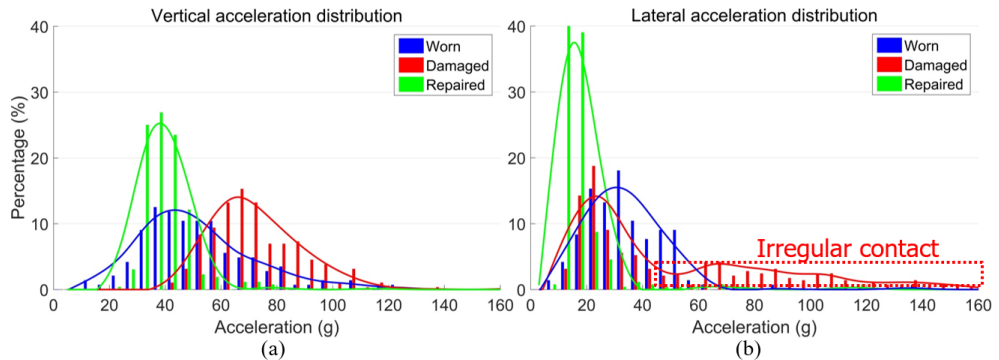


Figure 4.3. Vertical (a) and lateral (b) acceleration distributions.

In this figure, clear change in the vertical impact accelerations from “Worn” to “Damaged” states can be seen. The shape of the acceleration distribution shifted to the right, meaning that the vertical accelerations were increased (in agreement with Table 4.1).

Unlike the vertical responses, in the lateral direction only some of the passing wheels caused higher impact accelerations (from 60-160 g in Figure 4.3 (a)). These accelerations were mainly due to the negative contact. The increase of the negative contact explains the increase of the mean value of the lateral accelerations (Table 4.1).

After the repair, the impact accelerations in both vertical and lateral directions were significantly reduced. These results again show that the repair of the crossing was successful and the performance/condition of the crossing was improved.

### 4.3 Analysis of fatigue area

As mentioned in Section 3.1, the size and location of the fatigue area can be used as indicators for crossing condition assessment. The development of the fatigue area of this monitored crossing is shown in Figure 4.4.

In “Worn” state, the fatigue area was relatively large (more than 150 mm) and the impacts due to the passing wheels were widely spread on the crossing nose. That could explain the

fact that there was no visible damage observed at that time. In “Damaged” state, the fatigue area was narrowed to a 50 mm region (Figure 4.1 (b)) and the location of the fatigue area was shifted around 100 mm further from the crossing nose point. The shift and narrowing of the fatigue area can be explained as follows: the fatigue area was firstly moving further away from the nose point (in the direction of the wheel impacts) with the growth of the plastic deformations on the nose rail. When the fatigue area reached the critical location and could not move any further, the wheel impact area became increasingly more concentrated and eventually caused the cracks on the crossing nose. Such changes of the fatigue area can indicate the crossing condition deterioration, and the predictive maintenance should be performed somewhere between the “Worn” and “Damaged” state (especially when the location of the fatigue area stopped moving).

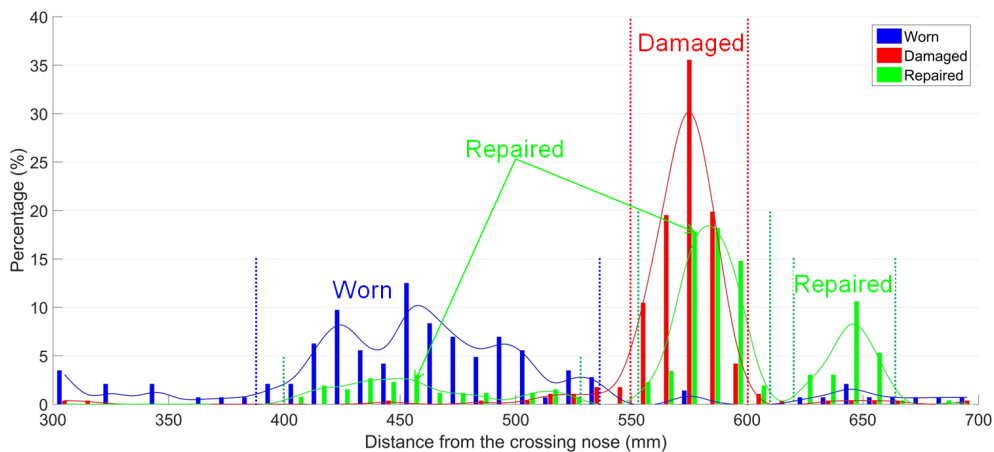


Figure 4.4. Fatigue area development.

After the repair of the crossing nose, three fatigue areas widely distributed along the crossing nose were appeared (Figure 4.4). Considering the reduction of the impact accelerations, it can be concluded that the repair work was successful and the wheel/rail contact properties were improved. In [12] it was shown that by deliberately changing the location of the wheel impact using welding and grinding repair the crossing life can be prolonged.

## 4.4 Summary

In the monitored crossing, several changes in the crossing condition from “Worn” to “Damaged” state can clearly be seen in the measured responses, such as the increase of the accelerations, increased number of the wheels with irregular negative contact and narrowed fatigue area. After the crossing repair, the measured responses reflected the improvements in the crossing performance (the reduced accelerations). Also, the repair resulted in changes of the fatigue area.

In crossing condition monitoring, these dynamic responses (impact acceleration, contact angle/irregular contact and fatigue area) of the crossing instrumentation can be used as the indicators for crossing condition assessment and for the maintenance effect analysis.

## 5 Wayside condition monitoring analysis

In railway track, there are some constructional irregularities, such as insulated or welded joints, turnout switches and crossings, etc. These irregularities make the sectional ballast settles faster due to the increase of wheel impact forces. In turn, the ballast settlement intensifies the track irregularity and accelerates track deterioration. Monitoring the dynamic performance of ballast and assessing the ballast condition is necessary for providing timely maintenance and for prevention of severe track damage. The local ballast settlement manifests itself in the increase of the vertical displacements of the rail and sleepers.

The DIC-based wayside condition monitoring system can detect and locate hanging sleepers in a track section through monitoring the vertical displacements of rail and sleepers. Based on the monitoring results, the ballast condition can be assessed. The ballast condition assessment can be used as guidance for timely track maintenance to prolong its service life. This wayside monitoring system is not specially designed for crossings, but can be applied in other tracks as well, which makes this system more versatile.

In this section, the rail displacement measurements in two locations are presented. One is a welding test section with very dense welding joints. The other one is in a moveable crossing section with visible hanging sleepers. These measurements aim to study the relationship between the rail displacements and the ballast condition, and the measurement results can be applied for the detection and quantification of ballast settlement in the crossing as well.

### 5.1 Wayside condition monitoring of welding joints

The monitored welding joints test section was built up to study the influence of welding joints introduced track irregularities. In this test section, the welding joints were very close to each other (Figure 5.1). After operation and testing for several months, the welded rail was replaced by a new rail. No action on ballast was performed, so the possible ballast settlement was still present in this track after rail replacement, which gave the opportunity to study the effect of ballast settlement. Meanwhile, the welding joints of the new rail were applied in the locations with compacted ballast, so the effect of the welds on the ballast settlement could be studied as well (Figure 5.2). The short wave irregularity excitation in the welding joint is similar to that in the crossing nose, which means that this study can be further applied in the monitoring of railway crossing. Another objective of this series of measurements is to set up a reference level of rail/sleeper displacement on compacted ballast that later can be used for ballast condition assessment.



Figure 5.1. Welding joints test section.

The rail displacements in two locations in this test section were measured using this wayside monitoring system before and after the rail replacement (Figure 5.2). One location was the normal track with compacted ballast (rail cutting point, Site 1-1) in the welding joints test section. After rail replacement, it became a welding joint on the new rail (Site 1-2). The other location was the old welding joints on the tested rail shown in Figure 5.1 (Site 2-1), which was later replaced by a whole piece of new rail (Site 2-2).

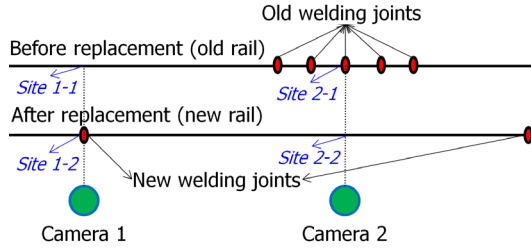


Figure 5.2. Schematic diagram of the field site.

In order to make the results more comparable, only the trains with the same configurations (Intercity train with one locomotive plus nine wagons) were recorded. The displacement results on the monitored sites are shown in Figure 5.3.

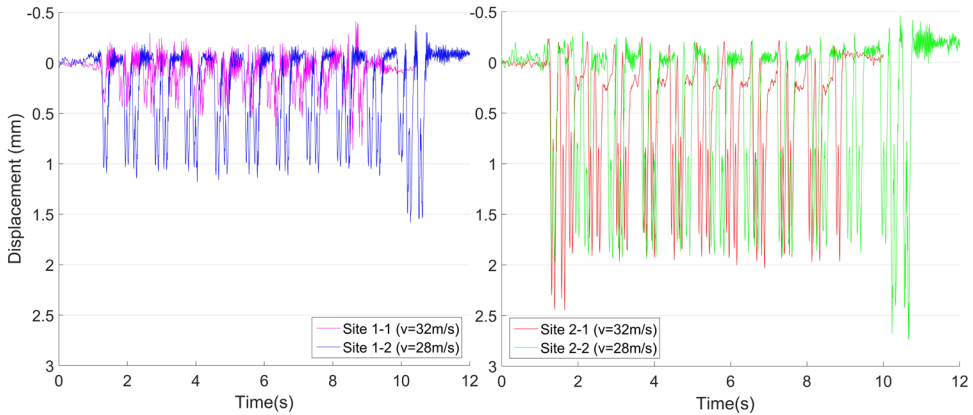


Figure 5.3. Displacement measurement results.

It can be seen that before the rail replacement, the maximum rail displacement in the normal track (Site 1-1) with compacted ballast is 0.8 mm (locomotive) / 0.5 mm (wagons). The maximum rail displacement in the old welding joints (Site 2-1) is 2.4 mm (locomotive) / 1.8 mm (wagons), which is more than 200 % higher than that in the normal track. These results indicate the formation of hanging sleepers under the welding joints. After replacement of the test rail, the maximum rail displacement in the new welding joint (Site 1-2) is 1.5 mm (locomotive) / 1.1 mm (wagons). Compared with the normal track, the increase is 100 %. This result reflects the increase of wheel impact forces due to the welding joint. The displacement of the new rail (Site 2-2) is 2.6 mm (locomotive) / 1.8 mm (wagons), which has no difference with the old welding joints (Site 2-1). This result illustrates that the ballast in this site has already settled. Only the replacement of the problematic rail without ballast

maintenance (track geometry correction) has very limited effect on the improvement of the performance of the track.

Type of vehicle	Displacement results, mm			
	Before rail replacement		After rail replacement	
	Site 1-1	Site 2-1	Site 1-2	Site 2-2
Locomotive	0.8	2.4	1.5	2.6
Trailer	0.5	1.8	1.1	1.8

Table 5.1. Displacement measurement results.



In these measurements, the effect of welds in initiation of ballast settlement has been studied using the wayside monitoring system. According to the measurement results, it can be concluded that the irregularities due to the welding joints will increase the wheel impact on the track and lead to higher rail/sleeper displacement. The accumulation of wheel impact will eventually lead to the ballast settlement. Additionally, for ballast condition assessment, the normal track (Site 1-1) can be used as a reference level of compacted ballast in practice.

### 5.2 Wayside condition monitoring of movable crossing

In Section 5.1, it is shown that the track irregularities can affect the dynamic performance of the track and cause ballast settlement. In this section, the monitoring results of a movable crossing are presented. The pre-monitoring track inspection has already indicated track deterioration (Figure 1.1 (c)), and the monitoring results were used to quantitatively assess the ballast condition. The effectiveness of maintenances including ballast tamping and crossing replacement was assessed as well.

In this crossing section, trains mainly run in the through facing direction. The rail displacements of the stock rail in two critical locations were measured using the wayside monitoring system. Specifically, one location was above the first switch machine close to the crossing nose (Target 1), and the other location was above the last switch machine (Target 2), as shown in Figure 5.4.

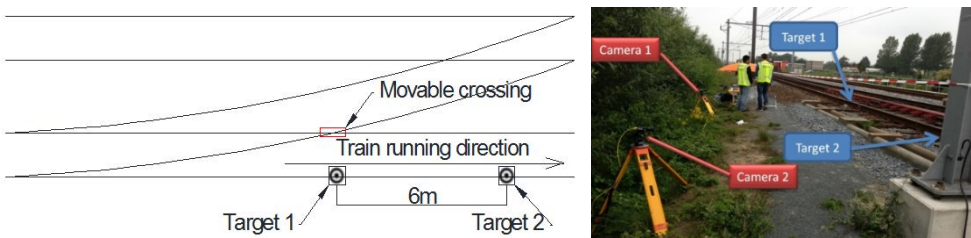


Figure 5.4. Overview of measurement location and cameras/targets setup.

This crossing section was totally measured four times. The first two measurements were carried out within a week, with track tamping performed in between. Therefore, the track conditions in these two measurements were respectively defined as “Before tamping” and

“After tamping”. About two weeks after tamping, the crossing was replaced, with another two measurements carried out right before and after the crossing replacement. The track conditions of these two measurements were then defined as “Before renewal” and “After renewal”. The type of monitored train is double decker train with six vehicle units, the difference of axle load between the locomotive and the wagons is limited. The monitoring results are shown in Figure 5.5.

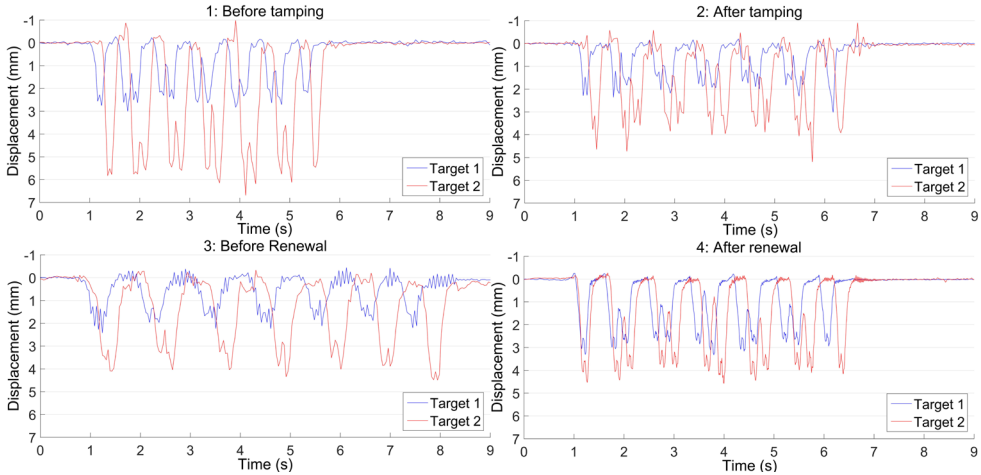


Figure 5.5. Rail displacement results.

It can be seen from this figure that the rail displacements of both monitored targets were much higher than the reference level (0.5 mm in Site 1-1 in Section 5.1). The maximum displacement of Target 2 before tamping was even 10 times higher than the reference level (6.5 mm). After tamping, the displacements of Target 1 and Target 2 were reduced 20 % and 30 %, respectively. It can be concluded from the results that tamping has positive effect on the performance of the track, but the settled ballast was not completely restored. Before and after crossing renewal, the displacement of Target 1 fluctuated between 2 mm and 3 mm while Target 2 remained at around 4mm. These results indicate that although the defects on the rail were eliminated, the ballast performance was not improved or even got worse.

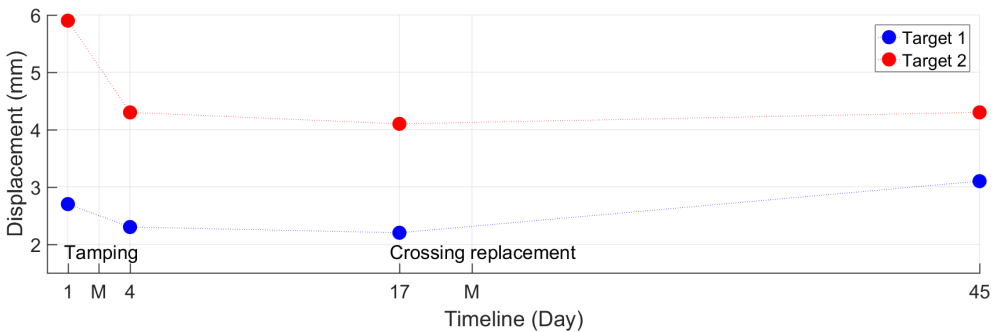


Figure 5.6. Rail displacements development of the monitored targets.

It can be concluded that the monitored two critical locations in this crossing section were suffering from severe ballast deterioration. This situation was not fundamentally improved by the track maintenances and the ballast settlement was continuously deteriorating afterwards.

It has to be noted that in this movable crossing section, the complicated track structure with several switch machines not only introduced extra track irregularity, but also made it difficult to maintain the settled ballast due to these mechanical components. Moreover, the rail irregularity caused the increase of wheel impact and initiated the ballast settlement. When it was formed, the settlement itself will also act as track irregularity and promote further deterioration.

A

### 5.3 Summary

This section presented the track displacement measurements using the wayside monitoring in a welded joints test section and in a movable crossing section. In both sections, the ballast settlement was detected and quantified, and the maintenance efficiency was assessed. Both measurements indicated that the track irregularities (welding joints and switch machine) were the sources of the ballast settlement initiation.

The measurements in the welding test section provided the reference (stable) level of ballast displacement and explained the initiation of ballast degradation. The measurements in the movable crossing section showed how the track maintenances could affect the ballast performance, which can provide guidance for effective and predictive ballast maintenance arrangement.

The wayside monitoring system has universal applicability that not restricted by railway crossings. Regarding to the condition monitoring of railway crossings, the rail displacement can be used as an indicator for ballast condition assessment.

## 6 Conclusions

This paper presented a selection of the condition monitoring tools for railway crossing. Both selected systems are tested in the field and are proved capable to perform track monitoring in long-term. The measurement results indicate that the condition of rail and ballast can be recognized. In addition, some malfunctioning components or damages, such as crossing rail defect and ballast settlement, can be detected and quantified.

Based on the measurement results, several indicators for crossing condition assessment are proposed. Specifically, the impact acceleration, irregular contact and the fatigue area can be used to assess the condition of crossing rail, and the rail displacement can be used to quantify ballast settlement.

The measurements obtained using the crossing instrumentation have shown that the proposed indicators were changing along with the crossing condition deterioration, such as the impact acceleration and the percentage of irregular contact were increased and the fatigue area narrowed. The wayside measurements in two track sections have clearly shown that the

ballast settlement was initiated by the track irregularities (welds).

The maintenance activities in the monitored tracks were mainly carried out reactively on the damaged components, which was actually too late since the tracks had been operated in the damaged condition for a while. The better way of track maintenance is to perform predictively before the occurrence of visible damage. The proposed indicators can be used to predict the crossing damage and timely perform the maintenance.

The presented monitoring tools have shown the capability of detecting the track condition through analysing the proposed indicators. In long-term condition monitoring, these tools can be used as the basis of structural health monitoring for railway crossings and further provide guidance for predictive maintenance.

A

## References

- [1] I.Y. Shevtsov, Rolling Contact Fatigue problems at Railway Turnouts, [http://www.slm-flanders.be/sites/default/files/events/Meeting\\_Materials\\_Nov2013/mm\\_13112013\\_ivan\\_shevtsov\\_prorail.pdf](http://www.slm-flanders.be/sites/default/files/events/Meeting_Materials_Nov2013/mm_13112013_ivan_shevtsov_prorail.pdf), 2013.
- [2] D. Huston, Structural Sensing, Health Monitoring, and Performance Evaluation. University of Vermont, Burlington, 2011.
- [3] D. Pines, A.E. Aktan, Status of structural health monitoring of long-span bridges in the United States, *Progress in Structural Engineering and Materials*, vol. 4, 2002, p. 372-380.
- [4] I.N. Robertson, Prediction of vertical deflections for a long-span prestressed concrete bridge structure, *Engineering Structures*, vol. 27, 2005, p. 1820-1827.
- [5] J.M. Ko, Y.Q. Ni, Technology developments in structural health monitoring of large-scale bridges, *Engineering Structures*, vol. 27, 2005, p. 1715-1725.
- [6] J.M.W. Brownjohn, Lateral loading and response for a tall building in the non-seismic doldrums, *Engineering Structures*, vol. 27, 2005, p. 1801-1812.
- [7] H.A. Toliyat, K. Abbaszadeh, M.M. Rahimian, L.E. Olson, Rail defect diagnosis using wavelet packet decomposition, *IEEE Transactions on Intelligent Transportation Systems*, vol. 39 (5), 2003, p. 1454-1461.
- [8] L.F. Molina, E. Resendiz, J.R. Edwards, J.M. Hart, C.P.L. Barkan, N. Ahuja, Condition Monitoring of Railway Turnouts and Other Track Components Using Machine Vision, *Proceedings of the Transportation Research Board 90th Annual Meeting*, 2010.
- [9] Y. Li, H. Trinh, N. Haas, C. Otto, S. Pankanti, Rail component detection, optimization, assessment for automatic rail track inspection, *IEEE Transactions on Intelligent Transportation Systems*, vol. 15 (2), 2014, p. 760-770.
- [10] N. A. Thakkar, J. A. Steel, R. L. Reuben, Rail-wheel contact stress assessment using acoustic emission: A laboratory study of the effects of wheel flats, *Proceedings of the Institution of Mechanical Engineers, Part F: Journal of Rail and Rapid Transit*, vol. 226, 2012, p. 3-13.
- [11] D. Cantero, B. Basu, Railway infrastructure damage detection using wavelet transformed acceleration response of traversing vehicle, *Structural Control and Health Monitoring*, vol. 22, 2015, p. 62-70.

- [12] C. Wan, V. Markine, I. Shevtsov, Improvement of Vehicle-Turnout Interaction by Optimising the Shape of Crossing Nose, *Vehicle System Dynamics*. vol. 52 (11), 2014, p. 1517-1540.
- [13] L. Xin, V. Markine, I. Shevtsov, Numerical procedure for fatigue life prediction for railway turnout crossings using explicit finite element approach, *Wear*, vol. 366-367, 2016, p. 167-179.
- [14] E. Kassa, C. Andersson, J. Nielsen, Simulation of dynamic interaction between train and railway turnout. *Vehicle System Dynamics*. Vol. 44 (3), 2006, p. 247-258.
- [15] E. Kassa, J. Nielsen, Dynamic interaction between train and railway turnout: full-scale field test and validation of simulation models. *Vehicle System Dynamics*. Vol. 46, 2008, p. 521-534.
- [16] A. Johansson, B. Pålsson, M. Ekh, J.C.O. Nielsen, Mats. K.A. Ander, J. Brouzoulis, E. Kassa, Simulation of wheel–rail contact and damage in switches & crossings, *Wear*, W-99618, 2010.
- [17] B. Pålsson, J. Nielsen, Wheel–rail interaction and damage in switches and crossings, *Vehicle System Dynamics*, Vol. 50 (1), 2012, 43-58.
- [18] C. Wan, Optimisation of vehicle-track interaction at railway crossings, Delft University of Technology, Delft, 2016.
- [19] V.L. Markine, I.Y. Shevtsov, Experimental Analysis of the Dynamic Behaviour of Railway Turnouts, The Eleventh International Conference on Computational Structures Technology, Dubrobnik, Croatia, 2012.
- [20] V. L. Markine, I. Y. Shevtsov, An Experimental Study on Crossing Nose Damage of Railway Turnouts in the Netherlands, the 14th International Conference on Civil, Structural and Environmental Engineering Computing, Cagliari, Sardinia, Italy, 3-6 September 2013.
- [21] X Liu, V.L. Markine, I.Y. Shevtsov, R.P.B.J. Dollevoet, Experimental Analysis of Key Parameters Investigation in Turnout Crossing Degradation Process, submitted to the 10th Contact Mechanics Conference, Colorado, USA, 2015.
- [22] X. Liu, V.L. Markine, I.Y. Shevtsov, Dynamic experimental tools for condition monitoring of railway turnout crossing, The Second International Conference on Railway Technology: Research, Development and Maintenance, Corsica, France, 2014.
- [23] H. Wang, V.L. Markine, R.P.B.J. Dollevoet, I.Y. Shevtsov, Improvement of train-track interaction in transition zones via reduction of ballast damage, The 24th International Symposium on Dynamics of Vehicles on Roads and Tracks, Graz, Austria, 17-21 August 2015.
- [24] V.L. Markine, C. Wan, Performance Optimised Geometry of Railway Crossings: Design and Implementation, *International Journal of Railway Technology*, vol. 5 (2), 2016, p. 1-25.



# Paper B

## MBS Vehicle – Crossing Model for Crossing Structural Health Monitoring

X. Liu, V.L. Markine

*Sensors*, vol. 20 (10), 2020, 2880.

<https://doi.org/10.3390/s20102880>

### Abstract

This paper presents the development of a multi-body system (MBS) vehicle–crossing model and its application in the structural health monitoring (SHM) of railway crossings. The vehicle and track configurations in the model were adjusted to best match the real-life situation. By using the measurement results obtained from an instrumented crossing and the simulation results from a finite element (FE) model, the MBS model was validated and verified. The results showed that the main outputs of the MBS model correlated reasonably well with those from both the measurements and the FE model. The MBS and FE models formed the basis of an integrated analysis tool, which can be applied to thoroughly study the performance of railway crossings. As part of the SHM system for railway crossings developed at Delft University of Technology, the MBS model was applied to identify the condition stage of a monitored railway crossing. The numerical results confirmed the highly degraded crossing condition. By using the measured degradation as the input in the MBS model, the primary damage sources were further verified. Through identifying the crossing condition stage and verifying the damage source, necessary and timely maintenance can be planned. These actions will help to avoid crossing failure and unexpected traffic interruptions, which ultimately will lead to sustainable railway infrastructure.

**Keywords:** Railway crossings; Structural health monitoring; Vehicle–crossing interaction; Multi-body system modelling; Model validation and verification; Condition-stage identification.

# 1 Introduction

Railway turnouts (also called switches and crossings (S&C)) are essential components of the railway infrastructure that provide the ability for the trains to transfer from one track to the other. A standard railway turnout contains three main parts:

- The switch panel that controls the train travelling directions;
- The crossing panel that provides the intersection of two tracks;
- The closure panel, which connects the other two panels.

A sketch view of a standard left-hand turnout is shown in Figure 1.1.

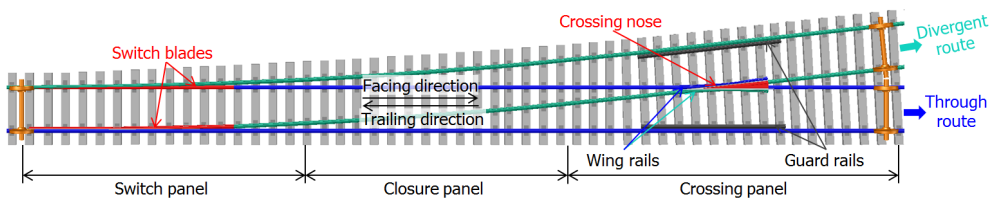


Figure 1.1. Standard left-hand railway turnout with a 1:9 crossing.

B

When a train is passing through a turnout crossing, the wheel on the inner rail has to pass the gap between the wing rail and the crossing nose rail. The presence of this gap leads to high impact forces acting on the wing rail/crossing rail. The higher the train velocity, the higher these forces are [1]-[3]. The magnitude of the impact forces also depends on the crossing angle, namely the bigger the angle, the higher the wheel forces [3]-[4]. It should be noted that in contrast to the divergent route where the maximum allowable speed of the passing trains depends on the crossing angle, there is no speed limit related to the crossing angle for the trains passing the crossing in the through route [5]. The speed limit in the through route is usually defined by the operational speed on the particular track section. Therefore, high impact forces due to the passing wheels occur on these crossings resulting in fast degradation and short service life of the crossings. As such, the turnout crossing is one of the weakest spots in the railway network.

In recent years, the dynamic performance of railway crossings has drawn much attention and several studies on the wheel–crossing interaction and the related problems have been performed. These studies consist of both experimental [6]-[16] and numerical approaches [1]-[4], [17]-[37]. The experimental studies can provide more realistic results than the numerical ones but are also more expensive and time-consuming. Sometimes, it is difficult to get any regular patterns from the measurement results due to the complexity of train–crossing interactions in the situ [12], and the development of the structural health monitoring (SHM) system for railway crossings is still in the primary stage regarding damage detection. In such cases, numerical models are needed to help to identify the crossing condition from the experimental data. For that purpose, the numerical models should be able to catch the main dynamic features of railway crossings and be also suitable for performing repetitive simulations.

The numerical models for crossing performance analysis available nowadays are mainly based on the multi-body system (MBS) methods and the finite element (FE) methods. The FE models that featured with detailed wheel–rail contact analysis are widely applied to address the local wheel–rail interaction problems. The related studies cover topics such as the development of numerical models [3]-[4], [17], critical contact pressure [18] and stress [19] analysis, damage-related studies [20]-[25], method aiming to improve the crossing performance [26], assessment of the maintenance effect [27] and damage prediction [28], etc. The primary deficiency of the FE models is the high requirement for computing resources. As it was mentioned in Ma et al. [4], one simulation of the wheel-crossing interaction may take hours or even days to finish. Therefore, the FE models are usually simplified to have only the wheel/wheelset-crossing part. Full-scaled turnout models are only applied in the static or semi-static analysis [29]-[30]. From this point of view, the FE models are difficult to apply for the verification of the measurement results due to the requirement of multiple trial calculations. Therefore, the MBS method that provides fast simulation is the better option. Furthermore, the MBS models are already applied in the parameter studies and design optimization of railway crossings [31]-[37], but their application combined with experimental studies are still limited, where the measurement results are mainly used for model validation.



Figure 1.2. A 1:9 cast manganese steel crossing: (a) View of a wing rail and crossing nose rail; (b) Crossing nose rail damage in the transition region.

In the Netherlands, the most commonly used type of crossings is the cast crossing made of the manganese steel with a crossing angle of 1:9 [38], as shown in Figure 1.2 (a). This type of crossings suffers greatly from severe plastic deformations and cracks leading to spalling defects or even to sudden fracture of the crossing nose (Figure 1.2 (b)). The service life of such crossings in the Netherlands has become prohibitively short, where in some cases, it is only 2-3 years [39]. To better understand the sources of their poor performance, the condition monitoring system based on the instrumentation devices has been developed and implemented in this type of crossings, as described in Markine et al. [12]. The experimental data provided the instant performance information about the monitored crossing and together with the proposed condition indicators, they were used to assess the crossing condition and to describe the degradation process of the crossing. The indicators and related condition stages were determined experimentally. To verify them, as well as to extend the SHM system to other operational conditions (e.g. different type of crossings), a numerical model is necessary.

Therefore, **the goal of this study** was to develop an MBS model for vehicle–crossing interaction that is suitable for SHM. By using this model, not only the crossing conditions

can be identified, but also the condition indicators can be verified.

To verify the MBS model, the FE wheel–crossing model developed and validated in Ma et al. [4] was used in this study. The FE model accounted for the plastic deformation and hardening of the material on a local scale, such as the stress and strain resulting from the wheel–rail interface. The procedure of the model verification is described in this paper. After that, the use of the MBS model in the SHM system is described and demonstrated. The outline of this study is given below.

In Section 2, the modelled real-life situation, the development of the MBS model, and the input data that was adjusted according to the analysed railway system are described. The MBS model validation using the field measurement results and the verification using the previously developed FE model are given in Section 3. Using the developed MBS model application, the identified crossing condition stage in the field monitoring is further verified, as presented in Section 4. In Section 5, the main conclusions are provided.

## 2 MBS model of vehicle–crossing interaction

As mentioned in the previous section, one of the purposes of the MBS model was to verify the previously proposed indicators. Therefore, in this section, the monitored crossing and the obtained measurement data are presented first, followed by detailed information about the MBS model.

### 2.1 Monitored crossings

In the railway track system, a crossover is a pair of turnouts that connects two parallel tracks and allows a train to pass over from one track to the other (Figure 2.1). Such a crossover is usually a part of a double crossover to allow all the trains to run on one track and gain more maintenance time for the other track. There are plenty of these crossovers on the Dutch railway network, and under the normal operating conditions, the trains pass the crossings only in the through (facing or trailing) route (Figure 1.1). In the Dutch railway network, the presence of bridges, culverts and level crossings limits the available space for the layout of the double crossovers. Therefore, the turnouts with the smallest crossing angle of 1:9, which requires relatively short layout distance, are commonly used in crossovers.



Figure 2.1. Typical crossover in the Dutch railway network.

To obtain insight regarding the crossing performance in the real-life situation and to provide guidance for the validation of the numerical models, a 1:9 cast manganese crossing from a double crossover in the Dutch railway was instrumented and monitored. The operational speed in the through route of the crossing is 140 km/h, which is much higher than the speed limit of 40 km/h in the divergent route [5]. The crossing instrumentation is based on the performance analysis device called ESAH-M, which has been introduced and actively used in previous studies [3]-[4], [8], [35]. An overview of the crossing instrumentation used in the situ is shown in Figure 2.2.

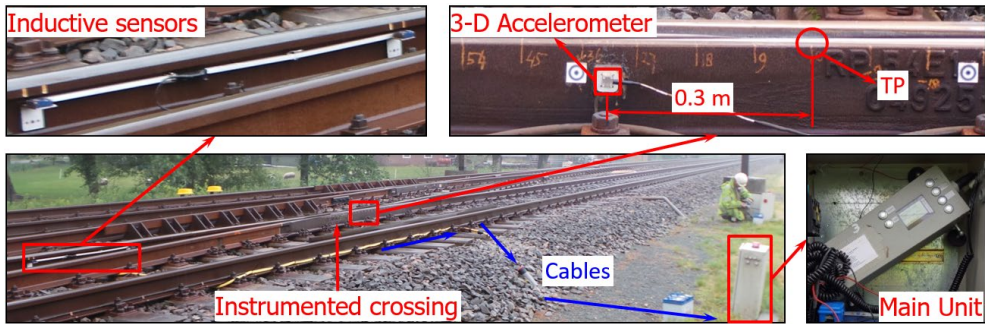


Figure 2.2. Overview of the crossing instrumentation, TP: Theoretical point.

As seen in Figure 2.2, the main components of this device are a 3-D accelerometer attached to the side of the crossing (0.3 m away from the theoretical point (TP)), a pair of inductive sensors attached in the closure panel and the main unit installed near the track. The inductive sensors are used for train detection and train velocity calculations. All the sensors are connected to the main unit for measurement control and data recording. The measurement range of the acceleration sensor is 500 g ( $\approx 5000 \text{ m/s}^2$ ) and the sampling frequency is 10 kHz.

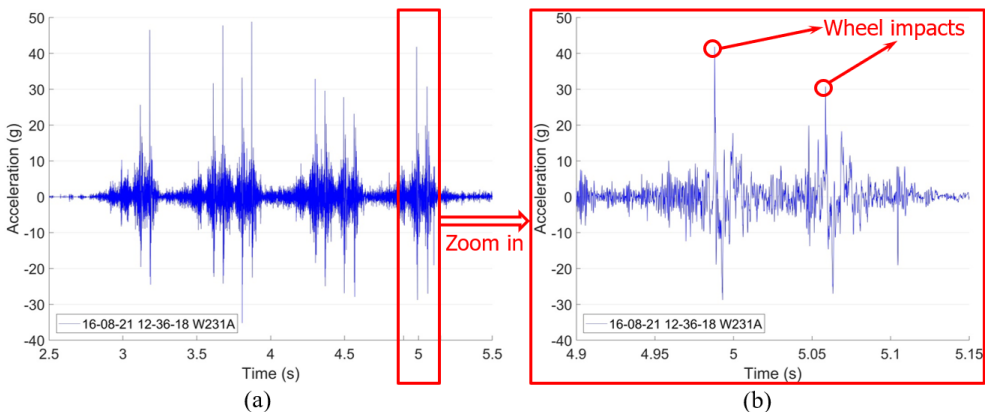


Figure 2.3. Measured crossing dynamic responses using the instrumentation. (a): Vertical acceleration response of one train (12 wheelsets); (b): Examples used for wheel impacts extraction.

When a train passes through the crossing, the wheel–rail interaction is directly reflected in the vertical acceleration responses (Figure 2.3 (a)). From these results, the impact due to each

passing wheel can be extracted (Figure 2.3 (b)). The statistical results of the impacts due to multiple passing wheels is considered to be a critical indicator for the crossing condition assessment [8].

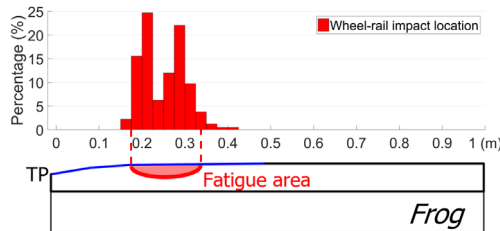


Figure 2.4. Example for the fatigue area detection.

Beside the wheel impacts, the impact location of each passing wheel could also be obtained, and the area where most of the wheel impacts were located was defined as the fatigue area, as shown in Figure 2.4. Practically, the fatigue area was simplified as the confidence interval of  $[\mu - \sigma, \mu + \sigma]$ , where  $\mu$  is the mean value of the wheel–rail impact locations, and  $\sigma$  is the standard deviation. Theoretically, 68% of the wheel impacts are located in this region. Although discrepancies exist, such a simplification can reflect the development of the wheel–rail contact condition. It has already been demonstrated in a previous study [8] that the fatigue area is a good representation of the crossing rail damage observed in the railway network, which makes it an important indicator for assessing a crossing’s condition. The wheel impacts and the fatigue area are further discussed later in combination with the developed MBS model.

B

## 2.2 Geometrical parameters

In the MBS model, the vehicle model was developed based on the double-deck train VIRM [39], which is the most commonly used train type in the monitored track section. The wheel type used in the VIRM train is S1002, and the rail type used in the track is UIC54 E1. The main parameters of the S1002 wheel profile and UIC54 E1 rail profile are shown in Figure 2.5.

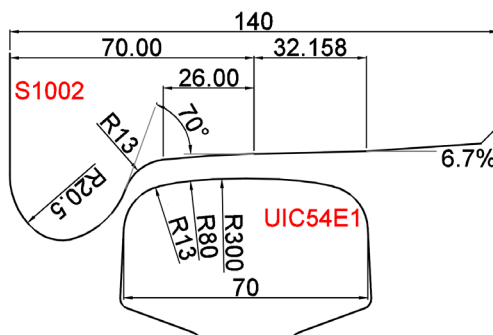


Figure 2.5. UIC54 E1 rail profile and S1002 wheel profile applied in the MBS model (dimensions in mm).

The design drawing of the modelled 1:9 cast crossing is shown in Figure 2.6 (provided by the Dutch railway infrastructure manager ProRail). In this drawing, a group of critical cross-

sections (from AA to GG) are defined to describe the crossing rail geometry. The total length of the crossing is approximately 3.7 m.

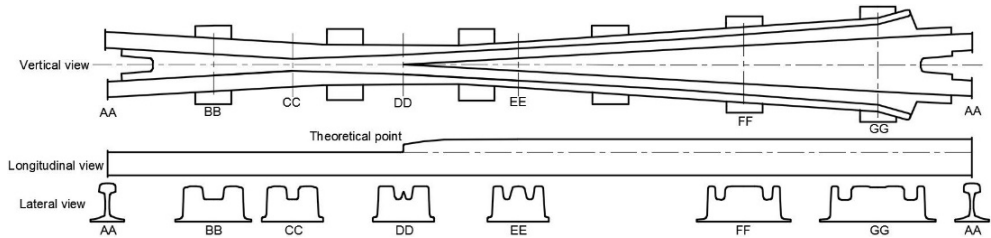


Figure 2.6. Geometry of the 1:9 cast crossing with defined critical cross-sections. (Drawing from Y. Ma)

The crossing geometry is one of the critical components in the development of the MBS vehicle-crossing model. According to the design, the TP is located in the section DD, the change of the rail geometry is mainly from section CC (-0.50 m from the TP) to section FF (1.51 m from the TP). For the nose rail, the geometry is gradually developed from an arc ( $r=2$  mm) in the TP to the UIC54 E1 profile in the section of 0.63 m from the TP (between sections EE and FF). Some additional sections are added to precisely define the crossing geometry, which can help to control the curvature of the arcs in the rail profiles and the height of the nose rail. The additional control sections between DD and FF are shown in Figure 2.7.

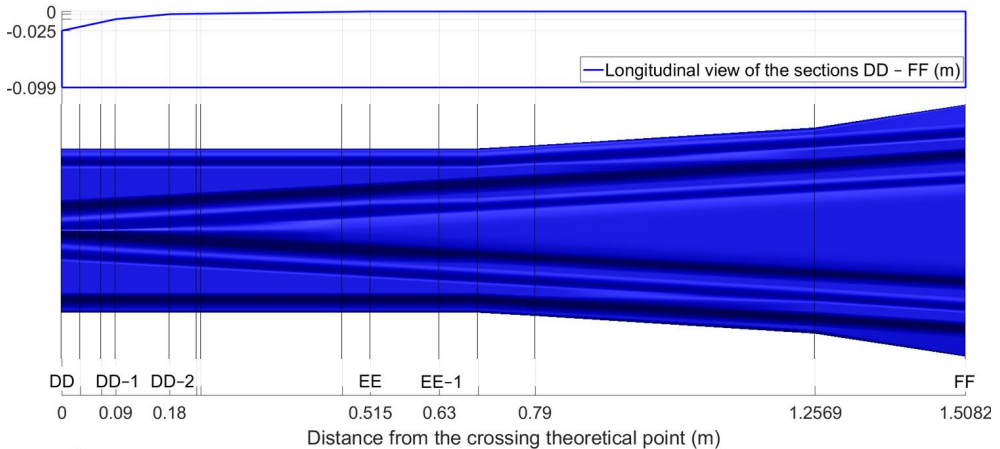


Figure 2.7. Additional cross-sections between DD and FF.

The height of the nose rail is defined by four control sections, namely section DD, two sections in every 0.09 m (DD-1 and DD-2, Figure 2.7) and section EE that is 0.515 m from DD. Similarly, the profile of the nose rail is defined by five control sections from the TP (DD) to the section EE-1 with the UIC54 E1 profile (0.63 m from the TP). Together with some auxiliary sections, the crossing geometry is defined by 23 control sections including AA, and the profiles between two control sections are automatically interpolated using the third-order spline curve.

## 2.3 Vehicle–crossing model

The model for the analysis of the vehicle–track interaction developed using the MBS method (implemented in VI-Rail software [40]) is shown in Figure 2.8 (a). The track model is a straight line with the crossing panel (Figure 2.8 (b), critical sections are marked in red) situated in the middle of the track. This study concentrated on the wheel–rail interaction in the crossing panel. Therefore, the switch panel (Figure 1.1) was simplified to a normal track. The profiles between two adjacent sections were automatically interpolated using the third-order spline curve. The total length of the track model was 100 m, which allowed for enough preloading space (around 1 m) before the vehicle entered into the crossing panel, as well as enough space after the vehicle passed through the crossing.

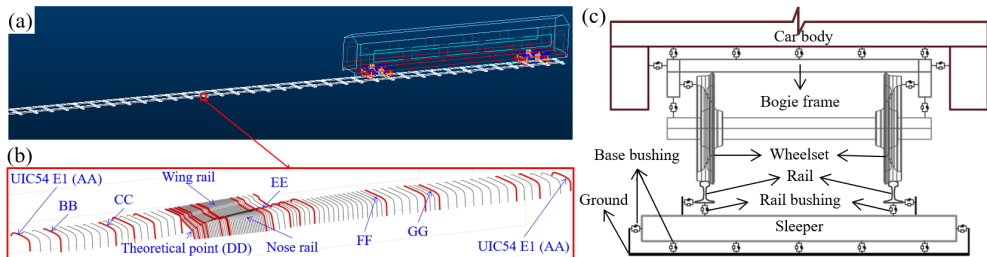


Figure 2.8. MBS model: (a) Vehicle–track model; (b) Flexible connections in the model; (c): Input crossing profiles (the control sections are marked in red).

The vehicle model was developed based on the VIRM train model with a total length of 27.5 m. The car body and bogie frames, as well as the wheelsets, were modelled as rigid bodies with both primary suspension and secondary suspension taken into account (Figure 2.8 (c)). The wheel–rail contact model was defined as the general contact element that used the actual wheel and rail profiles as the input, which allowed for variable wheel and rail profiles and a visualized contact graphic.

In the MBS simulation, the main outputs included the wheel displacements, rail accelerations (optional), wheel–rail contact forces and contact area, etc. The computation of the wheel–rail contact force was based on the Hertz contact theory. The elastic deformation was estimated according to the undeformed penetration, which was used for the contact area calculation. With the contact force and contact area, the wheel–rail contact pressure could be obtained. More information about the methodologies can be found in VI-Rail documentation [40].

## 2.4 Model parameters

Before the simulations, the properties of the track and the corresponding elements in the MBS models were thoroughly checked and adjusted to ensure that the MBS model and the FE model (used for the model verification) described the same real-life railway system (the monitored crossing). The vehicle/wheelset properties used in the MBS model are given in Table 2.1. The total axle load was calculated from the wheelset, bogie and car body masses, which was 10 t in this model. In the FE model [4], the axle load was also 10 t, while the weights of the bogies and the car body were all integrated into the simplified half-moving wheelset.

Table 2.1. Vehicle configuration of the MBS model

Item		Value
Wheel	Profile	S1002
	Radius (m)	0.46
Wheelset	Mass (kg)	1100
Bogie	Mass (kg)	3800
Car body	Mass (kg)	68000

The main properties of the rail model were Young’s modulus and density. For the rail pad and ballast, the stiffness and damping in both vertical and lateral directions were taken into account. The main track properties are given in Table 2.2, referring to Hiensch et al [41].

Table 2.2. Track properties of the MBS model

Track component		Value
Rail	Young’s modulus (GPa)	210
	Mass density (kg/m <sup>3</sup> )	7900
Rail pad	Vertical stiffness (MN/m)	1300
	Vertical Damping (kN·s/m)	45
	Lateral stiffness (MN/m)	280
	Lateral Damping (kN·s/m)	58
Ballast	Vertical stiffness (MN/m)	45
	Vertical Damping (kN·s/m)	32
	Lateral stiffness (MN/m)	45
	Lateral Damping (kN·s/m)	32

**B**

### 3 Model validation and verification

In the previous study [4], the FE wheel–crossing model for the crossing performance analysis was already developed and validated. The explicit FE model can take the plastic deformation and hardening of the material on a local scale into account, which is quite helpful for a better understanding for the wheel–rail interaction. To allow the combination of the MBS model with the FE model to thoroughly study the dynamic performance of railway crossings, it is of great importance that the MBS model is not only comparable with the measurement results but also close to the output of the FE model. Therefore, the developed vehicle–crossing MBS model was validated using the measurement results from the crossing instrumentation and verified using the simulation results from the FE model.

To better compare with the measurement and FE simulation results, the train running direction was set to the facing through route and the time step was adjusted to 0.0001 s, which was consistent with that in the FE simulation and the sampling frequency of the measurement data. The following response quantities that reflect the performance of the crossing were used to validate and verify the MBS model:

- The transition region where the wheel load transitioned from the wing rail to the nose rail, which is considered the most vulnerable region in the crossing.
- The vertical impact acceleration within the transition region.

Furthermore, some other output data from both the MBS and the FE simulations, including the vertical wheel trajectory and contact forces, were compared further to prove the compatibility of the two numerical models. All these results are presented and analysed in the following sections.

### 3.1 Transition region

In the MBS simulation, the transition region was where the wheel and crossing rail had two-point contact was recognized as the interval between the start of wheel–nose rail contact and the end of the wheel–wing rail contact. The size and location of the transition region reflected the smoothness of the wheel–rail contact transition from the wing rail to the nose rail. The transition region calculated using the MBS model was 0.196–0.227 m, as shown in Figure 3.1.

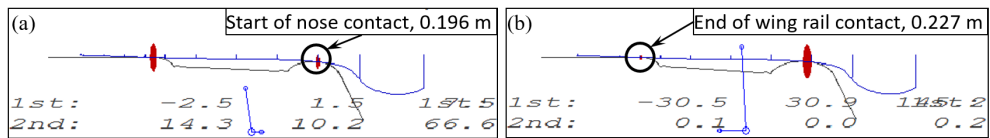


Figure 3.1. Transition region calculation in the MBS model. (a): Start contact with the nose rail; (b): End contact with the wing rail.

In real-life, the transition region was obtained through inspection and recognized as the overlapping shining bands on both the wing rail and the crossing nose. For the monitored crossing, the observed transition region was around 0.16–0.35 m with a size of 0.19 m, as shown in Figure 3.2. It can be seen that the transition region in the MBS simulation was within the observed one but was much smaller with a size of only 0.031 m. Such a phenomenon can be explained by the ideal initial conditions (no lateral angle or displacement) of the wheels used in the simulations and the absence of the wheel or rail irregularities. Moreover, the actual crossing was not new and had a certain level of plastic deformations and wear. In reality, every wheel passed the crossing with a certain angle and lateral shift that resulted in earlier/later contact in the transition region. The fact that the simulated transition region was included in the transition region of the real crossing proved the correctness of the MBS simulation results.

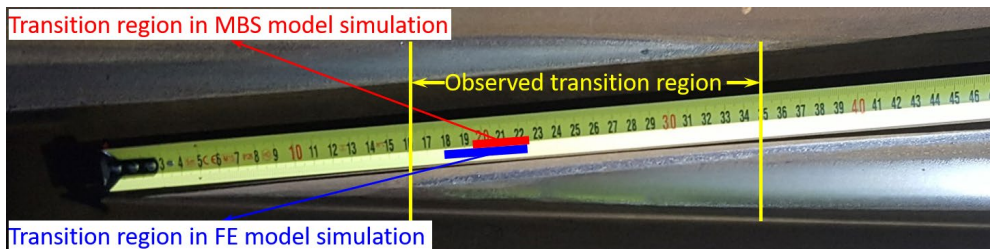


Figure 3.2. Transition regions obtained from the field observation and the numerical simulations.

The transition region in the FE model simulation [4] was 0.180–0.223 m with a size of 0.043 m, which was 30% larger than that obtained from the MBS simulation. Considering that in the MBS model the wheels and rails were simulated as rigid bodies without taking the material deformation into account, the transition regions in both methods were close to each other, which proved the compatibility of the MBS models with the FE model.

### 3.2 Impact acceleration and fatigue area

Due to the uncertainty of the wheel–rail contact situation, the measured impact accelerations of the passing wheels can vary a lot from one to another in amplitude and impact angles [8], as shown in Figure 3.3. In terms of extreme cases such as the wheel flange impact on the rail (Figure 3.3 (b)–(c)), the acceleration responses can be up to 10 times higher than that due to a normal passing wheel.

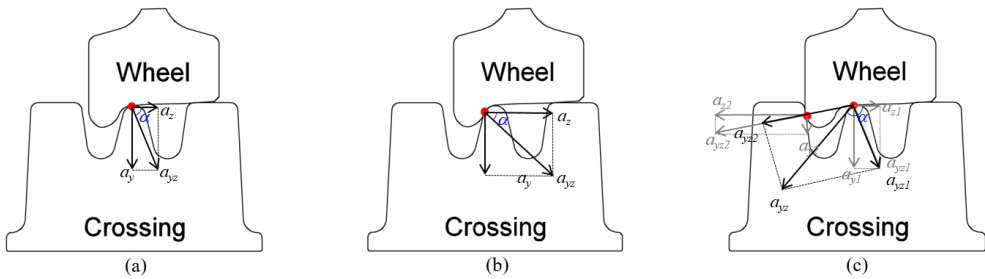


Figure 3.3. Wheel/rail contact situations: (a) Regular contact; (b) Irregular (positive) flange–nose rail contact and (c) Irregular (negative) flange–wing rail contact.

The measured acceleration signals for the model validation contained more than 1000 wheels from 90 trains. In both numerical models, no track or rail irregularities were considered, which means that in the numerical simulations the wheel (wheel-set) did not experience any additional disturbance when passing the crossing. As a result, the contact situation in these simulations is always regular (Figure 3.3 (a)). Therefore in the model validation, only the measured signals with the regular contact ( $|a_y| > |a_z|$ ) were used, which resulted in 500 selected passing wheels. The distribution of the impact accelerations due to these passing wheels is shown in Figure 3.4. The resulting histogram can be considered a normal distribution with a mean value of  $\mu = 47.15$  g and a standard deviation of  $\sigma = 17.65$  g.

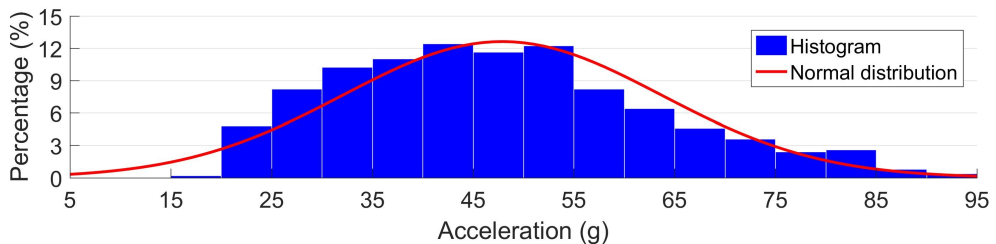


Figure 3.4. Histogram of the measured vertical accelerations used in the model validation.

The time-domain representation of the selected measured acceleration responses used in Figure 3.4 is given in Figure 3.5 (a). For a better interpretation, the time histories were aligned horizontally with the wheel–rail impact point (Figure 3.5 (b)), which were used for validation of the numerical model.

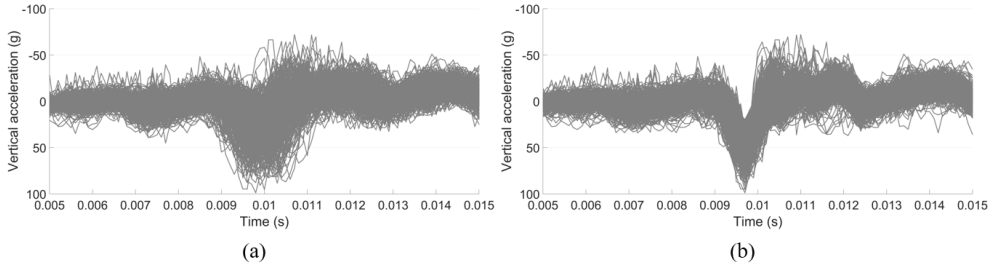


Figure 3.5. Measured acceleration responses: (a): Original time domain results; (b): Modified results with the time histories aligned horizontally with the impact point.

### Impact acceleration analysis

In the MBS model, the selected element used for the acceleration extraction was the rail with a lumped mass (Figure 3.6 (a)) located 0.3 m from the TP, which was the same as the location of the accelerometer in the crossing instrumentation (Figure 2.2). The comparison of the MBS simulation results with the measured responses and the FE simulation results is shown in Figure 3.6 (b).

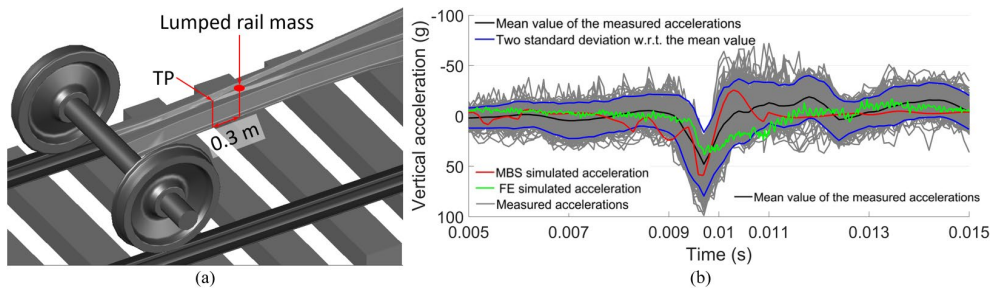


Figure 3.6. (a): Rail element for acceleration extraction in the MBS model; (b): Comparison of simulated accelerations with measured ones in the time domain.

From Figure 3.6 (b), it can be seen that the amplitude of the MBS simulated vertical acceleration was higher than the mean value of the measured acceleration as well as those from the FE simulation. It can also be noted that some of the measured accelerations had rebound after the impact (0.01–0.011 s). The MBS simulation also had such a rebound, while the FE simulation did not.

The discrepancy between the MBS and FE simulations were mainly due to the different assumptions in these models. In the MBS model, the wheelsets, rails and sleepers were all modelled as rigid bodies. In this case, the elasticity and damping of the vehicle–track system were underestimated, which led to the higher amplitude of the rail acceleration. While in the FE model, the crossing rail was modelled as a solid element without a hollow inside. This

means that the rail mass and stiffness were overestimated, which resulted in relatively small accelerations. Nevertheless, both simulation results were located within the interval  $[\mu-\sigma, \mu+\sigma]$  of the measured accelerations, meaning that although tolerable discrepancies existed, the MBS model was reasonably compatible with the field measurements, as well as with the FE model.

### Fatigue area analysis

The distribution of the wheel impact locations for the selected measurement data is shown in Figure 3.7. Based on these results, the fatigue area of the crossing was calculated, which was 0.221–0.249 m from the TP. In the MBS simulation, the wheel impact was located at 0.231 m from the TP, which was very close to the centre of the fatigue area, as marked in Figure 3.7. The fatigue area obtained from field measurement represents the degree of concentration of the wheel impacts, while the impact location in the MBS simulation was only from one wheel passage. Even so, the close results proved the correctness of the MBS model.

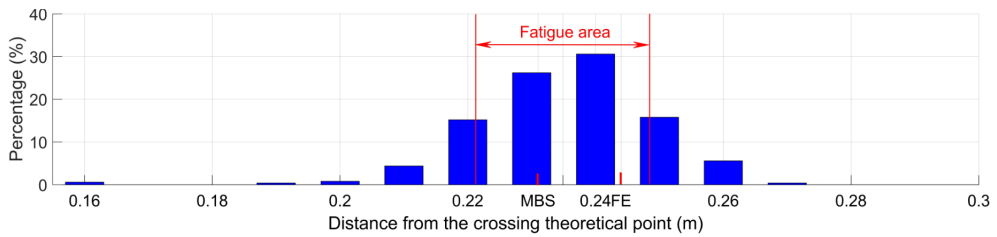


Figure 3.7. Distribution of wheel impact locations.

By comparison, the impact location in the FE simulation was 0.244 m, which was within the fatigue area as well. The close impact locations obtained from the MBS and FE simulations further proved the compatibility of these two models.

It must be noted that the wheel impacts and the fatigue area were calculated based on the selected wheels, which all involved in regular wheel–rail contacts, and the deviation was quite limited. Therefore, the resulting wheel impacts and fatigue area could not fully represent the real-life situation, and therefore should not be used to assess the crossing condition.

### 3.3 Other responses

In the numerical simulations, the wheel trajectory was related to the global responses of the models and characterised the correctness of the geometry representation in the models. On the other hand, the wheel–rail contact forces were related to the local properties and reflected the accuracy of the modelling of the wheel–rail contact. To further verify the compatibility of these two models, the vertical wheel trajectory, as well as the wheel–rail contact forces, were compared. The results and analysis are presented below. For the MBS simulation, the results from the first wheelset of the vehicle were applied.

#### Wheel vertical trajectory

The vertical wheel trajectory is the vertical displacement of the wheel relative to the rail. The change of the trajectory reflects the smoothness of the wheel passing through the crossing [35]. The vertical trajectories of the wheel in the MBS and FE simulations are shown in Figure 3.8. To provide a better comparison, the initial points of all the simulations were shifted to zero.

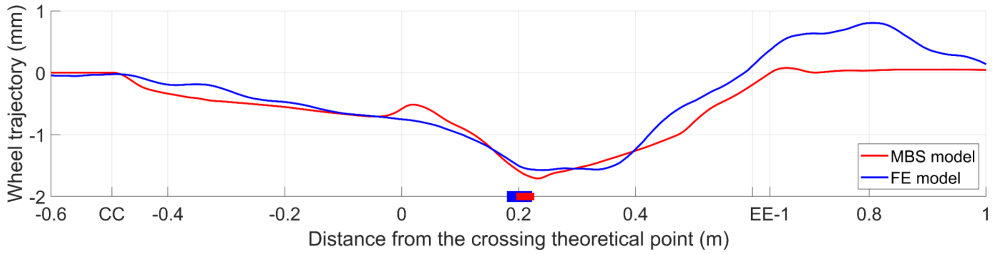


Figure 3.8. Wheel vertical trajectory comparison.

It can be seen from Figure 3.8 that despite some slight differences near the TP and after the transition region, the trajectories of both simulations were very close to each other. The maximum displacement in the MBS simulation was 1.71 mm at 0.231 m from the TP, while in the FE simulation, it was 1.57 mm at 0.242 m from the TP. The difference between these two models was only 9 %. It can be seen that the maximum values in both simulations occurred shortly after the transition of the wheel load, which was consistent with the impact acceleration.

In the MBS simulation, the trajectory showed several abrupt changes where the rail geometries were varied (e.g. in sections of CC, DD (TP), and EE-1). Such a development was in accord with the rigid body assumption in the MBS model. By comparison, the trajectory was more gently developed in the FE simulation, except for the slight rebound after section EE-1. Such a phenomenon can be explained by the fact that in the FE model, the wheel and rails were modelled as solid elements that allowed the material to deform. The material deformation due to the wheel-rail contact reduced the influence of small rail geometry variations. After the wheel passed the varied region (sections of CC – EE-1), the released wheel load led to the resilience of the rail and resulted in the slight rebound.

### Vertical contact forces

Figure 3.9 shows the vertical wheel-rail contact forces obtained from the MBS and FE models. Similar to the wheel trajectory comparison, the contact forces of both models were close to each other. In the MBS simulation, loss of wheel-rail contact occurred near the sections of CC, DD and EE-1, which were consistent with the locations where the wheel slightly rebounded (Figure 3.8). By comparison, the wheel-rail contact forces in the FE model developed smoother than those in the MBS models with less fluctuation.

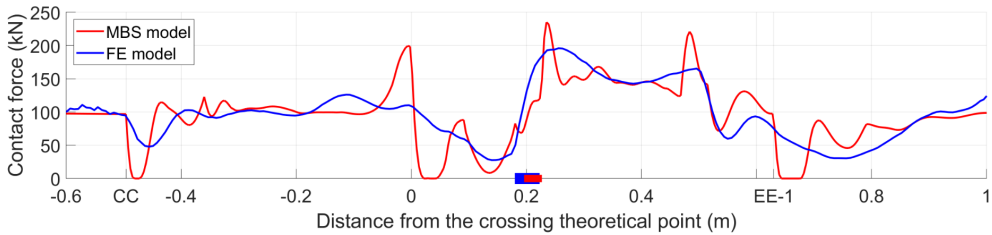


Figure 3.9. Comparison of the vertical wheel–rail contact forces.

The decrease in the contact forces of both models near section CC (Figure 3.9) indicated the beginning of the wing rail. At this point, the wheel–rail contact point on the wheel shifted farther from the wheel flange. In the MBS model, the sudden increase of the contact force near the TP reflected the effect of geometry change of the wing rail. It must be noted that the first peak values (after passing through the TP) of both models occurred after the respective transition regions. In the MBS simulation, the pick value was 235 kN, which was located at 0.235 m from the TP. Meanwhile in the FE model, it was 196 kN at 0.256 m. The second peak values were respectively 221 kN at 0.484 m in the MBS model and 165 kN at 0.496 m in the FE model.

It can be concluded that the contact forces obtained from the MBS model were comparable to those from the FE model. Some saltation in the MBS simulation was caused by modelling the wheel and rail elements as rigid bodies without considering the flexibilities of them. The slight hysteresis of the contact force calculation in the FE model was due to the effect of material deformation. From this point of view, the FE simulation was closer to the real situation. Even so, as a much more efficient alternative, the MBS model can also provide acceptable results.

The comparable results of the MBS model simulation with the FE model simulation further confirmed that both models described the same real-life system. For the same simulation presented in this section, the calculation time of the FE model was a few days, while that of the MBS model was only a few minutes. Therefore, the MBS model could be better applied in repetitive simulations such as rail geometry optimization and track irregularity analysis. For the dynamic performance analysis of railway crossings, this MBS model can be applied for the preliminary simulations to find out the critical situations. The obtained critical situations can then be used as the inputs into the FE model for detailed wheel–rail contact analysis. The combined MBS–FE methods form an integrated tool that can be applied to thoroughly study the dynamic performance of railway crossings.

In this section, the developed MBS model was validated and verified using both the measured results and the FE simulation results. Although tolerable discrepancies existed, the MBS model was reasonably compatible with field measurement and the FE model. It can be concluded that the MBS model can identify the main features of the wheel–rail impact at a crossing and can be used to analyse the crossing performance.

## 4 Application in crossing condition monitoring

In the crossing condition monitoring tool developed in [13], the condition assessment was made based on the changes in the dynamic performance indicators during the monitored period. In some cases, when the monitoring has to be performed on an already operating (not newly installed) crossing, its condition stage at that moment is difficult to determine, especially for a new type of crossing for which no monitored history is available. With the help of the MBS model developed in this study, the condition stage can be determined by comparing the measurement results with the simulation results that are based on the new (designed) crossing condition.

In a case where that the monitored crossing is identified to be in a degraded condition, the damage sources will need to be inspected. The inspected crossing damage can be then used as the input into the MBS model to simulate the crossing performance in the degraded condition. By comparing the simulation results with the measured ones, the damage sources of the crossing degradation can be verified. By knowing the crossing damage sources, proper maintenance actions can be implemented in a timely manner to avoid fatal defects and unexpected track disruptions.

In this section, the above-mentioned applications (identify condition stages and verify damage sources) are demonstrated in a monitored 1:9 trailing crossing, as presented below.

## B

#### 4.1 Condition stage identification

The studied 1:9 trailing crossing was located in the same double crossover as the facing crossing used for model validation in Section 3. Similarly, the trains were mainly passing the crossing mainly on the through route with the velocities up to 140 km/h. In contrast to the crossing analysed in Section 3, this crossing was passed in the trailing direction. Nevertheless, the same MBS model presented in Section 2 was used here to assess the crossing performance. The in situ performance of the crossing was obtained using the instrumentation (Figure 2.2). By comparing the measurement results with the simulation results of the crossing in the designed condition, the actual condition stage of the crossing was identified.

##### Measurement results and analysis

To process the measured data, the transition region in the crossing was inspected, as shown in Figure 4.1. The transition region was recognized as the region with overlapping shining bands. Using the track dimensions (the sleeper width was 0.20 m, and the clip is located at 0.30 m from the TP), the transition region of this crossing was located between 0.15–0.40 m from the TP.

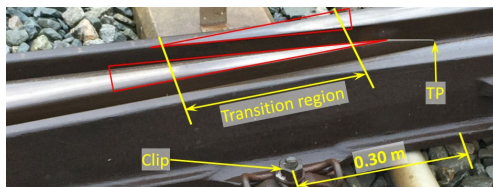


Figure 4.1. Transition region inspection of the monitored 1:9 trailing crossing.

The measurement data used for the crossing performance analysis consisted of the multiple wheel passages from one monitoring day. To be consistent with the numerical simulation, only the results from the VIRM trains with velocities of around 140 km/h, as used in the model, were selected, which resulted in a sample size of 78 passing wheels. The magnitude and location of the impacts due to these wheels were analysed and the results are presented in Figure 4.2.

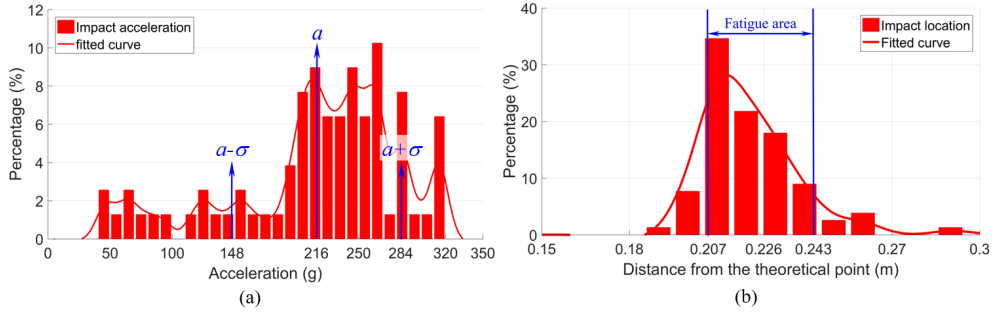


Figure 4.2. Measured dynamic responses. (a): Wheel impact distribution; (b): Impact location distribution.

Figure 4.2 (a) shows the magnitude distribution of the measured impact acceleration responses. The mean value was 216 g and the standard deviation was 68 g. The impact location distribution is shown in Figure 4.2 (b), from which it can be seen that the majority of the wheel impacts (the fatigue area) was located at a distance 0.207–0.243 m from the TP, resulting in a size of the fatigue area of 0.036 m.

The wheel-impact-based results were the most representative ones that reflected the condition of the crossing. In the next section, these results are compared with the simulation results of the crossing in the designed condition to identify the actual condition stage of the monitored crossing.

### Numerical simulation and condition stage identification

The MBS vehicle–crossing model used here to analyse the crossing performance in the designed condition was the same as the one presented in Section 2. The only difference was that the vehicle was now moving in the trailing direction, meaning that the wheel load on the crossing panel was transferred from the crossing nose to the wing rail. Using the designed (not worn) crossing shape and the other model parameters given in Section 2, the dynamic performance of the 1:9 trailing crossing was analysed.

The determination of the transition region using the simulation results is demonstrated in Figure 4.3. In contrast with the facing crossing, the wheel load in the trailing crossing moved from the crossing nose to the wing rail. Therefore, the transition region started from the wheel–wing rail contact (Figure 4.3 (a)) and ended up with the loss of wheel–crossing nose contact (Figure 4.3 (b)). The determined transition region is then was 0.182–0.225 m from the TP. This region was located within the one obtained during the field inspection (0.15–0.40 m), as shown in Figure 4.1. Thus, this confirmed that the MBS model developed for the trains passing in the facing direction was also valid for the trailing crossing analysis.

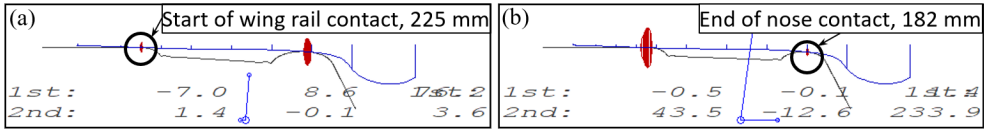


Figure 4.3. Transition region calculation of 1:9 trailing crossing in the designed condition. (a): Start of the contact with the wing rail; (b): End of the contact with the nose rail.

Figure 4.4 shows the vertical acceleration responses of the crossing rail due to the first passing wheel. It can be seen that the maximum acceleration (due to the wheel impact) was 95 g. This value was much lower than the mean value of the measured impact acceleration (216 g) shown in Figure 4.2 (a). Based on the significant difference (increase) between the measured and the simulated crossing accelerations (in the designed condition), it can be concluded that the monitored crossing was in highly degraded condition. This conclusion was in agreement with the experimental results of a 1:15 crossing presented in [13], wherein the significant increase (68%) in the observed measured acceleration was correlated with the visible damage of the crossing rail.

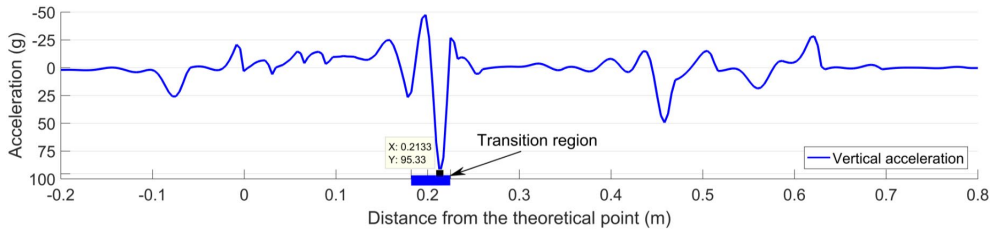


Figure 4.4. Rail vertical acceleration responses of a 1:9 trailing crossing in designed condition.

The fatigue area in the designed condition could not be determined from the numerical simulation. Yet, the wheel impact location could be obtained, which was 0.213 m from the TP (Figure 4.4). Similar to the transition region, the impact location was within the measured fatigue area (0.207–0.243 m, Figure 4.2 (b)).

It can be seen that in the degraded condition, the main change was the increased wheel impact acceleration, while the change in the impact location was rather limited. In the next step, the damage sources of this crossing were detected and verified, as presented in the next section below.

## 4.2 Damage source detection and verification

A typical SHM consists of five levels of activities, namely detection, localization, assessment, prediction and remediation [42]. In the previous section, the highly degraded condition of the monitored crossing was identified, which corresponded to the first step of SHM (determine the presence of structural damage). Then, the second step was to localize the damage to guide for crossing maintenance.

### Degraded crossing geometry

For a regularly degraded railway crossing, one of the typical damage sources is rail wear and deformation. For the monitored crossing, the rail profiles in the critical sections were measured, and compared with the designed profiles, as shown in Figure 4.5.

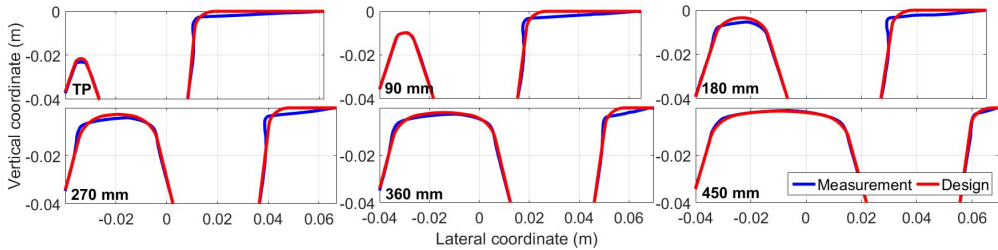


Figure 4.5. Measured crossing profiles in critical sections compared with the designed profiles.

It can be seen from Figure 4.5 that the crossing rail was worn and deformed. The most severe material damage on both the wing rail and the nose rail occurs in the section of 0.18–0.27 m, which was consistent with the distribution of the wheel impact locations (0.207–0.243 m, Figure 4.2 (b)). It can also be seen that the wear and deformation of the wing rail continued into the section of 0.00–0.18 m, meaning that the rail degradation extended out of the transition region. From this point of view, the crossing had been operated under degraded condition for a significant period.

**B**

### Numerical verification

The geometry measurement results presented in the previous section indicate the worn and deformed condition of the crossing and wing rails. To verify the effect of this damage on the crossing performance, the measured rail profiles were implemented in the MBS model and the numerical simulations were performed again.

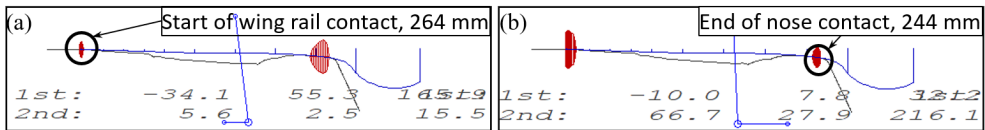


Figure 4.6. Transition region calculation of the 1:9 trailing crossing using measured rail geometry. (a): Start of the contact with the wing rail; (b): End of the contact with the nose rail.

The calculated transition region was 0.244–0.264 m, as shown in Figure 4.6. It can be seen that due to the severe wear and deformation of the wing rail, the initial wheel–wing rail contact (Figure 4.6 (a)) occurred earlier than that in the designed condition (0.225 m, Figure 4.3 (a)). Furthermore, the size of the transition region was reduced to only 0.020 m (compared with 0.043 m in the designed condition). The damaged rail geometry resulted in the transition region being shifted further away from the TP and there was a sharper transit of the wheel load from the crossing nose to the wing rail. The narrowed transition region with a shift farther from the TP can indicate a degraded crossing rail geometry. Such a changing pattern is in agreement with the development of the fatigue area that was observed in the previous

study of a 1:15 facing crossing in [13].

The simulation results of the crossing acceleration due to the first passing wheel is shown in Figure 4.7. Compared with the designed condition (Figure 4.4), the crossing acceleration in the degraded condition was increased from 95 g to 214 g, and such a result was quite close to the mean value of the measured results (216 g, Figure 4.2 (a)). These results indicated that the degraded rail geometry was the main cause of the increased accelerations.

It should be noted that the simulated wheel impact was located at 0.256 m from the TP, which was not consistent with the measured fatigue area (0.207–0.243 m, Figure 4.2 (b)). Furthermore, this location was 0.043 m farther than the wheel impact in the designed condition (0.213 m, Figure 4.4). Such a result indicated that besides the degraded crossing rail geometry, there might also be some other degraded elements in the monitored crossing (e.g. uneven ballast settlement) that need to be further investigated in combination with displacement measurement results.

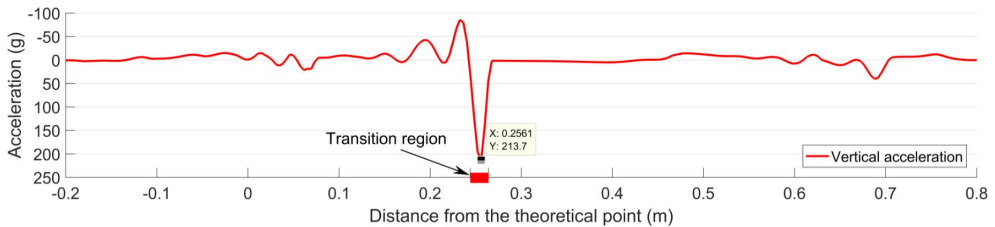


Figure 4.7. Simulation results of the 1:9 trailing crossing with rail wear and deformation taken into account.

To analyse the developments in the wheel–rail interaction, the contact forces in both the designed and degraded conditions were also compared. The results are presented in Figure 4.8. Beside the dramatically increased impact force (438 kN in the degraded condition vs 270 kN in the designed condition), the rail damage resulted in the loss of wheel–rail contact in the 0.27–0.46 m region. Such results show the influence of rail wear and deformation on the wheel’s behaviour. Due to the interaction with the other wheel from the same wheelset as well as the influence of the other wheelset within the same bogie, the wheel was running through the crossing could not fully follow the damaged rail profile. Consequently, when the wheel resumed contact with the rail, the contact force was dramatically increased and the wheel load was sharply shifted from the crossing nose to the wing rail. Such a sharp transition of the wheel load led to a higher impact on the crossing.

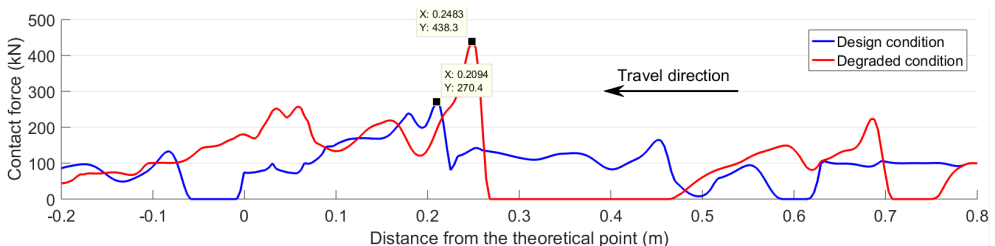


Figure 4.8. Wheel–rail contact forces in different rail conditions.

Based on the results and analysis in this section, it can be seen that the developed MBS model was successfully applied to help identify the condition stage of a crossing and to verify the damage sources in combination with field inspection. Furthermore, it can be concluded that the monitored 1:9 trailing crossing was in a highly degraded condition. The high wheel–rail impacts were mainly correlated with the worn and deformed rail geometry. Repair welding and grinding in this crossing are urgently required to avoid further damage (e.g. cracks, spalling, etc.).

The application of the MBS model in the condition monitoring of the 1:9 trailing crossing further confirmed that the condition indicators (proposed based on 1:15 facing crossing in the previous study [13]) are applicable for different types of crossings (e.g. angle, traffic direction, etc.), which provides a better opportunity for the promotion of the condition monitoring system.

The deformed crossing geometry in the studied crossing was the dominant factor causing the degradation, though there is still likely to be some other damage that was not detected, e.g. ballast settlement, track misalignment, etc. The developed MBS model proved to be sufficient for the crossing condition stage identification and damage source verification, yet a necessary track inspection was still required. A better way to master the crossing condition is to combine the MBS model with the condition monitoring. With sufficiently detected damage sources, proper and timely maintenance actions can be planned, which will help improve the crossing performance and ultimately lead to sustainable railway crossings.

## 5 Conclusions

In this study, an MBS model for the crossing performance analysis was developed. The model was validated and verified using the field measurement results and the FE simulation results. With the assistance of this MBS vehicle–crossing model, the condition stage of a monitored crossing is identified, and the source of the crossing damage is verified. Based on the results and analysis, the following conclusions can be drawn.

The MBS model was validated and verified using the field measurement and FE simulation results. The comparable results of the transition region, wheel impact acceleration and impact location proved the validity of the MBS model for the wheel–crossing dynamic analysis. The comparison of the simulation results from the MBS model and the FE model correlated very well. It was verified that the MBS model could identify the main features of the crossing’s dynamic behaviour. The differences between these two models could be explained by the different simplifications in each model, such as the simplified beam element of the rail (instead of solid element) in the MBS model and using a half wheelset (instead of a whole wheelset or bogie) in the FE model.

The MBS model displayed fast simulations, which is suitable for analysis that requires repetitive simulations. Therefore, it can be applied in the preliminary analysis (e.g. parametric study, rail geometry optimization and track irregularity analysis) seeking critical operating conditions. The FE model can then be used to perform detailed wheel–rail contact analysis based on the critical conditions obtained from the MBS simulations.

Using the developed MBS vehicle–crossing model, the degraded condition stage of a monitored 1:9 trailing crossing was successfully identified. The rail wear and deformation were further verified as the primary damage sources. The simulation results proved that the rail damage of the crossing was already at a severe level, showing a highly deteriorated crossing performance. With the assistance of the MBS model, the procedure for the crossing condition assessment can be dramatically simplified.

Combined with the simulation results, the measurement results regarding the degraded 1:9 trailing crossing also proved the applicability of the condition indicators for different crossing types (e.g. crossing angle, travel directions, etc.), which provides a sound basis for promoting the indicators in the condition monitoring of railway crossings.

The MBS model is a necessary supplement to the SHM system for railway crossings. Through identifying the crossing condition stage, necessary crossing maintenance actions can be better planned and implemented in a timely manner, which can help avoid fatal crossing damages and unexpected traffic interruptions. With sufficient condition information of railway crossings, the crossing maintenance strategy can be ultimately improved from “failure reactive” to “failure proactive” and lead to sustainable railway crossings with better performance.

## B

### References

- [1] C. Wan, V.L. Markine, I.Y. Shevtsov, Optimisation of the elastic track properties of turnout crossings. *Proceedings of the Institution of Mechanical Engineers Part F: Journal of Rail and Rapid Transit*, vol. 230, 2016, p. 360-373.
- [2] P. Torstensson, G. Squicciarini, M. Krüger, B. Pålsson, J. Nielsen, D. Thompson, Wheel-rail impact loads and noise generated at railway crossings – Influence of vehicle speed and crossing dip angle, *Journal of Sound and Vibration*, vol. 456, 2019, p. 119-136.
- [3] L. Xin, V.L. Markine, I.Y. Shevtsov, Numerical analysis of the dynamic interaction between wheelset and turnout crossing using explicit finite element method, *Vehicle System Dynamics*, vol. 54, 2016, p. 301-327.
- [4] Y. Ma, A.A. Mashal, V.L. Markine, Modelling and experimental validation of dynamic impact in 1:9 railway crossing panel, *Tribology International*, vol. 118, 2018, p. 208-226.
- [5] ProRail, *Ontwerpvoorschrift (Baan en Bovenbouw) Deel 6.1: Wissels en kruisingen Alignement, tussenafstanden, overgangsvrije zones en bedieningsapparatuur, V006*, the Netherlands, 2015, p. 12.
- [6] L.F. Molina, E. Resendiz, J.R. Edwards, J.M. Hart, C.P.L. Barkan, N. Ahuja, Condition Monitoring of Railway Turnouts and Other Track Components Using Machine Vision, *Proceedings of the Transportation Research Board 90th Annual Meeting*, November 2010.
- [7] A.T. Cornish, Life-time monitoring of in service switches and crossings through field experimentation, PhD thesis, Imperial College London, London, UK, 2014.

- [8] S. Kaewunruen, Monitoring structural deterioration of railway turnout systems via dynamic wheel/rail interaction, *Case Studies in Nondestructive Testing and Evaluation*, vol. 1, 2014, p. 19-24.
- [9] P. Wang, Li. Wang, R. Chen, J. Xu, J. Xu, M. Gao, Overview and outlook on railway track stiffness measurement, *Journal of Modern Transportation*, Vol. 24 (2), 2016, p. 89-102.
- [10] F. Balouchi, A. Bevan, R. Formston, Detecting Railway Under-Track Voids Using Multi-Train in-Service Vehicle Accelerometer, 7th IET Conference on Railway Condition Monitoring, Birmingham, United Kingdom, 27-28 September 2016.
- [11] G.J. Yeo, Monitoring Railway Track Condition Using Inertial Sensors on an in-Service Vehicle, PhD thesis, University of Birmingham, Birmingham, United Kingdom, June 2017.
- [12] V.L. Markine, X. Liu, A.A. Mashal, Y. Ma, Analysis and improvement of railway crossing performance using numerical and experimental approach: application to 1:9 double crossovers, *Proceedings of the 25th International Symposium on Dynamics of Vehicles on Roads and Tracks*, Queensland, Australia, 14-18 August 2017.
- [13] X. Liu, V.L. Markine, H. Wang, I.Y. Shevtsov, Experimental tools for railway crossing condition monitoring, *Measurement*, vol. 129, 2018, p. 424-435.
- [14] A. De Rosa, S. Alfi, S. Bruni, Estimation of lateral and cross alignment in a railway track based on vehicle dynamics measurements, *Mechanical Systems and Signal Processing*, vol. 116, 2019, p. 606-623.
- [15] H. Tsunashima, Condition Monitoring of Railway Tracks from Car-Body Vibration Using a Machine Learning Technique, *Applied Sciences*, vol. 9, 2019, No. 2734.
- [16] C. Chen, T. Xu, G. Wang, B. Li, Railway turnout system RUL prediction based on feature fusion and genetic programming, *Measurement*, vol. 151, 2020, No. 107162.
- [17] M. Pletz, W. Daves, H. Ossberger, A wheel passing a crossing nose: dynamic analysis under high axle loads using finite element modelling, *Proceedings of the Institution of Mechanical Engineers Part F: Journal of Rail and Rapid Transit*, vol. 226, 2012, p. 603-611.
- [18] M. Wiest, E. Kassa, W. Daves, J.C.O. Nielsen, H. Ossberger, Assessment of methods for calculating contact pressure in wheel-rail/switch contact, *Wear*, vol. 265, 2008, p. 1439-1445.
- [19] J. Xiao, F. Zhang, L. Qian, Numerical simulation of stress and deformation in a railway crossing, *Engineering Failure Analysis*, vol.18, 2011, p. 2296-2304.
- [20] E. Kassa, J.C.O. Nielsen, Dynamic train-turnout interaction in an extended frequency range using a detailed model of track dynamics, *Journal of sound and vibration*, vol. 320, 2009, p. 893-914.
- [21] A. Johansson, B. Pålsson, M. Ekh, J.C.O. Nielsen, M.K.A. Ander, J. Brouzoulis, E. Kassa, Simulation of wheel-rail contact and damage in switches & crossings, *Wear*, vol. 271, 2010, p. 472-481.

- [22] M. Pletz, W. Daves, H. Ossberger, A wheel set/crossing model regarding impact, sliding and deformation - explicit finite element approach, *Wear*, vol. 294, 2012, p. 446-456.
- [23] V.L. Markine, M.J.M.M. Steenberg, I.Y. Shevtsov, Combatting RCF on switch points by tuning elastic track properties. *Wear*, vol. 271, 2011, p. 158-167.
- [24] G. Kouroussis, D.P. Connolly, G. Alexandrou, K. Vogiatzis, Railway ground vibrations induced by wheel and rail singular defects, *Vehicle System Dynamics*, vol. 53(10), 2015, p. 1500-1519.
- [25] Z. Wei, C. Shen, Z. Li and R. Dollevoet, Wheel–Rail Impact at Crossings-Relating Dynamic Frictional Contact to Degradation, *Journal of Computational and Nonlinear Dynamics*, vol. 12 (4), 2017, p. 041016 1-11.
- [26] A.A. Mashal, Analysis & Improvement of railway crossing using explicit finite element method, MSc thesis, Delft University of Technology, Delft, the Netherlands, 2016.
- [27] L. Xin, V.L. Markine, I.Y. Shevtsov, Analysis of the effect of repair welding / grinding on performance of railway crossings using field measurements and finite element modelling, *Proceedings of the Institution of Mechanical Engineers Part F: Journal of Rail and Rapid Transit*, vol. 232, 2018, p. 645-662.
- [28] R. Skrypnik, M. Ekh, J.C.O. Nielsen, B.A. Pålsson, Prediction of plastic deformation and wear in railway crossings – Comparing the performance of two rail steel grades, *Wear*, Vol. 428-429, 2019, p. 302-314.
- [29] T.M.H. Arts, Measuring the neutral temperature in railway track during installation and use, MSc thesis, Delft University of Technology, Delft, the Netherlands, 2011.
- [30] J.S. Siew, O. Mirza, S. Kaewunruen, Torsional Effect on Track-Support Structures of Railway Turnouts Crossing Impact, *Journal of Transportation Engineering, Part A: Systems*, vol. 143(2), 2017, No. 06016001.
- [31] X. Shu, N. Wilson, C. Sasaoka, J. Elkins, Development of a real-time wheel/rail contact model in NUCARS and application to diamond crossing and turnout design simulations, *Vehicle System Dynamics*, vol. 44, 2006, p. 251-260.
- [32] E. Kassa, J.C.O. Nielsen, Dynamic interaction between train and railway turnout: full-scale field test and validation of simulation models, *Vehicle System Dynamics*. Vol. 46, 2008, 521-534.
- [33] B. Pålsson, J.C.O. Nielsen, Wheel-rail interaction and damage in switches and crossings, *Vehicle System Dynamics*, Vol. 50, 2012, p. 43-58.
- [34] C. Wan, V.L. Markine, I.Y. Shevtsov, Improvement of vehicle–turnout interaction by optimizing the shape of crossing nose, *Vehicle System Dynamics*, vol. 52, 2014, p. 1517-1540.
- [35] C. Wan, V.L. Markine, I.Y. Shevtsov, Analysis of train/turnout vertical interaction using a fast numerical model and validation of that model. *Proceedings of the Institution of Mechanical Engineers Part F: Journal of Rail and Rapid Transit*, vol. 228, 2014, p. 730-743.

- [36] C. Wan, V.L. Markine, Parametric study of wheel transitions in railway crossings. *Vehicle System Dynamics*, vol. 53, 2015, p. 1876-1901.
- [37] J.J.J. Wegdam, Expert tool for numerical & experimental assessment of turnout crossing geometry, MSc thesis, Delft University of Technology, Delft, The Netherlands, 2018.
- [38] I.V. Shevtsov, Rolling Contact Fatigue problems at Railway Turnouts, [http://www.slm-flanders.be/sites/default/files/events/Meeting\\_Materials\\_Nov2013/mm\\_13112013\\_ivan\\_shevtsov\\_prorail.pdf](http://www.slm-flanders.be/sites/default/files/events/Meeting_Materials_Nov2013/mm_13112013_ivan_shevtsov_prorail.pdf), 13 November 2013.
- [39] H. Wang, V.L. Markine, X. Liu, Experimental analysis of railway track settlement in transition zones, *Proceedings of the Institution of Mechanical Engineers Part F: Journal of Rail and Rapid Transit*, vol. 232 (6), 2018, p. 1774-1789.
- [40] VI-grade GmbH, VI-Rail 16.0 Documentation, © 2014 VI-grade engineering software & services, Marburg, Germany, 2014.
- [41] M. Hiensch, J. Nielsen, E. Verheijen, Rail corrugation in The Netherlands - measurements and simulations, *Wear*, vol. 253, 2002, p. 140-149.
- [42] D. Huston, Structural Sensing, Health Monitoring, and Performance Evaluation, University of Vermont, Burlington, USA, 2011.



# Paper C

## Correlation Analysis and Verification of Railway Crossing Condition Monitoring

X. Liu, V.L. Markine

*Sensors*, vol. 19 (19), 2019, 4175.

<https://doi.org/10.3390/s19194175>

### Abstract

This paper presents a correlation analysis of the structural dynamic responses and weather conditions of a railway crossing. Prior to that, the condition monitoring of the crossing as well as the indicators for crossing condition assessment are briefly introduced. In the correlation analysis, strong correlations are found between acceleration responses with irregular contact ratios and the fatigue area. The correlation results between the dynamic responses and weather variables indicate the influence of weather on the performance of the crossing, which is verified using a numerical vehicle-crossing model developed using the multi-body system (MBS) method. The combined correlation and simulation results also indicate degraded track conditions of the monitored crossing. In the condition monitoring of railway crossings, the findings of this study can be applied to data measurement simplification and regression , as well as to assessing the conditions of railway crossings.

**Keywords:** Railway Crossing; Condition Monitoring; Condition Indicator; Correlation Analysis; Weather Impact; Numerical Verification.

## 1 Introduction

Railway turnouts are essential components of railway infrastructure and provide the ability for trains to transfer from one track to the other. In the meantime, a gap between the wing rail and nose rail in the crossing panel (Figure 1.1 (b)) introduces a discontinuity in the rail. As a result of trains passing through, the high wheel–rail impact due to the high train velocity causes this type of crossing to suffer from severe damage such as cracks (Figure 1.1 (c)) and spalling (Figure 1.1 (d)), and the service lives of some railway turnouts are only 2-3 years. In order to improve the maintenance of the crossing and prolong service life, it is better to perform maintenance in a predictive way by developing a structural health monitoring (SHM) system for railway crossings [1].

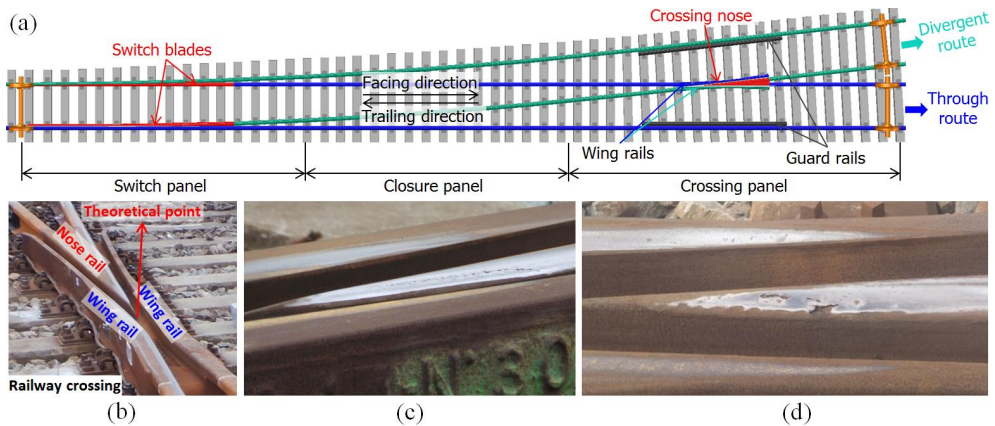


Figure 1.1. (a): Standard left-hand railway turnout with 1:9 crossing; (b): Crossing panel in site; (c): Plastic deformation with cracks; (d): Spalling.

In order to obtain information on damage detection, localization and condition assessment in SHM systems, it is important to get insight into the performance of the structures. In recent years, SHM has drawn increasingly more attention in the railway industry. D. Barke and W.K. Chiu reviewed the major contributions of condition monitoring in regards to wheels and bearings [2]. Based on digital image correlations, D. Bowness et al. measured railway track displacement using a high speed camera [3]. The axle box acceleration (ABA) system has been widely applied in the condition monitoring [4] and damage detection [5]-[6] of railway tracks. However, most of the contributions of SHM are based mainly on normal tracks. Z. Wei et al. have applied the ABA system in railway crossing damage detection [7]. However, as a special and vulnerable component in the railway track system, the study on crossings in terms of condition monitoring are still limited.

In the existing studies, the performance analysis of crossing has been based mainly on numerical approaches. For instance, finite element (FE) wheel-crossing models have been applied to calculate plastic deformation and frictional work [8], to simulate the distribution of stresses in the crossing nose [9] and to predict the fatigue life of a crossing [10]. Also, multi-body system (MBS) vehicle-crossing models have been used for general train-track interaction analysis [11], track elasticity analysis [12], crossing geometry optimization [13]-

[15] and so on. Due to restricted track access, high costs and time consumption, field measurements have mainly been used for numerical model validation [9], [16]. The numerical models are usually developed according to a certain hypothesis with a focus on specific problems. However, for damage detection and assessments of crossing conditions, the numerical approach alone is not enough, and monitoring the conditions of in-service railway crossings is highly necessary.

In real life, the wheel-rail contact in a crossing can be affected by many factors. Some factors are related to the train track system, such as train type [17], velocity [18], axle load [18]-[19], wheel-rail friction [18], crossing geometry [18]-[19], track alignment [19], track elasticity [12] and so on. Some factors are related to the crossing environment, such as the contaminants on the rail [19]-[21] and rail temperature variation [22]-[23]. All these factors, especially those introduced by the environment, make the measurement data noisy and the crossing condition cannot be clearly shown [24]. In order to properly analyse the measurement data for monitoring the crossing condition, the first step is to figure out the influence of the above mentioned factors on the performance of the crossing.

In this study, the influence of train track system-related factors is minimized through data selection and a filtering process. Specifically, train type, velocity and the bogie number are restricted to a certain scope. In order to estimate the influence level of the external factors (such as the weather condition), a correlation analysis using Pearson's correlation coefficient, which is usually applied to quantitatively evaluate the correlation strength between two variables, is performed. The correlation analysis results are verified using a vehicle-crossing model developed using the multi-body system (MBS) method. In this model, the weather changes are modelled according to changes in the properties of the affected track elements. The correlation between the weather condition and the dynamic responses of the crossing provides the foundation for long-term measurement data regression, which will be applied in the crossing degradation assessment procedure. In addition to weather factors, the correlation strengths between the dynamic responses of the crossing are also analysed, which can be applied to provide guidance for the selection and post-processing of the measurement data and to improve the efficiency of analysing a large amount of data.

The paper is organized as follows. The condition-monitoring procedure of a railway crossing, including the crossing instrumentation, is presented in Section 2. The indicators applied for the crossing condition assessment are briefly introduced in Section 3. The correlation analysis, including the dynamic responses and weather variables, are given in Section 4. In Section 5, the mechanisms of the weather effects are analysed and verified through numerical simulation. Finally, in Section 6, the conclusions based on the correlation analysis are provided and further applications for the degradation procedure description of the monitored crossing are discussed.

## 2 Railway crossing condition monitoring

In this section, monitoring the condition of a railway crossing is discussed. The crossing instrumentation and a brief procedure for processing the measurement data are described.

## 2.1 Crossing instrumentation

The monitored crossing in this study is a cast manganese steel crossing with an angle of 1:9, which is the most commonly used crossing for Dutch railway tracks (more than 60% [25]). As part of a double crossover, the crossing is mainly used for through-facing routes (Figure 1.1 (a)). This railway line is mainly used for passenger transportation with a velocity of passing trains up to 140 km/h. The crossing is instrumental for using the system that has been introduced, and has been actively used in previous studies[1], [17], [19], [26]. An overview of the crossing instrumentation is given in Figure 2.1.

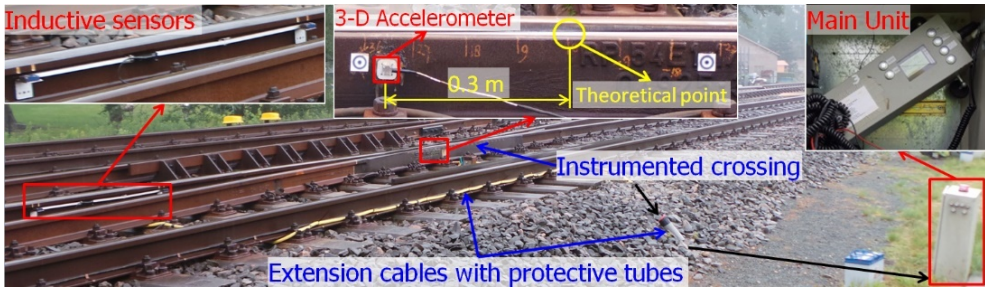


Figure 2.1. Overview of the crossing instrumentation

The main components of this device are a 3-D accelerometer attached to the crossing rail, a pair of inductive sensors attached to the rails in the closure panel and the data logger (main unit) installed on the outside of the track. The inductive sensors are used for train detection and the initiation of the measurements, as well as for train velocity determination. All of the sensors are connected to the data logger for data storage and basic analysis of the data. The measurement range and sampling frequency of the acceleration sensor are 500 g and 10 kHz, respectively. The main measured data are the 3-D acceleration responses (i.e.,  $a_x$ ,  $a_y$  and  $a_z$ ) of the crossing due to the passing trains.

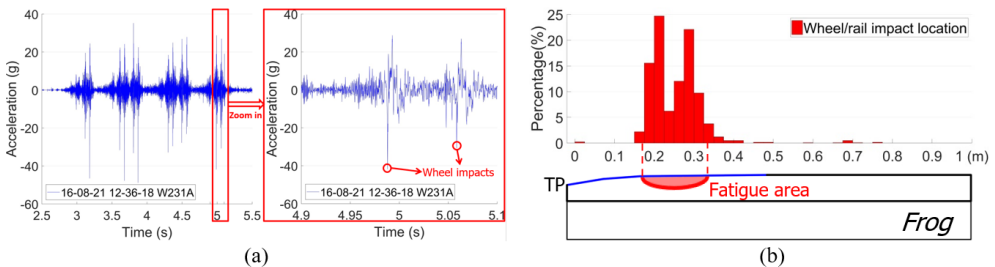


Figure 2.2. Examples of output of crossing instrumentation. (a): Vertical acceleration response due to one train passage; (b): Wheel impact location distribution.

An example of the vertical acceleration response in a time domain due to one passing train with 12 wheelsets is shown in Figure 2.2 (a). It can be seen from this figure that the time and location of each wheel's impact on the crossing can easily be obtained from the acceleration responses. The region where most of the wheel impact is located is defined as the fatigue area

(Figure 2.2 (b)), which can be used for assessing crossing conditions based on a large amount of data.

## 2.2 Measurement data selection and processing

The crossing monitored in this study was in a new state at the beginning of the observations. In order to reduce the influence of vehicle variations, the measurement results considered here were restricted to one type of train, namely the VIRM (double-deck) trains that pass with a velocity of around 140 km/h. Moreover, the accelerations caused only by the first bogie were considered. Thus, the remaining uncertainties in the measured data mainly coming from the environment (e.g., the weather). Depending on the amount of monitoring data, the measurement results will be analysed on three different levels, namely,

- the dynamic response due to the passage of a single wheel;
- the results of multiple-wheel passages from one monitoring day; and
- the statistical results from multiple monitoring days.

An example of vertical acceleration responses in different levels is shown in Figure 2.3.

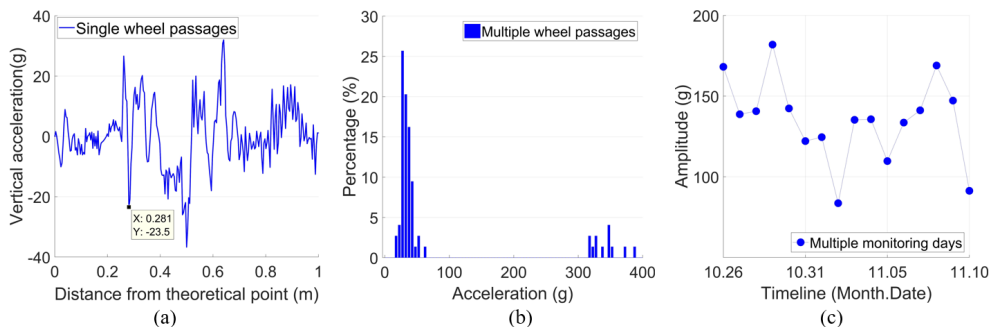


Figure 2.3. Example of measured vertical acceleration responses. (a): From single wheel passage; (b): From multiple wheel passages from one monitoring day; (c): From multiple monitoring days.

The response due to single wheel passages was directly obtained from the measured time domain signal (Figure 2.3 (a)). The distribution of the maximum impact acceleration from each passing wheel constituted the results of multiple wheel passages (Figure 2.3 (b)). For the statistical results from multiple monitoring days, each point represented the average value of the impact vertical accelerations of the recorded passing wheels from one monitoring day (Figure 2.3 (c)). It can be seen that each wheel passed the railway crossing differently. Based on a single wheel's passage it is difficult to assess the performance of the crossing. Yet, some conclusions on wheel–rail interaction can still be drawn based on these data. The statistical analysis based on multiple passing wheels was more applicable for assessing the condition of the railway crossing.

## 3 Condition indicators

In this section, the indicators for assessing a crossing's condition are briefly described. These indicators are calculated based on the transition region and consist of the irregular contact ratio, 3-D acceleration responses and the fatigue area. To demonstrate the condition analysis procedure, some typical examples of the measurement results from the monitored crossing are presented.

### 3.1 Transition region

The transition region of a crossing is the location where the wheel load is transferred from the wing rail to the nose rail (or vice versa, depending on the traveling direction). In practice, the wheel-rail contact points in the crossing can be recognized by looking at the shining band on the rail surface. An example of such a band on the monitored crossing is given in Figure 3.1 and denoted by the red triangle areas. Using these bands, the transition region can be then estimated by the overlapping area of the shining bands on the wing rail and nose rail. Based on this image, the transition region of the monitored crossing is located around 0.15-0.40 m as measured from the crossing's theoretical point (TP).

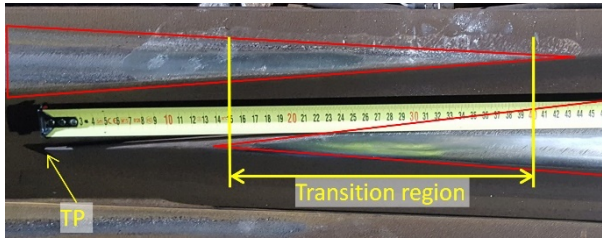


Figure 3.1. Transition region of the monitored crossing

From a performance point of view, the transition region is the most vulnerable part of the crossing, since the rail is thinner and the wheel forces are higher than in the other parts of the turnout. Therefore, to analyse the dynamic performance of the crossing, only the accelerations located within the transition region are taken into account.

### 3.2 Wheel-rail impact status

In an ideal situation, the wheel will pass through the transition region smoothly without flange contact (Figure 3.2 (a)). In such a case, the vertical acceleration ( $a_y$ ) will dominate the 3-D acceleration responses. However, in real life, due to disturbances existing in the track, each wheel passes the crossing at a different angle, which results in different impact accelerations in all the three directions. Referring to the measurement results, the impact angle can be defined by the factor of  $k = a_z/a_y$ . It has been found [1] that when the impact factor exceeds a certain level ( $|k| \geq 1$ ), there is a large chance that the wheel flange will hit the nose rail or wing rail of the crossing (depending on the direction). Such flange contact is recognized as irregular positive (Figure 3.2 (b)) or negative (Figure 3.2 (c)) contact.

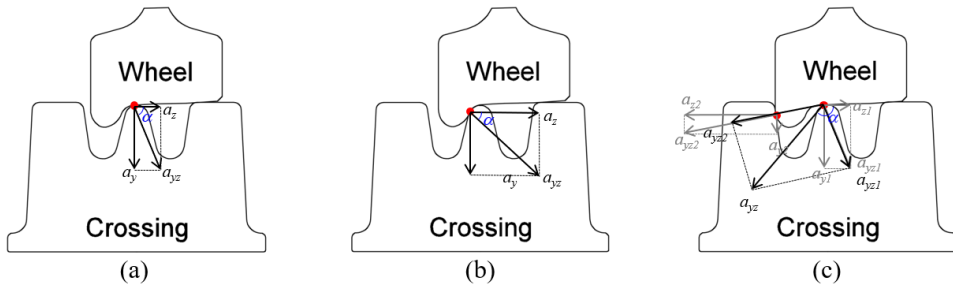


Figure 3.2. Wheel/rail contact situations. (a) Regular contact; (b) Irregular positive contact when wheel flange hits the crossing nose; (c) Irregular negative contact when wheel flange hits wing rail.

The irregular contact ratio is usually at a low level (below 3%) for well-maintained crossings, but might dramatically increase when damage occurs to the crossing (above 20%) [1]. Thus, the irregular contact ratio can be applied as a key indicator in assessing the conditions of railway crossings.

### 3.3 3-D acceleration responses

For the monitored crossing, the regular and irregular contact wheels showed dramatic differences in the 3-D impact acceleration responses ( $a$ ). For regular passing wheels, the impact vertical acceleration was usually below 50 g, while such impact could be above 300 g for irregular passing wheels. Examples of the 3-D acceleration responses from typical regular and irregular passing wheels are shown in Figure 3.3 and Figure 3.4, respectively. In order to better understand the wheel-rail contact, the transition region obtained from field observation (Figure 3.1) is marked in the figures as a green line on the horizontal axis.

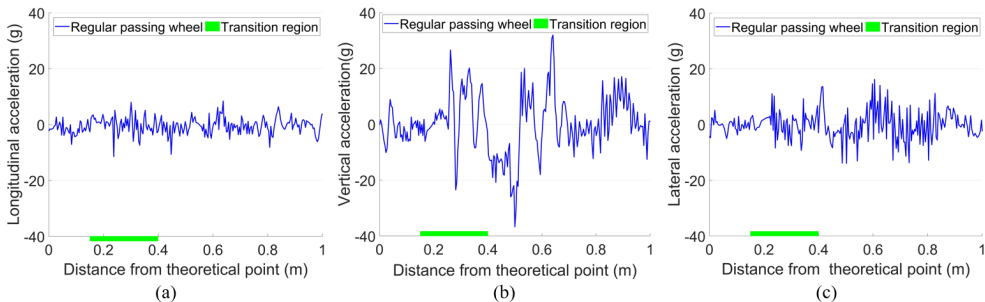


Figure 3.3. Examples of regular impact acceleration responses due to passing wheels.

It can be seen from Figure 3.3 that  $a_y$  is much higher than  $a_x$  for a regular passing wheel, while  $a_z$ , meaning that the impact factor ( $a_z/a_y$ ), is relatively small. It is also indicated that the wheel has two impacts on the crossing, with the first one (22 g) in the transition region and the second one (34 g) after the wheel load transit to the crossing nose rail. Even though the second impact has a higher amplitude, the first one is more damaging, since in the first impact location the nose rail is much thinner than in the second one.

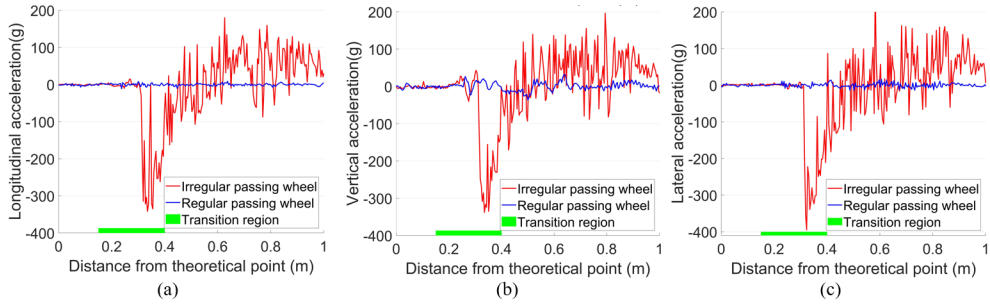


Figure 3.4. Examples of regular (same as Figure 3.3) and irregular impact acceleration responses due to passing wheels.

For the irregular passing wheel presented in Figure 3.4, it can be seen that the impact is located in the transition region and the accelerations in all three directions are very close to each other (in contrast to the regular passing wheel). Such strong correlation of the acceleration responses reflects the intense wheel impact on the crossing nose rail and the rough transition of the wheel load from wing rail to the crossing nose rail. The big difference between the two typical wheel-rail impacts gives an example of the violent fluctuation of the resulted dynamic responses that can be observed in such crossings.

### 3.4 Impact location and fatigue area

The impact location is defined as the point where the maximum wheel-rail impact occurs. As described previously, the impact location is restricted within the transition region. For the example given in Figure 2.3 (a), the impact location was 0.281 m from the TP.

The fatigue area is defined as the region where most of the wheel impacts are located and is calculated based on multiple wheel passages. In monitoring the conditions of railway crossings, the location and size of the fatigue area reflect the wheel load distribution along the crossing nose. In general, farther impact locations from the TP and wider fatigue areas indicate a better crossing condition.

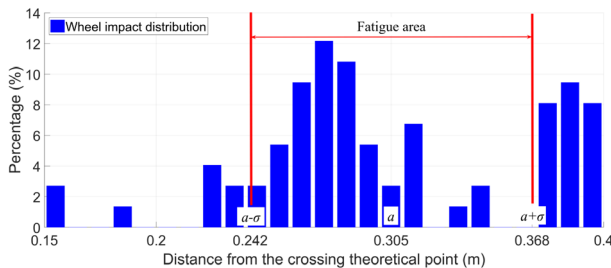


Figure 3.5. Example of fatigue area calculation.

In practice, to simplify the calculation procedure, the distribution of the wheel impacts due to multiple wheel passages is assumed to be normal distribution, the mean value  $a$  is the impact location and the confidence interval  $[a - \sigma, a + \sigma]$  is recognized as the fatigue area.

An example of the fatigue area of the monitored crossing during a single day is given in Figure 3.5.

In this example, the wheel impact location was  $a = 0.305 \text{ m}$ , and the standard deviation of the simplified normal distribution was  $\sigma = 0.063 \text{ m}$ . Therefore, the fatigue area for the crossing during this monitoring day was between 0.242 and 0.368 m, with a size of 0.126 m. It can be noticed that the calculated fatigue area is not accurate, yet for condition monitoring in the long term, such simplification can provide reasonably acceptable results and highly improve the efficiency of data analysis.

### 3.5 Results from multiple monitoring days

In order to describe the development of the crossing’s condition, the indicators are mainly used as statistical results over multiple monitoring days. An example of the development of vertical crossing acceleration responses as well as an irregular contact ratio is given for a span of 16 days in Figure 3.6. In this period, no track activities (e.g., maintenance) were performed, and the time frame was relatively too short for the condition of the crossing to degrade; therefore, the crossing condition can be assumed to be stable.

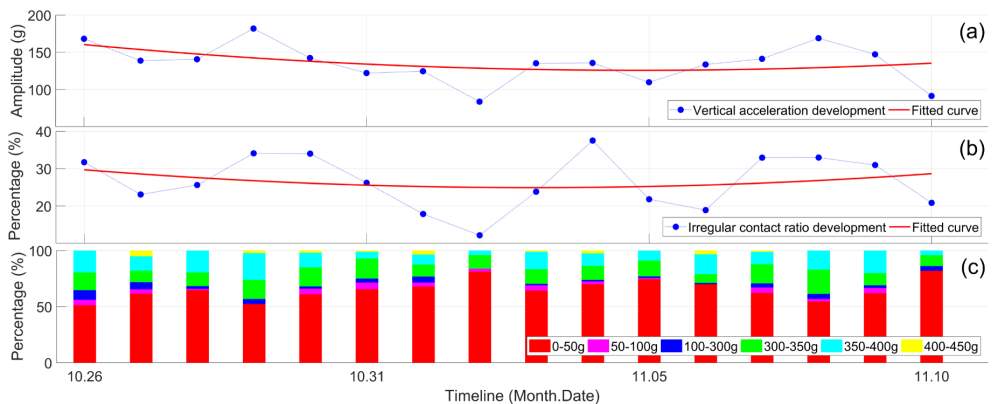


Figure 3.6. Development of the vertical acceleration responses in the monitored period. (a): Mean value of the vertical acceleration; (b): Irregular contact ratio; (c): Distribution of the acceleration responses in each day.

From Figure 3.6 (a) it can be seen that the overall trend of the mean value of the accelerations is relatively stable, while the fluctuations of the responses are quite significant. The vertical accelerations have the minimum value of 84 g and the maximum value of 182 g. Such fluctuations have resemblance with the fluctuations of the irregular contact ratio (Figure 3.6 (b)). This resemblance will be further studied in the correlation analysis. It should be noted that the irregular contact ratio in the monitored period was above 10%, and for some days even it was higher than 30%, which is much higher than the previously studied 1:15 crossing [1] and reflects the abnormal condition of the monitored 1:9 crossing.

To summarize, the analysed results have shown the following interesting features:

- The large difference of the dynamic responses from one passing wheel to another;

- The high irregular contact ratio due to multiple wheel passages in one monitoring day;
- The highly fluctuated acceleration responses as well as the irregular contact ratio in short monitoring period.

All these features of the monitored 1:9 crossing indicate quite different performances from the previously studied 1:15 crossing. Investigating the sources of the fluctuation is necessary for a proper assessment of the crossing condition. Also, some condition indicators such as impact acceleration and the irregular contact ratio show possible correlations with each other. Figuring out the relationships between these indicators can help to reduce the amount of the required data, which will improve the efficiency of the post processing of the measurement results. These two questions can be investigated using correlation analysis, which will be presented in the next section.

## 4 Correlation analysis

As discussed in the previous section, a high fluctuation was observed in the vertical acceleration responses to the monitored crossing over a short period of time, and was unlikely to be related to structural changes. Considering that the interference factors from the train were minimized by data selection, one possible cause of the fluctuating dynamic responses might have been the continuously changing weather conditions.

### 4.1 Influence of the weather

It was discovered in the previous study [24] that temperature variation shows a good correlation with the acceleration fluctuation. In that study, the temperature fluctuation was considered to be the result of the duration of sunshine or precipitation. In order to assess the impact of the weather more accurately, the influences of weather conditions—including mean value of the daily temperature, daily sunshine and precipitation duration—will be analysed. Figure 4.1 shows the fluctuation of crossing vertical acceleration responses with varying weather conditions.

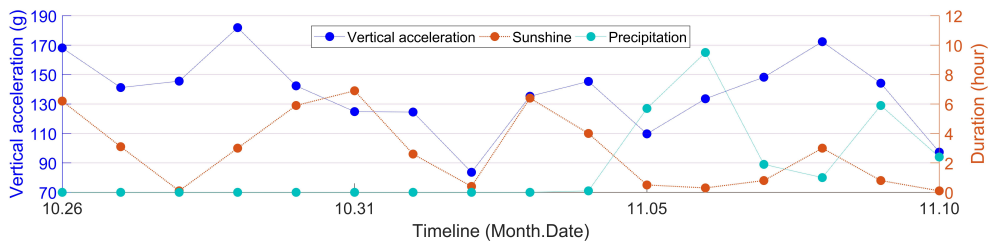


Figure 4.1. Development of vertical acceleration together with the sunshine and precipitation durations.

From Figure 4.1 it can be seen that the fluctuating durations of sunshine showed a similar pattern to the crossing's vertical acceleration responses. There seems to be connection between these two variables. For durations of precipitation, the connection with the vertical acceleration responses was lower. In order to quantitatively assess the impact of the weather, the correlations between the weather variables and condition indicators must be analysed.

The weather data are obtained from the Royal Dutch Meteorological Institute (KNMI) [27] in days, and mainly consist of the following items:

- Sunshine duration per day ( $D_s$ );
- Precipitation duration per day ( $D_p$ ).

The crossing condition indicators were obtained from the crossing instrumentation, and the statistical results based on multiple monitoring days have been applied. The analysed indicators include the following parts:

- Longitudinal, vertical and lateral acceleration responses ( $a : a_x, a_y$  and  $a_z$ );
- Irregular contact ratio ( $I_r$ );
- Wheel impact location ( $L_o$ ) and the size of fatigue area ( $F_a$ ).

## 4.2 Pearson's correlation coefficient

In statistics, the linear correlation between two variables is normally measured using Pearson's correlation coefficient  $r$ . For two variables  $X$  and  $Y$  with the same sample size of  $n$ ,  $r$  can be obtained using the following formula:

$$r_{X,Y} = \frac{\text{cov}(X,Y)}{\sigma_X \sigma_Y} = \frac{E[(X - \mu_X)(Y - \mu_Y)]}{\sigma_X \sigma_Y} = \frac{1}{\sigma_X \sigma_Y} \cdot \frac{1}{n} \sum_{i=1}^n [(x_i - \mu_X)(y_i - \mu_Y)] \quad (1)$$

$$X = X(x_1, x_2, \dots, x_n), Y = Y(y_1, y_2, \dots, y_n) \quad (2)$$

where

- $\text{cov}(X, Y)$  is the covariance of  $X$  and  $Y$
- $\sigma_X$  &  $\sigma_Y$  are respectively the standard deviations of  $X$  &  $Y$
- $\mu_X$  &  $\mu_Y$  are respectively the mean values of  $X$  &  $Y$
- $E[\dots]$  is expectation of the given variables

When  $X$  is in direct/inverse proportion to  $Y$ , then the correlation coefficient is

$$r_{X,Y} = \frac{E[(X - \mu_X)(Y - \mu_Y)]}{\sigma_X \sigma_Y} = \pm \frac{\sigma_X \sigma_Y}{\sigma_X \sigma_Y} = \pm 1 \quad (3)$$

If  $X$  and  $Y$  are independent, then the variable of  $(x_i - \mu_X)(y_i - \mu_Y)$  (1) could be a random positive or negative value. In case of large amount of data ( $n \rightarrow \infty$ ),

$$\lim \frac{1}{n} \sum_{i=1}^n [(x_i - \mu_x)(y_i - \mu_y)] = 0 \tag{4}$$

Therefore, the value range of the correlation coefficient is  $r_{x,y} = [-1, 1]$ .  $r_{x,y} = \pm 1$  means that the two variables  $X$  and  $Y$  are perfectly correlated, and  $r_{x,y} = 0$  means that  $X$  and  $Y$  have no correlation with each other. Otherwise,  $X$  and  $Y$  is considered partly correlated.

In different research fields, the gradation of correlation index may have notable distinctions [28]. In some domains such as medicine and psychology, the requirement of the correlation coefficient—that a strong correlation is defined as  $|r| \geq 0.7$ —is relatively strict, while in other domains such as politics,  $|r| \geq 0.4$  can already be considered a strong correlation. In this study, the structural responses and weather were indirectly associated. The three-level guideline modified from [29] is applied for the correlation strength analysis, as shown in Table 4.1.

Table 4.1. The three-level correlation strength guideline

$r$	Correlation Strength
$ r  < 0.3$	Weak
$0.3 \leq  r  < 0.5$	Moderate
$0.5 \leq  r  < 1$	Strong

### 4.3 Correlation analysis

In the analysis presented here, the correlations between the dynamic responses of the crossing ( $a$ ,  $I_r$ ,  $L_o$  and  $F_a$ ) and the weather-related variables ( $T_m$ ,  $D_s$  and  $D_p$ ) are studied. The data used for the correlation analysis are from 16 monitoring days (the same as in Figure 3.6,  $n=16$  in Equation (2)). The correlation within each group of parameters, as well as the cross-correlation between these two groups of parameters, will be analysed.

Table 4.2. Correlation coefficients for dynamic responses and weather variables

$r$	$a_x$	$a_y$	$a_z$	$I_r$	$L_o$	$F_a$	$D_s$	$D_p$
$a_x$	1	0.98	0.99	0.84	-0.30	-0.56	0.43	-0.23
$a_y$		1	0.99	0.79	-0.37	-0.51	0.36	-0.17
$a_z$			1	0.85	-0.32	-0.53	0.42	-0.22
$I_r$				1	-0.09	-0.42	0.40	-0.22
$L_o$					1	0.36	-0.39	0.14
$F_a$						1	-0.63	0.38
$D_s$							1	-0.54
$D_p$								1

The results are presented in Table 4.2. Nomenclature in the table is presented earlier in section 4.1. The strong, moderate and weak correlation coefficients are marked with red, blue and black colours, respectively. The correlation results will be analysed in the different categories presented below.

### Correlation of the dynamic responses

It can be seen from Table 4.2 that the 3-D acceleration responses ( $a_x$ ,  $a_y$  and  $a_z$ ) are very strongly correlated to each other. The irregular contact ratio ( $I_r$ ) and the size of the fatigue area ( $F_a$ ) are also strongly correlated with  $a$  ( $a_x$ ,  $a_y$  and  $a_z$ ). It can be noted that the correlations between  $F_a$  and  $a$  are negative, meaning that the increase of  $a$  is usually accompanied with the reduction of  $F_a$ . The correlations of the impact location ( $L_o$ ) with other dynamic responses are not strong, meaning that  $L_o$  is relatively independent from the other dynamic responses. Some typical correlation results of the dynamic responses (framed in Table 4.2) are further discussed below.

The very strong correlations of  $a_x$ ,  $a_y$  and  $a_z$  ( $r \approx 1$ ) indicate that the 3-D accelerations are synchronously developed. The correlation between  $a_y$  and  $a_z$  is demonstrated in Figure 4.2 (a). Therefore, in practice, it is possible to use the accelerations only in one direction, (e.g.  $a_y$ ) to analyse the crossing behaviour, which can help improve the efficiency in processing the measurement data.

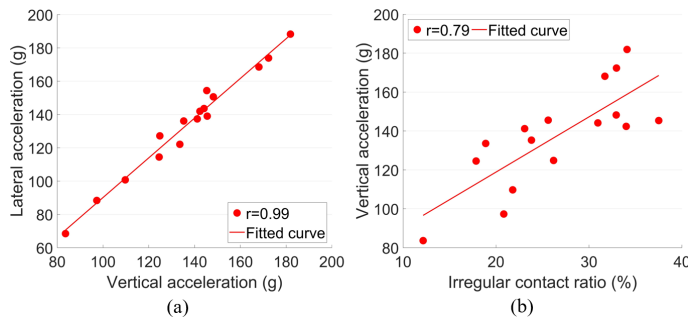


Figure 4.2. Correlations of the dynamic responses. (a):  $a_y$ - $a_z$ ; (b):  $I_r$ - $a_y$ .

The strong correlations between  $I_r$  and  $a$  (Figure 4.2 (b)) clearly indicate that the high acceleration responses are to a great extent contributed by the high ratio of irregular contact. This phenomenon could have been caused by temporary (not residual) rail displacements due to varying temperature forces in the rail. It has to be noted that all these responses ( $I_r$  and  $a$ ) fluctuated violently, a phenomenon that was likely caused by instable track conditions that were possibly affected by changes in weather conditions. This assumption will be verified later using a numerical model.

Figure 4.3 (a) shows the correlation between  $a_y$  and  $L_o$ . The negative result means that when  $a$  increased, there is a tendency for  $L_o$  to be shifted closer to the crossing's theoretical point, although the moderate correlation strength ( $r = -0.37$ ) indicates that the connection between  $a$  and  $L_o$  was rather limited. This might have been because the shift of  $L_o$  was a long-term effect of rail geometry degradation [1]. However, the rail geometry was unlikely to be changed during the relatively short monitoring period (16 days), so the temporary change of  $a$  might not have directly resulted in the shift of  $L_o$ .

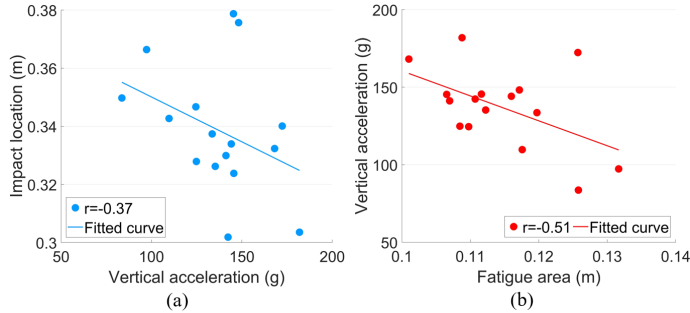


Figure 4.3. Correlations of the dynamic responses. (a):  $a_y$ - $L_o$ ; (b):  $F_a$ - $a_y$ .

The correlation between  $F_a$  and  $a_y$  is shown in Figure 4.3 (b). Compared with  $L_o$ ,  $F_a$  was more likely to be reduced due to the increase of  $a$ . Combined with the strong correlation between  $a$  and  $I_r$ , it can be deduced that the impact locations of the irregular contact wheels tended to be centralized, while those of regular contact wheels were decentralized. Such a result confirms that a wider fatigue area will to some extent indicate a better crossing performance.

C

**Correlation of the weather conditions**

As can be seen from Table 4.2, the precipitation duration ( $D_p$ ) had a strong negative correlation with the sunshine duration ( $D_s$ ), as shown in Figure 4.4.

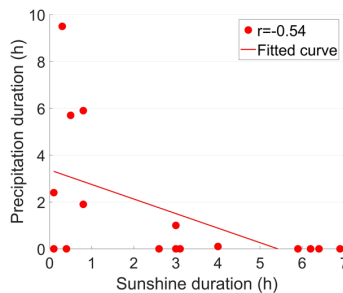


Figure 4.4. Correlation result between sunshine duration and precipitation duration ( $D_s$ - $D_p$ ).

For the weather variables,  $D_s$  and  $D_p$  can be considered as two opposite weather conditions. From this point of view, the correlation coefficient of  $r = -0.54$  is not very strong. Such results could be explained by the existence of cloudy/overcast conditions, and weather in a single day can switch among sun, rain and clouds/overcast. It can be noticed that in the monitored period, precipitation only occurred in 6 of the 16 days, which to some extent shows the complicity of the weather conditions.

### Cross-correlation between dynamic responses and weather conditions

According to the correlation results presented in Table 4.2, the cross-correlations of  $D_p$  with the dynamic responses were quite limited, except for a moderate correlation with  $F_a$ . Meanwhile,  $D_s$  was strongly correlated with  $F_a$  and moderately correlated with all the other dynamic responses.

The moderate correlation between  $I_r$  and  $D_s$  is shown in Figure 4.5 (a). Such a result can be explained by the fact that an increase of the rail temperature due to sunshine causes the displacements in the turnout. Due to these geometrical changes, the wheel cannot pass the crossing normally anymore, which results in an increase of irregular contact. Such a result is consistent with the moderate correlations between  $D_s$  and  $a$ .

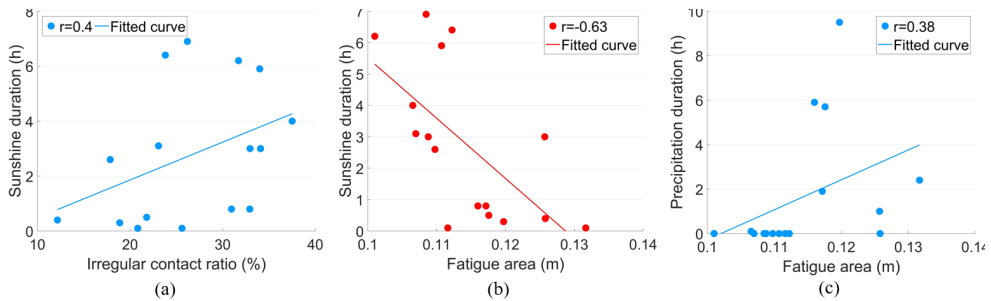


Figure 4.5. Cross-correlation results between dynamic responses and weather conditions: (a):  $I_r$ - $D_s$ ; (b):  $F_a$ - $D_s$ ; (c):  $F_a$ - $D_p$ .

The correlation of  $D_s$  with  $F_a$  is stronger than with the other dynamic responses ( $r = -0.63$ , Figure 4.5 (b)), meaning that sunshine-initiated rail displacements were likely to occur primarily in centralized impact locations, which may have increased the likelihood of irregular contact.

An example for demonstrating the influence of sunshine on the dynamic responses of the monitored crossing is given in Figure 4.6. In this example, there was hardly any sunshine on one day (11.02), and a long period of sunshine on another day (11.03) (Figure 4.1). It can be seen that on 11.03 (with sunshine),  $I_r$  is higher (Figure 4.6 (a)) and  $F_a$  is slightly narrower (Figure 4.6 (b)). Such results indicate that the temporary effect of sunshine can lead to the changes of the crossing performance.

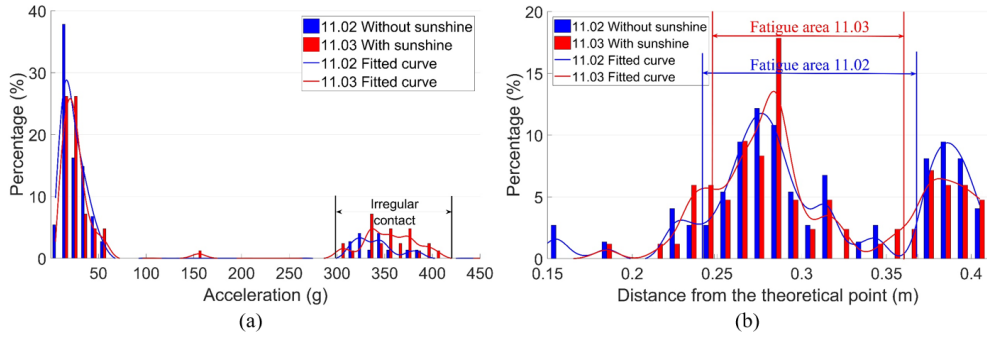


Figure 4.6. Influence of sunshine on the dynamic responses. (a): Vertical acceleration distribution; (b): Fatigue area analysis.

The moderate correlation between  $D_p$  and  $F_a$  is shown in Figure 4.5 (c). Considering that the correlation between  $D_p$  and  $D_s$  was not very strong, the moderate correlation between the dynamic responses and weather conditions can already indicate a measure of impact. An example of the measured dynamic responses of the crossing for a day without precipitation (11.04) and a day with precipitation (11.05, Figure 4.1) is shown in Figure 4.7.

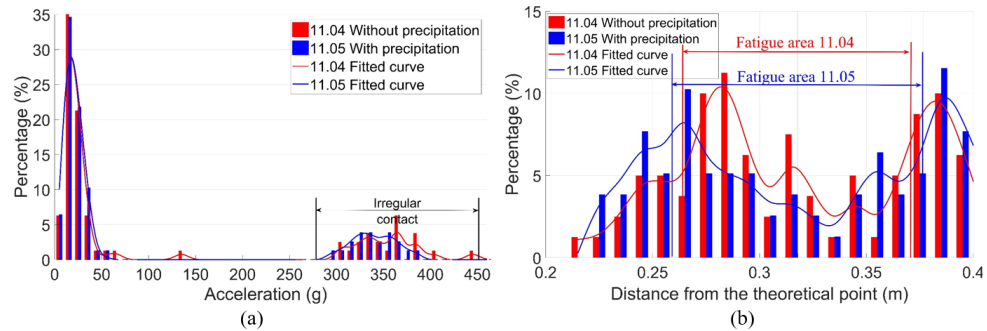


Figure 4.7. Influence of precipitation on the dynamic responses. (a): Vertical acceleration distribution; (b): Fatigue area analysis.

It can be seen in Figure 4.7 that on the day with precipitation (11.05),  $I_r$  was slightly lower than that on the day without precipitation (11.04) and  $F_a$  was wider. The reason for such results could be that precipitation may reduce the friction coefficient on the rail's surface and make the transition of the wheel load smoother. This assumption will be verified using a numerical model in the next section.

It should be mentioned that the subgrade of the monitored crossing was relatively soft, with canals on both sides of the track. Persistent precipitation could change the property of the subgrade and further affect the dynamic performance of the track. Therefore, the influence of precipitation can be quite complicated.

Based on the correlation analysis, the main conclusions can be drawn as follows:

- The accelerations in all three directions developed synchronously. In monitoring crossing conditions, it is sufficient to use vertical acceleration to represent the 3-D acceleration responses. Through this, the data processing procedure can be simplified.
- The strong correlation between  $I_r$  and  $a_y$  indicates that irregular contact is likely to result in high impact accelerations. Such a result confirms that  $I_r$  can be used as an indicator for the crossing condition assessment. A high value of  $I_r$  indicates a degraded condition of the monitored crossing.
- The high (moderate/strong) correlation results between  $D_s$  and the dynamic responses of the crossing clearly indicate the influence of weather. It can be concluded that significant fluctuations in accelerations during a relatively short period are caused by changes in weather conditions. To verify this, a numerical model will be used in the next section.

## 5 Numerical verification

In general, solar radiation is one of the major sources of rail thermal force. Depending on the sunshine duration, the associated rail temperature can rise to 40 °C higher than the ambient air temperature [30]. The change in rail temperature will increase the rail stress and amplify lateral displacements in the rail. The lateral displacements will then increase the uncertainty of the impact angle of a wheel in the railway crossing, eventually leading to an increase in the acceleration responses of some passing wheels, as shown in Figure 3.6.

Precipitation will introduce water to the rail surface that acts as a lubrication layer, which will reduce the friction coefficient in the wheel–rail interface [21]. It has been studied [31] that a low friction coefficient can be helpful in reducing hunting oscillation and, in contrast to sunshine, can reduce the impact angle of a wheel in the railway crossing.

The above-mentioned effects of temperature and friction variation corresponding to sunshine and precipitation are implemented in the multi-body system (MBS) model described below.

### 5.1 MBS model setup and validation

In order to verify the weather effect hypotheses, a model for analysing vehicle-crossing interaction developed according to the MBS method (implemented in VI-Rail software) will be used, as shown in Figure 5.1 (a). The track model is a straight line with the crossing panel (Figure 5.1 (b)) situated in the middle of the track. The total length of the track model is 100 m, which allows enough preloading time for the vehicle before it enters into the crossing panel, as well as enough space after the vehicle passes through the crossing.

The crossing geometry is defined by the control cross-sections, and the profiles between two pre-defined cross-sections are automatically interpolated using the third-order spline curve. In the track model, the rail is considered to be lumped masses on the sleepers connected with a massless beam. The flexible layers under the rail are the rail bushing that represents the rail pads and clips, and the base busing representing the ballast bed (Figure 5.1 (c)).

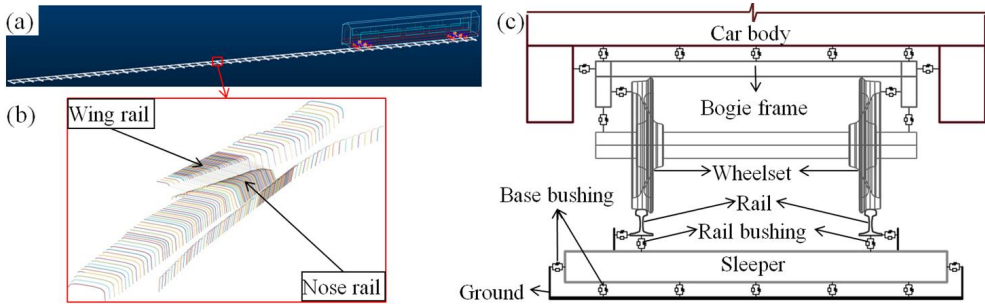


Figure 5.1. MBS model: (a) Vehicle-track model; (b) Crossing profiles; (c) Flexible connections in the model.

The crossing model is the same as the monitored 1:9 casted manganese crossing with a rail type of UIC54 E1. The track parameters of Dutch railways [32] applied in the model are shown in Table 5.1.

Table 5.1. Track parameters

Track components		Stiffness, MN/m	Damping, kN·s/m
Rail pad / Clips	Vertical	1300	45
	Lateral	280	580
	Roll	360	390
Ballast		45	32

The vehicle model was developed based on a VIRM locomotive with a total length of 27.5 m comprising a car body, front bogie and rear bogie. In the vehicle model, the car body and bogie frames, as well as the wheel sets, are modelled as rigid bodies with both primary and secondary suspensions taken into account (Figure 5.1(c)) [33]. The vehicle travels with a velocity of 140 km/h, the same as in the data analysis measurements. The wheels use a S1002 profile with a wheel load of 10 t. The wheel–rail contact model is defined as the general contact element and uses actual wheel and rail profiles as an input, which allows variable wheel and rail profiles.

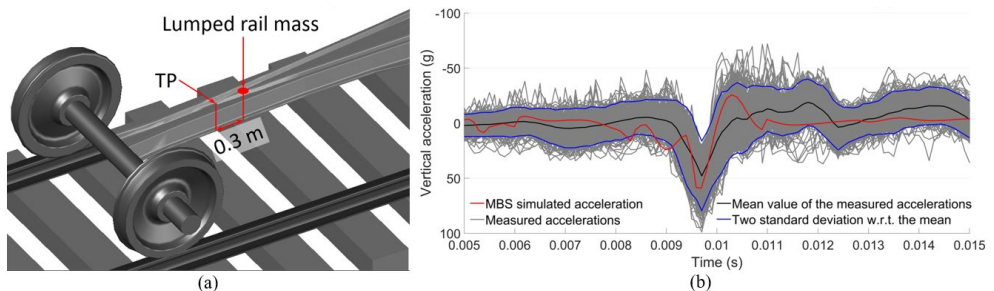


Figure 5.2. MBS model validation: (a): Rail element for acceleration extraction; (b): Comparison of MBS simulated acceleration with measured ones in time domain.

The MBS vehicle–track model was validated using the measured acceleration responses from the crossing with the same design and stable conditions. Since the validation simulation was

based on ideal track conditions, only the acceleration responses with regular wheel–rail contact were used in the comparison. The selected element for acceleration extraction was the rail with lumped mass (Figure 5.2 (a)) from the same location as the instrumented accelerometer (Figure 2.1).

The validation results are shown in Figure 5.2 (b). It can be seen that the simulation results (red line) are quite comparable with the measured accelerations (black line). The magnitude of the simulated vertical acceleration during impact was around 55 g, which is comparable with the mean value of the measured acceleration responses (47 g). Although tolerable deviations of the impact signals exist, the simulation results agree reasonably with the measurements. It can be concluded that the MBS model can catch the main features of the wheel–rail impact during crossing and can be used to analyse crossing performance. Further details about the numerical model development and validation can be found in [34].

## 5.2 Numerical analysis

### Effect of sunshine

In the previous study [35], the displacements of a turnout due to the change of the rail temperature were analysed using a finite element (FE) model. The simulation results indicated that when the rail temperature was increased (from a stress-free temperature) by 40 °C, the turnout rails were laterally displaced up to 4 mm, as shown in Figure 5.3(a). These results are applied in the MBS vehicle-crossing model as the sunshine-initiated lateral displacements. It should be noted that this simulation is based on ideal track conditions. In the case of a degraded track, the temperature-initiated lateral displacements could be amplified.

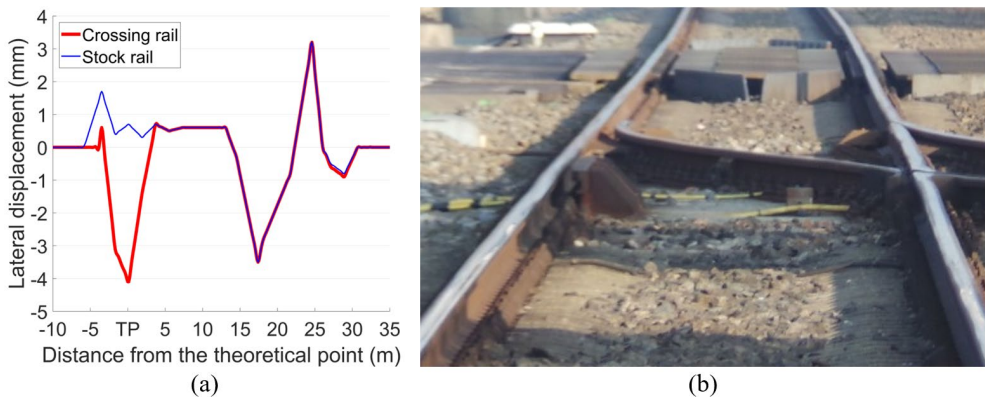


Figure 5.3. (a): Temperature initiated rail lateral displacement in FE simulation (Figure 11.15 in [35]); (b): Monitored crossing

In order to take the track degradation into account for the degraded track condition, the input lateral rail displacements in the MBS model are assumed to be twice as high as the ideal track condition (with maximum lateral rail displacements of 8 mm). The effect of precipitation is not taken into account and the friction coefficient of  $f = 0.4$  is used. Based on the above

assumptions, the vertical accelerations and transition regions of the rail are simulated and presented below.

The calculated transition regions under different track conditions are shown in Figure 5.4. In the reference condition with no lateral displacement in the track, the sizes of the transition regions for the front wheel and the rear wheel are both 0.031 m [34]. When the temperature-initiated track displacements are taken into account, the transition regions shift closer to the theoretical point and the sizes reduce dramatically to 0.015 m for the front wheel and 0.012 m for the rear wheel. For the degraded track with higher rail displacements, the size of the transition region is only 0.004 m.

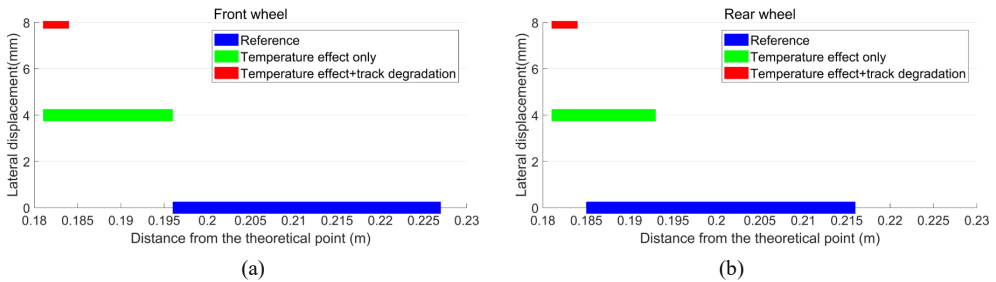


Figure 5.4. Transition regions of the crossing. (a): Front wheel; (b): Rear wheel.

The vertical acceleration response of the rail due to passing wheels is shown in Figure 5.5. It can be seen that lateral displacement in the rail can result in higher acceleration responses caused by both the front and rear wheels.

Combined with the results of the transition region (Figure 5.4), the simulation results confirm the correlation results (Figure 4.5 (a)-(b)) that the long sunshine duration, which will result in a higher temperature in the rail, can lead to a centralized impact location and higher impact acceleration responses at the crossing.

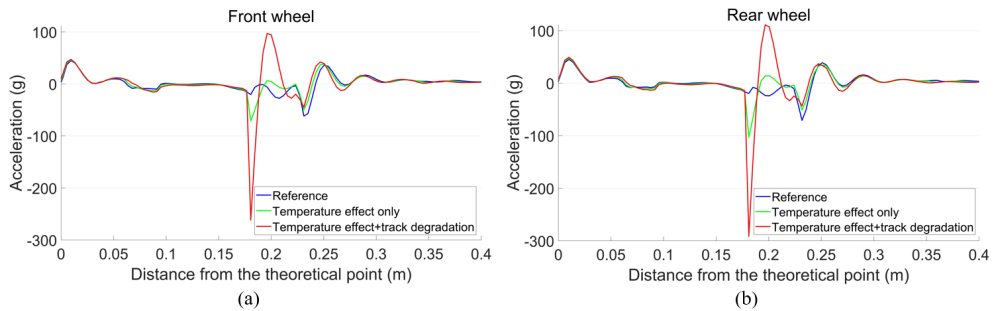


Figure 5.5. Vertical rail accelerations due to the passing wheels. (a): Front wheel; (b): Rear wheel.

It can be also seen that with the existence of rail displacement, the acceleration response caused by the rear wheel is higher than that caused by the front wheel from the same bogie. These results indicate that the performance of the rear wheel is not only affected by rail displacement, but also by the passing condition of the front wheel.

In case of a degraded track, higher rail displacements may lead to much higher acceleration responses as a result of both the front and rear wheels. Such impact accelerations (near 300 g) are close to the amplitude of the acceleration responses due to the irregular impacts in the

measurements (Figure 4.6 (a), Figure 4.7 (a)). The simulation results prove that the lateral rail displacements caused by increases in rail temperature, in combination with track geometry deviations, can result in high wheel–rail impact accelerations.

### Effect of precipitation

With the influence of precipitation, the friction coefficient ( $f$ ) in the wheel–rail interface can vary from 0.4 to 0.05 [35]. In this study, the precipitation effect is simulated by a reduction of  $f$ . The temperature-initiated rail displacements under ideal track conditions are taken into account. Calculations of rail accelerations resulting from passing wheels are shown in Figure 5.6.

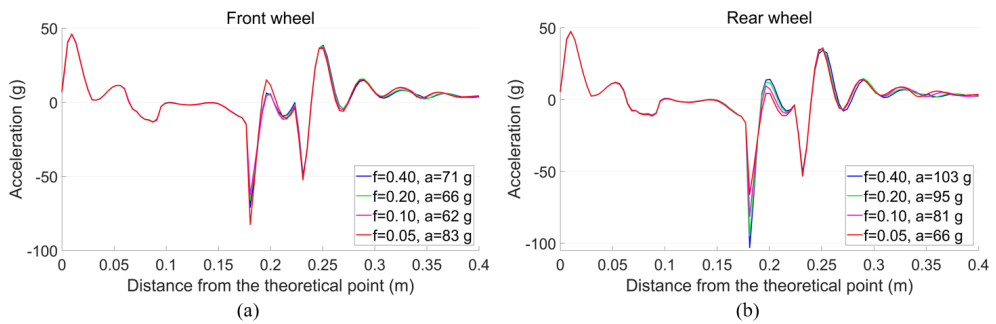


Figure 5.6. Vertical accelerations of the rail due to the passing wheels. (a): Front wheel; (b) Rear wheel.

For the front wheel, when  $f$  is reduced from 0.4 to 0.1, the impact acceleration gradually reduces from 71 g to 62 g. However, when  $f = 0.05$ , the maximum impact acceleration is increased to 83 g. Such results show that reducing the friction coefficient is not always helpful for the dynamic performance of the crossing. For the rear wheel, the reduction of  $f$  results in a decreased impact acceleration from 103 to 66 g. As discussed previously, the high rail acceleration responses due to the rear wheel are affected by the movement of the front wheel. In this case, the lowered  $f$  can help the wheelset return to a balanced position faster due to lower lateral restraint, which reduces the influence of the front wheelset on the rear wheelset from the same bogie.

It can be concluded that the change of  $f$  due to precipitation has an influence on the dynamic performance of the crossing, but the effect of a lower  $f$  is not always positive. Such results prove the correlation results indicating that an increase of  $D_p$  tends to result in lower acceleration responses, but the correlation strength is not high. The moderate correlation between  $D_p$  and  $F_a$  is also consistent with the simulation results that each wheel passes through the crossing more independently, which leads to less centralized impact locations.

### 5.3 Discussion

In this section, the MBS model for vehicle–crossing interaction analysis was briefly introduced. Using this model, the sunshine and precipitation effects were simulated as rail displacements and reduced  $f$  in the wheel–rail interface, respectively. The simulation results indicate that the rail displacements due to sunshine can lead to an increase in wheel-crossing impact acceleration. Combined with track degradation, such an effect could be highly amplified. Meanwhile, a lower  $f$  in the wheel–rail interface due to precipitation might reduce the interaction effect of two wheelsets from the same bogie, but cannot help improve track conditions. Combined with the measurement results, it can be concluded that the monitored crossing was not in the ideal condition, and possessed a certain degree of track degradation that made it more sensitive to changes in weather conditions.

## 6 Conclusions and future work

### 6.1 Conclusions

In this study, the conditions of a railway crossing were monitored, and the results were presented. The indicators for assessing the conditions of a crossing were briefly introduced. Inspired by the observed connection between vertical acceleration responses of the crossing and variations in the sunshine duration, correlations of the dynamic responses and weather conditions were calculated. Using the vehicle-crossing MBS model, the influence of weather on the performance of the crossing was verified. The main conclusions of this study can be drawn as follows:

- The strong correlations between the dynamic responses show that the measurement results can be simplified and the crossing conditions can be assessed by only a few indicators (e.g., vertical acceleration, irregular contact ratio and fatigue area).
- The correlation results between the dynamic responses of the crossing and sunshine duration explain the fluctuation of dynamic responses over a short period of time. Such results confirm the temporary influence of weather on the performance of a crossing.
- The correlation results between sunshine duration and precipitation duration, as well as between precipitation duration and the dynamic responses of the crossing, indicate the complexity of the effect of precipitation.
- The simulation results not only verify the impact of weather on the dynamic performance of the crossing, but also indicate that the condition of the track at the monitored crossing was degraded. In cases of track degradation, the influence of weather can be amplified.

In monitoring the conditions of railway crossings, the correlation results among dynamic responses can be used to simplify measurement data. The verified weather effects explain the fluctuation of the dynamic responses over a short time period, which provides the basis for the measurement data regression. It should be noted that although sunshine variation is a short-term effect, the interaction of sunshine with the degraded track can turn this temporary interruption into a permanent track deformation, which will further accelerate the degradation of the track. In monitoring the conditions of railway crossings, the influence of weather can be eliminated through data regression to describe the structural degradation procedure, but the reflected track problem has to draw enough attention. Ensuring good track condition will

not only help prolong service life of the crossing, but will also reduce the influence of varying weather conditions.

## 6.2 Future work

This study was based on monitoring the conditions of railway crossings. It can be imagined that weather variation might also have an impact on other track sections, especially vulnerable parts such as transition zones, insulated joints, sharp curves, and so on. In the future, the effects of weather on other parts can be further investigated, which will improve the universality of this study and provide broader information for railway track management.

## References

- [1] X. Liu, V.L. Markine, H. Wang and I.Y. Shevtsov, Experimental tools for railway crossing condition monitoring, *Measurement*, vol. 129, 2018, p. 424-435.
- [2] D. Barke, W.K. Chiu, Structural health monitoring in the railway industry: A review, *Structural Health Monitoring*, vol. 4, 2005, p. 81-94.
- [3] D. Bowness, A.C. Lock, W. Powrie, J.A. Priest, D.J. Richards, Monitoring the dynamic displacements of railway track, *Proceedings of the Institution of Mechanical Engineers Part F: Journal of Rail and Rapid Transit*, vol. 221, 2007, p. 13-22.
- [4] A. Chudzikiewicz, R. Bogacz, M. Kostrzewskim, R. Konowrockim, Condition monitoring of railway track systems by using acceleration signals on wheelset axle-boxes. *Transport*, vol. 33, 2018, p. 555-566.
- [5] B. Sowiński, Interrelation between wavelengths of track geometry irregularities and rail vehicle dynamic properties, *Archives of Transport*, vol. 25, 2013, p. 97-108.
- [6] H. Tsunashima, Condition Monitoring of Railway Tracks from Car-Body Vibration Using a Machine Learning Technique, *Applied Sciences*, vol. 9, 2019, 2734.
- [7] Z. Wei, A. Núñez, Z. Li, R. Dollevoet, Evaluating degradation at railway crossings using axle box acceleration measurements, *Sensors*, vol. 17, 2017, 2236.
- [8] Z. Wei, C. Shen, Z. Li, R. Dollevoet, Wheel–Rail Impact at Crossings-Relating Dynamic Frictional Contact to Degradation, *Journal of Computational and Nonlinear Dynamics*, vol. 12 (4), 2017, p. 041016 1-11.
- [9] Y. Ma, A.A. Mashal, V.L. Markine, Modelling and experimental validation of dynamic impact in 1:9 railway crossing panel, *Tribology International*, vol. 118, 2018, p. 208-226.
- [10] L. Xin, V. Markine, I. Shevtsov, Numerical procedure for fatigue life prediction for railway turnout crossings using explicit finite element approach, *Wear*, vol. 366-367, 2016, p. 167-179.
- [11] E. Kassa, C. Andersson, J.C.O. Nielsen, Simulation of dynamic interaction between train and railway turnout, *Vehicle System Dynamics*. Vol. 44, No. 3, 2006, 247-258.

- [12] C. Wan, V.L. Markine, I.Y. Shevtsov, Optimisation of the elastic track properties of turnout crossings. *Proceedings of the Institution of Mechanical Engineers Part F: Journal of Rail and Rapid Transit*, vol. 230, 2016, p. 360-373.
- [13] B.A. Pålsson, Optimisation of railway crossing geometry considering a representative set of wheel profiles, *Vehicle System Dynamics*, vol. 53, 2015, p. 274-301.
- [14] C. Wan, V.L. Markine, I.Y. Shevtsov, Improvement of vehicle–turnout interaction by optimizing the shape of crossing nose, *Vehicle System Dynamics*, vol. 52, 2014, p. 1517-1540.
- [15] C. Wan, V.L. Markine, R.P.B.J. Dollevoet, Robust optimisation of railway crossing geometry. *Vehicle System Dynamics*, vol. 54, 2016, p. 617-637.
- [16] E. Kassa, J.C.O. Nielsen, Dynamic interaction between train and railway turnout: full-scale field test and validation of simulation models, *Vehicle System Dynamics*. Vol. 46, 2008, 521-534.
- [17] V.L. Markine, I.Y. Shevtsov, An Experimental Study on Crossing Nose Damage of Railway Turnouts in the Netherlands, *Proceedings of the 14th International Conference on Civil, Structural and Environmental Engineering Computing*, Cagliari, Italy, 3-6 September 2013.
- [18] L. Xin, V.L. Markine, I.Y. Shevtsov, Numerical analysis of the dynamic interaction between wheelset and turnout crossing using explicit finite element method, *Vehicle System Dynamics*, vol. 54, 2016, p. 301-327.
- [19] C. Wan, V.L. Markine, Parametric study of wheel transitions in railway crossings. *Vehicle System Dynamics*, vol. 53, 2015, p. 1876-1901.
- [20] O. Arias-Cuevas, Low Adhesion in the Wheel-Rail Contact, PhD thesis, Delft University of Technology, Delft, the Netherlands, 2010.
- [21] H. Chen, T. Ban, M. Ishida, T. Nakahara, Effect of water temperature on the adhesion between rail and wheel, *Proceedings of the Institution of Mechanical Engineers, Part J: Journal of Engineering Tribology* vol. 220, 2006, p. 571-579.
- [22] M. Ertz, F. Bucher, Improved creep force model for wheel/rail contact considering roughness and temperature, *Vehicle System Dynamics*, vol. 37, 2002, p. 314-325.
- [23] T.M.H. Arts, Measuring the neutral temperature in railway track during installation and use, MSc thesis, Delft University of Technology, Delft, the Netherlands, 2011.
- [24] V.L. Markine, X. Liu, A.A. Mashal, Y. Ma, Analysis and improvement of railway crossing performance using numerical and experimental approach: application to 1:9 double crossovers, *Proceedings of the 25th International Symposium on Dynamics of Vehicles on Roads and Tracks*, Queensland, Australia, 14-18 August 2017.
- [25] J.J.J. Wegdam, Expert tool for numerical & experimental assessment of turnout crossing geometry, MSc thesis, Delft University of Technology, Delft, the Netherlands, December 2018.

- [26] V.L. Markine, I.Y. Shevtsov, Experimental Analysis of the Dynamic Behaviour of Railway Turnouts, Proceedings of the 11th International Conference on Computational Structures Technology, 4-7 September 2012, Dubrobnik, Croatia.
- [27] Koninklijk Nederlands Meteorologisch Instituut, <https://www.knmi.nl/nederland-nu/klimatologie/daggegevens>, (accessed on 10 November 2015).
- [28] H. Akoglu, User's guide to correlation coefficients, Turkish Journal of Emergency Medicine, vol. 18, 2018, p. 91-93.
- [29] J. Cohen, Statistical Power Analysis for the Behavioral Sciences 2<sup>nd</sup> Edition, New York University, New York, USA, 1988.
- [30] ProRail, Instruction of Procedures at Extreme Weather Conditions RLN00165, Version 002, Utrecht, the Netherlands, 10 December 2003.
- [31] T. Ohyama, Tribological studies on adhesion phenomena between wheel and rail at high speeds. Wear, vol. 144, 1991, p. 263-275.
- [32] M. Hiensch, J.C.O. Nielsen and E. Verheijen, Rail corrugation in The Netherlands – measurements and simulations, Wear, vol. 253, 2002, p. 140-149.
- [33] VI-grade GmbH, VI-Rail 16.0 Documentation, © 2014 VI-grade engineering software & services, Marburg, Germany, 2014.
- [34] X. Liu, V.L. Markine, MBS Vehicle-Crossing Model for Crossing Structural Health Monitoring, *submitted*, 2020.
- [35] T.M.H. Arts, V.L. Markine, I.Y. Shevtsov, Modelling Turnout Behaviour when Achieving a Neutral Temperature, Proceedings of the First International Conference on Railway Technology: Research, Development and Maintenance, Las Palmas de Gran Canaria, Spain, 18-20 April 2012.



# Paper D

## Train Hunting Related Fast Degradation of a Railway Crossing — Condition Monitoring and Numerical Verification

X. Liu, V.L. Markine

*Sensors*, vol. 20 (8), 2020, 2278.

<https://doi.org/10.3390/s20082278>

### Abstract

This paper presents the investigation of the root causes of the fast degradation of a railway crossing. The dynamic performance of the crossing was assessed using the sensor-based crossing instrumentation, and the measurement results were verified using the multi-body system (MBS) vehicle-crossing model. Together with the field inspections, the measurement and simulation results indicate that the fast crossing degradation was caused by the high wheel-rail impact forces related to the hunting motion of the passing trains. Additionally, it was shown that the train hunting was activated by the track geometry misalignment in front of the crossing. The obtained results have not only explained the extreme values in the measured responses, but also shown that crossing degradation is not always caused by the problems in the crossing itself, but can also be caused by problems in the adjacent track structures. The findings of this study were implemented in the condition monitoring system for railway crossings, using which timely and correctly aimed maintenance actions can be performed.

**Keywords:** railway crossing; wheel-rail impact; train hunting; numerical verification; railway track maintenance

## 1 Introduction

In the railway track system, turnouts (switches and crossings) are essential components that allow trains to pass from one track to another. A standard railway turnout is composed of three main parts: switch panel, closure panel, and crossing panel, as shown in Figure 1.1. In a railway turnout, the crossing panel is featured to provide the flexibility for trains to pass in different routes.

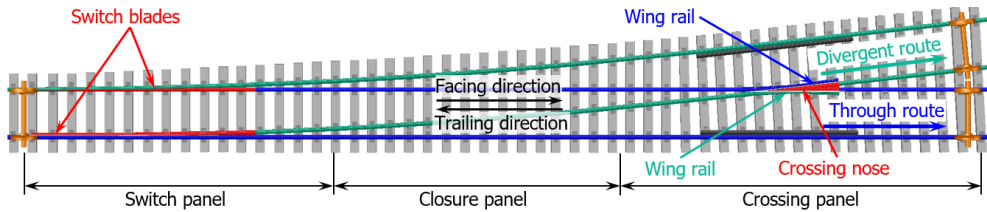


Figure 1.1. Standard left-hand railway turnout and the definition of the passing routes.

For rigid crossings that are commonly used in conventional railway lines, the gap between the wing rail and the nose rail usually results in high wheel-rail impacts in the transition region where the wheel load transits from the wing rail to the nose rail (vice versa, Figure 1.2), which makes the crossing a vulnerable spot in the railway track. In the case of crossings that are mainly used for the through route traffic (e.g., crossings in the crossover), there is no specific speed limit [1] and trains can pass through the crossings with a high velocity of up to 140 km/h. The high train velocity makes the wheel-rail impact more serious. In the Dutch railway system, around 100 crossings are urgently replaced every year [2] due to unexpected fatal defects, which not only result in substantial maintenance efforts, but also lead to traffic disruption and can even affect traffic safety.

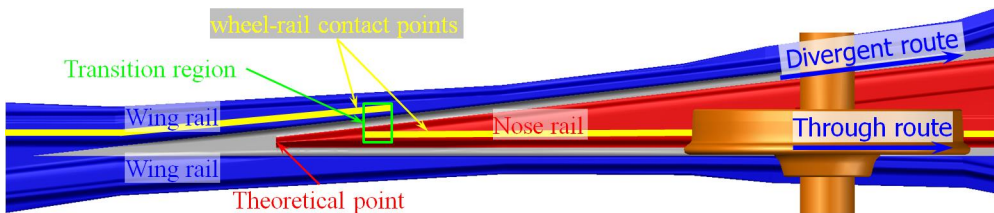


Figure 1.2. Wheel-rail interaction in the railway crossing for through route traffic.

In contrast to a switch panel, wherein sensors are instrumented for condition monitoring [3]-[4] and remaining useful life prediction [5], monitoring in a crossing panel is usually absent. As a result, the real-time information on the condition of railway crossings is limited. The present maintenance activities are mainly reactive and based on the experience of the contractors. In this case, the root causes of the crossing degradation are not always resolved by the maintenance actions, and the crossings are likely to be operated in a degraded condition. To improve this situation, necessary guidance for maintenance actions is highly required.

Proper crossing maintenance usually relies on condition assessment and degradation

detection, which can be realized through field monitoring. In recent years, condition monitoring techniques have been frequently applied in the railway industry. Aside from the above-mentioned instrumentation on the turnout switches, vehicle-based monitoring systems have been applied in track stiffness measurement [6] and estimation [7], track alignment estimation [8], hanging sleepers detection [9], and track fault detection [10], etc. Compared with the normal track, the current studies on railway crossings are mainly based on numerical simulation. Typical contributions include wheel-rail interaction analysis [11]-[21], damage analysis [16], [17], [22], [23], and prediction [18], [24], [25] as well as crossing geometry and track stiffness optimization for better dynamic performance [16], [26]. Field measurements are mainly used for the validation of numerical models. The monitoring of railway crossings for condition assessment and degraded component detection is still limited.

In the previous study, key indicators for the crossing condition assessment based on the field measurement were proposed [27]-[28]. Additionally, a numerical vehicle-crossing model was developed using a multi-body system (MBS) method to provide the fundamental basis for the condition indicators [29]. In this study, the condition indicators, as well as the MBS model, were applied in the condition monitoring of a fast degraded railway crossing. The main goals of this study were to investigate the root causes of the crossing degradation as well as to assess the effectiveness of the current maintenance actions.

Based on the objectives, this paper is presented in the following order. The experimental and numerical tools, including the crossing condition indicators, are briefly introduced in Section 2. The measurement results and the crossing degradation analysis as well as the effectiveness of the current maintenance actions are presented in Sections 3 and 4. Based on the measurement results and field inspections, the root causes for the fast crossing degradation were investigated with the assistance of the MBS model, as presented in Section 5. In Section 6, the verification of the effectiveness of the maintenance actions is given. Finally, in Section 7, major conclusions are provided.

## 2 Methodology

In this section, the experimental tools for the crossing condition monitoring, as well as the indicators for the crossing condition assessment, are briefly introduced. The MBS vehicle-crossing model for the verification of the experimental findings is also presented.

### 2.1 Experimental Tools

The experimental tools mainly consisted of the in-site instrumentation system modified from ESAH-M (Elektronische System Analyse Herzstückbereich-Mobil) and the video gauge system (VGS) for wayside monitoring, as briefly described below. Both tools have already been introduced and actively applied in previous studies. Detailed information regarding the installation and data processing can be found in [27], [30].

#### Crossing Instrumentation

The main components of the crossing instrumentation are an accelerometer attached to the crossing nose rail for 3-D acceleration measurement, a pair of inductive sensors attached in

the closure panel for train detection as well as train velocity calculation, and the main unit for data collection. An overview of the instrumented crossing is shown in Figure 2.1.

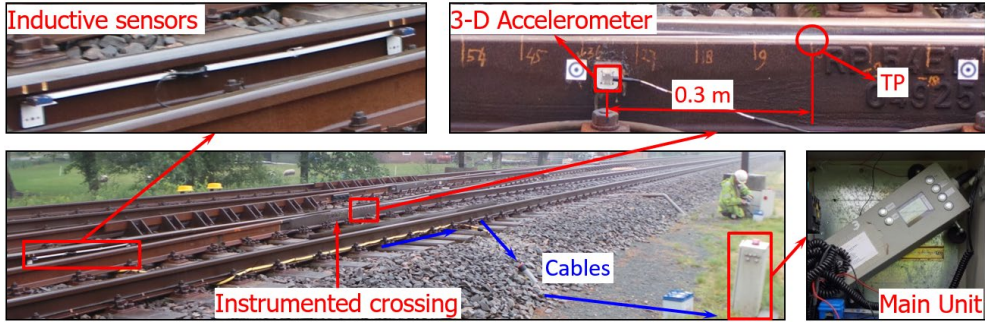


Figure 2.1. Crossing instrumentation based on ESAH-M.

The main outputs of the crossing instrumentation were the dynamic responses of the crossing nose, including the wheel-rail impact accelerations and locations, etc. All these responses were calculated within the transition region, which can be obtained through field inspection [29]. Based on these measured responses and the correlation analysis between the responses [28], two critical condition indicators related to the wheel impact and fatigue area, respectively, were proposed.

The wheel impact is reflected by the vertical accelerations, which were obtained from the crossing and processed through statistical analysis. This indicator is mainly based on the magnitude of the impacts due to each passing wheel (Figure 2.2 (a)), and the changes in time indicate the different condition stages of the crossing (Figure 2.2 (b)).

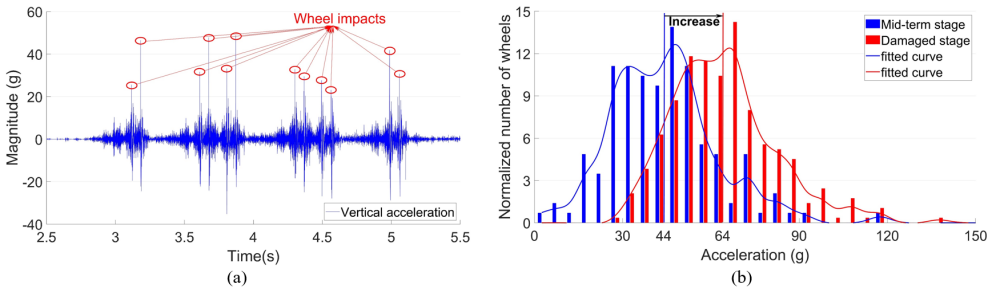


Figure 2.2. Indicator for the wheel impact. (a): Procedure for the obtainment of wheel impacts; (b): Example of the variation of the wheel impacts in different condition stages.

D

The fatigue area is defined as the region where the majority of wheel impacts are located on the crossing, and where ultimately the crack initiates (Figure 2.3 (a)). In practice, the fatigue area can be simplified as the confidence interval of  $[a - \sigma, a + \sigma]$ , where  $a$  is the mean value of the wheel-rail impact locations, and  $\sigma$  is the standard deviation. The location and size of the fatigue area are critical values for the assessment of crossing wear and plastic deformation. A wide fatigue area usually represents well-maintained rail geometry. As demonstrated in Figure 2.3 (b), when the crossing condition was degraded from “Worn” to “Damaged”, the

fatigue area was dramatically narrowed and shifted further from the theoretical point (TP) of the crossing. More information about the fatigue area can be found in the previous study [27].

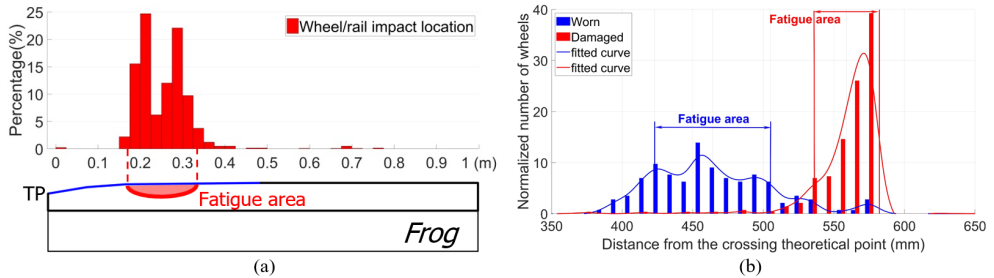


Figure 2.3. Demonstration of the crossing fatigue area detection; (a): Definition of the fatigue area. (b): Example of the fatigue area changes in different crossing condition stages.

### Wayside Monitoring System

The VGS for wayside monitoring is a remote measurement device based on digital image correlation (DIC). It uses high-speed digital cameras to measure the dynamic movements of the selected targets in the track. The system, set up together with the targets installed on the crossing rail next to the instrumented accelerometer, is shown in Figure 2.4 (a), and the demo of the displacement measurement is shown in Figure 2.4 (b). The main outputs are the vertical displacements of the tracked targets with a stable sampling frequency of up to 200 Hz.

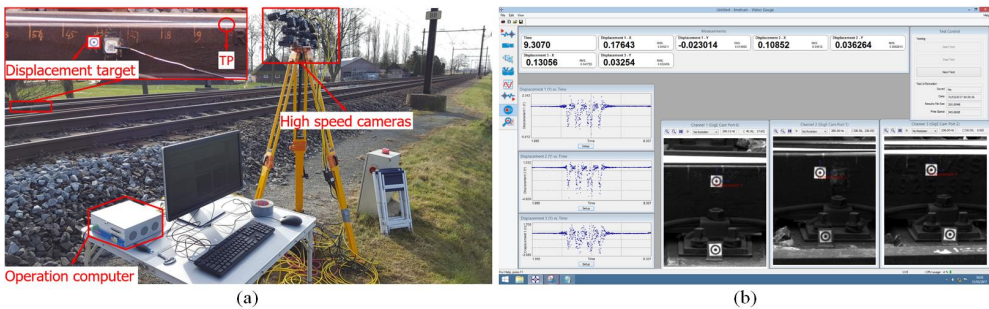


Figure 2.4. Wayside monitoring. (a): System setup; (b): The screen of displacement measurements.

Due to the limitation of the experimental conditions, the wayside monitoring system is usually set up close by the side of the track, which will introduce extra noise in the measured displacement results. To improve the accuracy of the measurement, the noise part needs to be eliminated. The noise mainly comes from the ground-activated camera vibration, which can be manually activated by hammering the ground near the camera. The measured camera vibrations in both the time and frequency domains are given in Figure 2.5.

Despite the differences in the displacement responses in the two monitored crossings, the main resonance of the camera vibration was around 15–45 Hz. In the previous study [30], the main components in the displacement signal were elaborated. The train-track components related to displacement responses are mainly distributed below 10 Hz, which do not overlap

with the camera vibration introduced noise. The noise part due to camera vibration can then be reduced through low-pass filtering, as shown in Figure 2.6.

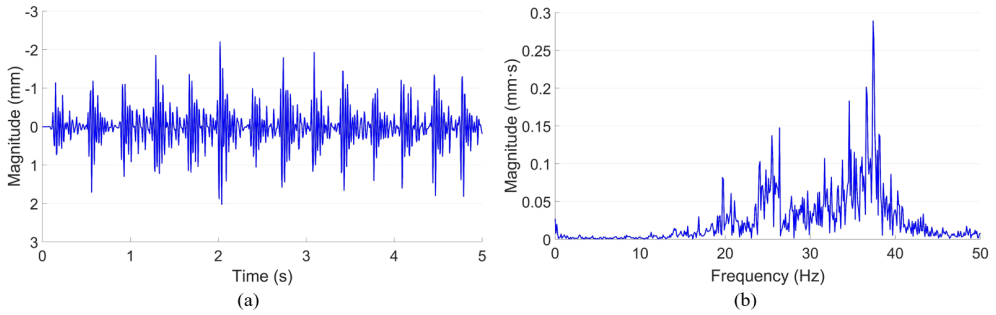


Figure 2.5. Ground activated camera vibration. (a): Time domain signal; (b): Frequency domain responses.

The magnitude of the dynamic vertical displacement of the rail directly reflects the intensity of the track movement due to the passing trains. By comparing the measured rail displacement with the reference level, which can be obtained from numerical simulation using the parameters in the designed condition, the ballast settlement level of the monitored location can be estimated. The MBS model for the crossing performance analysis is described later in this section.

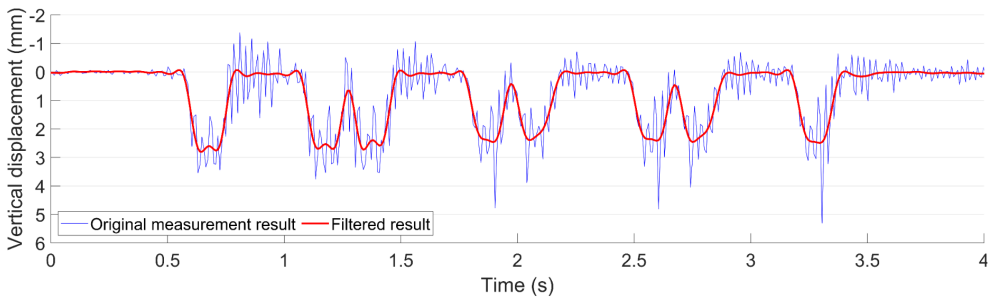


Figure 2.6. Examples of the measured rail vertical displacement.

## 2.2 Multi-Body System (MBS) Vehicle-Crossing Model

The numerical model for the crossing performance analysis was developed using the MBS method VI-Rail (Figure 2.7 (a)). The rail pads, clips, and ballast were simulated as spring and damping elements (rail busing and base busing, Figure 2.7 (b)).

D

In the vehicle model, the car body, bogie frames and the wheelsets were modelled as rigid bodies with both the primary suspension and secondary suspension taken into account (Figure 2.7 (b)). The track model was a straight line with the crossing panel (Figure 2.7 (c)) situated in the middle of the track. The rail element for the acceleration and displacement extraction was the lumped rail mass located 0.3 m from the TP of the crossing (Figure 2.7 (d)), which is consistent with the setup of the field measurements (Figure 2.1 and Figure 2.4 (a)).

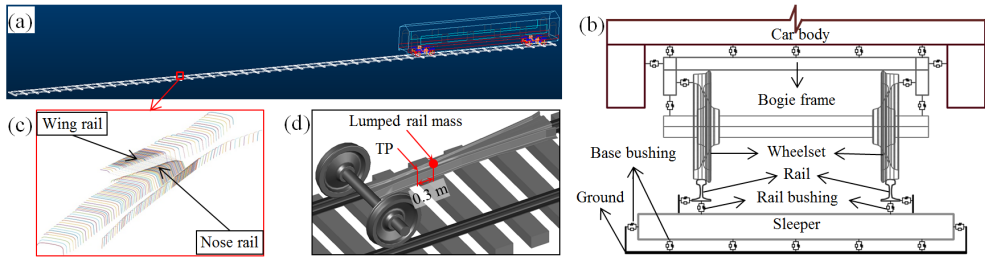


Figure 2.7. Multi-body system (MBS) model. (a): Vehicle-track model; (b): Flexible connections in the model; (c): Crossing profiles; (d): Rail element for acceleration extraction.

The detailed model development, experimental validation, and numerical verification can be found in the previous study [29]. Corresponding to the condition indicators, the main outputs of the MBS model are the wheel impact acceleration, transition region and wheel-rail contact forces. Using the MBS model, the condition of the monitored crossing, as well as the detected track degradations, can be verified.

### 3 Field Measurements and Analysis

The monitored crossing was a cast manganese crossing with an angle of 1:9. As part of a crossover, trains mainly pass the crossing in the facing through route (Figure 1.2) with a velocity of around 140 km/h. The on-site view of the crossing is shown in Figure 3.1 (a). According to the maintenance record, this crossing was suffering from fast degradation with the service life of only around three years (18 years on average [2]). At the beginning of the condition monitoring, the damaged crossing was completely renovated.

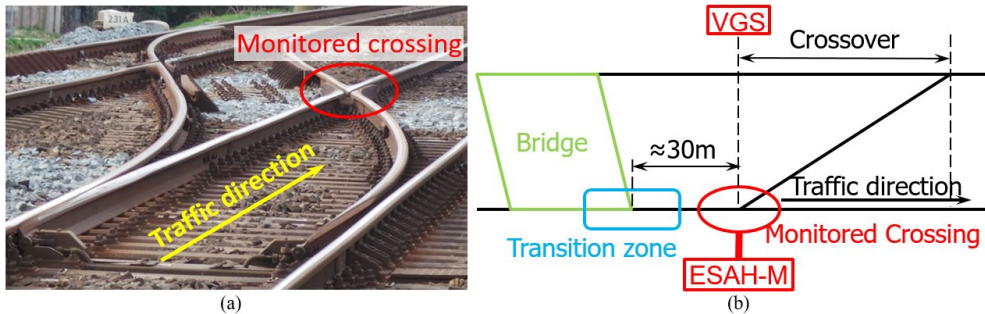


Figure 3.1. Overview of the monitored crossing. (a): On-site view; (b): Sketch view.

Figure 3.1 (b) gives a sketch view of the crossing, including the setup of the monitoring devices and the layout of the adjacent structures, especially the small bridge in front of the crossing. Considering that the bridge is located quite close to the monitored crossing, the performance of the crossing might be affected by the bridge, which will be discussed later. The measurement results from the crossing instrumentation were based on multiple train passages in one monitoring day. For the wayside monitoring, one sufficient train passage is enough to estimate the ballast condition. To maximally reduce the influence of the vehicle-related variables, the selected results were restricted to the commonly operated VIRM trains

with velocities of around 140 km/h.

### 3.1 Wheel Impacts

Based on the estimated transition regions, the wheel impact accelerations were calculated. The distribution of the wheel impacts due to multiple wheel passages is shown in Figure 3.2 (a). The sample size, in this case, was 78 passing wheels. It can be seen that the wheel impacts presented a bimodal distribution. Around 80 % of the wheel impacts were below 50 g, while the remaining 20 % of the wheel impacts were extremely high with a mean value of around 350 g. Such a polarized distribution of impacts indicates the highly unstable wheel-rail interaction in this crossing. It was demonstrated in a previous study [29] that for this type of railway crossing, the average level of the wheel impact is around 50 g, meaning that the 20 % of high impacts of the monitored crossing are already more than seven times higher than the average impact level. It can be imagined that such high impacts will dramatically accelerate the degradation procedure of the crossing.

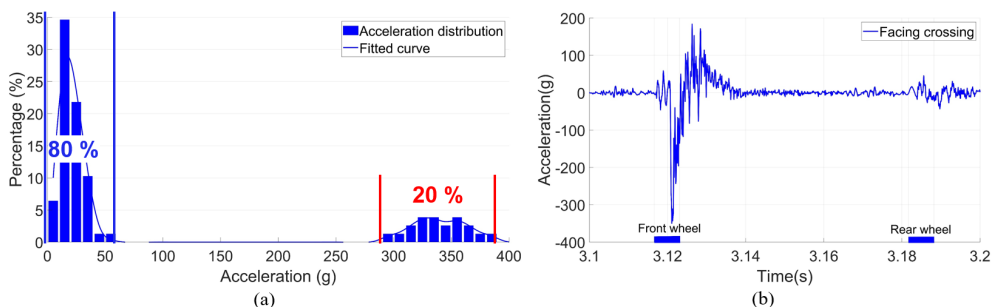


Figure 3.2. Vertical acceleration responses of the monitored crossings. (a): Distribution based on multiple train passages in one day; (b): Example of impacts due to one bogie.

An example of the impact acceleration response in the time-domain due to the first bogie of a VIRM train is shown in Figure 3.2 (b). It can be seen that for the two passing wheels from the same bogie, the impacts can be quite different. The impact due to the front wheel was up to 350 g, while the rear wheel activated vertical acceleration was only 20 g. It has to be noted that the high impacts were not always introduced by the front wheel, but appeared to have random occurrences. Such results further confirmed the instability of wheel-rail interaction at this crossing.

### 3.2 Fatigue Area

The measured fatigue area of the monitored crossing is presented in Figure 3.3. It can be seen that the wheel impacts were widely distributed at 0.22-0.38 m from the TP with the fatigue area size of 0.16 m. According to the previous study [28], the transition region (Figure 1.2) for this type of crossing is around 0.15-0.4 m. The fatigue area widely covered 64 % of the transition region, which can be considered to be in line with the expectation of a new crossing profile. Such results further confirmed that the crossing rail was not worn or deformed.

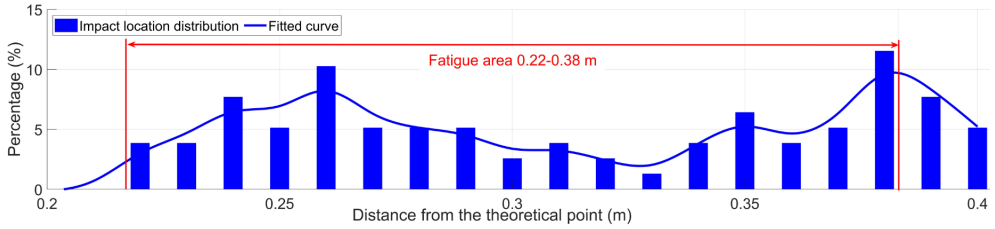


Figure 3.3. Measured fatigue area of the monitored crossing.

It has to be noted that the fatigue area does not conform to the normal distribution (referring to the “Worn” stage demonstrated in Figure 2.3 (b)). Combined with the results of the wheel impacts such a fatigue area further confirmed the instability of the wheel-rail contact in the monitored crossing.

In a previous study [27], it was found that the crossing degradation was accompanied by the increase of wheel-rail impacts and the reduction in the fatigue area. The large number of extremely high wheel-rail impacts and relatively wide fatigue area clearly indicate the abnormal performance of the monitored crossing. Finding the root causes of such abnormality is the key to improving the dynamic performance of the crossing.

### 3.3 Ballast Settlement

The measured vertical displacement of the crossing rail is presented in Figure 3.4. It can be seen that the vertical rail displacement was around 4 mm. The measured displacement result can be considered to have two main parts: the elastic deformation and the gap between the sleeper and ballast. Considering that the ballast settlement is the accumulated effect due to multiple wheel passages, the plastic deformation caused by each passing train can be neglected. Due to the high impacts in the crossing panel, the ballast is usually settled unevenly, which results in hanging sleepers. Using the validated MBS model, it was calculated that the rail displacement in the reference condition was 1.4 mm (Figure 3.4), which only consisted of the elastic deformation part. By comparing these two results, it could be calculated that the gap between the sleeper and ballast was 2.6 mm, which can be estimated as the settlement of ballast. It was observed that the rail displacement obtained from the MBS simulation was much higher than that in a normal track (less than 1 mm [27], [31]), which indicates the vulnerability of the ballast in the railway crossings.

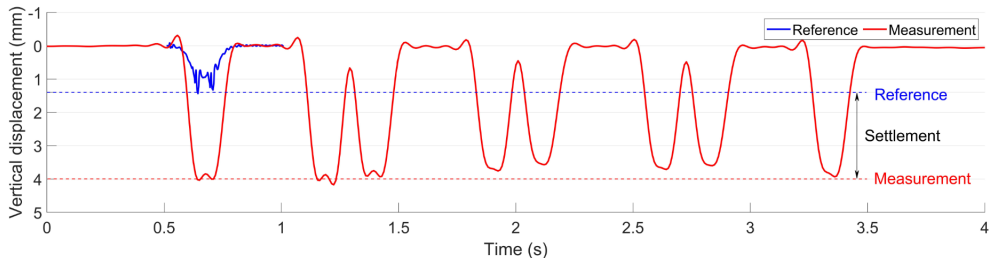


Figure 3.4. Ballast settlement in the monitored crossing.

In a previous study [27], it was found that track irregularities such as rail joints and turnout crossings can lead to the fast deterioration of the ballast, and the ballast settlement will in turn accelerate the degradation procedure of other related track components. In this study, the 2.6 mm ballast settlement was already higher than those in the previously monitored welded joints ( $\approx 1.5$  mm) and movable crossings ( $\approx 2$  mm), which revealed the seriously deteriorated ballast condition.

It can be concluded that the monitored crossing was suffering from rapidly occurring, extremely high wheel-rail impacts and severe ballast settlement. For a recently renovated crossing, such performance is quite abnormal.

## 4 Effectiveness Analysis of the Maintenance Actions

The constantly occurring extremely high wheel-rail impacts as well as serious ballast settlement clearly indicate the degraded condition of the crossing. In order to improve such a situation, various maintenance actions were implemented in this location including ballast tamping, fastening system renovation, etc. In this section, the effectiveness of the maintenance actions are briefly discussed, as presented below.

### 4.1 Ballast Tamping

Considering that the crossing rail was lately renovated with limited wear or plastic deformation, the severe ballast settlement was suspected to be the main cause for the high wheel-rail impacts. Therefore, ballast tamping actions were frequently performed in this location by the local contractor. However, due to the lack of maintenance facilities, the tamping actions were mainly performed using the squeezing machine (Figure 4.1 (a)) without track geometry correction. It can be imagined that the settled ballast cannot be fully recovered with such tamping action. As shown in Figure 4.1 (b), after tamping, the rail displacement was not dramatically reduced.

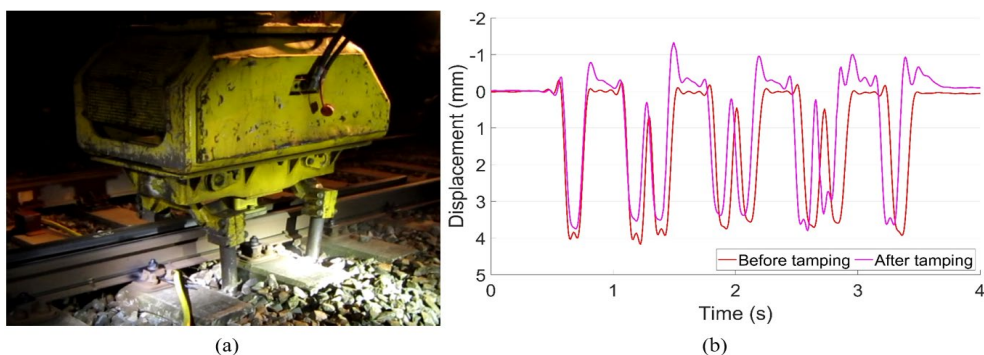


Figure 4.1. (a): Squeezing machine used for ballast tamping in the monitored crossing; (b): Measured rail displacement before and after ballast tamping.

The development of the wheel-rail impacts before and after tamping are presented in Figure 4.2. In this figure, each point represents the mean value of the impact accelerations based on

multiple wheel passages in one monitoring day. It was discussed in a previous study [28] that the fluctuation of the wheel impacts was highly affected by external disturbances such as the weather. Still, it can be seen that the regression values before and after tamping were both around 100 g.

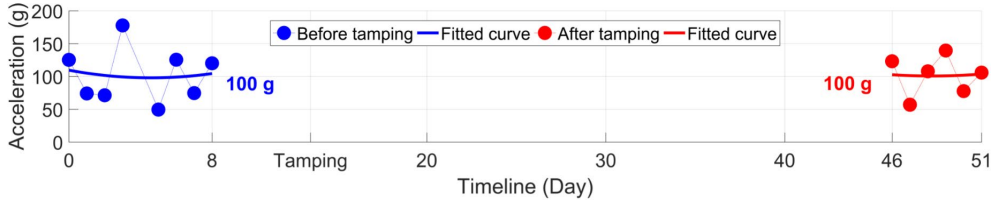


Figure 4.2. Development of the wheel-rail impacts before and after ballast tamping.

It can be concluded that such frequently implemented ballast tamping had no improvement in either the ballast condition or the dynamic performance of the monitored crossing. Without figuring out the root causes for the fast crossing degradation, such ineffective ballast tamping should be suspended.

## 4.2 Fastening System Renovation

During the monitoring period, the fastening system was found to be degraded with some broken bolts. Such degradation affected the lateral stability of the track. Therefore, the fastening system, mainly the bolts in the guard rails and the clips, was renovated, as shown in Figure 4.3.

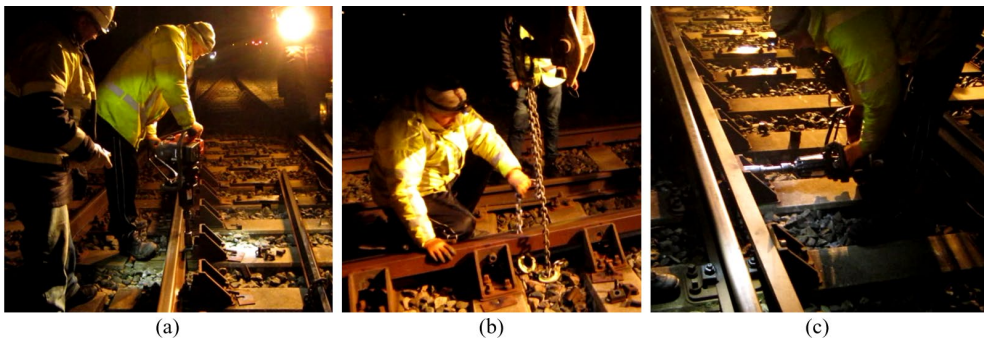


Figure 4.3. Fastening system renovation. (a) Remove the broken bolts. (b) Reposition the guard rail. (c) Install new bolts.

The development of the wheel-rail impacts before and after renovation is shown in Figure 4.4. The upper figure is the development of the mean value, and the lower figure gives the ratio of different impact levels in each monitoring day, corresponding to the value in the upper figure.

It can be seen from Figure 4.4 that before the renovation, the wheel-rail impact showed a clear increasing trend with the impact values widely distributed from 0 to 450 g. Such a degradation trend indicates that maintenance is urgently required due to the defects of the fastening system. After the renovation, the wheel-rail impacts were dramatically reduced in

terms of the mean value and separated into two distribution modes, which is similar to those shown in Figure 3.2 (a). Such improvement is due to the enhancement in the track integrity. However, the wheel-rail impacts above 300 g were still a large proportion after maintenance, which means that the sources for such high wheel-rail impacts were not found.

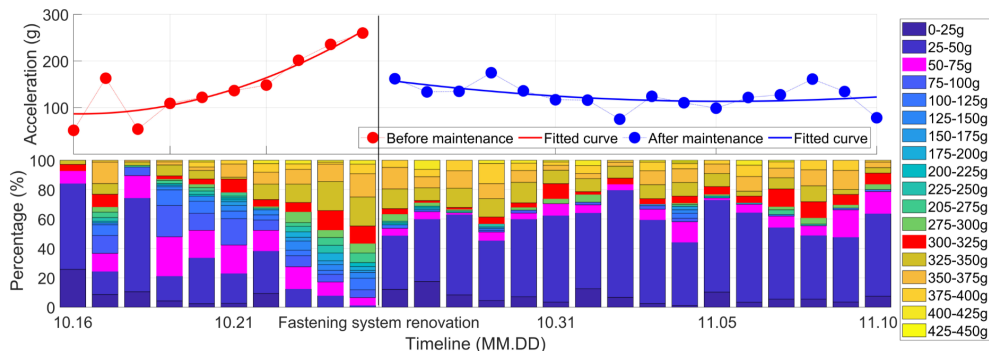


Figure 4.4. Effect of fastening system renovation on the dynamic performance of the crossing.

In practice, ballast tamping is currently one of the few options for contractors to maintain the track. However, the unimproved crossing performance clearly indicates the ineffectiveness of tamping. The fastening system renovation was a forced action to repair damaged components. Although the crossing performance was improved, the extremely high wheel-rail impacts were not reduced, thus the sources for the fast crossing degradation were not eliminated. To figure out the root causes for the crossing damage, the track inspection was extended to the bridge in front of the crossing (Figure 3.1 (b)). The results for the track inspection, as well as the numerical verification using the MBS model, are presented in the next section.

## 5 Damage Sources Investigation

In this section, the track inspection, including the whole turnout and the adjacent bridge, is presented. The inspected degradations will be input into the MBS model to verify the influence on the crossing performance. As a reference, the dynamic responses in the designed condition with no track degradations were also simulated and compared with those in degraded conditions. The verification results, followed by the analysis, are also presented.

### 5.1 Track Inspection

In the field inspection, it was found that the bridge was not well aligned in the track, but deviated around 15 cm, as shown in Figure 5.1 (a). Such deviation introduced a curve into the track, which was likely to be out of design since no elevation was set up in the outer rail. It can be imagined that the passing trains could not pass the track along the central line but tended to have wheel flange contact with the outer rail, which eventually leads to the severe wear in the switch blade (Figure 5.1 (b)).

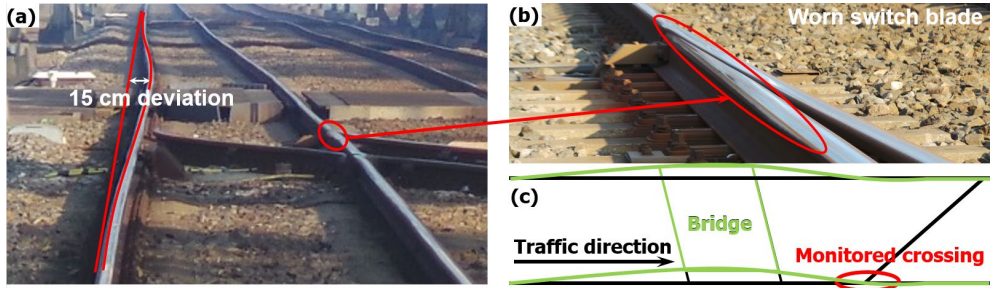


Figure 5.1. Track deviation in front of the crossing. (a) Inspected curve introduced by the bridge. (b) Worn switch rail. (c) Demonstration of the bridge deviation.

The accumulated effect of the track deviation was also reflected in the varied track gauge. It was shown in the measurement results that the gauge variations along the whole turnout were up to 3 mm, as presented in Table 5.1. Considering that the monitored crossing is located quite close to the bridge (Figure 5.1 (c)), such track misalignment, including the track deviation in the bridge and track gauge variation along the turnout, may affect the wheel-rail interaction in the crossing.

Table 5.1. Track gauge measurement results in critical sections along the turnout

Location	A	B	C	D	E	F	G
Deviation (mm)	+2	+3	-2	-2	+2	+3	0

## 5.2 Numerical Verification and Analysis

In order to verify the effect of the track lateral misalignment on the performance of the crossing, both the bridge-introduced curve and the track gauge variation were input into the MBS vehicle-crossing model (Figure 2.7). The equivalent track lateral irregularities as the model input are shown in Figure 5.2.

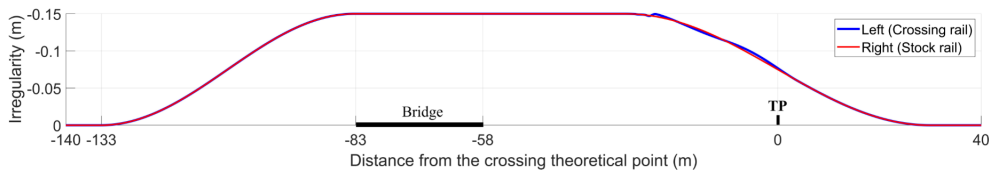


Figure 5.2. Equivalent lateral irregularities in the track.

In the MBS model, the crossing type is the same as the monitored 1:9 crossing with the rail

type of UIC54 E1. The vehicle model is consistent with the recorded VIRM train with the wheel profile of S1002. The initial track parameters of Dutch railways [32] applied in the model are given in Table 5.2.

Table 5.2. Track parameters

Track components		Stiffness, MN/m	Damping, kN·s/m
Rail pad / Clips	Vertical	1300	45
	Lateral	280	580
	Roll	360	390
Ballast		45	32

With the track misalignment taken into account, the crossing condition was considered as degraded. The simulation results of both wheels in the bogie, including the wheel impact accelerations and transition regions, were compared with the results in the designed condition [29], as shown in Figure 5.3.

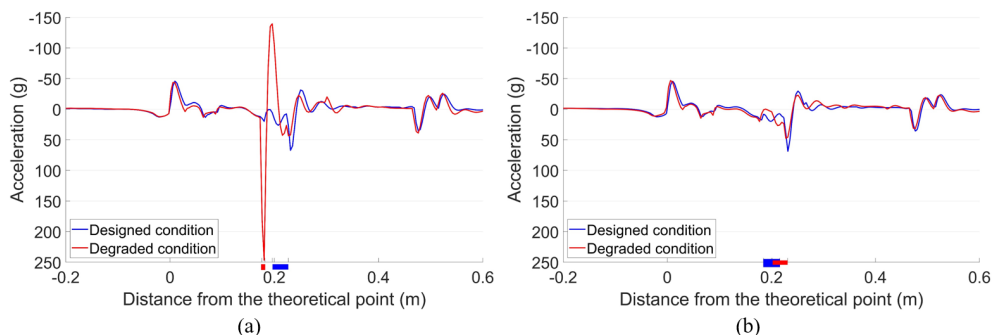


Figure 5.3. Vertical impact acceleration responses and transition regions. (a) Front wheel. (b) Rear wheel.

It can be seen from Figure 5.3 (a) that with the lateral irregularity taken into account, the impact of the front wheel was dramatically increased to 247 g, which was 4 times higher than the reference value (around 62 g) in the designed condition. While for the rear wheel from the same bogie, the impact was 48 g (Figure 5.3 (b)), which was even lower than the reference value. Despite the slight difference in the absolute values, the simulation results were consistent with the measurement results (Figure 3.2). Meanwhile, the transition region of the front wheel was 0.176–0.182 m from the TP with a size of only 0.006 m. Compared with the reference level (0.196–0.217 m with a size of 0.031 m, [29]), it was much narrower and closer to the TP, indicating earlier wheel impact and much sharper wheel load transition in the crossing. For the rear wheel, although the transition region was located farther from the TP, the size was almost the same as the reference value.

Such results clearly show that the curve and lateral track misalignment in front of the crossing can lead to unstable wheel-rail contact in the crossing and sometimes result in extremely high impacts. Additionally, the front and rear wheels pass through the crossing quite differently, which indicates that the performance of the rear wheel is not independent, but is affected by the front wheel.

For the wheel-rail contact forces, the tendency was similar to the acceleration responses, as shown in Figure 5.4. With the degraded track condition, the maximum contact force of the front wheel in the degraded condition was 468 kN, which was twice as high as that in the designed condition (235 kN). While for the rear wheel, the difference between the degraded condition and the designed condition was limited.

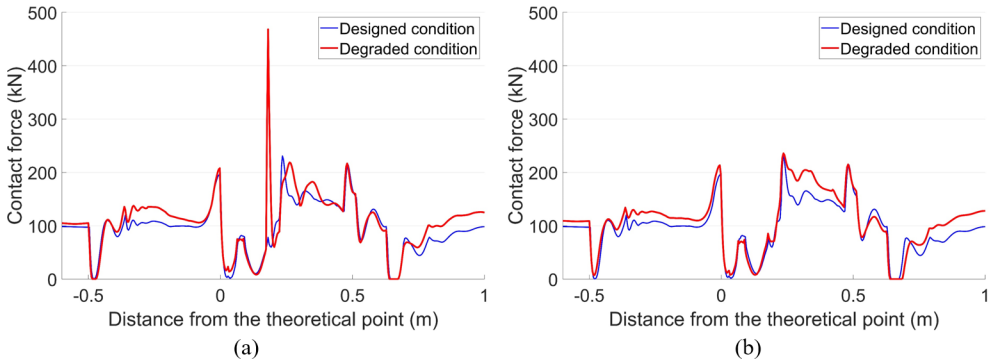


Figure 5.4. Vertical wheel-rail contact responses of the facing crossing. (a) Front wheel. (b) Rear wheel.

To understand how the track misalignment affects the wheel-rail interaction in the crossing, the relationship between the wheel lateral displacements and wheel-rail contact forces were analysed. Before that, the wheel lateral displacement in the designed condition is presented in Figure 5.5. When the train enters the crossing panel, the varied rail geometry will lead to the lateral movement of the wheel. The maximum lateral displacement was around 0.7 mm.

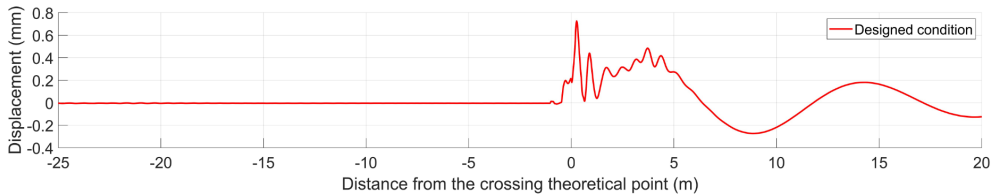


Figure 5.5. Wheel lateral displacement in the designed condition.

In the degraded condition with track lateral irregularities, the lateral displacements of the wheels were dramatically changed, as shown in Figure 5.6. It can be seen that both the front wheel and the rear wheel showed activated hunting oscillation before and after passing through the crossing, but the trajectories were quite different. For the front wheel, the lateral movement was more intense and ran toward the crossing nose rail near the TP. The maximum lateral displacement corresponding to the position with the highest contact force was 2.3 mm, which means that compared with that in the designed condition, the wheel flange was around 1.6 mm closer to the nose rail. Comparatively speaking, such displacement of the rear wheel was only 0.3 mm. Such results indicate that the wheel-rail impact was profoundly affected by the movement of the wheel. When the wheel approaches closer to the crossing nose, the wheel-rail impact is likely to be increased. It can be concluded that the train hunting activated by the lateral track misalignment in front of the crossing is the main cause of the extremely high wheel-rail impacts.

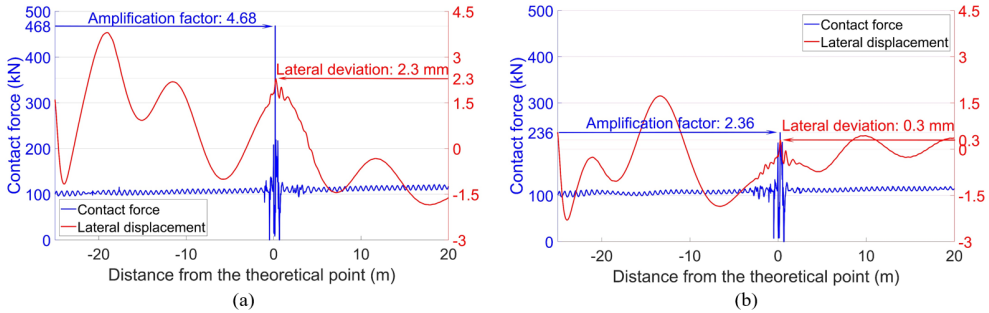


Figure 5.6. Wheel-rail contact forces and wheel lateral displacements. (a) Front wheel. (b) Rear wheel.

The train hunting effect also explains the unstable wheel-rail impacts. For the rear wheel, the lateral movement was affected not only by the track misalignment but also by the front wheel from the same bogie. As a result, these two wheels led to quite different wheel trajectories. It can be imagined that in the real-life situation, there are much more factors that may affect the hunting motion of each passing wheelset such as the initial position of the wheel when entering the misaligned track section, the mutual interaction between the adjacent wheelsets, the lateral resistance of the track, and even the weather condition [28], etc. The combined effect of all these factors ultimately resulted in the polarized distribution of the impact acceleration responses (Figure 3.2 (a)).

### 5.3 Respective Effect of Lateral Curve or Track Gauge Deviation

It can be noticed that in the previous analysis, the input track misalignment consisted of two parts: the lateral curve introduced by the bridge and the track gauge deviation. In order to understand the effect of each part in the wheel-rail interaction, these two parts were further analysed, and the results are presented below.

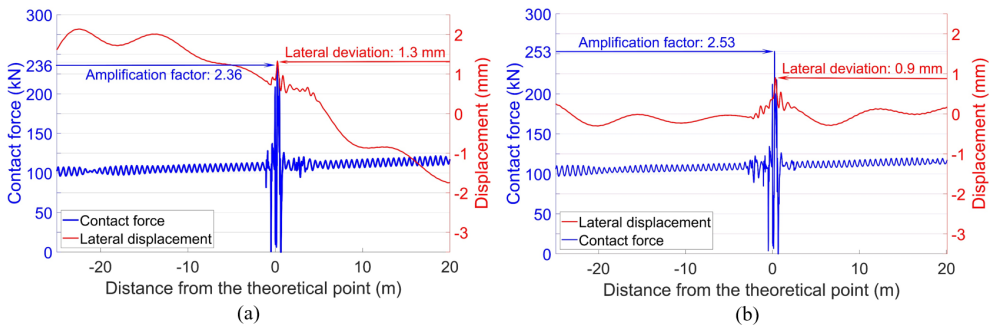


Figure 5.7. Wheel-rail contact forces and lateral wheel displacements. (a) Front wheel. (b) Rear wheel.

Considering the bridge-introduced lateral curve, the wheel-rail contact forces and the lateral wheel displacements were calculated, as presented in Figure 5.7. It can be seen that in the front wheel, the bridge-introduced curve mainly resulted in the lateral shift of the wheel trajectory due to the centripetal force. Such a shift was only 0.5 mm near the crossing nose

when compared with the designed condition, and the effect on the wheel impact was limited. For the rear wheel, the combined effect of the curve and the motion of the front wheel resulted in the lateral deviation of 0.9 mm, which was quite close to that in the designed condition and had no significant influence on the wheel-rail impact.

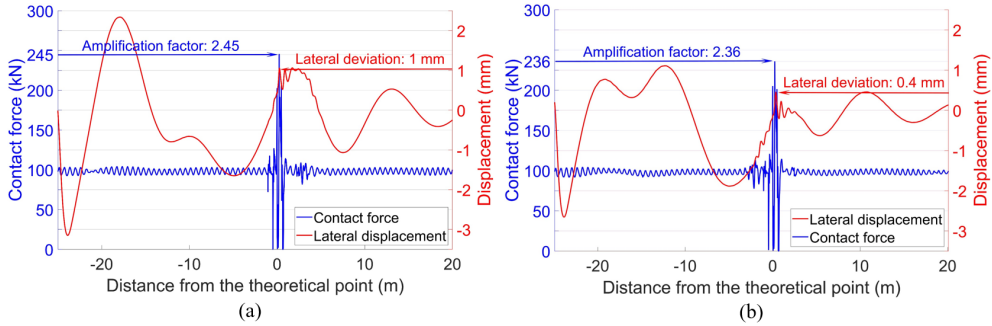


Figure 5.8. Wheel-rail contact forces and wheel lateral displacements. (a) Front wheel. (b) Rear wheel.

The effect of the track gauge deviation on the wheel-rail interaction is demonstrated in Figure 5.8. Different from the effect of the bridge-introduced curve, the deviated track gauge activated the hunting motion of the passing wheels. Still, the resulted lateral wheel displacements were not large enough to amplify the wheel-rail impact. The maximum displacements corresponding to the wheel impacts were 1 mm in the front wheel and 0.4 mm in the rear wheel, respectively.

## 5.4 Summary

Based on the above analysis, it can be concluded that the extremely high wheel-rail impacts in the monitored crossing were caused by the hunting oscillation of the passing trains. Such train hunting was the combined effect of the bridge-introduced curve in front of the crossing and the deviated track gauge along the turnout. When the maximum wheel lateral displacement reaches a certain level (e.g., 2.3 mm), the wheel-rail impact will be dramatically amplified.

It has to be noted that although the curve in front of the crossing did not directly activate train hunting, the activated lateral shift of the passing wheels resulted in the wear in the switch blade (Figure 5.1 (b)) and contributed to the track gauge deviation. Therefore, such a curve can be considered as the root cause of the fast degradation of the monitored crossing. To improve the performance of the crossing, this curve has to be first eliminated.

In the previous study [28], it was proven that high rail temperature due to the long duration of sunshine would amplify the existing track geometry deviation in turnout and lead to the increase in the wheel-rail impacts. The train hunting activated by the track gauge deviation in this study further confirmed these results.

## 6 Effect of Maintenance-Related Degradation

According to the measurement results, the monitored crossing also suffered from ballast settlement and broken clips. In order to better simulate the real-life situation, these track defects were respectively added to the degraded MBS model developed in Section 5.2. The combined effects were simulated and analysed, as presented below.

### 6.1 Effect of Ballast Settlement

It is shown in Figure 3.4 that the detected ballast settlement was around 2.6 mm. To simplify the problem, a vertical irregularity was introduced in the MBS model to simulate the ballast settlement, as shown in Figure 6.1. In this irregularity function, the amplitude was 1.3 mm, and the wavelength was 10 m. The trough of the wave was located 0.3 m from the TP of the crossing, which was consistent with the instrumented accelerometer and the installed displacement target.

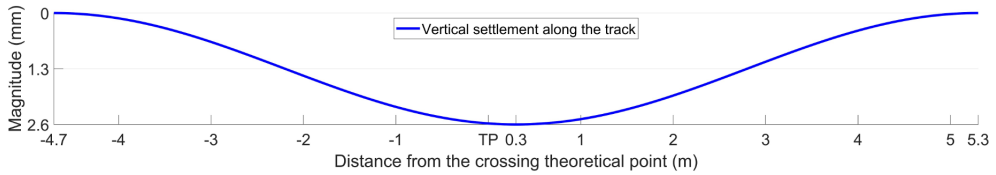


Figure 6.1. Ballast settlement introduced in the MBS model.

With the ballast settlement taken into account in the MBS model, the dynamic performance of the crossing was simulated. The representative results are shown in Figure 6.2. It can be seen that the simulation results were almost the same as those without ballast settlement (Figure 5.6), despite the slightly increased impact force of the front wheel (from 468 kN to 487 kN). It can be concluded that the existence of ballast settlement had a limited influence on the dynamic performance of the crossing. From another point of view, the ballast settlement was more likely to be the accumulated effect of the high wheel-rail impacts. Such results further explain the ineffectiveness of the frequently performed ballast tamping since ballast settlement is not the main cause of the extremely high wheel-rail impacts.

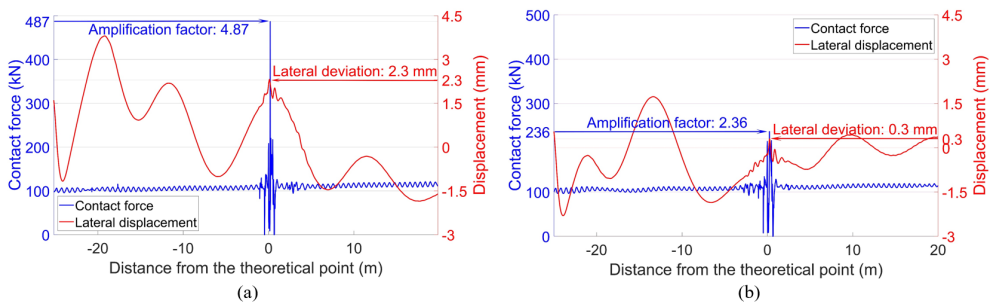


Figure 6.2. Wheel-rail contact forces and lateral wheel displacements. (a) Front wheel. (b) Rear wheel.

### 6.2 Influence of Reduced Lateral Support

It is shown in Figure 4.3 that the defects of the fastening system can increase the instability of the wheel-rail impact in the crossing. Combined with the maintenance action and the simulation results in Section 5, it can be inferred that this effect was caused by the reduced lateral track resistance. To verify this inference in the degraded model (Section 5.2), the input lateral stiffness of the clips in the crossing panel was reduced from 280 MN/m (Table 5.2) to 2.8 N/m, and the corresponded damping was reduced from 580 kN·s/m to 5.8 N·s/m. Based on these inputs, the wheel-rail contact forces and the lateral wheel displacements were calculated, as presented in Figure 6.3.

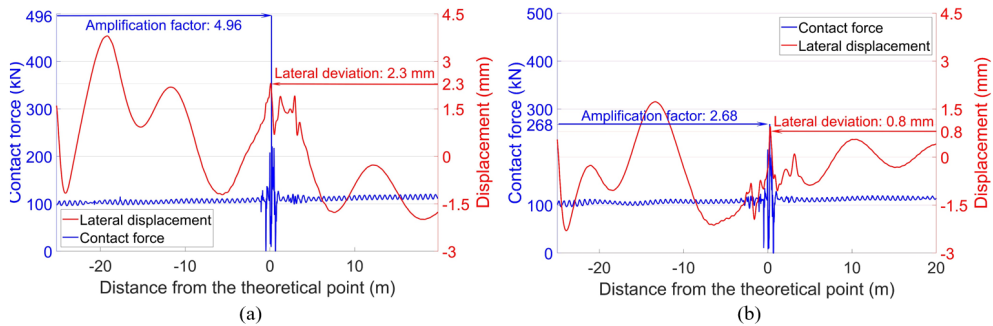


Figure 6.3. Wheel-rail contact forces and lateral wheel displacements. (a) Front wheel. (b) Rear wheel. Note: Ballast settlement was not taken into account.

It can be seen from Figure 6.3 that with the reduced lateral stiffness and damping of the clips, the impacts of both the front wheel and the rear wheel were slightly increased (compared with the results in Figure 5.6). Moreover, the hunting motion of wheels in the crossing panel was more intense. As a result, the lateral deviation of the rear wheel increased from 0.3 mm to 0.8 mm. It can be imagined that with the impacts of the passing trains, the track alignment will continuously be changing due to the reduced structural integrity. The changed track alignment will, in return, act on the wheel-rail interaction and eventually lead to more unstable wheel impacts in the crossing (Figure 4.4). From this point of view, renovating the defected fastening system is necessary for a monitored crossing. Enough track lateral resistance can help to maintain better crossing performance.

## 7 Conclusions

In this study, the root cause of the fast degradation of a 1:9 crossing in the Dutch railway system was investigated. The effectiveness of some typical track maintenance actions was also assessed and verified. Based on the measurement and simulation results, the following conclusions can be drawn:

- The fast crossing degradation was directly caused by the extremely high wheel-rail impacts, and the root cause for such high impacts was the hunting of the passing trains that were activated by the track lateral misalignment in front of the crossing. When the lateral deviation of the passing wheel exceeds a certain extent (e.g., 2.3 mm), the wheel-rail contact situation will change and the wheel impacts will be dramatically increased. To improve the current situation, such track misalignment needs to be eliminated;
- Ballast settlement is likely to be the accumulated effect of the high wheel-rail impacts. The

influence on the crossing performance is somewhat limited. Ballast tamping, especially with only the squeezing machine, cannot improve the dynamic performance of the crossing. In the case of not knowing the sources of damage, it is better to take no action, rather than implement ballast tamping;

- Fastening system renovation helped improved the crossing performance by providing better lateral support in the track but was not targeted to the fundamental problem. Therefore, such damage repair action is useful, but not enough for an improvement in the crossing performance.

This study further verified the effectiveness of the previously proposed condition indicators in the investigation of the damage sources of the crossing. Since the root causes for the fast degradation were the deviated track in front of the crossing, this means that the degradation detection is not only restricted to the crossing itself but can also take the adjacent structures into account.

The activated train hunting reasonably explained the instability of wheel-rail interaction in the crossing, which pointed out a possible direction to maintain the problematic crossings in the Dutch railway network. As part of the Structural Health Monitoring System for railway crossings developed in TU Delft, the findings in this study will help improve the current maintenance philosophy from “failure reactive” to “failure proactive”, and eventually lead to sustainable railway crossings.

## References

- [1] ProRail, Ontwerpvoorschrift Baan en Bovenbouw Deel 6.1: Wissels en kruisingen Alignement, tussenafstanden, overgangsvrije zones en bedieningsapparatuur, V006, The Netherlands, 2015, p. 12.
- [2] I. Shevtsov, Rolling Contact Fatigue problems at Railway Turnouts, [http://www.sim-flanders.be/sites/default/files/events/Meeting\\_Materials\\_Nov2013/mm\\_13112013\\_i\\_van\\_shevtsov\\_prorail.pdf](http://www.sim-flanders.be/sites/default/files/events/Meeting_Materials_Nov2013/mm_13112013_i_van_shevtsov_prorail.pdf), 2013
- [3] A.T. Cornish, Life-time monitoring of in service switches and crossings through field experimentation, PhD thesis, Imperial College London, London, United Kingdom, May 2014.
- [4] L.F. Molina, E. Resendiz, J.R. Edwards, J.M. Hart, C.P.L. Barkan, N. Ahuja, Condition Monitoring of Railway Turnouts and Other Track Components Using Machine Vision, Proceedings of the Transportation Research Board 90th Annual Meeting, November 2010.
- [5] C. Chen, T. Xu, G. Wang, B. Li, Railway turnout system RUL prediction based on feature fusion and genetic programming, Measurement, vol. 151, 2020, No. 107162.
- [6] P. Wang, Li. Wang, R. Chen, J. Xu, J. Xu, M. Gao, Overview and outlook on railway track stiffness measurement, Journal of Modern Transportation, Vol. 24 (2), 2016, p. 89-102.
- [7] G.J. Yeo, Monitoring Railway Track Condition Using Inertial Sensors on an in-Service Vehicle, PhD thesis, University of Birmingham, Birmingham, United Kingdom, June 2017.

- [8] A. De Rosa, S. Alfi, S. Bruni, Estimation of lateral and cross alignment in a railway track based on vehicle dynamics measurements, *Mechanical Systems and Signal Processing*, vol. 116, 2019, p. 606-623.
- [9] F. Balouchi, A. Bevan, R. Formston, Detecting Railway Under-Track Voids Using Multi-Train in-Service Vehicle Accelerometer, 7th IET Conference on Railway Condition Monitoring, Birmingham, United Kingdom, 27-28 September 2016.
- [10] H. Tsunashima, Condition Monitoring of Railway Tracks from Car-Body Vibration Using a Machine Learning Technique, *Applied Sciences*, vol. 9, 2019, No. 2734.
- [11] E. Kassa, J.C.O. Nielsen, Stochastic analysis of dynamic interaction between train and railway turnout, *Vehicle System Dynamics*. Vol. 46, No. 5, 2008, p. 429-449.
- [12] S. Alfi, S. Bruni, Mathematical modelling of train-turnout interaction, *Vehicle System Dynamics*. Vol. 47, No. 5, 2009, p. 551-574.
- [13] Z. Ren, S. Sun, G. Xie, A method to determine the two point contact zone and transfer of wheel rail forces in a turnout, *Vehicle System Dynamics*. Vol. 48, No. 10, 2010, p. 1115-1133.
- [14] M. Pletz, W. Daves, H. Ossberger, A wheel set/crossing model regarding impact, sliding and deformation - explicit finite element approach, *Wear*, vol. 294, 2012, p. 446-456.
- [15] A. Anyakwo, C. Pislaru, A. Ball, A New Method for Modelling and Simulation of the Dynamic Behaviour of the Wheel-rail contact, *International Journal of Automation and Computing*, Vol. 9(3), 2012, p. 237-247.
- [16] B.A. Pålsson, Optimisation of Railway Switches and Crossings, PhD thesis, Chalmers University of Technology, Göteborg, Sweden, February 2014.
- [17] Z. Wei, C. Shen, Z. Li, R. Dollevoet, Wheel–Rail Impact at Crossings-Relating Dynamic Frictional Contact to Degradation, *Journal of Computational and Nonlinear Dynamics*, vol. 12 (4), 2017, p. 041016 1-11.
- [18] L. Xin, Long-Term Behaviour of Railway Crossings – Wheel-Rail Interaction and Rail Fatigue Life Prediction, Delft, The Netherlands, June 2017.
- [19] S. Chiou, J. Yen, Modeling of railway turnout geometry in the frog area with the vehicle wheel trajectory, *Proceedings of the Institution of Mechanical Engineers Part F: Journal of Rail and Rapid Transit*, vol. 232(6), 2018, p. 1598-1614.
- [20] R. Skrypnik, J.C.O. Nielsen, M. Ekh, B.A. Pålsson, Metamodeling of wheel-rail normal contact in railway crossings with elasto-plastic material behaviour, *Engineering with Computers*, Vol. 35, 2019, p. 139-155.
- [21] P.T. Torstensson, G. Squicciarini, M. Krüger, B.A. Pålsson, J.C.O. Nielsen, D.J. Thompson, Wheel-rail impact loads and noise generated at railway crossings – influence of vehicle speed and crossing dip angle, *Journal of Sound and Vibration*, vol. 456, 2019, p. 119-136.
- [22] M. Wiest, W. Daves, F.D. Fischer, H. Ossberger, Deformation and damage of a crossing nose due to wheel passages, *Wear*, vol. 265, 2008, p. 1431-1438.

- [23] A. Johansson, B. Pålsson, M. Ekh, J. Nielsen, M. Ander, J. Brouzoulis, E. Kassa, Simulation of wheel–rail contact and damage in switches & crossings, *Wear*, Vol. 271, 2010, p. 472-481.
- [24] J.C.O. Nielsen, X. Li, Railway track geometry degradation due to differential settlement of ballast/subgrade – Numerical prediction by an iterative procedure, *Journal of Sound and Vibration*, vol. 412, 2018, p. 441-456.
- [25] R. Skrypnik, M. Ekh, J.C.O. Nielsen, B.A. Pålsson, Prediction of plastic deformation and wear in railway crossings – Comparing the performance of two rail steel grades, *Wear*, Vol. 428-429, 2019, p. 302-314.
- [26] C. Wan, Optimisation of vehicle-track interaction at railway crossings, PhD thesis, Delft University of Technology, Delft, The Netherlands, September 2016.
- [27] X. Liu, V.L. Markine, H. Wang, I.Y. Shevtsov, Experimental tools for railway crossing condition monitoring, *Measurement*, vol. 129, 2018, p. 424-435.
- [28] X. Liu, V.L. Markine, Correlation Analysis and Application in the Railway Crossing Condition Monitoring, *Sensors*, vol. 19 (19), 2019.
- [29] X. Liu, V.L. Markine, Validation and Verification of the MBS Models for the Dynamic Performance Study of Railway Crossings, *submitted*, 2019.
- [30] H. Wang, V.L. Markine, X. Liu, Experimental analysis of railway track settlement in transition zones, *Proceedings of the Institution of Mechanical Engineers Part F: Journal of Rail and Rapid Transit*, vol. 232 (6), 2018, p. 1774-1789.
- [31] L. Xu, Z. Yu, C. Shi, A matrix coupled model for vehicle-slab track-subgrade interactions at 3-D space, *Soil Dynamics and Earthquake Engineering*, vol. 128, 2020, 105894.
- [32] M. Hiensch, J.C.O. Nielsen, E. Verheijen, Rail corrugation in The Netherlands – measurements and simulations, *Wear*, vol. 253, 2002, p. 140-149.

## Publications

**X. Liu**, V.L. Markine, H. Wang, I.Y. Shevtsov, Experimental tools for railway crossing condition monitoring, *Measurement*, vol. 129, 2018, p. 424-435.

**X. Liu**, V.L. Markine, MBS Vehicle-Crossing Model for Crossing Structural Health Monitoring, *Sensors*, vol. 20 (10), 2020, 2880.

**X. Liu**, V.L. Markine, Correlation Analysis and Application in the Railway Crossing Condition Monitoring, *Sensors*, vol. 19 (19), 2019, 4175.

**X. Liu**, V.L. Markine, Train Hunting Related Fast Degradation of a Railway Crossing – Condition Monitoring and Numerical Verification, *Sensors*, vol. 20 (8), 2020, 2278.

H. Wang, V.L. Markine, **X. Liu**, Experimental analysis of railway track settlement in transition zones, *Proceedings of the Institution of Mechanical Engineers Part F: Journal of Rail and Rapid Transit*, vol. 232 (6), 2018, p. 1774-1789.

J. Mao, J. Xiang, C. Yu, **X. Liu**, K. Gong, Wear and stability analysis of the train-curve rail system with an elastic anti-friction guard rail, *Dyna*, vol. 90(5), 2015, p. 532-539.

L. Xu, **X. Liu**, Matrix coupled model for the vehicle-track interaction analysis featured to the railway crossing, *Mechanical Systems and Signal Processing*, 2020, (*under review*).





## Xiangming Liu

05 August 1987, Born in Qinhuangdao, China

### EDUCATION

September 2006 – June 2010

**Bachelor in Civil Engineering**, Central South University, Changsha, China

September 2010 – November 2012

**Master in Railway Engineering**, Central South University, Changsha, China

December 2012 – December 2020

**Ph.D. in Railway Engineering**, Delft University of Technology, Delft, The Netherlands.